Control of volatile organic chemical emissions by adsorption onto hydrophobic and organophilic adsorbents

Yee, Lee Lai

Award date:
1997

Awarding institution:
University of Bath

CONTROL OF VOLATILE ORGANIC CHEMICAL EMISSIONS BY ADSORPTION ONTO HYDROPHOBIC AND ORGANOPHILIC ADSORBENTS

submitted by Lai Yee, Lee B. Eng. (Hons.)

for the degree of Ph.D.

of the University of Bath

1997

ProQuest LLC
789 East Eisenhower Parkway
P.O. Box 1346
Ann Arbor, MI 48106-1346

To Eng and my parents,

for their love and support.

Summary

With the advent of the Environmental Protection Act 1990, the control of volatile organic chemical (VOC) emissions has become necessary. Complying with regulations may result in additional costs, but these may be alleviated if solvent recovery by means of low pressure drop monoliths is considered. Monoliths, in comparison with traditional packed beds, have a very low pressure drop and high surface areas. The principal aims of the research were to determine the effectiveness of high silica zeolites as adsorbents for the recovery of VOCs and to utilise the zeolites in the monolithic configuration. Silicalite and ZSM-5 were selected as the adsorbents and propane, ethanol and methylene chloride were selected as representative VOCs.

The project was divided into two phases. The first was concerned with optimising the chemical formulation of pastes containing a high percentage of silicalite such that they can be extruded to form monolith structures. The second phase of the project involved comparing the equilibrium and kinetic performances of the manufactured monoliths with the performance of an equivalent packed bed containing commercially available silicalite pellets.

Multichannel monoliths containing up to 90 % silicalite and with cell densities up to 29 cells/cm^2 and adsorbent wall thicknesses down to 0.6 mm were produced. A square channel monolith having a channel size of 1.0 mm, a wall thickness of 1.0 mm and a cell density of 25 cells/cm^2 was selected for further study due to its relatively high mechanical strength, ease of fabrication, and to the fact that its overall dimensions were comparable with those of an equivalent packed bed. The single component adsorption of VOCs onto high silica zeolites is highly favourable and isotherms of rectangular shape were obtained. The equilibrium capacities for the VOCs were found to be broadly similar for the two adsorbent forms whilst, in their favour for air pollution control applications, the manufactured monoliths were determined to have a much lower affinity for water than the pellets. The isotherms for single component VOC adsorption for both the monolith and the packed bed are well represented by the Langmuir model. While the isotherms for the adsorption of VOC and water vapour mixtures onto the monolith can be predicted well with the extended Langmuir model, those for adsorption

onto the packed bed do not agree well with the model. The kinetics of uptake onto the monoliths were found to be somewhat inferior to those on the packed bed and this was believed to be due to a less than optimum macropore structure and a lower external mass transfer coefficient in the former. A mathematical modelling study by Shah et. al., 1995 revealed that there would be no difference in performance between a monolith and an equivalent packed bed if the rate of adsorption in both cases were to be controlled by micropore diffusion. The external mass transfer coefficient calculated for the monolith is lower than that for the packed bed.

The desorption of VOCs from the monoliths by back flushing with a nitrogen purge at room temperature was found to be complete, which augurs well for the recovery of VOCs. The fact that silicalite monoliths perform advantageously in humidified air streams means that the principal disadvantage of using granular activated carbon (GAC) for VOC control can be overcome. Other advantages of silicalite over GAC include the avoidance of self-combustion in the presence of ketones and the ability to regenerate the inorganic adsorbent in air, rather than resorting to the use of inert gases as is necessary with GAC.

Acknowledgements

The work presented in this thesis was carried out under the supervision of Prof. B.D. Crittenden, Head of the School of Chemical Engineering, University of Bath and Dr. S. Perera, Lecturer in the same School. The author wishes to express her sincere gratitude to Prof. Crittenden and Dr. Perera for their constant interest, enthusiasm and guidance.

The author would like to thank Mr. John Bishop of the University of Bath for reading the thesis and for his invaluable suggestions. Gratitude is also extended to the members of staff and colleagues in the Schools of Chemical Engineering and Material Science, University of Bath, for their active support and technical assistance, especially to Mr. Robert Vincent Brain, Mr. Tony Comer, Miss Elaine Odgers, Mrs. Ann O'Reilly and Mr. Mervyn Newnes. Technical support provided by Mr. Leslie Steele, superintendent of the University of Bath Inter-schools Workshop, Mr. Mac Forysth, chief technician of the School of Chemical Engineering, and his predecessor Mr. Tom Walton, is also gratefully acknowledged.

Finally, the funding of the project by the EPSRC is acknowledged and the author is indebted to UOP for supplying the silicalite powder and pellets.

List of Contents

List of Tables

List of Figures

Nomenclature

b	Langmuir adsorption equilibrium constant ($mmHg^{-1}$)
C	adsorbate concentration in the effluent at any general time t (ppm)
C_o	initial feed adsorbate concentration (ppm)
d	pipe diameter (m)
d_c	monolith channel diameter (m)
d_h	hydraulic diameter (m)
d_p	particle diameter (m)
D_{ax}	axial dispersion of packed bed (m^2/s)
D_{axm}	axial dispersion of monolith (m^2/s)
D_v	molecular diffusivity (m^2/s)
f	friction factor (dimensionless)
f_F	Fanning friction factor (dimensionless)
f_{PB}	modified friction factor defined in Equation 6.15
$F_{sorbate}$	adsorbate feed flowrate (m^3/s)
k	external mass transfer coefficient (m/s)
l_c	concentration entrance length in monolith channel (m)
l_v	velocity entrance length in monolith channel (m)
L	bed length (m)
LUB	length of unused bed (m)
MTZ	mass transfer zone length (m)
ΔP	pressure drop (Pa)
q	adsorbate concentration in the adsorbed phase (mol/g)
q_{de}	total amount of adsorbate being desorbed (mol/g)
q_{eq}	equilibrium loading (mol/g)
q_{max}	concentration in the adsorbed phase when the monolayer is complete as defined in Equation 4.2 (mol/g)
Re	Reynolds number defined as $\frac{\rho u d}{\mu}$ (dimensionless)
Re_{PB}	modified Reynolds number defined in Equations 4.9 (dimensionless)
Re_{d_h}	Reynolds number defined in Equation 6.5 (dimensionless)

Sc Schmidt number defined as $\frac{\mu}{\rho D_v}$ (dimensionless)

Sh Sherwood number defined as $\frac{kd}{D_v}$ (dimensionless)

t_b breakthrough time (s)

t_{eq} equilibrium time (s)

u average velocity (m/s)

u_i interstitial velocity (ms/)

u_s superficial velocity (m/s)

u_{mf} minimum fluidisation velocity defined in Equation 6.1 (m/s)

u_{max} maximum allowable interstitial velocity in the packed bed defined be Equation 6.2 (m/s)

W adsorbent weight (g)

Symbols

α selectivity factor defined in Equation 5.1 (dimensionless)

ρ fluid density (kg/m^3)

μ fluid viscosity (Ns/m^2)

ε packed bed voidage defined in Equation 4.9 (dimensionless)

ε_m monolith voidage (dimensionless)

ε_{mf} voidage of fluidised bed (dimensionless)

ε_p bed voidage defined in Equation 6.12 (dimensionless)

Ψ adsorption-desorption reversibility factor defined in Equation 4.10 (dimensionless)

φ surface roughness (m)

Subscripts

i	volatile organic compound
j	water vapour

Chapter 1

Introduction

1.1 Background to the work

The term "volatile organic compounds" (VOCs) refers to a wide range of organic chemicals including aliphatic, aromatic and chlorinated hydrocarbons, aldehydes, ketones, esters, acids and alcohols (Table 1.1). VOCs evaporate readily at ambient temperature and, as an approximation, they are those organic compounds having room temperature vapour pressures greater than about 0.0007 atm and boiling points up to about 260°C at atmospheric pressure, which is true of most organic compounds with less than about 12 carbon atoms (De Nevers, 1995). Complex mixtures such as crude oils, paints, aerosols and adhesives can contain a high proportion of volatile material as well.

Table 1.1 Summary of the main classes of VOCs

Class	Structures	Examples
Alkanes	Hydrocarbon (HC) chains	Ethane (C2), propane (C3), butane (C4), hexane (C6), heptane (C7), octane (C8)
Alkenes	HC chains	Ethene, propene, butene
Alkynes	HC chains	Ethyne, butyne
Aromatics	HC rings and their derivatives	Benzene, toluene, xylene
Alcohols	HC chains with oxygen (-OH)	Methanol, ethanol
Aldehydes/ ketones	HC chains with oxygen (=O)	Ethanal, propanone, acetone
Acids	HC chains with oxygen (-OOH)	Formic acid, acetic acid
Halogenates	HC chains with halogens (e.g. chlorine, fluorine) attached	Chlorofluorocarbons (CFCs), vinyl chloride, chloroform

Methane is the most abundant VOC on the global scale, produced mainly by natural processes such as the decomposition of organic matter in woodlands. However, it has limited importance in pollution health considerations due to its relatively low reactivity, except perhaps indirectly in that it is an important greenhouse gas and contributes to global warming. It is therefore common to restrict studies of the health effects of VOCs to non-methane (NM) VOCs.

The major sources of the VOCs present in the UK atmosphere are shown in Table 1.2 and summarised in Figure 1.1 (DoE, 1993). Other data published by the European Community (EC) are shown in Table 1.3 and Figure 1.2 (Kiely, 1997). The data in Table 1.3 are expressed in kg VOC per capita and are incomplete as some countries include methane while others do not. The data from DoE (1993) are expressed in ktonnes VOC per year and do not include methane. The two sets of data show that the VOC sources are diverse and include natural sources such as release from forest trees, forest fires and anaerobic processes as occur in bogs and marshes. Figure 1.1 indicates that, of the man-made sources, vehicle emissions are by far the most significant, accounting for some 36 % (972,000 tonnes) of total VOC emissions in 1988. Almost all of this arose from the use of petrol engined vehicles, either in the form of exhaust emissions (83 %) or evaporation of fuel (17 %). Other significant sources of VOCs include the use of industrial solvents (particularly for painting), the petrochemical industry (which covers losses in crude oil production and distribution, refinery processes and product distribution), domestic solvents (e.g. painting, aerosols and other non- aerosol products) and the chemical industry. A similar distribution of VOC sources is shown in Figure 1.2, which indicates that road transport, including exhaust emissions and evaporative fuel losses, is the major contributor, followed by solvents usage. Figure 1.2 shows that during 1985 in the EC, 27 % of VOCs emissions arose from road transport, 17 % from the solvents industry, 15 % from coal mining, 17 % from landfilling (methane), 12 % from natural sources, 10 % from gas distribution and 2 % from other sources.

Table 1.2 NM VOC emissions inventory for UK, 1988 (ktonnes/year) (DoE, 1993)

Source	Emission (kt/yr)	% of total emissions
Painting	278	10.22
Printing	41	1.50
Surface cleaning	43	1.58
Dry cleaning	11	0.40
Adhesive	58	2.13
Pharmaceuticals	40	1.47
Aerosols	86	3.16
Non-aerosol consumer products	73	2.68
Agrochemical	39	1.43
Seed oil extraction	10	0.36
Other solvent use	73	2.68
Oil production	92	3.38
Oil distribution	107	3.93
Refineries	180	6.62
Product distribution	128	4.70
Other oil industry	25	0.91
Chemical industry	200	7.36
Domestic combustion - coal	51	1.87
Domestic combustion - other fuel	8	0.29
Industrial combustion	17	0.62
Other combustion	1	0.04
Baking	21	0.77
Alcoholic beverages	44	1.62
animal by-products	< 1	< 0.04
Other food	20	0.73
Iron and steel	9	0.33
Waste disposal	49	1.80
Gas industry	34	1.25
Miscellaneous	9	0.33
Petrol exhaust	644	23.68
Petrol evaporation	137	5.04
Diesel exhaust	167	6.14
Other transport	24	0.88
Total	2719	100

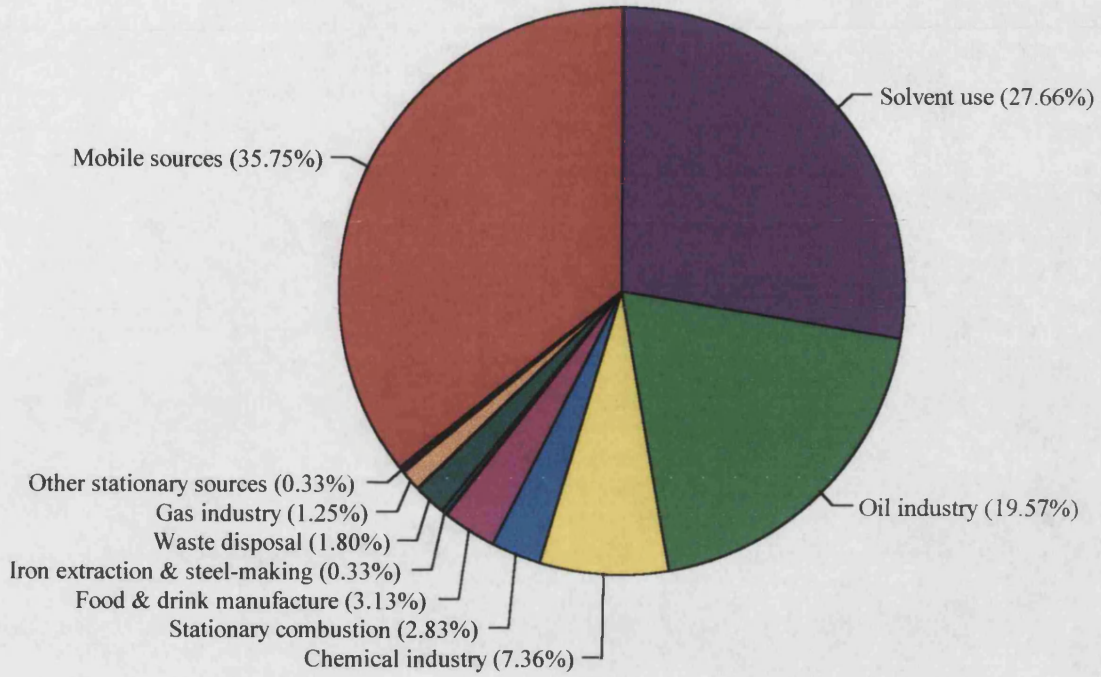

Figure 1.1 UK emissions of NM VOCs during 1988, categorised by source (DoE, 1993)

Table 1.3 VOC emissions per capita for 1985 (Kiely, 1997)

Source	Total VOC emissions (kg VOC/capita)				
	EC12	West Germany	Netherlands	UK	Ireland
Road transport	16	19	15	14	~7
Solvent evaporation	10	18	11	12	~7
Solid fossil fuel mining	8	17	-	16	-
Landfilling	10	29	-	12	-
Distribution of gas	5	4	-	7	~8
Production process	< 2	< 0.1	< 1	4	-
Combustion industry	< 0.5	< 0.1	< 1	< 1	< 1
Oil refineries	< 0.5	< 0.1	< 1	< 1	< 1
Heat for commerce, residential and institutional	2	< 0.5	< 0.5	< 1	-
Nature/miscellaneous	7	4 - 3	1	1.5	7
Total	~60	~95	~29	~69	~31

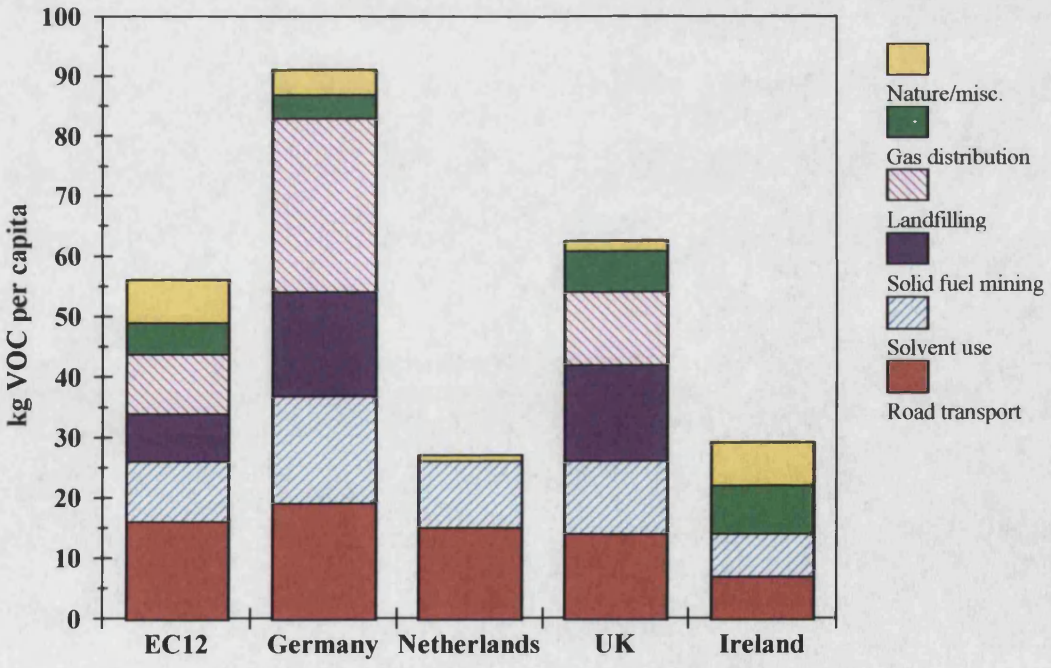

Figure 1.2 VOC emissions per capita during 1985 (Kiely, 1997)

Although much of the evidence presented concerns emissions of VOCs into the atmosphere, the significance of indoor VOC pollution should not be overlooked. Most people spend 80-90 % of their time in enclosed structures such as office buildings, schools, shopping malls and homes, and the indoor levels of VOCs are often higher than in the outdoor air (ENDS, May 1996). VOCs are present in many common materials and products, such as construction materials, furnishings, consumer products and pesticides. A large number of VOCs, including several carcinogenic compounds, have been identified in indoor air and some examples are shown in Table 1.4 (Sterling, 1985). Principal sources of the aliphatic hydrocarbons are cooking and heating fuels, aerosol propellants such as propane and butane and cleaning compounds, glues and thinning solvents such as hexane. Halogenated VOCs, such as methyl chloroform and methylene chloride, are widely used as degreasing, dewaxing and dry cleaning solvents, and in home products. Alcohols, such as ethanol and methanol, come from window cleaners, paints, paint thinners, cosmetics and adhesives. New types of building material (e.g. pressed board) and some forms of cavity wall insulation (and chipboard and other wood products made with urea-formaldehyde resins) can also emit formaldehyde and affect indoor air quality under certain circumstances (ENDS, May 1996).

Table 1.4 Examples of indoor VOCs and potential sources

Pollutant class	Example	Indoor sources
Aliphatic hydrocarbon (HC)	Propane, butane, hexane, limonene	Cooking and heating fuels, aerosol propellants, cleaning compounds, refrigerants, lubricants, flavouring agents, perfume base
Halogenated HC	Methyl chloroform, methylene chloride, PCBs	Aerosol propellants, fumigants pesticides, refrigerants, degreasing, dewaxing and dry cleaning solvents
Aromatic HC	Benzene, toluene, xylenes	Paints, varnishes, glues, enamels, lacquers, cleaners
Alcohols	Ethanol, methanol	Window cleaners, paints, thinners, cosmetics, adhesives, human breath
Ketones	Acetone	Lacquers, varnishes, polish removers, adhesives
Aldehydes	Formaldehyde, nonanal	Fungicides, germicides, disinfectants, artificial and permanent-press textiles, paper, particle boards, cosmetics, flavouring agents

The concerns regarding the concentrations of VOCs in the polluted atmosphere include the following :

- some VOCs are known to be toxic or carcinogenic.

- most of them contribute, in varying degree, to the formation of ground level (or tropospheric) ozone.

- some of them contribute to the problem of ozone depletion in the upper atmosphere (or stratosphere).

- some of them are powerful infrared absorbers, and thus contribute to the greenhouse effect or global warming.

Some VOCs may cause eye and skin irritation, drowsiness, coughing and sneezing, nausea and headaches, and damage to the liver and kidneys, whereas others such as benzene and 1,3-butadiene are also carcinogenic. Benzene is classified as a genotoxic carcinogen, which means it directly affects the genetic material of the cell (the DNA), causing leukaemia in workers exposed to high concentrations well over the air quality standard of 5 parts per billion (annual average) recommended by the UK Expert Panel on Air Quality Standards. The Panel is considering a longer term target of 1 ppb rolling annual average (Harrison, 1996). A study of 748 workers in the rubber industry who were exposed to benzene over ten years showed that this group of people were 5.6 times more likely to have low white blood cell counts and develop leukaemia than the general population. According to WHO and US EPA, 0.3 ppb (1 μg/m3) produces an estimated lifetime risk of leukaemia of 4-8 per million, with the risk being proportional to the concentration. Estimates of the number of people who may develop leukaemia in the Los Angeles basin as a result of exposure to benzene are put at 100-780 per million people exposed (Elsom, 1996). Benzene occurs naturally in crude oil and is also formed during the upgrading of fuel oil. The dominant emissions of benzene in urban atmospheres are from petrol exhaust and by evaporation of petrol from fuel tanks and during refuelling. In unleaded fuel, aromatic hydrocarbons (as well as

alkenes) replace lead as the means of raising the octane level. This results in higher exhaust emissions of benzene (and butadiene from alkenes) if vehicles without catalytic converters are fuelled with unleaded petrol. In the European Union, the benzene content of petrol is limited to 5 % by volume, although fuels typically contain about 2-4 % in most European countries. Diesel accounts for only a relatively small proportion of benzene emissions (about 9 % in the UK in 1991). People inside vehicles in a slow-moving stream of traffic may be exposed to concentrations of benzene two or three times higher than those experienced by pedestrians walking alongside the road, due both to leaks into the interior from the vehicle's own exhaust system, and to emissions from the exhausts of the cars in front. A few researchers have suggested that the higher rates of leukaemia among children in the suburbs and commuter villages could be linked to benzene exposure during prolonged car journeys (Elsom, 1996).

1,3-Butadiene has been shown to cause cancer in animals. There is also evidence that workers in the synthetic rubber industry, exposed to high concentrations of this compound, have had a slightly higher than expected risk of contracting cancers of the lymphoid system and bone marrow, lymphomas and leukaemia. The Expert Panel on Air Quality Standards has set a recommended standard for 1,3-butadiene of 1 part per billion rolling annual average (Harrison, 1996).

Aldehydes are widely used in industry and have been evaluated as to their environmental and health effects. Some aldehydes may irritate the skin or eyes. Formaldehyde, a common indoor pollutant, has been widely studied and though not yet demonstrated to be a human carcinogen, has been shown to cause cancer in rats (ENDS, May 1996). Aldehydes are present in vehicle exhaust fumes and the concentration of aldehydes in urban air has been increasing in recent years. This is thought to be due to the inefficient operation of catalytic converters under certain circumstances. Other toxic VOCs such as 1,2,4-trimethylbenzene (emitted from printworks) are potential lung cancer-inducing agents.

The second cause of concern regarding VOCs is their role as precursors in the formation of tropospheric ozone. In order to form ozone, two other components are required, *viz.*, nitrogen oxides (NO_x) and ultraviolet ($h\nu$) radiation. NO_x formation is related to the combustion of fossil fuels (e.g. power generation, petroleum refining, vehicles) and ultraviolet radiation is supplied by the sun. The photochemical oxidation reactions involved are simplified as follows (Harrison, 1996) :

$$NO_2 + h\nu \xrightarrow{J} NO + O(^3P) \qquad (\lambda < 430 \text{ nm}) \qquad (1.1)$$

where J is the photodissociation rate constant of NO_2. The oxygen atom then combines with an oxygen molecule to produce ozone, O_3 :

$$O(^3P) + O_2 + M \longrightarrow O_3 + M \qquad (1.2)$$

where M is an unreactive molecule such as nitrogen. Normally the ozone formed is short-lived as it reacts again with NO to return to the original starting point:

$$NO + O_3 \xrightarrow{r} NO_2 + O_2 \qquad (1.3)$$

where r is the rate coefficient of the reaction between NO and ozone. All three reactions are rapid and an equilibrium is reached when the rate of ozone formation (which is equal to the rate of NO_2 photolysis if all $O(^3P)$ leads to O_3 formation) equals the rate of O_3 removal, i.e. $J[NO_2] = r[O_3][NO]$. Thus,

$$[O_3] = \frac{J[NO_2]}{r[NO]} \qquad (1.4)$$

However, VOCs interfere with this removal mechanism; together with sunlight they create competing radicals (e.g. HO_2, RO_2) which convert NO to NO_2 (without using up O_3), thereby increasing the ratio $[NO_2]/[NO]$, and hence increasing the concentration of ozone. The potential of VOCs to create ozone varies with each compound and they are classified according to their "photochemical ozone creation potential" (POCP). Table 1.5 shows the POCPs for a number of chemical classes (Marlowe, 1992). The VOCs

with high photochemical reactivity usually contain double bonds such as the alkenes and the aromatics. The POCPs of some typical members of each VOC class are shown in Appendix I).

Table 1.5 Examples of photochemical ozone creation potential (POCP) values

Compound	Average POCP
Alkenes	84
Aromatics	76
Aldehydes	44
Alkanes	42
Ketones	41
Esters	22
Alcohols	20
Chlorinated Hydrocarbons	2

Ozone is a secondary pollutant and constitutes 90 % of the total products of the photochemical reactions. Other secondary pollutants created include peroxyacetyl nitrate (PAN), hydrogen peroxide and nitric acid. The photochemical reactions also create fine particulates which give photochemical smog a hazy appearance. Ozone concentrations near the ground can be raised to levels considered dangerous to human health. Being an irritant to the respiratory system, ozone can produce asthma-like symptoms. The UK Expert Panel on Air Quality Standards has recommended an ambient air quality standard of 50 ppb as an eight-hour average maximum exposure. In addition to these environmental effects, ozone is also known to be responsible for damaging plants, particularly growing crops and beech trees, and for damaging building materials such as rubber and painted surfaces. The Department of the Environment estimates the annual cost of the damage to building material as ranging from £170 to £354 million.

Stratospheric ozone is formed at altitudes between 12 and 40 km, in a region known as the ozone layer, by sunlight splitting oxygen molecules into oxygen atoms which then combine to form ozone. Stratospheric ozone is being depleted by chlorine-containing VOCs such as CFCs, carbon tetrachloride and methyl chloroform, which are stable enough to survive removal processes in the troposphere (~0-14 km). The photolytic decomposition of these compounds in the stratosphere leads to the initiation of ozone-destructive chain-reactions :

$$Cl^{\bullet} + O_3 \rightarrow ClO^{\bullet} + O_2 \qquad (1.5)$$

$$ClO^{\bullet} + O \rightarrow Cl^{\bullet} + O_2 \qquad (1.6)$$

The depletion is accentuated at the cold poles, especially in Antarctica during springtime, where it has created what is popularly referred to as the 'ozone hole'. Stratospheric ozone plays a vital part in protecting people, plants and animals, by absorbing harmful ultraviolet radiation from the sun which would otherwise increase skin cancer, cause cataracts, damage crops and kill phytoplankton. Another benefit of the ozone layer is that it is warmed during the process of absorption of ultraviolet radiation and forms a thermal lid to the atmosphere. This lid traps virtually all atmospheric moisture below it, so enabling cloud and precipitation processes to operate, which in turn sustain life on the earth. Some stratospheric ozone diffuses down into the lower atmosphere, producing a naturally occurring background concentration of ozone of about 10-15 % of the tropospheric total. Occasionally, brief intrusions of stratospheric air, rich in ozone, can plunge toward the surface, temporarily increasing surface concentrations. This usually happens during disturbed weather conditions such as those associated with the passing of a cold front, when urban-generated levels of ozone are not particularly high anyway. The depletion of ozone levels in the upper atmosphere will allow increased levels of ultraviolet radiation and this will speed up the rate of photochemical reactions which produce ozone in the lower atmosphere and so worsen air quality.

Almost all the VOCs emitted as a result of human activities are emitted into the atmospheric boundary layer, the shallow region of the troposphere next to the earth's surface, whose depth varies between typically a few hundred metres in winter to perhaps 2 km at the height of summer. Many of the more reactive VOCs are quickly oxidised in the atmospheric boundary layer. However, some survive and are transported into the free troposphere above the boundary layer during particular meteorological events such as the passage of fronts. Some of these compounds may absorb infrared radiation (wavelengths > 4 μm) emitted from the surface of the earth; they are termed radiatively active gases and may contribute to global warming. They trap much of the earth's outgoing radiative energy, thereby heating the atmosphere and subsequently radiating this energy back to the earth and out to space. These greenhouse gases act like a thermal blanket around the globe, raising its temperature. The relative impacts of the gases per unit mass are expressed in terms of Global Warming Potentials (GWP). These are estimates of the radiative forcing per kilogram of substance relative to the effect of 1 kg of carbon dioxide (Harrison, 1996). Table 1.6 shows the GWP of some VOCs (AEA Technology, 1993). Methane and the halogenated VOCs are the most significant greenhouse gases and have relatively long atmospheric lifetimes.

Table 1.6 Example GWP of VOCs

Compound	Emission (kt/a)	GWP	Atmospheric lifetime (days)
Methane	5000	17	3780
Other alkanes	220	1.2-2.9	4-116
Aromatics	195	1.6	0.6-25
Acetates	35	-	-
Halocarbons	79	166-4329	5-2410
Ketones	93	-	2-137
Alcohols	13	-	2-33

Those long lived VOCs which are not classed as radiatively active gases may perturb the concentration of gases which are radiatively active in the free troposphere by taking part in the reactions which produce a net increase in ozone concentration. Ozone levels

in this region are believed to be rising steadily and this is of some concern because ozone is also an important greenhouse gas and an increase in its concentration will contribute to global warming (Harrison, 1996).

Due to concern regarding these adverse environmental effects of VOCs, legislation has been drafted throughout the developed world to control emissions. In the UK, considerable progress has been made in recent years in reducing VOC emissions from a number of sources, in particular from vehicle exhausts. The main driving forces behind this progress have been the United Nations Economic Commission for Europe (UNECE) Convention on Long Range Transboundary Air Pollution (the LRTAP Convention) and the Environmental Protection Act 1990 (EPA 90). Under the terms of the 1991 VOC (Geneva) Protocol of the UNECE Convention, the UK (and other signatories) are committed to a reduction of 30 % in total annual emissions of VOC by 1999 from a 1988 base. A number of measures have already been taken to ensure that the UK meets this commitment. Of these, the most significant are the EC Directives relating to petrol and petrol-engined vehicles. These include:

- 91/441/EC which (from 1.1.93) requires all new petrol cars to meet strict emission limits, effectively requiring the fitting of catalytic converters and carbon canisters.

- 93/59/EC which (from 1.10.94) applies stricter emissions standards to all new light vans, off-road vehicles and heavy cars up to 3.5 tonnes.

- 67/584/EC and 87/416/EC which control the benzene and butadiene content of petrol.

- 94/63/EC (Stage I) which (from 31.12.94) controls VOC emissions resulting from the storage of petrol and its distribution from terminals to service stations (ENDS, Jan 1997).

Further EC measures include tighter emission limits on diesel vehicles, the Stage II Directive which controls VOC emissions during the refuelling of petrol-engined vehicles (ENDS, Mar 1997), and a proposal to set VOC emission limits on industrial

processes that use large amounts of solvents (e.g. printing, surface cleaning and painting) (AEA Technology, 1993).

In the UK, VOC emissions into the atmosphere are controlled under Part I of the EPA 90, through Integrated Pollution Control (IPC) or Local Authority Air Pollution Control (LAAPC). Because of the detailed requirements applicable to individual processes, the emission limits and recommended control technologies are given in official guidance notes. The Process Guidance Notes applicable to solvent-using industries under local authority control are in the PG 6 series (Appendix II). The emission limits laid down in these guidance notes were set with the aim of achieving a 30 % reduction in VOC emissions between 1988 and the year 1999, i.e. the Europe-wide target agreed under the UNECE VOC protocol. The guidance notes are flexible and are constantly being changed to meet tighter controls.

Under the EPA 90, the emission limits set for VOCs are based on the VOC type, the process emitting the VOC, and the abatement technique. Processes are classified into Part A and Part B depending on the process throughput, process type and types of emissions released. Under Part A processes, solvents are separated into Class A or Class B, depending on their potential to cause environmental damage. Examples of Class A and Class B VOCs are shown in Table 1.7, together with their emission standards. For the most damaging VOCs the limits are even tighter, and are given for the individual VOC (Table 1.7).

Table 1.7 Example solvents under Part A processes

Class	Solvent	UK guideline (mg/m^3)
A	Acetaldehyde, acrylic acid, benzyl chloride, methylene chloride, carbon tetrachloride, chlorofluorocarbons, ethyl acrylate, halons, maleic anhydride, 1,1,1-trichloroethane, trichloroethylene, trichlorotoluene	20 • mass release limit of 100 g/hr is exceeded
B	Toluene, acetone, methanol, ethanol, propylene, ethyl acetate, isopropyl alcohol, tetrahydrofuran	80 • expressed as toluene • where the mass release limit of 5 tonnes/year or 2 kg/hr (whichever is greater) is exceeded
More damaging type	Benzene	5
	Amines	10
	Formaldehyde	5
	Total phenols, cresols and xylols	10
	Triethylamine	2

Part B processes have a range of limits and these are given in the guidance notes for the specific process. However, for a vast majority of processes the limit is 50 mg/m^3 (expressed as total carbon). For all of the concentration limits stated above, the introduction of dilution air to achieve emission concentration limits is not permitted. The other important criterion for the VOC emission is that it must be free of offensive odour outside the process boundary. This can have particular implications for processes using odorous VOCs such as aldehydes and ketones.

Both national and Europe-wide measures for tighter regulation of VOC emissions, and a public information campaign designed to reduce domestic emissions should ensure that the UK meets its UNECE 30 % VOC reduction commitments by 1999. Current estimates suggest that the UK will fulfil its international commitments by achieving a reduction of some 35 % in total annual emissions of VOCs by 1999 (from the 1988 level) which is well inside the 30 % target (Environmental Management, 1995).

Following the introduction of such regulations, with their accompanying economic implications, the technologies for the control of VOC emissions have acquired an increased importance. The various options for treating the VOC emissions will now be discussed.

1.2 VOC Abatement Technologies

Emissions of VOCs can be controlled by one or both of the following:

- the addition of end-of-pipe control technologies to clean up effluent streams; this category can be subdivided into those methods which destroy VOCs and those methods which recover VOCs.

- minimisation of waste at the source by strategic process design such as substitution of raw materials to reduce VOC input to the process, changes in operating conditions and the modification of equipment to minimise the formation of VOC pollutants.

The project described in the thesis is concerned with the first method, with the intention to recover the VOCs. There are twelve existing and emerging end of pipe VOC abatement technologies, as discussed by several authors (AEA Technology, 1993, EPA 90 Technical Guidance Note, 1994 and Mukhopadhyay and Moretti, 1993). Seven are standard technology: adsorbers, thermal oxidisers, catalytic oxidisers, flares, boilers/process heaters, absorbers and condensers. Three are relatively recent technologies: biofilters, membrane separators and ultraviolet oxidisers. Two technologies are still under development: corona destruction reactors and plasma technology devices. The major VOC emissions control techniques are briefly discussed below, and some of their essential features are compared in Table 1.8 (Ruddy and Carroll, 1993).

1.2.1 Thermal Oxidation (Incineration)

This is a process in which VOCs are combusted to form carbon dioxide and water at high temperatures by either direct flame incineration or by passing the preheated gas stream through a catalyst bed. The catalyst is generally a precious metal, a transition metal or a zeolite (Dowd et. al., 1992). The VOC-laden air is captured by an air handling system, preheated, thoroughly mixed, and transported to the treatment system via a system of ducts and fans. With suitable temperatures and residence times, direct flame incineration can provide greater than 99 % removal of most of the compounds. Catalytic systems generally have lower removal efficiencies - between 90 and 95 % (Ruddy and Carroll, 1993). Catalytic systems also operate at lower temperatures and require less auxiliary fuel. Incineration systems operate at very low residence times (of the order of seconds). Thermal oxidation will require supplementary fuel to support combustion if the calorific value of the waste stream is low and therefore it cannot release enough heat to maintain autothermal firing conditions. Thermal oxidisers also produce NO_x. Catalytic systems can be expensive due to the cost of catalyst and heat recovery systems. Although an effective technique, there is a need to consider how an incineration device will operate safely when organic concentrations are near the explosive range. The lower explosive limit (LEL) is typically in the range 1 % to 3 % for organics. The operation and efficiency of incinerators are very sensitive to fluctuations in flowrate and VOC concentration. These issues usually imply that additional instrumentation is needed. When chlorinated organics are burnt, a caustic scrubber is required to neutralise acid gases that would be formed and a final waste treatment system would mean additional capital and operating costs. As it is a destructive technique, incineration provides no option for future recovery or reuse of solvents.

1.2.2 Condensation

VOCs can be removed and recovered by condensation processes utilising liquid cryogens, typically liquid nitrogen in either a direct or an indirect contact process. The driving force for condensation is over-saturation, which is achieved by chilling or pressurisation (or both). Condensation is most efficient for VOCs with boiling points above 38°C at relatively high concentrations, i.e. above 5000 ppm (Ruddy and Carroll, 1993), and can recover up to 99 % of the compounds. However, capital costs are high and after treatment would be required to remove condensed water and possibly to separate a mixture of volatiles. Low boiling VOCs can require extensive cooling or pressurisation, which sharply increases the operating cost. Furthermore, the formation of clathrates or hydrates and the freezing of vapours is a concern in condensation systems (Spencer, 1992).

1.2.3 Absorption

The absorption of gases in liquids is a well established technology, suitable for compounds with a favourable distribution coefficient. However, a suitable, inexpensive absorbent may not be available for every compound. The compounds transferred to the liquid phase must also be recovered before the absorbent can be reused, making an after treatment system a necessity.

1.2.4 Chemical Oxidation

Organics in dilute air streams can be easily oxidised in an extremely fast energy efficient gas-solid photocatalytic oxidation process. Chemical oxidation is provided solely by photo-excitation over a solid catalyst by near ultraviolet light. The catalyst is generally a semiconducting oxide such as titania. Complete oxidation of a number of organics including acetone, benzene and trichloroethylene has been reported by Raupp et. al. (1992). The oxidation is hypothesised to proceed through a surface mediated, hydroxyl radical initiated, chain reaction. The highly involved mechanism has a

complex dependence on water vapour concentration. Chemical oxidation is a promising new technology. However, it suffers from the disadvantages associated with any solid catalyst system including catalyst poisoning and attrition losses. Also, the distribution of ultraviolet light must be studied in detail for large systems before they can become practical.

Table 1.8 VOC control technologies (Ruddy and Carroll, 1993)

Control technology	Thermal oxidation	Catalytic oxidation	Condensation	Carbon adsorption	Absorption
Concentration range (ppm)	100-2,000	100-2,000	> 5,000	20-5,000	500-5,000
Capacity range (m^3/min)	28-14160	28-2830	3-570	3-1700	57-2830
Removal efficiency	95-99 + %	90-95 %	50-90 %	90-98 %	95-98 %
Capital costs (£ per m^3/min)	Recup; 210- 4200 Regen; 620-9300	Fixed; 410-5200 Fluid; 730-4600	210-1700	310-2500	310-1500
Annual operating cost (£ per m^3/min)	Recup; 310-1900 Regen; 420-3100	Fixed; 210-1600 Fluid; 310-1900	420-2500	210-730	520-2500
Secondary wastes	Combustion products	Combustion products	Condensate	Spent carbon; collected organic	Wastewater; captured particulate
Advantages	Up to 95 % energy recovery is possible.	Up to 70 % energy recovery is possible.	Product recovery can offset annual operating costs.	Product recovery can offset annual operating costs. Can be used as a concentrator in conjunction with another type of control device. Works well with cyclic processes.	Product recovery can offset annual operating costs.
Limitations	Halogenated compounds may require additional control equipment downstream. Not recommended for batch operations.	Thermal efficiency suffers with swings in operating conditions. Halogenated compounds may require additional control equipment downstream. Certain compounds can poison the catalyst (lead, arsenic, phosphorus, chlorine, sulphur, particulate matter).	Not recommended for materials with boiling points > 38°C. Condensers are subject to scale build-up, which can cause fouling.	Not recommended for streams with relative humidity > 50 %. Ketones, aldehydes and esters clog the pores of the carbon, decreasing efficiency.	Might require exotic scrubbing media. Design could be difficult in the event of lack of equilibrium data. Packing is subject to plugging and fouling if particulates are in the gas stream. Scale formation from absorbent/absorber interaction can occur.

1.2.5 Membrane Separation

Membrane separation systems can be used for a wide range of organic vapours. They are ideally suited for concentrated low volume single-compound streams where the recovery of the compound is highly desirable. The success of a membrane process depends upon the availability of a high selectivity membrane which can be formed into a high flux, low cost module (Baker et. al., 1992). Membrane separations have limited utility in the case of high volume, low pressure atmospheric emissions containing multiple compounds at low concentrations and pressure, because of the low driving force for separation and the after treatment of the separated mixture.

1.2.6 Biofiltration

Microbial oxidation is based on the ability of many micro-organisms (bacterial, moulds and yeasts) to degrade a number of compounds (Visscher and Brinkman, 1989). Part of the compound (substrate) is oxidised to products such as carbon dioxide and water and the remaining part is transformed into new cell material (cell synthesis). The degree of oxidation is dependent upon the solubility of the VOC in the inlet stream as the oxidation occurs in or on the surface of the water phase. Some long chain VOCs are difficult to treat by biofiltration due to their chemical robustness. The long contact time required between the VOC and the liquid phase for complete oxidation means that large areas are required for biodegradation. However, the technique is relatively cheap, reliable, and kind to the environment if the VOCs are easily oxidised. It can handle chemically different compounds and does not require after-treatment.

1.2.7 Adsorption

One of the most effective techniques for controlling emissions of VOCs, and also one of the most economical, is adsorption, usually using activated carbon as the adsorbent. This process is cost-effective as it is typically able to recover many VOCs for reuse. A particularly common application of carbon adsorption for VOCs control is solvent recovery. In general, solvent recovery using adsorption is a logical consideration for any industrial process exhausting considerable quantities of valuable solvent. The most commonly recovered solvents include toluene, heptane, hexane, carbon tetrachloride, acetone, ethyl acetate, methyl ethyl ketone (MEK), naphthalene and methylene chloride. Many other solvents are also suitable for recovery by adsorption. The adsorption of VOCs using molecular sieve zeolites, particularly the high silica zeolites, is gaining wider popularity, (Crittenden, 1994, Blocki, 1991 and Hairston, 1996) and will be discussed in detail in a later part of the chapter.

A broad range of zeolitic adsorbents of different pore sizes and relatively high selectivities is available for the adsorption of VOCs of various molecular weights and functionalities (Hairston, 1996). Flowrates varying from 3 to 1700 cm^3/min and VOC concentrations of 20 to 5,000 ppm can be used on activated carbon adsorbers (Ruddy and Carroll, 1993). The adsorbers can easily handle VOC concentrations in excess of the 25 % lower explosive limit (LEL) threshold. The adsorption system is sized according to the maximum expected flow and concentration and anything less usually improves efficiency. Adsorption systems are flexible and comparatively simple to design. They are inexpensive to operate and the installation costs are often lower than those of the other VOCs control systems (Table 1.8). In most cases the annual operating costs are offset by recovery of the product. Regeneration of spent adsorbent can be performed with steam, hot air or hot nitrogen. An advantage of nitrogen regeneration is that it provides an inert atmosphere for operation under otherwise potentially explosive conditions.

1.3 Adsorption Techniques

Figure 1.3 illustrates a typical commercial solvent recovery plant, where the VOC laden air passes through a column containing a bed of adsorbent. The VOC is adsorbed onto the adsorbent surface and clean air is exhausted to the atmosphere. To recover the solvent for reuse, it must be released from the adsorbent surface. This is most commonly done by heating the carbon with steam. The mixture of steam and solvent is condensed by cooling and then separated, in the simplest case by gravity decanting. If the solvent is soluble in water, distillation is required instead of decanting. The adsorbent can then be reused.

The batch process of adsorption and desorption as described above can be made continuous by the use of multiple beds where one is off-line for desorption while the others are adsorbing (Figure 1.3).

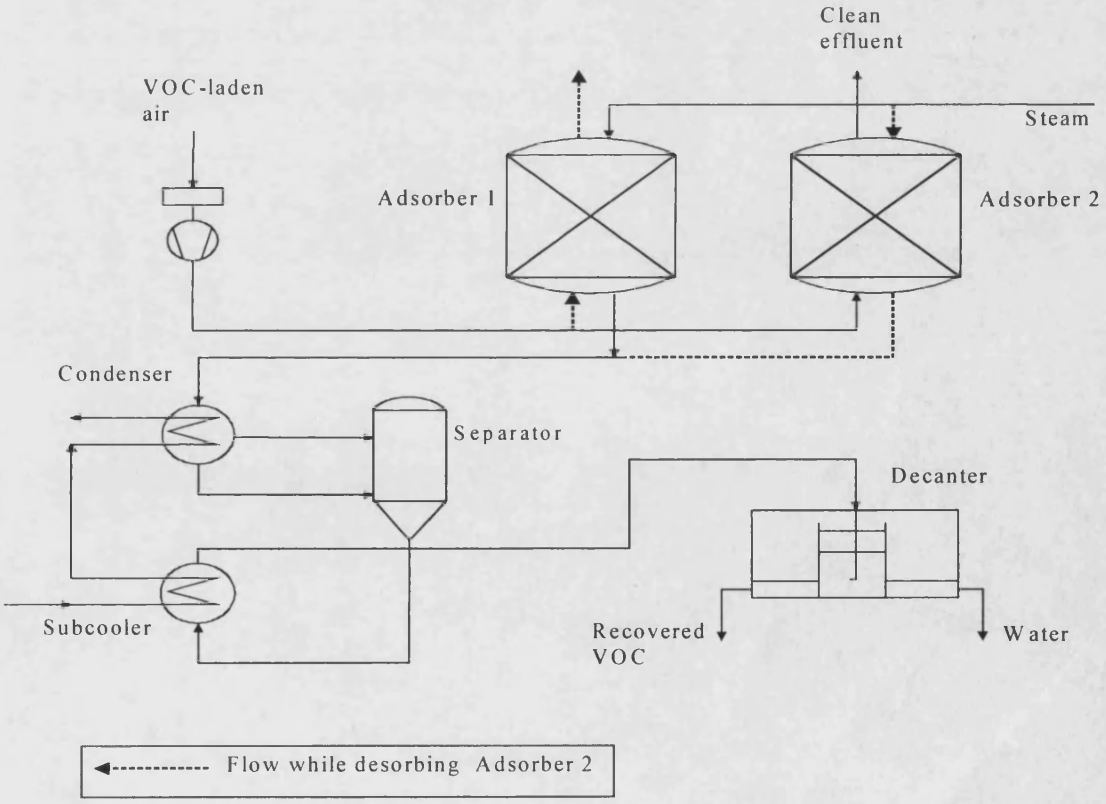

Figure 1.3 A typical solvent recovery plant

1.3.1 Principles of adsorption

Adsorption is the process by which residual molecular forces at the surface of solids (i.e. the adsorbent) attract molecules of gases and vapours (i.e. the adsorbates). In the case of air pollution control the relevant adsorbates are the VOC pollutants which have to be separated from an inert gas stream emitted into the atmosphere. Adsorption therefore is a useful means of concentrating the pollutants, thereby facilitating their disposal or recovery. Adsorption of gas molecules occurs at active sites on the solid surface which is described as homogeneous when all active sites contain the same energy potential. With different energy potentials the sites are known to be heterogeneous. The adsorbed phase consists of a thin gaseous layer which includes the adsorbate and a thin solid layer containing the active sites.

1.3.1.1 Adsorption Equilibria

In practice, adsorption capacity data are most often presented at given fixed temperatures using plots known as isotherms. An isotherm is a graph showing the loading of the adsorbate on the adsorbent as a function of the adsorbate concentration in the feed at the given temperature. Figure 1.4 shows the types of isotherms, as classified by Brunauer (Ruthven, 1984). Type I is concave downward and is referred to as a favourable isotherm, representing an adsorbent-adsorbate system in which the adsorbent pore size is not much greater than the adsorbate molecular diameter. Type II is known as an unfavourable isotherm. Adsorption systems having favourable isotherms produce breakthrough curves that are self-sharpening, whereas the breakthrough curves produced by unfavourable isotherms are known as proportionate. Types III, IV and V have alternating convex and concave regions. Types II and III are common for adsorbents with a wide range of pore sizes, where a continuously increasing loading occurs from monolayer to multilayer adsorption, and then to capillary condensation. The Type V isotherm is typical of a system with significant intermolecular attraction effects. Type IV is characteristic of a system having pores much wider than the adsorbate molecular diameter and the formation of two adsorption layers either on a plane surface or on the walls of the pore. Types IV and V may exhibit hysteresis, which occurs when desorption

takes place along a different isotherm from that for adsorption, usually as a result of liquid filling pores in a certain way that is not followed when they are emptied. Detailed discussions of the models for adsorption isotherms have been given by Ruthven, 1984, Yang, 1987 and Tien, 1994. Models include Langmuir, Freundlich, Brunauer-Emmett-Teller (BET), Polanyi, and Vacancy Solution Theory. Other principles of adsorption described in the standard works are forces of adsorption, adsorbent surface polarity, distribution and classification of pore sizes, different mechanisms of adsorption, adsorbent physical strength and different types of adsorbent materials.

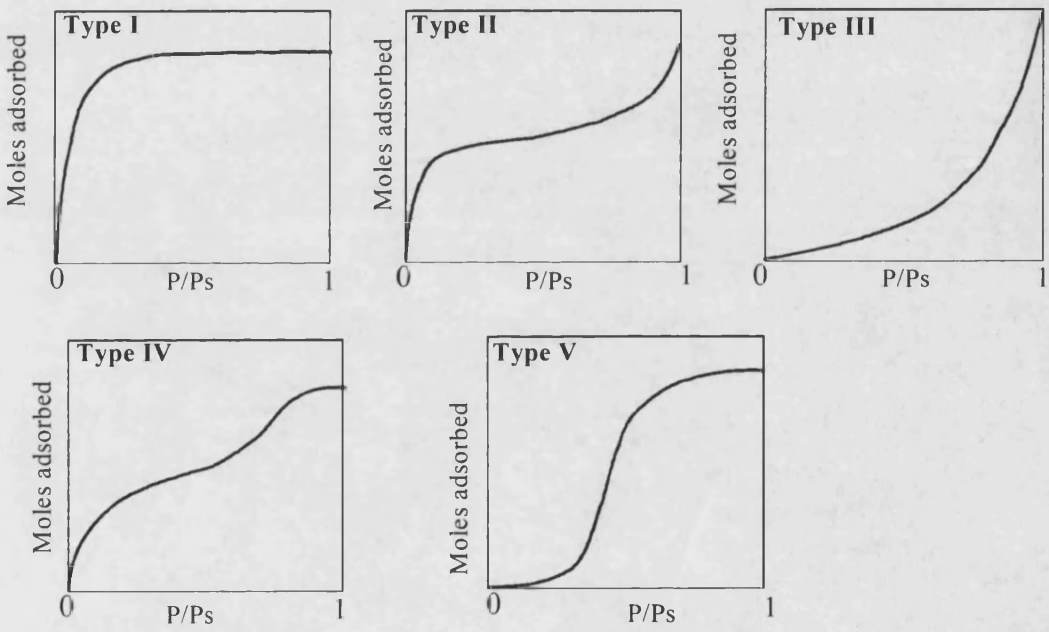

Figure 1.4 The Brunauer classification of isotherms

1.3.1.2 Adsorption Kinetics

The overall rate of adsorption for a porous adsorbent is usually controlled by mass and/or heat transfer resistances. Mass transfer kinetics is important as it controls the cycle time (or the depth) of a packed bed adsorption process. With fast kinetics, a plot of effluent concentration *vs.* time will remain level until the adsorbent is almost saturated and will then rise sharply. Such a plot, i.e. a sharp breakthrough curve, is desirable in practice. On the other hand, where poor kinetics cause the effluent concentration to begin varying soon after the start of the adsorption run, a distended breakthrough curve is produced. The rate of adsorption is a function of the concentration of the adsorbate in the bulk gas stream, the surface area of the adsorbent, the pore volume of the adsorbent and other properties of the adsorbent and adsorbate. Most commercial adsorbents consist of small microporous crystals formed into a macroporous pellet with a binder. Hence, two distinct diffusional resistances, i.e. microporous and macroporous, can arise. Table 1.9 shows the definitions of the pore sizes (Sing et. al., 1985). Since adsorption is carried out from the fluid phase, transport through the fluid boundary layer surrounding the particle leads to an additional mass transfer resistance. The physical rate of adsorption at the adsorbed phase is usually sufficiently high that it can be assumed to be instantaneous. The mass transfer resistances associated with a porous adsorbent particle are shown schematically in Figure 1.5. The kinetics of mass transfer can be investigated experimentally by monitoring and analysing either the transient uptake curve during a batch study or the breakthrough curve of a packed column.

Table 1.9 Classification of pore sizes

Pore type	Pore width, d (nm)
Macropores	$d > 50$
Mesopores	$2 < d < 50$
Micropores	$d < 2$

As adsorption is an exothermic process, the heat released has to be transferred from the adsorbent particle to the fluid. In a packed column, the heat is carried out by the flowing fluid or is dissipated through the column wall. The heat of adsorption provides a measure of the energy required for regeneration, low values being desirable. Ruthven (1984) gives a detailed account of the heat and mass transfer processes which occur in adsorption beds. Much attention is given to the analysis and interpretation of transient uptake curves for batch systems and on the determination of the most significant heat and mass transfer resistances for different conditions.

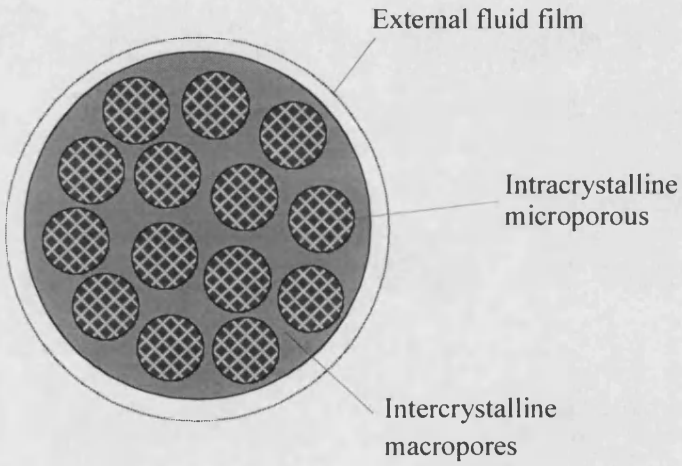

Figure 1.5 Idealised representation of mass transfer resistances in a composite adsorbent

1.4 Scope for Activated Carbon in VOC Adsorption

Although activated carbon is an effective adsorbent for the recovery of VOCs, its application has several drawbacks. Carbon attrition is one of the major problems associated with the adsorption system as its structure is relatively weak being manufactured by pyrolysis of organic material. Carbon is flammable and can promote fire when heated above 120°C. Because of this limitation, higher boiling VOCs (e.g. those with boiling points over 150°C) cannot be efficiently removed from exhausted carbon beds during the regeneration process (Blocki, 1991). Eventually, loss of bed capacity results in decreased performance and the bed has to be replaced. Carbon bed performance is sensitive to the moisture content of the gas stream being treated. As the relative humidity of the gas stream exceeds 50 %, the performance of the carbon decreases. Carbon adsorption is not recommended for VOC streams containing ketones. The carbonyl carbon can polymerise exothermically on the carbon surface (Ruddy and Carroll, 1993) resulting in bed fires. Impurities naturally occurring in carbon can act as catalysts and promote polymerisation or oxidisation of some solvents such as styrene, MEK and cyclohexane, resulting in by-products which cannot be desorbed or which might be hazardous. Activated carbon is not particularly selective and will adsorb most organic chemicals whether desirable or not. Its preference for higher molecular weight organic chemicals could lead to the premature breakthrough of lower molecular weight compounds from the bed. This could be a particular problem in controlling the emissions of VOCs of relatively low molecular weight.

Many of the disadvantages of carbon could be overcome if the adsorbent were hydrophobic and inorganic. It is the purpose of this research project to investigate the use of such an adsorbent in the control of VOC emissions. The next section of the thesis describes some inorganic adsorbents and their potential for use in environmental control.

1.5 Hydrophobic Zeolites

Zeolites are crystalline aluminosilicates with a framework based on an extensive three-dimensional network of oxygen ions. Situated within the tetrahedral sites formed by the oxygen there can be either a Si^{+4} or an Al^{+3} ion. The AlO_2^- tetrahedra in the structure determine the framework charge. This is balanced by cations that occupy the nonframework positions. The crystalline framework results in a precise uniformity of micropores which confers the ability to 'sieve' molecules.

The Si to Al ratio indicates the contribution of both atoms to a zeolite's framework. The ratio is never less than 1.0 but there are pentasil zeolites having a double five-ring unit such as silicalite which has a ratio towards infinity and ZSM-5 which has a ratio ranging from about 20 to 8000 (Olson et. al., 1981). The ratio has a strong influence over the adsorptive properties, with a systematic transition from the aluminium-rich zeolites, which have a strong affinity for water and other polar molecules, to silica-rich zeolites which are hydrophobic. In the absence of strong field gradients due to framework aluminium and exchangeable metal cations, silicalite exhibits a high degree of organophilic-hydrophobic character. It is capable of separating organic molecules out of water-bearing streams (Flanigen et. al., 1978). Therefore, it is potentially suitable for those VOC control applications where moisture is always present.

It is important to clarify the definition of hydrophobicity with respect to silicalite. Whilst it is electrically neutral, van der Waals forces are always present, their intensity correlating with the amount of attracted molecule if sufficiently close to the adsorbent surface. Strictly, heavier organic molecules are attracted more strongly than lighter ones. In aqueous solution, heavier organics are bound more strongly than water. Therefore the hydrophobicity should be interpreted in the sense that water is less strongly adsorbed than most organics.

Silicalite was first developed by the Union Carbide Corporation in 1977, while ZSM-5 was discovered by the Mobil Oil Company in 1972. The synthesis, crystal structure and properties of silicalite and ZSM-5 can be found in Flanigen et. al. (1978)

and Olson et. al. (1981), respectively. There are two type of silicalite, i.e. silicalite-1 and silicalite-2, which correspond structurally to ZSM-5 (orthorhombic) and ZSM-11 (tetragonal), respectively. The structure consists of a series of intersecting channels, straight and zigzag in silicalite-1 and straight only in silicalite-2. Both channels are defined by ten-oxygen rings resulting in an effective channel diameter of about 0.6 nm, unlike zeolites of the faujasite type which have twelve-oxygen rings. Therefore, at ambient temperature, silicalite can adsorb molecules as large as benzene with its kinetic diameter of 0.585 nm, but rejects larger molecules such as neopentane (Flanigen et. al., 1978). The unit cell of silicalite which contains 96 tetrahedral (SiO_2) units is shown schematically in Figures 1.6 and 1.7. The unit cell contains two straight channel sections (the central one plus one quarter of each of the four corner channels) and four zig-zag channels with four channel intersections as shown in Figures 1.6 and 1.7(i). The cross section of the straight channels is about 0.57-0.58 x 0.51-0.52 nm (elliptical) while the zig-zag channels have a nearly circular cross section of free diameter 0.54 nm. The length of the straight channel sections which is the cell constant, *b*, is equal to 1.98 nm while the other cell dimensions *a* and *c* are 2.006 nm and 1.336 nm respectively (*a*, *b*, and *c* are shown in Figures 1.7(ii) and (iii)). The three-dimensional framework density of silicalite is approximately 1.8 g/cm^3 and the specific micropore volume is about 0.19 cm^3/g. Its void fraction is about 33 % of the crystal volume and surface area is in the range of 390-450 m^2/g.

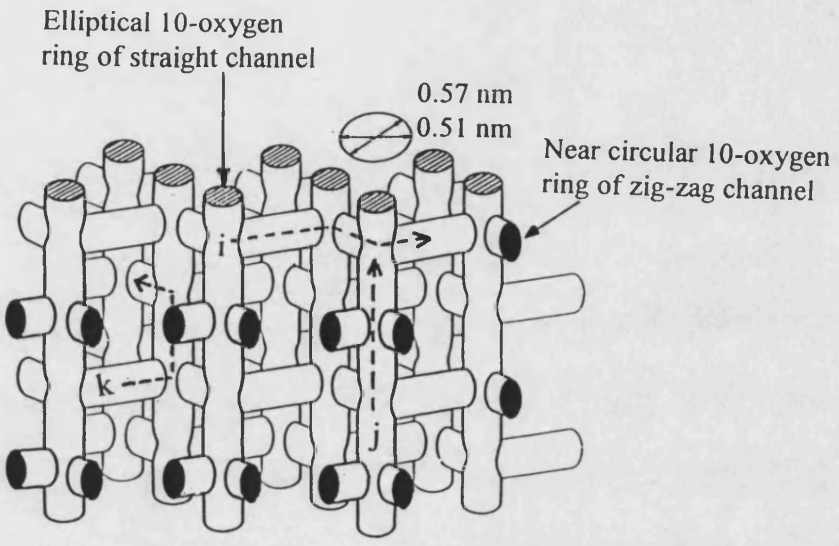

i : Zig-zag channel
j : Straight channel
k : Combination of i and j

Figure 1.6 Idealised internal structure of silicalite crystals determined from X-ray diffraction data

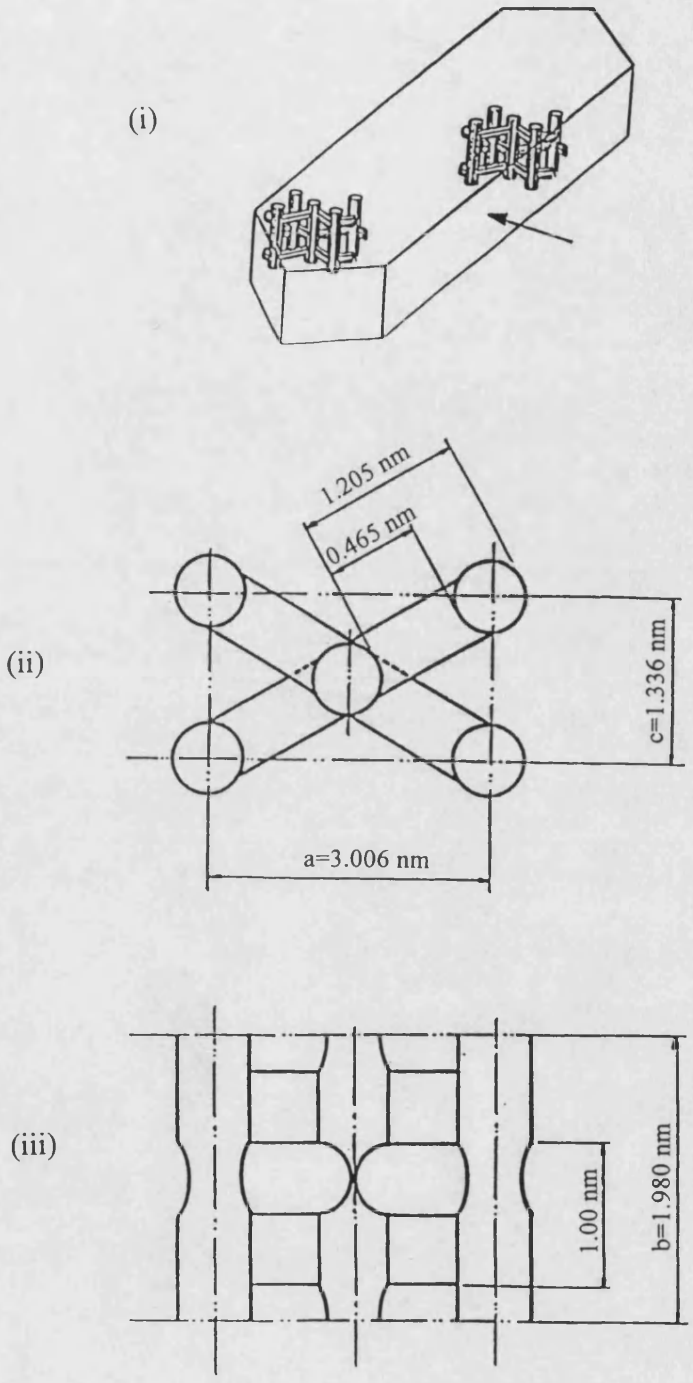

Figure 1.7 The channel system of silicalite/ZSM-5 showing (i) the orientation of the straight and zig-zag channels; (ii) a plan view looking at the top face of the crystal in (i); (iii) a view from the side face in the direction of the arrow in (i). Dimensions are shown in nm.

The fact that silicalite is completely inorganic and essentially hydrophobic means that it would not suffer many of the drawbacks of activated carbon described above when used in VOC control applications. The main disadvantage of silicalite is its relatively small pore size, which means that it would be suitable only for adsorbing organic molecules having kinetic diameters up to approximately 0.6 nm. The merits of the hydrophobic zeolite over activated carbon are discussed in the following section.

1.6 Hydrophobic Zeolites *vs.* Activated Carbon

Silicalite, composed entirely of inorganic oxides, is non-flammable and therefore will not contribute to a fire in a solvent laden atmosphere. Readily oxidising solvents such as ketones should not initiate a fire when adsorbed onto silicalite. By contrast, activated carbon has been demonstrated to catch fire when used to adsorb ketones from air under certain circumstances. Ketones react exothermically on the carbon in the presence of air and if the heat generated is not removed from the bed, the combustible adsorbent may catch fire. The exotherm and the ignition point of two activated carbons are shown in Figure 1.8 (Akubuiro and Wagner, 1992). The first peak (in Figure 1.8) represents the exothermic reaction, which is larger for type PCB carbon than for BPL carbon, which in turn is greater than JXC carbon. This order of reactivity confirms what was demonstrated in the literature (Akubuiro and Wagner, 1992). The second peak corresponds to the carbon ignition which starts at about the same point (500°C) for all three carbon adsorbents. Figure 1.9 shows the same test carried out on silicalite type MHSZ-773, T101 and T102 (UOP, 1992). The high silica zeolites reduce the exothermic reaction considerably in comparison with the activated carbon. As expected, these adsorbents are not ignited because of their inorganic oxide composition (Figure 1.9).

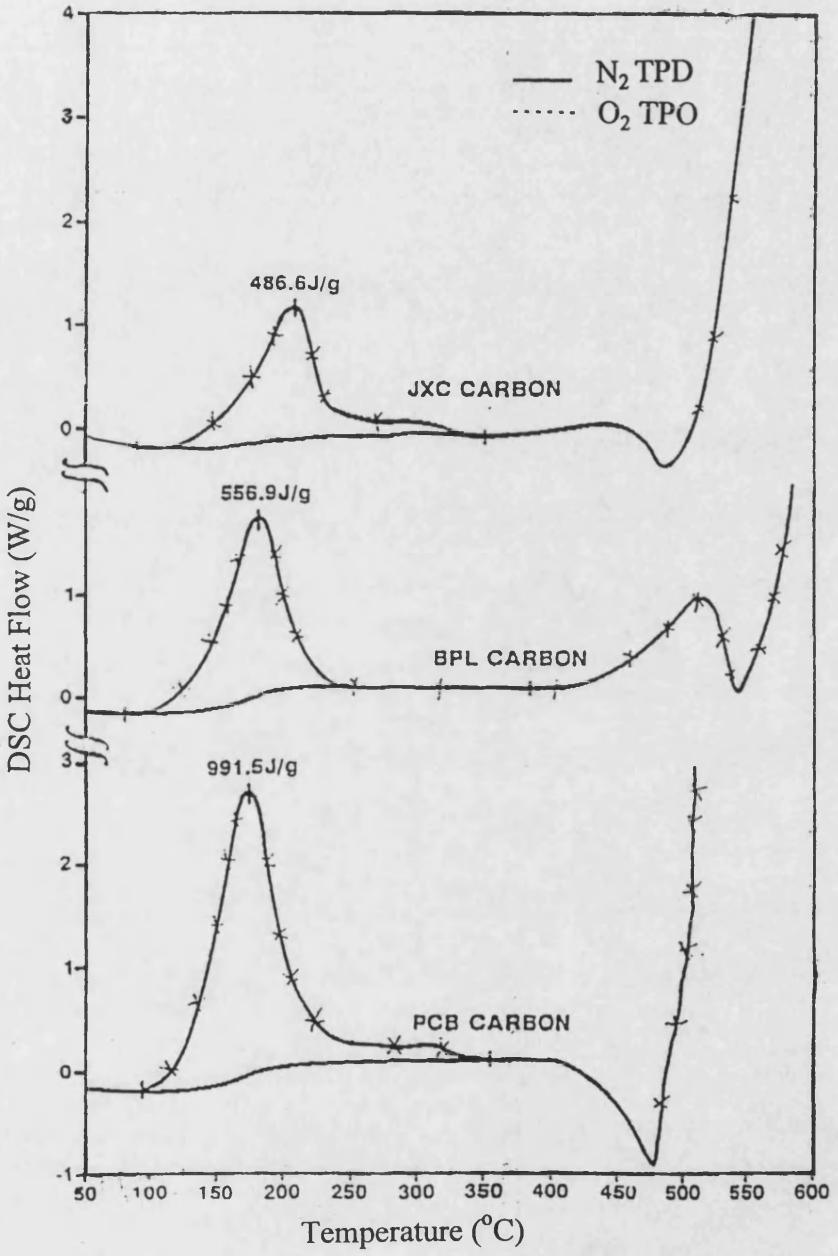

Figure 1.8 MEK on carbon DSC (UOP, 1992)

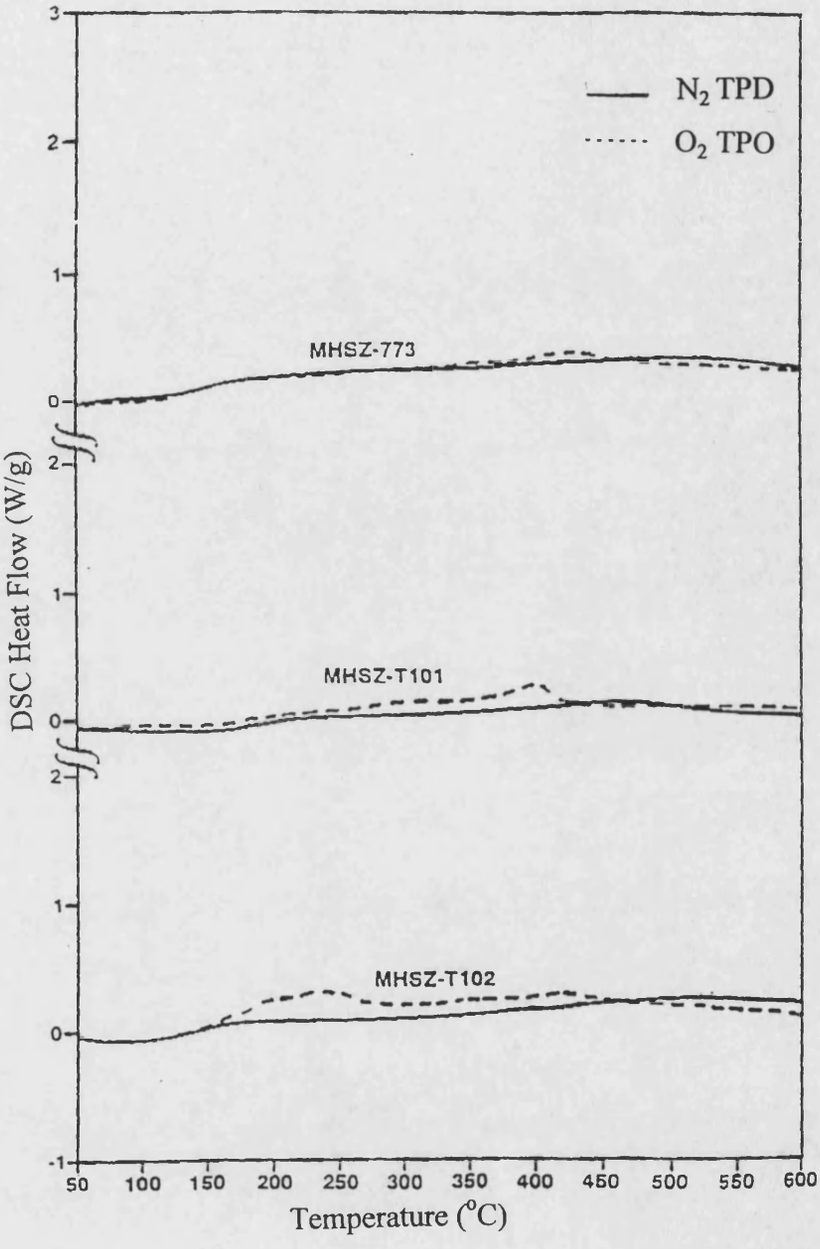

Figure 1.9 MEK on silicalite DSC (UOP, 1992)

Silicalite can withstand temperatures up to 1000°C in most gases, including air (Flanigen et. al., 1978). It is inert and remains chemically stable from a pH of 3 to 10 (UOP, 1992). It can therefore be regenerated at higher temperatures than activated carbon, effectively removing solvents boiling in excess of 175°C, thereby maximising its working capacity. Its thermal stability in an oxidising environment allows silicalite to be regenerated using high-temperature air without the risk of fire. Hot air regeneration avoids contamination of the condensate with steam and concentrates organic compounds for downstream recovery or disposal. It also enables the adsorbent to undergo controlled reactivation by burning off any remaining high-boiling compounds, tars, or carbonaceous materials which normal regeneration cannot remove. These advantages may enable the application of silicalite adsorptive treatment to a wider range of effluents.

Being essentially hydrophobic, silicalite has a low affinity for water and is selective due to its precise crystalline structures. Most VOCs have a kinetic diameter below 0.6 nm and thus would be capable of entering the zeolitic structure. Few molecules of a size greater than 0.6 nm pose an environmental threat through their volatility. Silicalite exhibits rectangular isotherms for organic compounds and this results in a sharper dynamic breakthrough curve than that exhibited by an activated carbon as shown in Figure 1.10 (UOP, 1992). This figure also shows that silicalite is less sensitive to humidity. Though carbon has a higher equilibrium loading, the breakthrough from activated carbon occurs earlier than from the silicalite bed. As shown in Figure 1.11 (UOP, 1992), silicalite has a greater adsorption capacity than activated carbon at low VOC concentrations. This supports the proposed usage of silicalite in environmental control, as most polluted streams consist of low levels of VOCs. The disadvantages of carbon, and the advantages of high silica zeolites in VOC adsorption are summarised in Table 1.10.

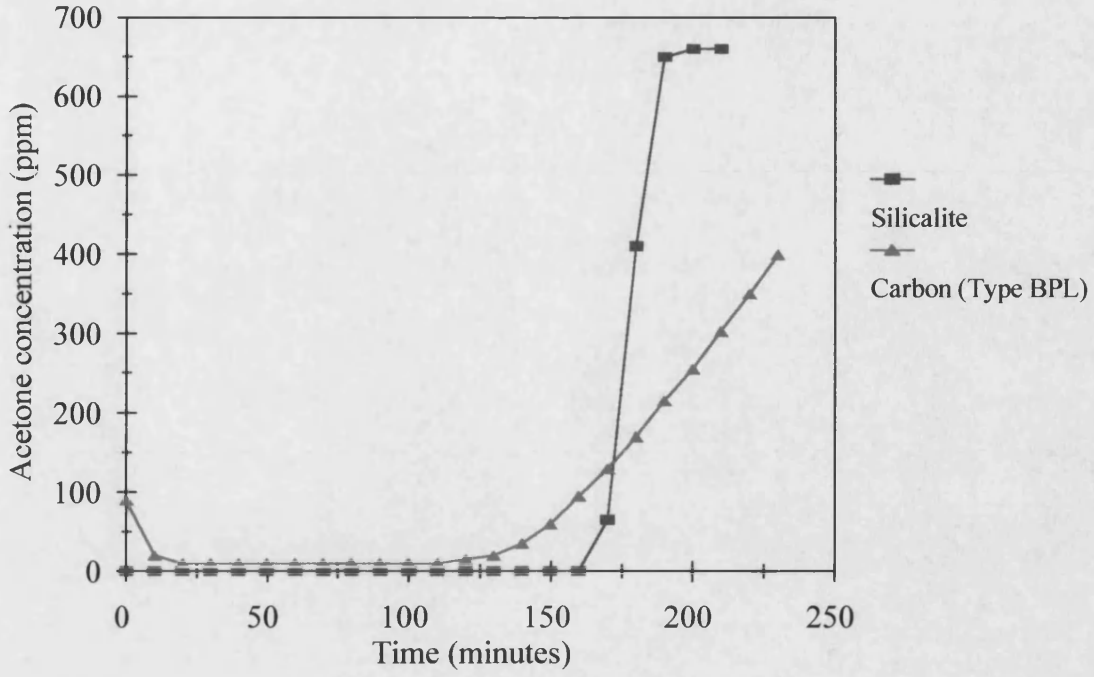

Figure 1.10 Acetone adsorption at 65 % relative humidity (UOP, 1992)

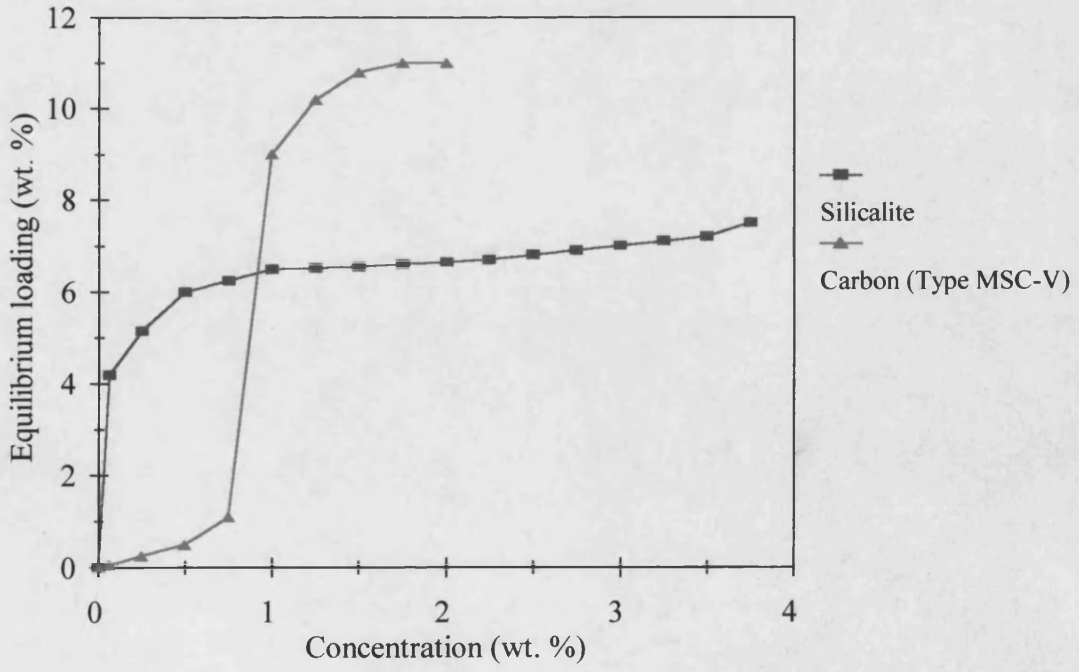

Figure 1.11 Adsorption of phenol from aqueous solution (UOP, 1992)

Table 1.10 Hydrophobic zeolite *vs.* carbon

Disadvantageous of carbon	Advantageous of using high silica zeolite
Flammable	Non-flammable
Cannot desorb high-boiling solvents (>150°C)	Can withstand temperatures up to 1000°C
Promotes polymerisation or oxidisation of some solvents to toxic or insoluble compounds	Can handle a wide variety of solvents
Can efficiently handle only minor concentration fluctuations	Efficient adsorption at a wide range of concentrations
Hygroscopic, requires relative humidity control	Does not promote solvent polymerisation or reaction
Non-selective	Hydrophobic, repels moisture
	Highly selective, especially for low molecular weight VOCs

Even though the cost of a high silica zeolite would probably be higher than that of an activated carbon, it is possible that the overall cost of the VOC control system would not be significantly greater provided the investment in the adsorbent is a relatively small fraction of the total cost of the process.

1.7 Environmental Applications of High Silica Zeolites

As a consequence of their shape-selective behaviour, high stability, high activity and very high resistance to deactivation due to coking, ZSM-5 and silicalite have been gaining importance in a variety of industrial petroleum and petrochemical industries. They have been used for isomerisation of xylene, conversion of methanol to gasoline, disproportionation of toluene, and alkylation of benzene and toluene. In addition to their proven applications within the petrochemical industry, the high silica zeolites have attracted attention as a potential adsorbent for the selective removal of organics from the environment. The potential and limitations of the zeolites in the control of environmental pollution have been discussed by Crittenden (1994) and Blocki (1991).

1.7.1 Alkanes

The earliest studies of the adsorption of VOCs onto silicalite were performed by Flanigen et. al. (1978) for Union Carbide. They also examined the effect of adding water vapour to the VOC feedstocks. It was determined that silicalite has a very low selectivity in favour of the adsorption of water and a very high preference for the adsorption of organic molecules smaller than its limiting pore size. Adsorption of VOC molecules onto silicalite occurs by the volume filling of micropores as in zeolite molecular sieves and other microporous adsorbents. The filling of micropores occurs by physical adsorption at low relative pressures and is characterised by enhancement of the adsorption energy due to an increase in dispersion forces resulting from the comparable sizes of the adsorption volume and the adsorbed molecule. This results in a Type I and near rectangular shaped adsorption isotherm of hexane onto silicalite. Total pore filling of 0.199 cm^3/g is essentially completed at a relative pressure of 0.03. In contrast, water does not fill the pores at any relative pressure. Other alkanes studied were butane and neo-pentane and the determined adsorption volumes were 0.190 and 0.029 cm^3/g, respectively. The volume of adsorbed water, at a relative pressure near one, was about 25% of the saturation pore volume for hexane. In gaseous or liquid mixtures of organic molecules and water, silicalite selectively adsorbs the organic molecule and thus is capable of removing organic molecules from VOC-water streams.

Hampson and Rees (1992) studied the control of hydrocarbon emissions using silicalite-1 and NaY. These zeolites were chosen because of the large differences in the electric field gradients present in their channels and cavities and also for the differences in channel/cavity size. The thermodynamics of adsorption of ethene and propane onto the zeolites, both singly and in binary mixtures, were examined using the isosteric method. This method allows the direct measurement of adsorption isosteres and involves the collection of pressure-temperature (P,T) data for the adsorbent-adsorbate system at constant adsorbate loadings. The separation factors for ethene-propane mixtures adsorbed onto silicalite were found to be larger than for those adsorbed onto NaY zeolites. The adsorption of the VOCs onto silcalite-1 depends mainly on the maximisation of dispersion force interactions within the zeolite channels. In comparison, the adsorption of the VOCs onto NaY zeolite depends on dispersion and electrostatic force interactions. Silicalite-1 is seen to be homogeneous with respect to adsorption site energies, whereas the various sodium ion sites in NaY zeolite contribute to its heterogeneity regarding adsorption site energies. Silicalite-1 is found to be the better adsorbent for the separation of ethene/propane mixtures.

A substantial amount of work on the adsorption of alkanes has been directed toward the measurement of micropore diffusion coefficients of silicalite and ZSM-5. A summary is given by Hufton and Danner (1993) and Karger and Ruthven (1992). Different experimental techniques have been devised for determining the diffusion coefficients in gas-solid systems, for example, concentration pulse and tracer pulse chromatography with small commercial crystals, the membrane technique, zero-length chromatography (ZLC) and the pulse field gradient nuclear magnetic resonance (PFG-NMR), classified under macroscopic and microscopic techniques. These methods are described and discussed by Karger and Ruthven (1992). Data on the diffusion of light alkanes and other simple organic molecules in these zeolites are also found in Karger and Ruthven (1992). Comparison of these data for a given adsorbate, such as propane, shows discrepancies of up to six orders of magnitude. The large discrepancy in the diffusion coefficient data has been discussed by Karger and Ruthven (1992). These authors methodologically analysed different experimental techniques and tabulated more reliable results for diffusion in the silicalite and ZSM-5 zeolites (and other zeolites such as 4A, 5A and 13X). A key finding was that agreement was obtained with the

slower systems and, conversely, disagreement occurred regarding quickly diffusing adsorbates. A "dual-mode" description of diffusion, where both mobile and immobile states exist in the solid, was hypothesised. Despite the differences, remarkable qualitative consistencies were demonstrated, such as the trend of the diffusion coefficients with concentration or cation loading. A summary of the literature data is given in Appendix III.

1.7.2 Alcohols

The adsorption of alcohols onto silicalite from aqueous mixtures has been studied for both liquid and vapour phase systems (Crittenden, 1994). The primary aim was to determine the feasibility of the adsorption process as an alternative to distillation. In some instances, low energy process alternatives to separate alcohol from azeotropic mixtures (particularly the ethanol-water azeotrope) and from dilute fermentation products, were being determined. However, the results show the potential value and limitations of silicalite in environmental protection applications. In general, the adsorption loading from aqueous solution of straight chain alcohols increases with increasing chain length from methanol to pentanol (Table 1.11). This is in accordance with the decrease in hydrophilicity of the molecule as the chain length increases. In addition, the adsorption loading was found to decrease as the extent of chain branching increases (Table 1.11). This may be attributed to, in the first case, the dependence of the hydrophilic-hydrophobic nature of an alcohol on its structure and, in the second case, the higher kinetic diameters of branched chain alcohols compared with those of straight chain alcohols.

Table 1.11 Adsorption capacities of alcohols from aqueous solution at 20°C

Liquid phase concentration (mg/l)	Adsorbate	Loading (mg/g)
10,000	Methanol	10
	Ethanol	57
	Propanol	83
	1-butanol	98
	2-butanol	86
	i-butanol	45
	l-butanol	34

For straight chain alcohols in the range ethanol-butanol, a maximum equilibrium loading up to about 0.13 grams of alcohol per gram of silicalite could be anticipated for the liquid phase at temperatures up to 60°C, and up to 0.1 g/g for the vapour phase at temperatures up to 130°C (Crittenden, 1994). The data obtained for the binary adsorption system are adequately represented by the extended Langmuir model (Klein and Abraham, 1983). Some studies confirm that water is also adsorbed with an alcohol. Despite this, the observation that ethanol can be concentrated from a 2 % w/v solution to 35 % and 1-butanol from 0.5 to 98 % by adsorption onto silicalite with subsequent desorption augurs well for environmental control applications, provided that the alcohol kinetic diameter is less than about 0.6 nm.

1.7.3 Phenol, Cresols and Benzyl Alcohol

The equilibrium loadings of benzyl alcohol, phenol and cresols are adequately correlated with aqueous solution concentration by the Freundlich equation for both silicalite and ZSM-5 (Crittenden, 1994). Example loadings for silicalite are given in Table 1.12. The adsorbability of benzyl alcohol is higher than that of phenol and aliphatic alcohol. The adsorption capacity of ZSM-5 is lower than that of silicalite, as might be expected due to the ability of ZSM-5 to adsorb water. The loadings of the cresols on silicalite are found to be considerably higher than that of phenol but similar to that of benzyl alcohol, indicating that the addition of a $-CH_2-$ group gives an equivalent

increase in adsorbability. The position of this functional group affects the adsorbability, most probably through the steric effect. Thus, as might be expected for the same solution concentration, the adsorption loading onto silicalite generally is greatest for m-cresol and lowest for o-cresol. For a solution concentration of 100 mg/l the equilibrium loading of phenol on silicalite is reduced from 24 mg/g at 25°C to 17.6 mg/g at 45°C, thereby illustrating the possibility for regeneration by temperature elevation.

Table 1.12 Adsorption capacities of phenol, cresols and benzyl alcohol from aqueous solution at 25°C

Liquid phase concentration (mg/l)	Adsorbate	Loading (mg/g)
100	Benzyl alcohol	44.5
	Phenol	24.0
	o-cresol	36.9
	p-cresol	45.6
	m-cresol	48.0

1.7.4 Halogenated VOCs

Chlorinated volatile organic compounds (CVOCs) released from water treatment operations, such as aeration, air stripping and aerobic biodegradation, are a major source of air pollution. A study of the ability of fresh and dealuminated ZSM-5 type zeolites to adsorb the CVOCs at room temperature and also to catalytically destroy the compounds was published by Prakash et. al. (1995). The adsorption of pure component CVOCs [e.g. trichloroethylene (TCE), methylene chloride ($MeCl_2$) and carbon tetrachloride (CCl_4)] on chromium-exchanged H-ZSM-5 (Cr-ZSM-5) was performed using the flow-through reactor method. The Lennard-Jones interactions of the CVOC with the ZSM-5 framework were estimated in order to determine the type of sites occupied. The effects of water vapour and pre-adsorbed CVOC on the adsorption of TCE are discussed. While the presence of water, either as vapour in the feed or pre-adsorbed onto the bed, resulted in a reduction of the adsorption of TCE due to competitive effects, pre-adsorbed $MeCl_2$ or CCl_4 did not affect subsequent TCE sorption. The presence of chromium or palladium cations in ZSM-5 did not appreciably affect humid TCE pickup as compared

with hydrogen-exchanged ZSM-5 (H-ZSM-5), but a decrease in capacity from 0.079 to 0.04 g TCE/g sorbent was noted with cobalt-exchanged H-ZSM-5 (Co-ZSM-5). When decreasing the aluminium content in ZSM-5, it was discovered that the adsorption of water was reduced by approximately 75 % and the sorption of TCE was increased. Also mentioned in the paper is a process whereby Cr-ZSM-5 could be used as a dual function medium for first storing and later catalytically destroying TCE from a low concentration (~110 ppm) stream. It was suggested that considerable energy savings might be obtained using this method.

Other investigations into the potential environmental applications of silicalite include those by Chorley et. al. (1991) and Utiger et. al. (1991). Trihalogenated methanes, including chloroform, dichlorobromomethane, dibromochloromethane and bromoform, can be formed in drinking water through complex reactions between chlorine used as a disinfectant, and humic and fulvic substances. At least on equilibrium grounds, silicalite offers a performance comparable with GAC for the removal of low concentrations of THMs (Chorley et. al., 1991). As an example, for a liquid phase concentration of 60 mg/l, the loadings on silicalite are 72 and 100 mg/g for chloroform and dibromochloromethane, respectively. The higher loading of the latter is due to its lower solubility in water when compared with chloroform (Chorley et. al., 1991).

The capacity of silicalite to adsorb 1,2-dichloroethane (EDC) is greater than that of GAC which is in turn greater than that of the resin Amberlite XAD4 (Utiger et. al., 1991). An example is shown in Table 1.13.

Table 1.13 Adsorption capacities of 1,2-dichloroethane onto various adsorbents

Liquid phase concentration (ppm)	Adsorbent type	Loading (mg/g)
10	Silicalite	73
	GAC	50
	Amberlite resin	16

1.7.5 Vehicle Emissions

Otto et. al. (1991) carried out a sorption study of several hydrocarbons onto silicalite powder and silicalite deposited onto a monolithic substrate. Their aim was to investigate the possibility of installing an adsorption device upstream of the catalytic converter in motor vehicles to enable temporary storage of the exhaust gases during cold-start. Experiments were performed using the gravimetric technique with the powder form and a flow-through type reactor with the monolith structure. The equilibrium loadings of the hydrocarbons (i.e. methane, ethane, propane, butane and hexane), alcohols (i.e. methanol and ethanol), carbon monoxide, carbon dioxide, and water, which were obtained using a microbalance, were represented well by the Langmuir isotherm. Experiments with preadsorption of water vapour, a major component of automotive exhausts, show that competitive water adsorption can substantially lower the adsorption of organic molecules. The adsorption capacity of wet silicalite for butane was reduced by 9 %, and that for methanol was reduced by about 20 % when compared with the adsorption capacity of dry silicalite. It was concluded that the size of adsorption device required under wet conditions was impractically large for the intended application.

The limited amount of equilibrium data which is available for some VOCs shows that silicalite has potential in environmental pollution control, including gas and aqueous phase applications. Due to its relatively small (~0.6 nm) and homogeneous pore size, silicalite exhibits limited performance for some common VOCs, and thus cannot be considered simply as a replacement for granular activated carbon. High silicalite zeolites represent a technology complimentary to, rather than competing with, activated carbon. Thus, silicalite should be considered for specific applications where selective removal and recovery of valuable VOCs from dilute polluted streams is desired.

1.8 Monolithic Adsorbents

There are several adsorption devices including fixed regenerative (or packed) beds, disposable and rechargeable canisters, travelling beds, fluidised beds and chromatographic baghouses. The most common and cheapest device is the packed bed. The problems associated with the packed bed are bed lifting, attrition with the entrainment of resultant fines and a relatively high pressure drop across the bed. The pressure drop may be reduced by using a larger particle size, but this may cause problems in dissipating the heat of adsorption and may increase mass transfer resistances within the pellet.

An alternative to such a system, and the subject of the present study, is a novel bed configuration featuring adsorbent incorporated into a monolithic structure. A monolith is an integral bundle of small and parallel channels, the cross-sections of which being any shape including square, circular, triangular, hexagonal and sinusoidal. Monoliths with hexagonally shaped channels are often referred to as honeycombs. The use of monolithic adsorbers may overcome many of the operational problems associated with packed beds. The flow within monoliths with straight channels is usually laminar, which results in a very low pressure drop. In fact, the pressure drop is typically two or three orders of magnitude lower than for a packed bed composed of spherical particles with a diameter of the same order of magnitude as the channel width of the monolith (Irandoust and Andersson, 1988). In addition to lower pressure drop, the monolithic configuration has a high surface to volume ratio. This is an important feature for pollution control applications where the flowrate is often high but with only trace amounts of VOC. In addition, it offers minimal resistance to the flow of particulates present in the gas phase, important if the adsorption of VOCs from motor vehicle exhausts is to be considered. The monolithic configuration also enables operation in the horizontal mode without plugging or channelling. Furthermore, the simple flow pattern and reactor structure make for more reliable scale-up. The main disadvantage of the monolith is its lower mass transfer compared with packed bed (Irandoust and Andersson, 1988). This may be countered by using a monolith with a higher cell density. A reduction in the channel diameter by a factor of three will increase the mass transfer coefficient by a factor of nine (Irandoust and Andersson, 1988). The structure

and manufacturing of the monolithic adsorber will be described in Chapter 3. The need to reduce cost is an important requirement in VOCs pollution control and this can be achieved by using the monolithic device.

1.9 Application of Monoliths to Air Pollution Control

Since the beginning of the 1970s, there has been a growing awareness of the potential applications of monolithic honeycomb supports within the air pollution control sector. Some prominent examples are as follows:

- automobile exhaust control (Howitt, 1980).
- NOx abatement from industrial emissions (Irandoust and Andersson, 1988).
- woodstove combustors (Irandoust and Andersson, 1988).
- ozone abatement in jet aircraft passenger cabins (Patil and Lachman, 1988).
- control of VOC emissions from organic solvents (Kenson, 1985).

Other non-environmental applications include decolorisation of nitric acid tail gas, methanation of carbon oxides (DeLuca and Campbell, 1977), steam cracking of naphtha, and methanol conversion to gasoline-range hydrocarbons (Antia and Govind, 1995). Irandoust and Andersson (1988) have reviewed the potential interest of monolithic catalysts for non-automobile applications and have published other papers concerning the use of this type of reactor in gas-liquid systems. An enhanced mass transfer in the liquid phase can be obtained by introducing plugs of a non-miscible liquid or gas into the flow. This disturbs the laminar flow and increases the radial mass transfer. In these processes, monoliths have generally been used as catalyst-supports in reacting environments, often at elevated temperatures. In contrast however, the monolith configuration is being seriously considered as a carrier for adsorbing material,

particularly for the abatement of VOC emissions. The review which follows shows the increasing importance of monolith adsorbents since the beginning of 1990.

Otto et. al. (1991) investigated the adsorption of automobile exhaust gases onto a silicalite monolith during the cold-start period. The silicalite powder was deposited onto a ceramic monolithic medium using a wash-coating technique. Blocki (1991) reviewed a cost effective solvent emission control plan involving a hydrophobic zeolite adsorbent impregnated into a honeycomb structure. The honeycomb was operated as a rotating disk. Crompton and Gupta (1993) have performed a pilot scale study on the adsorption of VOCs onto carbon and zeolite in a honeycomb structure. The adsorption was conducted using a rotary type device. Kenson (1994) reported that a honeycomb-based rotary adsorber or concentrator system employing activated carbon fibre could be more cost-effective than a conventional packed-bed for VOC/ROG (reactive organic gases)/air toxic emissions control in aerospace painting and stripping applications. His claim was confirmed following full scale installations. The difficulty in removing low concentrations (< 200 ppm) of methylene chloride with carbon was also identified. DeLiso (1991) discloses the manufacture of an activated carbon monolith for adsorbing evaporative hydrocarbon emissions in automotive anti-pollution applications, for example, from motor vehicle fuel tanks and petrol pumping stations. Extrusion and low temperature firing methods were employed in the fabrication process.

A search of the literature reveals that publications relevant to the topic of this research are very limited. Indeed comparatively little adsorption data has been published. More research therefore needs to be carried out in order to obtain sufficient adsorption information for an in-depth understanding of the operation of a monolith adsorbent to be established. It is a requirement for the research described in this thesis for the monolith prepared to have a high adsorption capacity, good kinetics and a low affinity for moisture. The monolith should be useable at high air flow rates and concentrations of VOCs.

The research project has an interest in the treatment of VOCs by adsorption onto high silica zeolites. For the reasons described earlier, it is proposed that the high silica adsorbents will provide better performance than the well-established activated carbon for VOC recovery. The following part of the thesis describes the objective and scope of the project.

1.10 Objectives of Research and Scope of Work

The objectives of the project include:

- to study the effectiveness of high silica zeolites, i.e. ZSM-5 and silicalite, as adsorbents for the recovery of VOCs in the vapour phase.
- to manufacture silicalite in monoliths having a high silicalite to binder ratio.
- to optimise the monolith design by means of adsorption breakthrough experiments.
- to compare the adsorption performance of silicalite monoliths with that of silicalite packed beds.
- to study the effect of humidity on the adsorption performance.

The work is limited to:

- the recovery of propane, ethanol and methylene chloride from the vapour phase.
- the use of the zeolite adsorbents, namely silicalite and ZSM-5, and comparing the adsorption equilibria of both zeolites in packed beds.

- the manufacture of silicalite powder into monolithic configurations and the carrying out of breakthrough studies to compare the performance with commercially available silicalite pellets.

- the investigation of adsorption effectiveness at room temperature and atmospheric pressure and determination of the influence of humidity.

- the investigation of the regeneration of adsorbents by back flushing with nitrogen under conditions similar to those employed during adsorption.

1.11 Structure of Thesis

The research described in the thesis is purely experimental. As described earlier, there exist many opportunities to employ silicalite in the recovery of VOCs, especially in a low pressure drop monolith configuration. Experiments were set up to formulate the silicate monoliths, to study their dynamic VOC adsorption properties, and to compare the results with those obtained under the same conditions using commercially available pellets. Chapter 2 describes the adsorption apparatus and experimental techniques which were used to assess the dynamic performances of the packed bed and the monoliths. A flow through apparatus was constructed to enable breakthrough curves of packed bed and monolith adsorption to be measured at room temperature and atmospheric pressure. In Chapter 3, a detailed description of silicalite monolith manufacture and design optimisation are given. The design of the monoliths is optimised using the breakthrough experimental set up described in Chapter 2. The experimental results obtained from packed bed studies are described in Chapter 4. The adsorptive properties of commercially obtained silicalite and ZSM-5 pellets are compared. These results form a basis of comparison for those described in Chapter 5, which contains the results of experiments into VOC adsorption onto the manufactured monoliths. Chapter 6 describes the evaluation of the pressure drop and external mass transfer coefficient both in the monolith and the packed bed. The thesis is concluded and future work is recommended in Chapter 7. A summary illustrating the work included in the thesis is given in the following Table 1.14.

Table 1.14 Summary of the thesis

Chapter	Work described	Future work
1	Background of work	
2	Description of the experimental apparatus and methods	
3	Manufacturing of silicalite monoliths	To manufacture monoliths of higher cell density and thinner wall.
4	Results of VOC adsorption onto packed bed of silicalite and ZSM-5. The effects of water vapour on VOC adsorption are also described.	To study the adsorption of multi-component VOCs mixtures onto the packed beds.
5	Results of VOC adsorption onto monoliths of silicalite. The effects of water vapour on VOC adsorption are also described. Comparison of results with those described in Chapter 4.	To study the adsorption of multi-component VOCs mixtures onto the monoliths.
6	Evaluating the external mass transfer resistance and pressure drop of both the monolith and the packed bed.	To carry out experiments to measure the external mass transfer coefficient.
7	Conclusion	To study the adsorption of multi-component VOC mixtures. To test the mathematical model on monolith adsorption developed by Shah et. al. (1995) with the experimental data obtained from this research.

Chapter 2

Experimental Apparatus and Procedure

2.1 Introduction

The equilibrium capacities and the kinetics of uptake of propane, ethanol, methlyene chloride, water and organic-water vapour mixtures were investigated using an adsorption column in the flow system shown schematically in Figure 2.1. A photograph of the experimental apparatus is shown in Figure 2.2. This chapter, which describes the apparatus and experimental procedure used for the study, can be divided into three sections. The first is concerned with the materials, that is with the adsorbents and gases; the second deals with the adsorption apparatus; and the third involves the experimental procedure.

2.2 Materials

2.2.1 Adsorbents

The adsorbents used in this study were monoliths of silicalite, pelletised silicalite and ZSM-5 beads. The zeolites were described in detail in Chapter 1 including the structure of silicalite and ZSM-5. Silicalite, both the powder and pellets, was purchased from UOP. It was labelled as MHSZ-420 for the powder form and MHSZ-423 for the pelletised form. The silicalite powder was fabricated into monoliths as described in Chapter 3. The ZSM-5 pellets were purchased from BDH. All these adsorbents have average micropore diameters of approximately 0.6 nm. Other physical properties supplied by the zeolite manufacturers are summarised in Table 2.1. Further analysis of the microporosity of these adsorbents is described in Chapter 3.

Table 2.1 Properties of zeolites obtained from the manufacturers

Adsorbent type	Silicalite		ZSM-5
Supplier	UOP		BDH
Product code	MHSZ-420	MHSZ-423	29882
Physical form	Powder	Sphere	Sphere
Physical appearance	White colour	White colour	White colour
Nominal particle size	< 200 mesh	8x10mesh and 14x16mesh	2 mm spheres
Average bulk density (g/cm^3)	-	0.833	0.72
Si/Al	Infinity		50

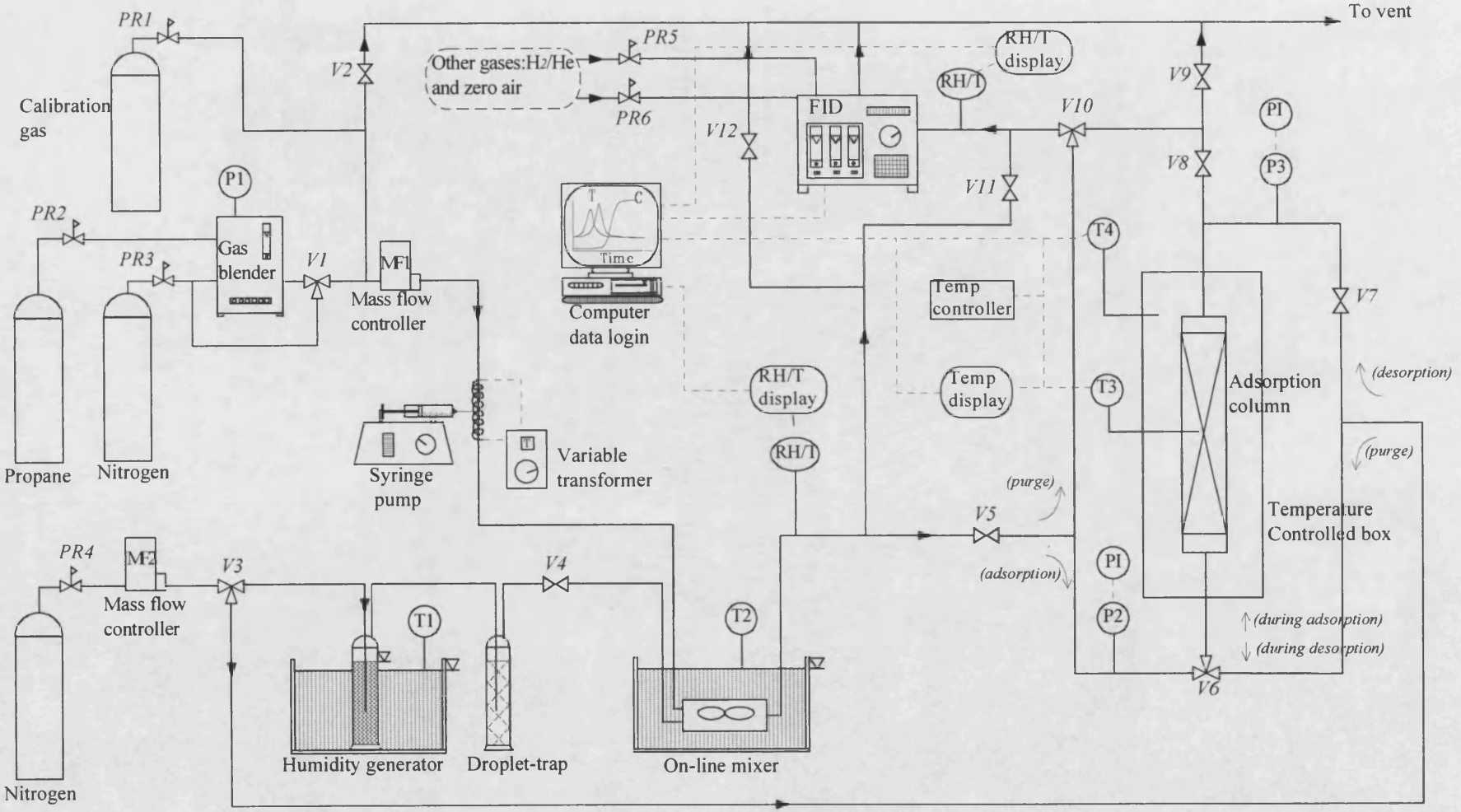

Figure 2.1 A schematic diagram of the apparatus used in the adsorption/desorption experiment

Figure 2.2 A photograph of the experimental apparatus

2.2.2 Adsorbates and Gases

The three organic adsorbates together with their relevant properties and concentrations used in the experiments are listed in Table 2.2. These adsorbates are representative of a broad range of commercial VOC pollutants. Furthermore, they have varying degrees of physical and chemical properties and therefore are expected to have different interactions with the adsorption media. The concentrations were selected to reflect typical concentration ranges that might be encountered in environmental or solvent recovery applications.

Ethanol is an important commercial solvent and a highly polar molecule. It was selected in order to study the effect of a polar molecule on adsorption in the presence of water vapour. It has the highest boiling point of the three organics and a molecular weight intermediate among the three solvents. It is completely soluble in water.

Propane on the other hand, being a pure hydrocarbon, is non-polar and also has the lowest molecular weight. It is an important product in the petrochemical industry and is widely used as a fuel. Its solubility in water is the lowest amongst the solvents studied here.

Methylene chloride was selected as a model chlorinated volatile organic compound (CVOC). It is difficult to remove by adsorption on activated carbon and therefore requires an energy/cost intensive VOC abatement technology such as thermal/catalytic destruction. Methylene chloride has a moderate polarity and the highest molecular weight when compared with the other two organics.

Table 2.2 Adsorbates used in this research and related properties

Adsorbates	Propane, C_3H_8	Methylene chloride, CH_2Cl_2	Ethanol, C_2H_5OH	Water, H_2O
POCP[2.1]	52[2.2]	1[2.3]	35[2.4]	-
Molecular weight[2.5]	44	85	46	18
Molecule diameter[2.6] (nm)	5.12	4.89	4.53	2.64
Solubility[2.7], at 25°C, (ppm weight)	62.40	1938	Total	-
Boiling point[2.8] at 1 atm (K)	231.11	312.90	351.44	373
Concentrations used	1000, 2500, 5000, 7500 and 10000 ppmv (volume)	3500, 20000 and 44000 ppmv	1000, 3000, 5300, 10000, 18500 and 44000 ppmv	20, 40, 50, 55, 70 and 80 % relative humidity (% RH)

Apart from the adsorbate species mentioned above, several other gases were used in this research including the carrier gas, system purge, regeneration gas, calibration gas and supply gases to the analytical instrument. Specifications are provided in Table 2.3. Nitrogen was used as the carrier gas because it was readily available, safer to use than helium and is not adsorbed significantly except at cryogenic temperatures. Thus it does not interfere with the adsorption of the VOCs.

[2.1] Photochemical Oxidant Creation Potential (POCP) is a measure of the ozone forming potential per unit mass emitted (Hayman and Jenkin, 1991). POCP factors are expressed relative to ethene (POCP=100).

[2.2 - 2.4] Data obtained from Reid and Sherwood, 1958.

[2.5 - 2.8] Data obtained from Perry and Chilton, 1973.

Table 2.3 Specification of gases and solvents

Type	Purpose	Supplier	Grade	Purity
Propane	Adsorbates, made to various concentrations in nitrogen carrier	BOC	Technical grade[2.9]	95 %
Propane	FID calibration	BOC	Special mixture	1000 ppmv balance nitrogen
Ethanol	FID calibration	BOC	Special mixture	967 ppmv balance nitrogen
Methylene chloride	FID calibration	BOC	Special mixture	1118 ppmv balance nitrogen
Compressed air	FID fuel	BOC	Zero grade[2.10]	95 %
Compressed air	FID by pass	BOC	Commercial[2.11]	-
Nitrogen	Carrier	BOC	Commercial[2.12]	99.99 %
	System purge			
	Regeneration			
Hydrogen-helium mixture	FID fuel	BOC	Commercial	40 % hydrogen balance helium
Ethanol (liquid)	Adsorbate	Sigma	HPLC	Denatured
Methylene chloride (liquid)	Adsorbate	Sigma	HPLC	99.90 %

[2.9] Total impurities 5 % maximum, i.e. ethane 100-300 ppmv, propylene 500 ppmv, isobutane 200-1500 ppmv, n-butane 550 ppmv, trans-2-butene 200 ppmv, cis-2-butene 100 ppmv and air 500 ppmv.

[2.10] Contains less than 1 ppm (vol) of carbon dioxide, < 2 ppmv of moisture and < 2 ppmv THC.

[2.11] Contains no other impurities which will influence the classification of the product. Typical composition of dry air : N_2 (78.09 %vol), O_2 (20.94%), Ar (0.93%), CO_2 (0.033%), Ne (18.16 E^{-4}), He (5.239E^{-4}), Kr (1.139E E^{-4}), H_2 (0.5 E^{-4}), Xe (0.086 E^{-4}) and Rn (6E-10).

[2.12] Contains less than 5 ppmv of oxygen and < 8 ppmv of moisture.

2.3 Apparatus

The apparatus consisted principally of an adsorption column, a flow system for supplying the feed stream, and an analytical system for monitoring the effluent gas composition (Figure 2.1). A separate adsorbent regeneration system was also constructed and a schematic diagram for this is shown in Figure 2.3. Flowlines consisted of quarter inch (OD) 316 stainless steel tubing as it was self-supporting, had a high temperature and chemical tolerance, and a negligible pressure loss for the particular test flow rates employed. The joints were made using 316 stainless steel Swagelok fittings and Whitey low temperature and high temperature ball valves. The equipment used can be sub-divided as follows:

- feedstock generation.
- inlet flowrate and temperature measurements.
- adsorption/desorption column.
- analysis of the column influent and effluent concentrations.
- high temperature regeneration.

2.3.1 Feedstock Generation

The feed system was designed to supply a constant flow of VOC vapour in nitrogen to the adsorption column. The feedstocks of VOC were prepared by using: (i) a Signal gas blender for propane-nitrogen mixtures, and (ii) a syringe pump for ethanol-nitrogen and methylene chloride-nitrogen mixtures. Gas-tight glass syringes of 10 ml, 20 ml and 50 ml were used for continuous injection of liquid VOC by the syringe pump into the carrier gas stream of nitrogen within a heated line. Trace heating for the line was provided using lengths of nickel-chrome wire covered in glassfibre sleeving (RS Component 398-751). For reasons of safety, these were powered by a controllable 50 V

isolating transformer. Selection of the syringe size was dependent on the desired composition. Humid streams were created by passing a known flowrate of nitrogen through a Dreschel jar filled with distilled water. This humidified nitrogen stream was then blended with the VOC laden stream of nitrogen. The humidity of the resultant gas was measured with an on-line hygrometer (Humitec HMP 36). The relative humidity was maintained constant by keeping flowrate and temperature of the system constant.

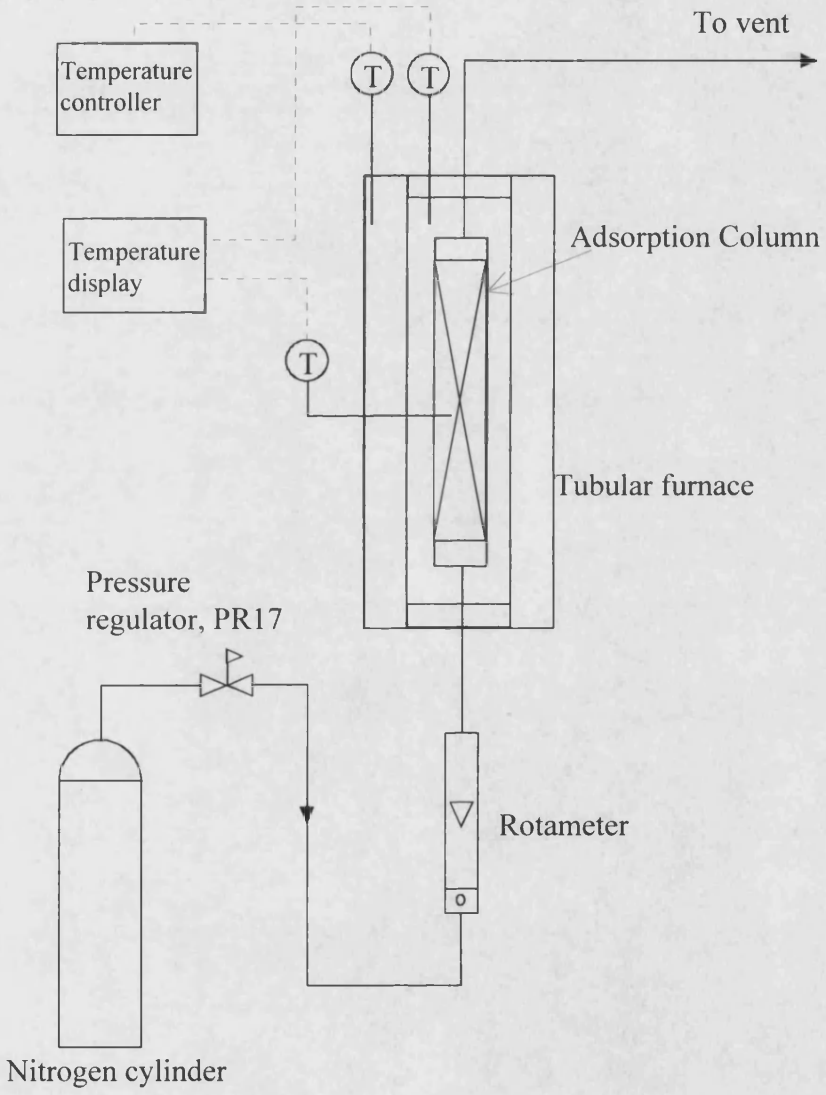

Figure 2.3 A schematic diagram of the regeneration apparatus

2.3.2 Inlet Flowrate and Temperature Measurements

The gas flowrate was controlled using thermal mass flow control units (Brooks Instruments 5850). These were supplied by the manufacturer ready-calibrated for the gases used. A suitable power supply/digital readout unit was constructed in-house. It was considered unnecessary to provide a computer interface for this. A mass flow meter was placed temporarily at the exit point to check for any gas leakage from the system, and once this had been completed the mass flow meter was then removed from the system. Gas leakage checks were also performed by applying soap solution to joints of slightly pressurised piping. An in-line gas mixer was fitted between the feedstock generator and the adsorption column to ensure that the gas was uniformly mixed prior to entering the bed. A thermocouple was placed after the mixer to monitor the gas temperature into the adsorption column.

2.3.3 Adsorption/Desorption Column

The adsorption apparatus consisted of a 1 inch OD x 40 cm long 316 stainless steel tube with both ends fitted with Swagelok stainless-steel reducers. These reducers enabled connection of the column to the rest of the system which was constructed mainly of quarter inch OD stainless steel piping. In order to accommodate different lengths of adsorbent in the column, a number of solid stainless-steel cylinders were fabricated, each with a quarter-inch hole bored along its axis. These could be used to take up any dead space in the column, and were a less expensive option than providing several columns of different length. A gas distributor, which was a stainless-steel perforated basket consisting of glass beads, was placed at the inlet section of the column to ensure good flow distribution.

Schematic drawings of columns containing monolith and pellets are shown in Figures 2.4 and 2.5, respectively. Further details of the adsorption beds which are specific to the adsorption systems under investigation are included in later chapters. When used in monolith form, the adsorbent was held within the column by packing silanised glass wool, which is non-adsorbing, in the gap between the outer edge of the

monolith and the stainless steel tube. A thermocouple positioned at the top of the monolith was used to monitor effluent temperature. For the packed column, the adsorbent beads were supported by a wire screen positioned on the gas distributor. Thermocouples, equally spaced at axial positions as shown in Figure 2.5, protruded through the tube wall and into the bed radially. Pressure transducers were placed at the column inlet and exit points. The pressure transducers were type 810 strain gauge devices manufactured by Druck Ltd. Each was supplied ready-calibrated with its own power supply/readout module by R.S. Components Ltd.

A tubular furnace obtained from Severn Science Ltd., was used in conjunction with a temperature controller (Eurotherm type K thermocouple input) to regulate the temperature of the column. In order to save time and effort in disconnecting and reconnecting the column, the same furnace was used during all three phases of the experiment i.e adsorption-desorption-regeneration. It was initially found that the power rating of the furnace (3.3 kW) was far too high to obtain satisfactory control at around 25°C. The solution adopted was to reduce the effective power rating to around 200 W by interposing a step-down transformer (4:1 ratio) between the furnace and the temperature controller. The transformer was bypassed for the desorption-regeneration parts of the experiments.

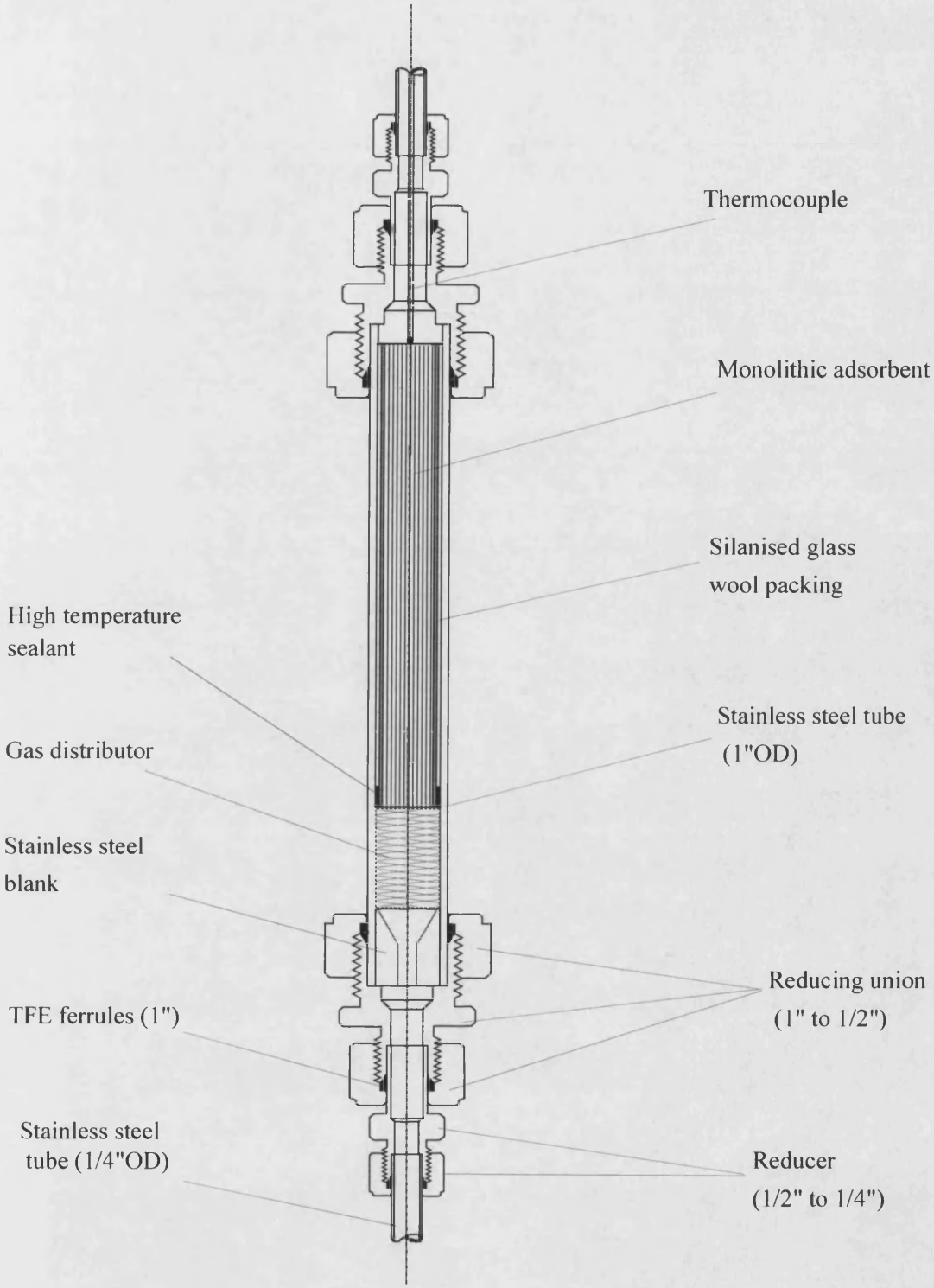

Figure 2.4 Monolith adsorption column

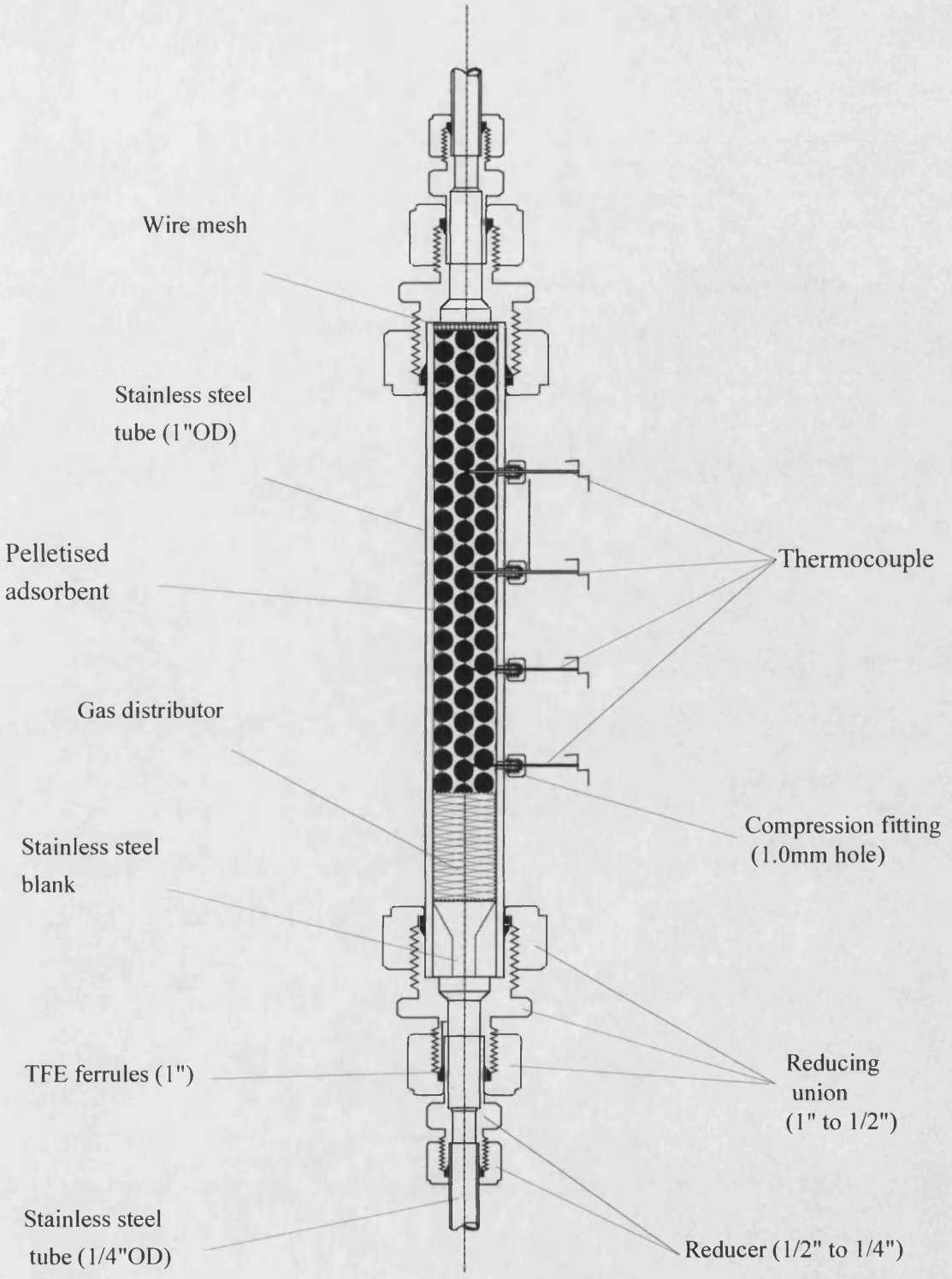

Figure 2.5 Packed bed adsorption column

2.3.4 Analysis of the Column Influent and Effluent Concentrations

The inlet and outlet concentrations were monitored continuously using an on-line flame ionisation detector (FID). The FID was calibrated using the calibration gases obtained from BOC. Properties of these ready-mixed gases are listed in Table 2.3. The FID has a heated sample system and detector which maintains a sample temperature of up to 200°C. The flow control system in the FID allows for sample flow rates of between 100 cm^3/min and 5000 cm^3/min with no variation in sample flow rate to the detector.

Data logging was accomplished using an IBM PC fitted with a PC Super interface card from CIL Ltd. The card was capable of logging up to eight differential voltage inputs at a resolution of 16 bits. The gain for each channel was software programmable. In addition, four 12-bit digital-to-analogue converters were provided (unused), together with sixteen logic lines (TTL levels 0-5 V) which could be configured for input or output. The output from the FID gas analyser was in the form of a 0-10 mA current signal which was converted to a voltage signal in the range 0-1 V by means of a suitable burden resistor (100 ohm) before being fed to the interface card. Relative humidity and temperature outputs from the humidity sensor electronics required no additional conditioning and were connected directly. Readings from the thermocouples were selected using a reed relay multiplexer controlled by logic lines from the interface card, and displayed on a digital panel meter (Digitron type 3750K). A 1 mV/°C output provided by the panel meter was connected to the interface card, making it possible to log all six temperatures automatically.

Software for data logging was written entirely in Borland Turbo basic. (A listing is included in Appendix IV). The program allowed all analogue data to be logged to a spreadsheet-compatible disk file every ten seconds. VOC concentrations were displayed in the form of graphs (versus time). All other data were displayed numerically at the top of the screen, together with the time elapsed since the start of the experiment. Menu options were also provided to facilitate calibration of the FID detector, which was carried out at the start of each experiment.

2.3.5 High Temperature Regeneration

Two regeneration units were used for the reactivation of adsorption beds. One of them was the temperature controlled furnace shared by adsorption-desorption runs (Figure 2.1). A separate regeneration facility consisting of a tubular furnace identical to the one described above, and a flow system providing the purge gas and a venting system were also available to increase the number of experiments. When one apparatus was used for adsorption over long periods, say > 12 hours, the other equipment was used for the regeneration of another bed. This is shown in Figure 2.3.

2.4 Experimental Procedure

The experimental procedure was devised with the aim of elucidating the column exit gas concentration history, ie. the breakthrough curve. In this section, the procedure is described in the order shown below :

- Packing and reconditioning of adsorbent
- Calibration of the FID
- Feedstock generation
- Check of operating conditions
- Adsorption run
- Regeneration

2.4.1 Packing and Reconditioning of Adsorbent

The first step in the experimental procedure was to fill the adsorption column with the appropriate adsorbent. For adsorption on a monolith, a fixed weight of the silicalite monolith (the preparation of which is to be described in Chapter 3) was placed in the column. Glass wool was inserted into the gap between the monolith and steel tube to hold the monolith centrally in the tube. A thermocouple was inserted through the top of the column sufficiently far to just avoid touching the top of the bed. A gas distributor was placed at the bottom of the column as shown in Figure 2.4. With adsorbent beads, a known weight of the desired adsorbent was poured randomly into the column while tapping the tube gently to promote a compact bed (Figure 2.5). Before using a pelletised adsorbent, it was necessary to screen the beads to give a uniform particle size. This was accomplished using British standard screens. The two size ranges used were 8 to 10 mesh and 14 to 16 mesh.

Initial drying of the zeolite adsorbents was carried out in a furnace at 150 to 200°C for 4 hours. Reactivation was carried out at 350 to 400°C for a duration of 16 to 24 hours. The lower temperature period was to remove moisture from the pores and the higher temperature period was to remove any other contaminants. A nitrogen purge of

1000 to 2500 cm^3/minute at atmospheric pressure was also introduced into the column during the reconditioning process. On completion, the furnace was switched off and the bed was cooled down over several hours to room temperature by a nitrogen flow. The furnace set point temperature was then adjusted to give the required adsorption experiment temperature (20 to 26°C), and the column was left for a time sufficient for the adsorbent to reach the desired temperature.

2.4.2 Calibration of the FID

The FID was switched on 30 minutes prior to the calibration in order to allow ample time for it to reach a steady temperature. The fuel gases (hydrogen and zero grade air) and by-pass air were supplied to the FID at a pressure of 2 barg and with the ignition button switched on. A duration of five minutes was allowed for gases to flush through the detector. The ignition button was pressed again to ensure that a flame was present, signified by a momentory full scale indication on the LED bar display. A further 5 minutes were allowed for the flame to settle before the span/calibration and zero gases were introduced. A zero grade air was used to set the zero reference of the analyser. To span the FID, a premixed gas with a fixed concentration (obtained from BOC with the specification shown in Table 2.3) was introduced after having selected an appropriate range to co-ordinate with gas concentration. The span knob was adjusted until the correct gas concentration was indicated by the digital display. A calibration gas flow rate of 500 cm^3/min was always used when spanning the FID.

2.4.3 Feedstock Generation

The propane-nitrogen mixture was prepared by passing the hydrocarbon and carrier gases into the Signal Gas Blender. Both gas supplies were set at 2.4 barg to the inlet of the gas blending unit. A calculation method provided by the manufacturer was followed in order to obtained the appropriate settings of the Gas Blender for the desired mixture.

A syringe pump was used for the generation of a vapour from a liquid organic. The organic liquid was infused into a nitrogen flow within a heated line. The line was maintained at a temperature between 100 and 150°C, and lagged with fibre glass. After a mixture of constant composition had been made up, the concentration of the VOC was measured as it by-passed the adsorption column. Fine adjustments were then made to the feed generator until the exact required concentration was obtained. The by-pass line is shown in Figure 2.1.

For experiments involving a humidified carrier gas, the water vapour was produced by bubbling a controlled nitrogen flow into a Dreschel jar containing distilled water. The jar was placed in a water bath set at 25°C. The humidified nitrogen stream, having passed through a droplet-trap, was mixed with the organic-laden nitrogen stream in the on-line mixer. The resultant stream was then passed through a hygrometer to measure the relative humidity. It was important to allow ample time for the mixture to stabilise before passing it to the adsorption column. This typically required 2 to 4 hours.

2.4.4 Check of Operating Conditions

Having completed the feedstock preparation, checks of the FID, feed, column, water bath, and ambient temperatures were performed. The FID has a built in temperature controller and this was set to 198°C. The FID temperature seldom fluctuated by more than ±1°C while the room temperature variations were usually about ±2°C during the day and ±5°C during the night. When using a humidity generator, the water bath was monitored less frequently because the on-off control was capable of holding the desired value within ± 0.1°C.

The temperature of the inert gas flowing through the bed prior to adsorption was usually in the range 24-26°C. The flowrates of the FID gases were then inspected by checking the rotameters on the FID. It was also vital to ensure sufficient gas supplies for the entire breakthrough experiment which might last for more than 12 hours. The last item checked was the feed stream concentration and flowrate prior to the adsorption run.

2.4.5 Adsorption Run

While the various operations mentioned above were being checked and recorded, the adsorption bed was purged with nitrogen to remove any remaining traces of impurities including moisture which might have been prematurely adsorbed when the column was installed, and also to cool down the bed to the adsorption temperature. If the bed had been previously reactivated in the separate regeneration unit, it was transferred into the test-system with great care to avoid exposing the adsorbent to air which could result in contamination.

Gas flow through the adsorption column was vertically upwards during all adsorption experiments. Once the bed had reached the desired temperature, it was then isolated from the rest of the system by means of the 3-way valve at the bottom (V6 in Figure 2.1) and a 2-way plug valve at top of the column (V8). This left the adsorbent in a stagnant pure nitrogen environment while the nitrogen flow bypassed the bed and flowed to the vent. After ensuring that the feed composition and flowrate were steady and as required, the adsorption run was commenced by switching the 3-way valve (V6) to permit feed flow. At this instant the feed check-bypass valve (V11) was closed and the 2-way valve (V8) at the top of column was opened to direct effluent to FID, and data logging was initiated. Throughout the experiment, the feed flowrate and temperature together with the column pressure were monitored manually, while the effluent concentration and temperature of the column were acquired by the computer every ten seconds. The various gas supplies were constantly checked throughout the experiment. The run was terminated when the effluent concentration detected by the FID was approximately the same as the feed concentration or when the changes between sample measurements became almost imperceptible. The experimental runs lasted between a few hours to several days. Following each run, the feed concentration and flowrate, and all temperatures were again checked and recorded.

2.4.6 Regeneration

After completion of the adsorption experiment the column was sealed in the manner described above and the supply of VOC was switched off. The system pipe lines were flushed with the carrier gas until all organic chemicals were completely removed from the system. This was indicated by the inert gas being VOC free. The carrier was then switched to the column and the desorption experiment was initiated. Desorption was performed under two types of condition. The first type was desorption under conditions similar to adsorption except that the purge flow was in the reverse direction. In the second type desorption was carried out at elevated temperature. Desorption was continued until the effluent stream concentration approached zero. The temperatures, column pressure, nitrogen purge flowrate and concentration were monitored throughout the desorption experiment. The flow for desorption was downwards in order to simulate industrial practice and to minimise attrition of the adsorbent particles. However, the flowrate was always such that the downward force was not sufficient to crush the particles.

After the desorption experiment, the bed was regenerated to prepare for the next adsorption experiment. The reconditioning was carried out at 300-400^{o}C for 16-24 hours under a nitrogen purge flowrate of 1500-2000 cm^{3}/min.

2.5 Conclusions

The experimental apparatus and procedure described in this chapter has enabled the dynamic adsorption of the single component VOC and that of the mixtures of VOC-water onto high silica zeolitic monoliths and pellets to be investigated. The simplicity of the equipment has enabled all the required process variables to be accurately maintained and monitored. Hence, in the subsequent analysis and assessment of the experimental data, errors (Appendix V) have been minimised.

Chapter 3
Fabrication, Characterisation and Optimisation of Monoliths

3.1 Introduction

This chapter describes the technique used to manufacture the monolith adsorbent used in this research, *viz.*, extrusion and the factors which influence the extrusion process. The experimental apparatus and methodology are explained in detail, followed by an overview of the major problems encountered during the formulation and fabrication of the monolith adsorbent. Characterisation of monoliths using several analytical techniques is described. In addition, determination of the optimum structure of the monolith using the adsorption equipment and procedure described in Chapter 2 is described.

3.2 Monolith Configurations

A monolith is composed of parallel channels which may be circular, hexagonal, square, triangular or sinusoidal. The channel size and the wall thickness can be controlled during fabrication along with the cell geometry. These factors determine the cell density, void fraction, geometric surface area and hydraulic diameter which affect the adsorption performance of the monolith. Ceramic monoliths have been designed and used as catalytic converters. Since their inception in the 1970's, considerable progress in the design and quality of cellular monoliths has been made (Howitt, 1980). For example, the square channel monolith was initially produced in only 31 cells/cm^2, then a structure of 46 cells/cm^2 was introduced and accepted as a great improvement as it provided 17 % greater surface area for catalyst deposition within the same overall volume. A further development in the design of the monolith structures including cell densities of 62 and 93 cells/cm^2 is also described by Howitt (1980). In addition, the thickness of the cell walls is reduced from the conventionally used 0.030 cm nominal to

0.015 cm. The benefit of higher cell density and thinner wall geometry are larger geometric surface area and lower pressure drop. In principle the cell density or wall thickness could have an infinite number of variations. However this is limited by the manufacturing methods presently used. The length of the monoliths typically ranges from 1 cm to 1 m and monoliths with diameters up to 2 m have been formed (DeLuca and Campbell, 1977). As described in Chapter 1, a monolith adsorbent has several potential advantages over the traditional packed bed. In addition to the relative high surface-to-volume ratio which enables low pressure drops to be obtained, monoliths can be operated horizontally without plugging or channelling. Once the channel size has been selected the simple flow pattern and structure make for more reliable scale-up, simply by increasing the monolith diameter. Monoliths can be stacked and/or cemented together to produce any desired length and diameter. Monoliths are more durable and dust-free than pellets which become abraded with time. Also, monoliths are possibly easier and more cost effective to manufacture than the pellets.

3.3 A Review of Monolith Manufacturing Methods

One of the major tasks of this research has been to prepare a monolith adsorbent which is suitable for use as a VOC control device. Particular applications include evaporative emissions of VOCs to the atmosphere from motor vehicle fuel tanks and gasoline pump nozzles. Other potential areas of application are the capture of emissions of automobile exhaust during the cold-start period, fugitive VOC releases from industrial solvent storage-tanks and the removal of a broad range of VOCs from air streams in a variety of manufacturing process. Otto et. al. (1991) designed a silicalite monolith for vehicle exhaust entrapment during the cold-start period. However, it was found that the monolith would have been too large for the application where size and cost are critical components of cars. The large size may have been due to the method of preparing the silicalite monolith. The wash-coating method allows only a limited amount of the zeolite adsorbent to be deposited on to the external surface for a fixed volume of monolith. Also there may have been loss of adsorption capacity due to adhesion-effects. In the research described in this thesis a different technique has been

used to improve the amount of silicalite per unit volume. Furthermore, it is intended that the molecular sieve zeolite will be strongly held and integrated to the overall structure.

Monoliths made from, or coated with, molecular sieve zeolites have been produced by several methods including extrusion, corrugation, wash-coating and hydrothermal-crystallisation. A summary of the literature is given in Table 3.1. All these methods have been used to fabricate monoliths as catalysts. Accordingly, full descriptions of each technique can be found in the literature including Deluca and Campbell (1977) and Irandoust and Andersson (1988).

Table 3.1 A review of methods for producing monolithic adsorbents and their uses

Techniques	Literature	Monolith type	Field of applications
Extrusion	Patil and Lachman (1988)	Silicalite	Methanol conversion
Extrusion	DeLiso (1991)	Activated carbon	Hydrocarbon vapour adsorption
Extrusion	Mizuno et. al. (1983)	Activated carbon	Hydrocarbon vapour adsorption
Extrusion	Liepa (1977)	X- and Y-types	Carbonation of soft drink
Corrugation	Kodama and Hirose (1993)	Silica gel	Dehumidification of air
Corrugation	Kuma (1995)	Silica gel	Dehumidification of air
Zeolite crystallisation onto monolith substrates	Lachman and Patil (1989)	ZSM-5, X and Y types	Catalytic cracking of petroleum, NOx abatement, etc.
Zeolite crystallisation onto monolith substrates	Brown and Woltermann (1979)	ZSM-5	Catalytic reduction of NOx
Zeolite washcoating	Otto et. al. (1991)	Silicalite	Vehicle cold-start adsorption
Zeolite washcoating	Patil and Lachman (1988)	Silicalite	Methanol conversion
Zeolite washcoating	Antia and Govind (1995)	ZSM-5	Methanol conversion

Corrugation, wash-coat and crystallisation, although suitable for forming monoliths of constant cross-section, have not been completely satisfactory due to the fact that cell shapes are limited, cell channels are prone to blockage by crystal/binder mixtures, and resultant wall thicknesses may not be uniform. Furthermore, these processes are relatively slow, complicated and difficult, and may require costly materials. For example, in corrugation each corrugated sheet must first be produced and coated with the desired adsorbent. Then it has to be stacked against a corresponding corrugated or uncorrugated sheet, this operation being continued until the desired number of layers has been assembled. The completed stack is then kilned. With this construction there is always doubt as to whether the corrugated and uncorrugated sheets will actually become bonded together along their contact lines in the manner intended. Also this technique gives rise to the formation of channels of a shape with narrow portions which can offer a considerable resistance to flow which is undesirable as pointed out by Eichhorn and Sauber (1969). General problems associated with wash-coating and crystallisation methods are channel plugging and poor adhesion of the crystals, which have a tendency to flake off under gas flow.

Extrusion is the most common technique for shaping monoliths of constant cross-section. The method has been employed for the past two decades to produce ceramic monoliths for catalytic converters. Extrusion has also been used to form materials for applications in a wide variety of industrial applications such as micro-electronics, food, agricultural and pharmaceutical chemicals, and the formation of engine components (Benbow et. al., 1991). The advantages of the extrusion technique include:

- it is a well studied and established method.

- it is an efficient process for high volume production.

- it has high flexibility in manufacturing, e.g. :
  - * very complicated cross-sections are possible.
  - * a variety of channel shapes can be made.
  - * continuous casting allows any bed length to become possible.

- uniformity is ensured, e.g. :
  * uniformity of weight is important because non-uniformity of manufacture would cause non-uniformity of adsorbent loading.
  * channel size uniformity is essential because flow through cells of different size would be non-uniform and this would lead to the adsorption capacity varying in line with flowrate or space velocity. Flowrates can also vary through channels of different shapes but containing the same flow cross sectional area.
  * variation in wall thickness can affect strength and adsorption if these parameters vary from sample to sample.
  * dimensions need to be accurate enough for satisfactory mounting.

- it is capable of shaping very hard powders, and different ratios of zeolite to binder are possible.

However, some disadvantages of the extrusion techniques are:

- uniformity of longitudinal shape is harder to control, particularly for long monoliths.

- final monolith structure depends on the powder properties.

- monolith strength is not imparted during the extrusion itself.

- structure or strength are not in general adjustable by changing the way the extrusion equipment operates.

- binders and rheology modifiers can adversely affect monolith adsorption properties.

3.4 Background to Extrusion Processes

Extrusion is a forming process in which a plastic material is forced through a constricting nozzle or die that produces a product with a controlled cross-section. A plastic material is usually defined as having the ability to deform continuously and permanently, without rupture, during the application of a stress that exceeds its yield value, and to maintain such shape once the imparting force is removed (Ryan, 1978).

Clay, the main raw material in the ceramic industry, is a naturally occurring hydrated aluminium silicate mineral. There are a number of species called clay minerals, which contain mainly mixtures of kaolinite ($Al_2O_3.2SiO.2H_2O$), montmorillonite [$(Mg,Ca)O.Al_2O_3.5SiO_2.nH_2O$], and illite ($K_2O$, MgO, Al_2O_3, SiO_2, H_2O, all in variable amounts). Clays are plastic and mouldable when sufficiently finely pulverised and wet, rigid when dry, and vitreous when fired at a suitably high temperature. Accompanying these clay minerals are varying amounts of feldspar, quartz, and other impurities such as oxides of iron. The plasticity developed by clays when water is added is dependent on the size and the shape of the particles. The finer the particle the greater the plasticity of the clay. As well as size, the shape of the particles is important. Clay particles are thin plates and hexagonal in shape which enable them to slide over one another with the presence of water molecules. Due to fineness the particle surface area is very high and the atoms at the surface attract water molecules to satisfy their valency balance resulting in a film of water around the particles. The water film enable the movement of one clay plate over another producing the plasticity effect (Ryan, 1978).

The principles involved in plastic material formulation are extremely diverse and complex. Successful fabrication may be based on the application of principles of colloid chemistry, rheology, organic and inorganic chemistry, physical chemistry, mechanics, surface chemistry, and other special disciplines to pottery problems. Many studies have been carried out on the extrusion of paste and its governing parameters. For example, Parks and Hill (1959) have studied both the transport of clay along the single-auger extruder and flow through dies of different geometry, and have provided a semi-empirical equation. Griffith (1966) described the extrusion of moist alumina and silica powders, and used a simplified expression to relate the pressure required to produce

flow with a yield value of the material which was deduced from the plastic behaviour of metals in compression. Isenhour (1979) experimentally demonstrated the influence of die design on the occurrence of surface defects in extrusion. He studied the effect of velocity and entrance taper angle on these defects, both before and after firing. Important phenomena were surface tearing and bulk lamination. Price and Reed (1983) studied conditions at the surface during the extrusion of electrical porcelain and indicated that there was slip at the wall of the die-land (Figure 3.1). Slip was enhanced by the segregation of fine particles and liquid binder into a surface layer less than a few micrometers in thickness. Benbow et. al. (1987) studied the paste rheology with a ram extruder in which there is convergent flow followed by extrusion through a tube of constant diameter, the die-land (Figure 3.1). The pastes were made from particles of known size distribution and liquids of known rheology. The flow was described successfully by regarding the convergent flow to be governed by a yield mechanism and the plug flow in the die-land by wall resistance. This results in two extrusion parameters namely the yield value and wall stress. Seven different alumina pastes were studied and found to comply with the proposed flow model. The two parameters are dependent on velocity. In each instance, the velocity effect is proportional to the effective viscosity of the liquid phase. Particle size distribution and liquid phase content each have a substantial effect on the extrusion parameters. Benbow et. al. (1991) studied the flow of pastes through dies of complicated geometry. They extended the relationship between pressure drop and extrudate velocity during flow from a circular barrel into a circular die-land to characterise the flow of paste through non-circular barrels and die-land sections that are square, triangular and rectangular. It was found that generally theory and experiment are in satisfactory accord. Conditions under which particle size affects paste flow are discussed. Flow instability causing the surface fluff and the adverse effect of sharp corners on the smoothness of the product are reported. The list of references surveyed is long, but it is neither the intention of this research to investigate the properties of extrusion, nor to study the large number of mathematical equations which are applicable to extrusion and dies. Empirical practice and an understanding of some basic extrusion variables similar to that of pottery work are sufficient to formulate a suitable paste for making the desired monolith.

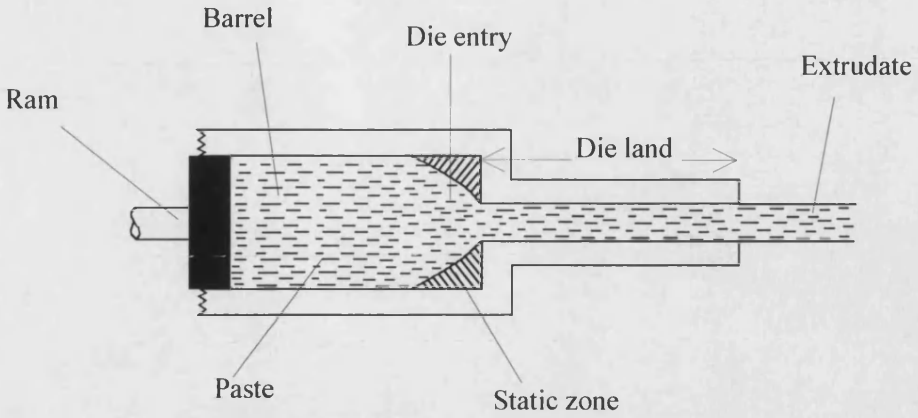

Figure 3.1 Terminology for paste extrusion through a cylindrical die

The manufacture of a successful monolith depends on obtaining the proper balance between the starting powder, the plasticiser, the mixing and de-watering procedure, and the die design. These aspects are all discussed in the following sections.

3.4.1 Starting Powder

The quality of the powder is related to the size, shape and size distribution of the constituent particles. To ensure success, it is important to use a fine powder as then the tendency of phase separation during extrusion is reduced and the rate of sintering is enhanced. A limited particle size distribution ensures that particles can be mixed symmetrically and the particle packing density is increased (Benbow et. al., 1987).

3.4.2 Plasticiser

The plasticiser should impart clay-type properties to the mass being extruded, such as relatively high plasticity and binding effects. Experimental work is required to arrive at the proper plasticiser for use with each individual composition to be extruded. High plasticity and low water content are desirable to avoid solid-liquid phase separation/surface tearing during extrusion, and to ensure safe drying. During preliminary paste formulation, several clays, such as ball clays with the commercial names of Hyplas 71 and CCB, and bentonite, were blended to find the appropriate plasticity for extrusion. After numerous trials, only bentonite was selected for this research.

Bentonite, derived from volcanic ash, belongs to the family group of montmorillonites which contain the finest minerals of clay. Montmorillonite minerals are unique in that water molecules can enter between the sheets of oxygen molecules lying on both sides of the sandwich, and cause a 'swelling' effect. Swelling, as well as the extremely small particle size of bentonite (substantially less than 0.5 micrometers, i.e., some 20 times less than that of the ball clays) makes it a very effective plasticiser. It is readily available locally at very low cost and, being non-adsorbing, it has been used in

the commercial granulation of adsorbents such as disclosed by Seidel and Staudte (1993) and Mitchell et. al. (1961).

3.4.3 Blending and De-watering

Experience with extrusion processing has shown that intensive mixing is desirable. Intimate mixing of the powders in the right proportion and in the right degrees of fineness will produce a mixture of the right water content and consistency required for the extrusion process. Thorough mixing is essential if the body is to have the same proportions throughout and hence behave consistently. In the research described in this thesis, the blending technique was adapted from the potter's traditional slip-mixing technique which is a free-flowing of suspension of powder in water. The technique was slightly modified to speed up de-watering by the addition of the right amount of water such that a thick slip of high viscosity is obtained. This method enabled very intimate mixing to be carried out using the available agitator.

De-watering is the process of removing part of the water from the wet-mixed bodies to a carefully controlled extent. In this study water filtering was by gravity and under room conditions. Careful attention was paid to the texture of the drying cake, and constant kneading of the soft paste in the filter bag was necessary to ensure uniformity. After checking moisture and hardness, the filter cake is either stored in a humidified container or used directly. Storing the cake over a long period of time enables it to mature and this results in a homogeneous body with high plasticity (Ryan, 1978).

3.4.4 Extrusion Press

Extrusion equipment may be of two types, the piston extruder and the auger extruder. A horizontal, non-deairing single auger extruder is used in the research described in this thesis. Extrusion may be more successful with a vacuum facility in order to remove air from the material during extrusion and so to minimise phase separation. Extrusion is possible only when there is sufficient fluid to overcome the

intraparticle friction and the frictional forces between the die walls and the powder. Thus, careful control of powder quality, water content and plasticity are essential.

The flow of paste through the conveying zone and through the shaping zone is the result of a force applied to the extruded mass that causes its forward movement. A Bingham plastic material requires an initial force to start the flow. Forward movement depends on friction between the clay and the barrel lining to restrain it from turning with the auger. To move forward the paste must either slide on the surfaces of the auger or shear at intermediate surfaces between the auger surface and the interior barrel surface. The paste is discharged as a single rope at the tip of the auger. The twisting of the auger causes the rope to be discharged as a coil, while the spacer and die tapers cause compression of the coil into a single column of extrudate. The coils may fracture in low-plasticity materials to produce a series of concentric and tapered cones, which are then forced together during travel through the die taper. Thus auger extrusion has the potential of producing a number of weakness planes that may develop into flaws in the finished product.

The design of extrusion dies is a state-of-the-art. As with the selection of plasticisers, nearly any die design could be made to work given sufficient time to experiment with it. Various monolith dies which have developed empirically, are described in the literature (Bagley, 1973, Refractory Co., 1977, Ogawa and Asami, 1981 and Yamamoto et. al., 1982). A typical extrusion die for a square monolith is diagrammatically represented in Figure 3.2.

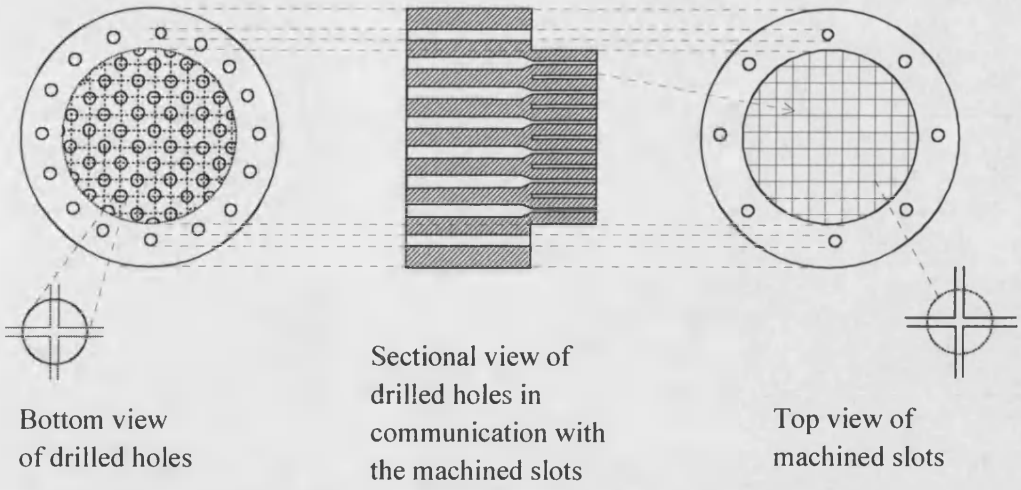

Figure 3.2 A schematic diagram of a die for shaping a square channel monolith

All the previously described forming processes require the further steps of satisfactory drying and firing to produce a sound monolith. Often these processes can be the critical ones in determining the outcome.

3.4.5 Drying

Drying is concerned with the removal of water by evaporation. Drying the green monolith at room temperature is a very delicate process which is essential prior to firing. It is most important that the water is removed slowly and uniformly to avoid problems like warping. During drying there is a continuous movement of water from the internal pores between the particles to the surface until the particles come into contact with each other. This is observed as a shrinkage on the monolith. A fast rate of evaporation from the surface would lead to a greater moisture gradient and hence greater drying stresses, with the higher risks of cracking or warping. The slow drying of the monolith is controlled by applying a thin layer of non-adsorbing powder on the monolith surface

followed by draping a polythene sheet around it in storage. When the green body is dry enough it is ready for firing.

3.4.6 Firing

Firing is the process which converts the green body of the monolith which is still weak and soft, into strong, hard monolith. The initial firing rate must be low to remove traces of pore water without rupturing the structure. The maximum temperature for the firing process is the highest temperature at which the molecular sieve is structurally stable. For silicalite the temperature stability is up to 800°C (UOP, 1992). The minimum firing temperature for the bonded zeolite is that temperature at which the product will dry to give a bound product and at which the loss of the water of hydration of the zeolite will be effected. For best results, the clay-bonded silicalite monolith should be fired at the temperature where the clay undergoes an irreversible phase change (Mitchell et. al., 1961). Bentonite undergoes an irreversible phase change above 700°C, which is below the temperature limit of the silicalite. Thus, when bentonite is used as the plasticiser, the bonded product is dried and calcined at 750°C. Seidel and Staudte (1991) show that calcination temperatures of 550-650°C are sufficient to give the mechanical stability and sorption properties of the molecular sieve studied.

3.5 Experimental Fabrication of Silicalite Monolith

This section describes the apparatus and the methodology used to produce silicalite monolith using the extrusion method. Before attempting to form the silicalite adsorbent, several clay types, e.g. Hyplas 71 and CCB, were used to develop a workable procedure, and also to gain familiarity with the problems associated with extrusion. The design of the die was purely empirical, and was refined at this preliminary stage. After numerous trials, the methodology was applied to mixtures of silicalite and bentonite.

3.5.1 Material and Apparatus

The extrusion was carried out horizontally with a single-auger extruder obtained from Baughan Ltd. A schematic drawing of the extruder is shown in Figure 3.3. This extruder was not equipped with a de-airing facility and, being of single auger design, the force that could be applied to the paste was limited. The paste quality was therefore adjusted to enable extrusion with minimum force, i.e, a paste of relatively high plasticity was required.

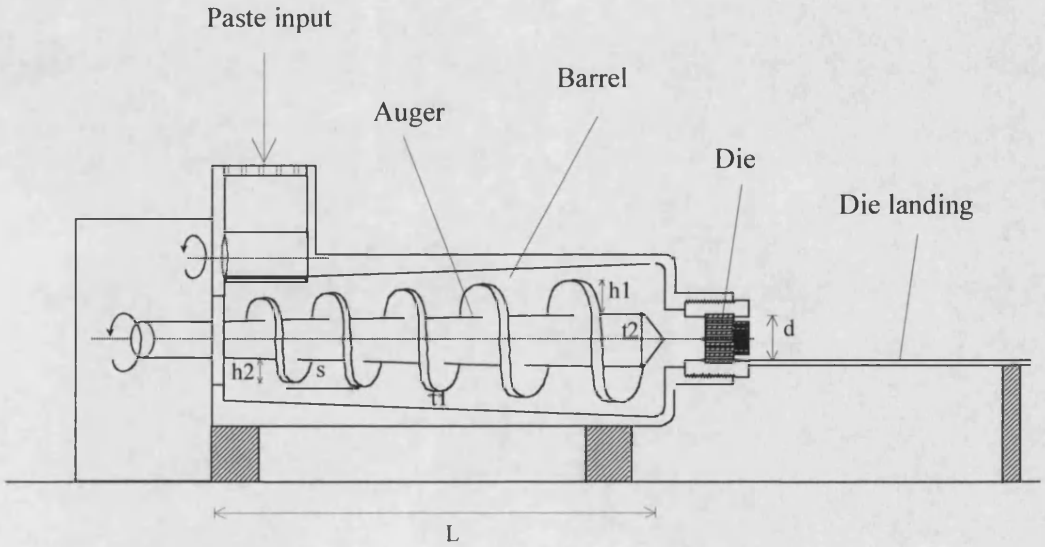

(Dimensions: L=410mm, h1=4.65mm, h2=7.15mm, t1=1.0mm, t2=37.9mm, s=49 mm andd=21mm)

Figure 3.3 A schematic diagram of the extruder

Several dies of different channel geometry were made from brass by the University Workshop, as illustrated in Figure 3.4. These dies were tested and refined in extrusion trials. Their dimensions are given in the Appendix VI. The workability of the dies greatly depended on the texture of the paste, and in most cases high plasticity ensured good success in monolith forming. It was found to be important that all sharp edges were smoothed to avoid surface tearing during the extrusion process.

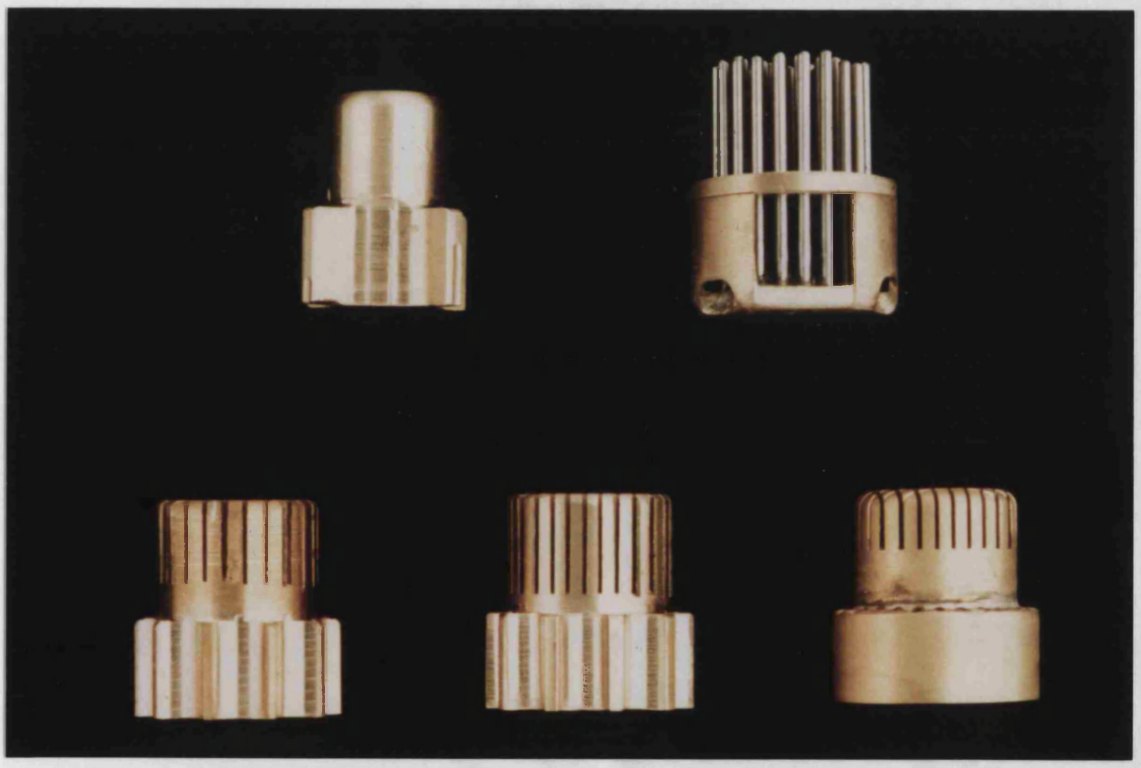

(Scale 1:1)

Figure 3.4 Photograph of the dies

A Hobart model AE200 industrial 3-speed food mixer was used to aid the powder mixing process. The agitator used was a balloon whisk. To ensure thorough mixing, and to avoid overloading the mixer motor, a relatively large proportion of water was added at this stage.

A Carbolite furnace was available for the firing stage. This was capable of operating at temperatures up to 1000°C and was equipped with a temperature programmer. Inlet ports enabled the supply of compressed air or other gases.

The adsorbent material used for the monolith was 200 mesh silicalite powder obtained from UOP (see Chapter 2). The binding agent selected was bentonite obtained from Bath Potters Ltd., the properties of which are tabulated in Appendix VII. Other clays, such as the commercial CCB and Hyplas 71, were also purchased from Bath Potters Ltd. for trial runs and their properties also are described in Appendix VII.

3.5.2 Procedure for Monolith Fabrication

The set of methods established for the making of silicalite monolith were as follows:

3.5.2.1 Paste Formulation

Pastes were prepared by weighing individual portions of silicalite powder and bentonite clay. The compositions of paste prepared are given in Table 3.2. These powders were then blended together by sieving in a British Standard sieve of 120 mesh. The sieving also had the effect of removing any large particulate material. A total of 1.0 kg of powder was prepared for each paste.

The powders were then poured into the bowl of the food mixer and a measured quantity of distilled water was added to make a thick slip. The amount of water added depended on the bentonite content. The higher the clay content, the larger was the amount of water required to produce a mixable slip. Mixing was carried out for at least

one hour in the Hobart blender, initially at the lower speed and then at the higher speed once a relatively smooth slip had been obtained.

When a homogeneous mixture was achieved, it was necessary to break down any agglomerates using a squeegee to force the slurry through a sieve of 120-mesh. During this stage, air pockets were also removed. The smooth slip was next poured into a filtering bag and allowed to de-water by gravity until an extrudable, 'cheese-hard' cake was formed.

The dewatering process usually required 2 to 4 weeks depending on the water content. Throughout this period the bag was regularly checked and kneaded to ensure that the cake dried uniformly. It was generally found that the paste was of the right plasticity and consistency when the water content was approximately 35-40% of the total weight of the paste. The 'cheese-hard' dewatered cake was removed from the filtering bag and kneaded thoroughly.

Vigorous throwing and kneading of the filtered cake ensured a uniform paste mixture, de-aeration and consolidation of the paste. Any large air pockets in the paste could adversely affect its mechanical strength. The paste was finally allowed to mature in a humidified enclosure for at least one week. This was to improve plasticity, homogeneity and workability of the cake.

Before extrusion, a wire was used to cut across the cake to check for any air pockets. Finally, the paste was kneaded and divided into small lumps.

Table 3.2 Compositions of pastes

Paste type	Silicalite powder (wt %)	Bentonite (wt %)	Distilled water (as wt % of solid)	Pore forming agent (as wt % of solid)
A	70	30	150	-
B	80	20	130	-
C	85	15	110	-
D	90	10	100	-
E	80	20	130	10
F	85	15	110	10

3.5.2.2 Extrusion Process

Before any extrusion could be carried out, all internal surfaces of the extruder that would come into contact with the paste were cleaned. These included the auger, internal barrel wall, and die. It was important to ensure there were no particulates left from a previous run as these would cause blockage of the flow of paste through the die, resulting in cracking of the extrudate.

The extruder chamber was first packed with the paste by plugging the exit with a solid-block, rotating the auger at 10 rpm and pushing in lumps of paste with a solid bar. Then the die was placed with care on the extruder such that it was aligned with the axis of the auger. (An off-centre die would encourage the monolith to twist in one direction or another, and might introduce strains that would later appear as cracks).

Extrusion was initiated by increasing the auger speed to 30 rpm while manually feeding lumps of paste continuously into the chamber until a monolith of the desired length was formed. Care was taken to ensure continuity of the feed in order to avoid entrapment of air and separation of the paste, which would eventually result in an unsuccessful extrusion. It was also essential to keep the operation as short as possible. The rise in temperature of the metal parts of the extruder and over-long exposure of the

paste to the environment could cause problems such as cracking due to localised changes in the water content of the paste.

3.5.2.3 Sectioning of Monolith

The green monolith was cut to the desired length using a length of 0.8 mm diameter nichrome wire. The sectioned monolith was then transferred with great care from the die landing on to a working surface.

3.5.2.4 Drying

Special techniques were developed following numerous trials, to minimise problems of warping and cracking during the drying stage. After extrusion, the green monolith was immediately covered with a thin layer of silicalite powder, sprinkled from a 60 mesh sieve, in order to reduce the rate of water evaporation from the outer surface. The monolith was then transferred with great care into a perforated 1 inch OD stainless steel tube that had been axially sectioned into two halves. The tube was designed to provide ease of handling, reduce drying and prevent the green monolith from warping. At this stage of the work, the least human contact with the extrudate is desirable, as uneven handling may cause stresses to build up in the green product that might result in cracking during the final firing stage.

3.5.2.5 Firing

The final part of the fabrication process involved the high temperature treatment of the extruded monolith. The monolith was fired in the stainless steel support according to the temperature programme shown in Figure 3.5. During the initial stage, any remaining water is removed from the pores of the adsorbent particles. The temperature was increased very slowly to ensure the uniform removal of water and to reduce any risk of cracking. The second stage was to oxidise any organic or impurities present in

bentonite. Compressed air was supplied at a rate of 1-2 l/min to ensure complete combustion. During the third (highest temperature) stage, fusion of the monolith occurred, imparting the necessary mechanical strength to the structure. The temperature programme was determined empirically to ensure a crack-free monolith.

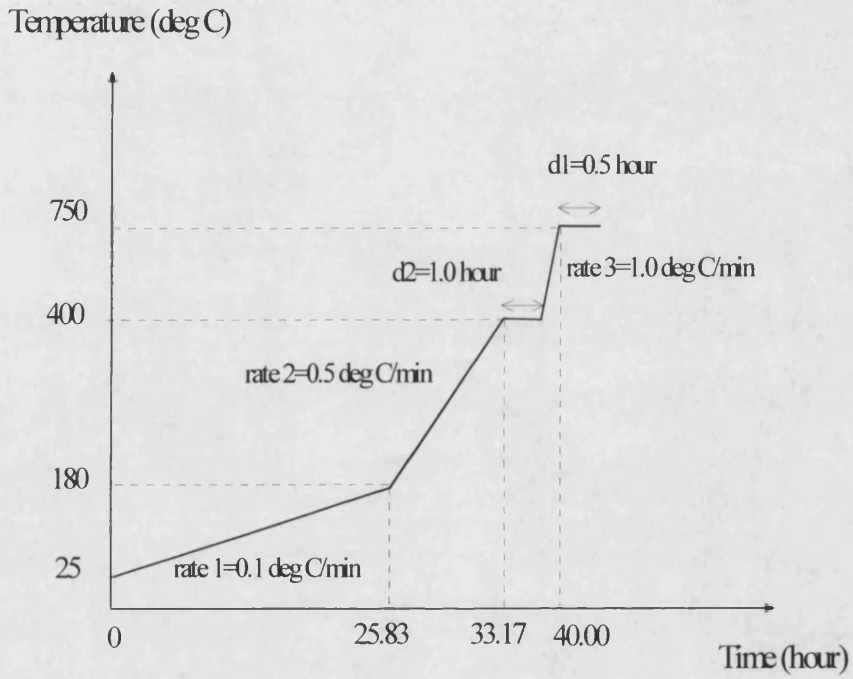

Figure 3.5 A plot of the firing rates

3.6 Results of Fabrication

Zeolitic monoliths containing various compositions of silicalite, i.e. 70, 80, 85 and 90 weight % silicalite were manufactured. The fired monoliths were white in colour and of various channel shapes including square and circular. Both the single and multichannel monoliths having length up to 1 m, and diameters of approximately 2 cm and 4 cm, were prepared. A photograph of these monoliths is shown in Figures 3.6. These monoliths of silicalite were characterised for their physical and adsorption properties using the methods described in the subsequent sections of this thesis.

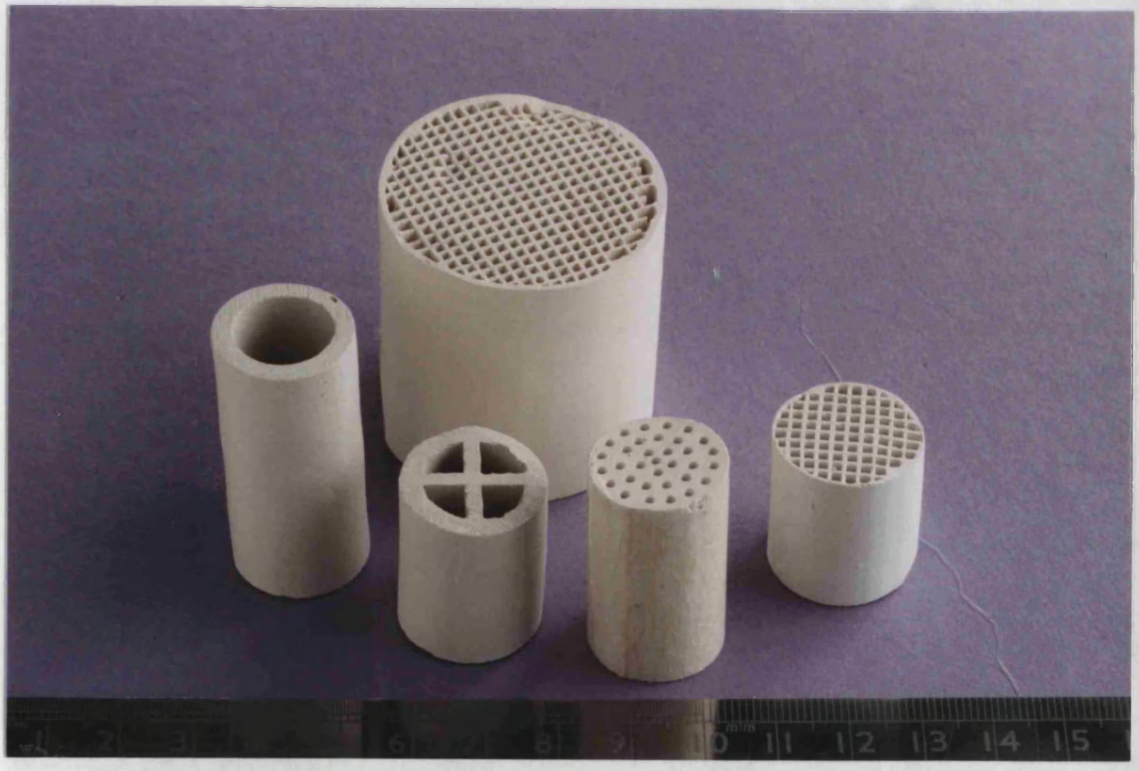

Figure 3.6(a) Photographs of the manufactured silicalite monoliths

Figure 3.6(b) Photographs of the manufactured silicalite monoliths

3.7 Problems Arising in Extrusion

Some of the problems encountered during the forming of silicalite monoliths by extrusion are discussed below.

3.7.1 Cracking

The formation of cracks in monoliths during or soon after extrusion was a major problem. Initially, cracking was found to be due to a lack of plasticity preventing the body knitting together after being sheared by the auger and in the die. Faulty die design was another factor, resulting in tearing of edges. The cracking problem was overcome by adjusting the moisture content, by increasing the plastisicing effect and by enlarging the back orifice and smoothing the sharp edges of the die. Examples of cracks formed on a monolith are shown in Figure 3.7.

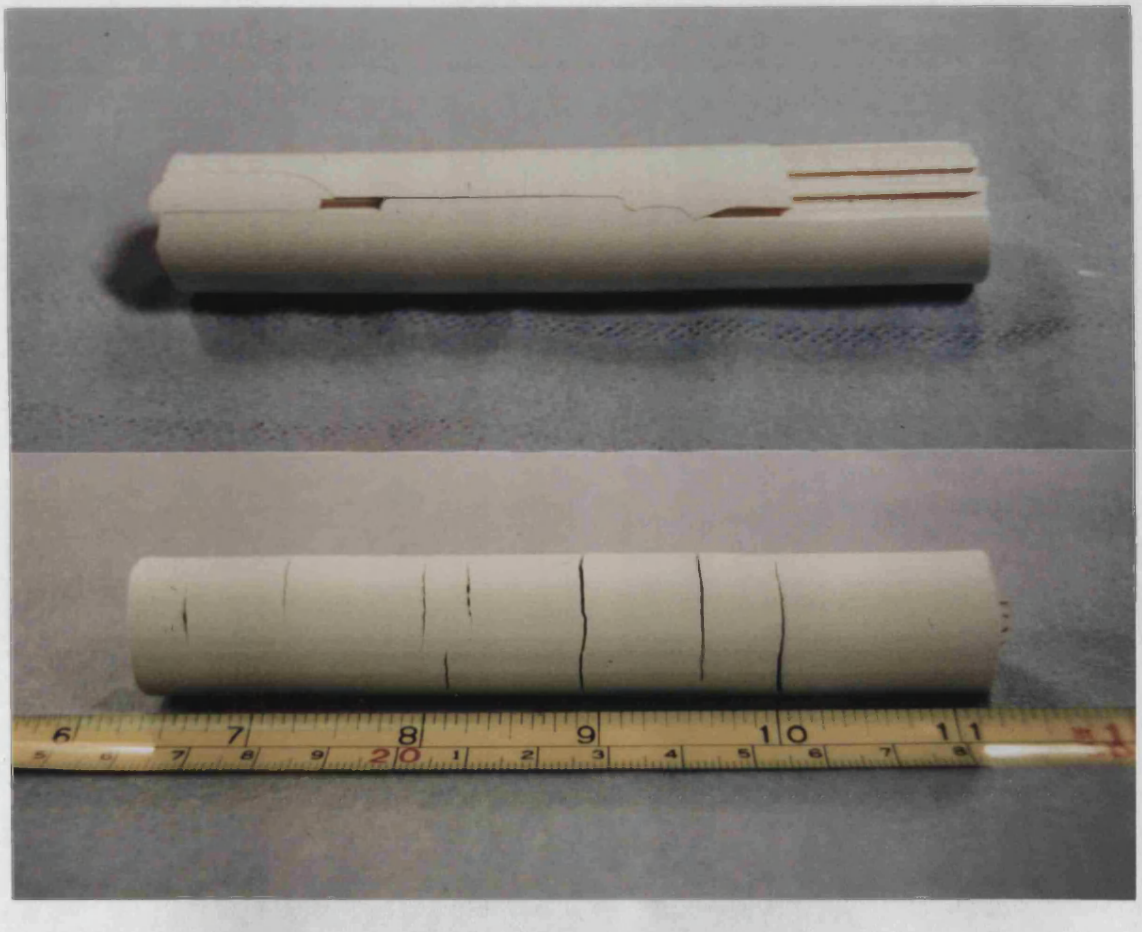

Figure 3.7 Examples of cracks formed on monolith

3.7.2 Warping

This often appears in the form of bending or bowing of the monolith tube before drying, but it can also occur during drying. It may be caused by uneven plasticity arising from unsatisfactory mixing, by hard compacted bodies or foreign matter in the die, or through careless handling. Careful and thorough mixing of the paste and scrupulous cleaning of the extruder parts were found to be essential to avoid the problem.

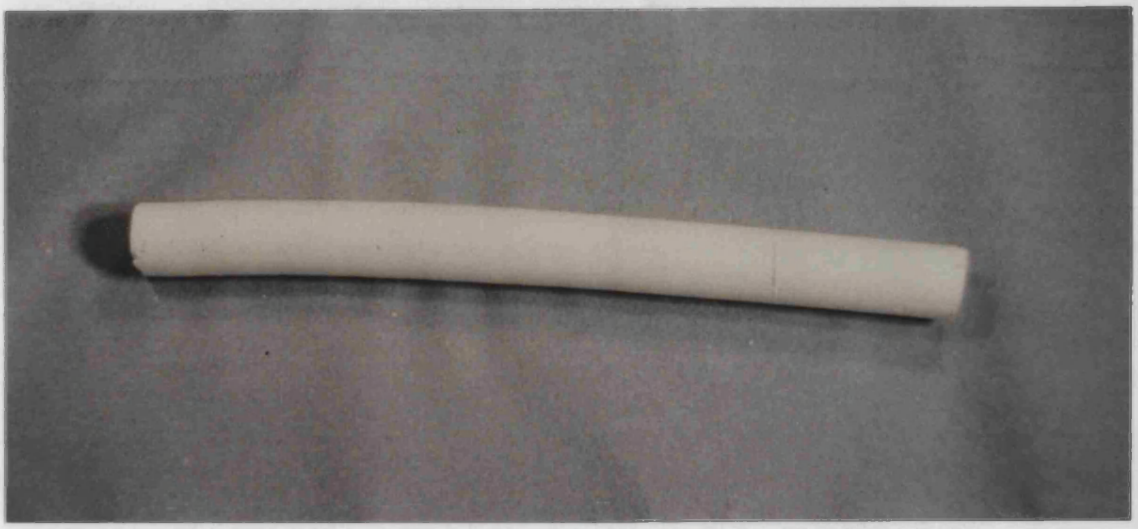

(Scale 1:2)

Figure 3.8 An example of warping formed on monolith

3.7.3 Lamination and Differential Drying Shrinkage

The particles of clay are plate-like in shape and the problem of lamination is due to the re-orientation of these plate-like particles when pressure is applied to them. The sliding of particles at the interfaces of paste and extruder/die may cause poor cohesion between adjacent streams within the extrudate. Poor cohesion may be due to alignment of particles within the extrudate or by any mechanism which inhibits the fusion of the planes. This will develop weak zones which during drying will be subjected to

mechanical stresses that can be sufficient to cause internal fracture. Elimination of lamination cracks can be accomplished by improving the drying method, changing the die design to minimise displacement, or improving the plasticity of the paste.

3.7.4 Choking of the Extruder

Here the extrusion may slow down or stop completely. The die becomes plugged with comparatively hard material, while the softer material is simply churned round inside the extrusion barrel. Possible causes are too great a moisture content, so that the body sticks to the screw instead of being propelled forward, the presence of large particles, and thixotropy of the paste which allows the body to remain very soft in the barrel where the rate of shear is high, but to harden as it approaches the die. The consequent heating of the paste in the barrel makes matters worse and it may be necessary to stop the machine and clean out the die and the extruder. Possible remedies are shortening the finishing section of the die, cooling the barrel, or increasing the speed of the extrusion auger or modifying the plasticity of the paste.

3.7.5 Eccentricity of the Cell of Monolith

This gives uneven wall thickness and would be most unsatisfactory in a thin wall monolith. The cause may be incorrect centring of the die or hard material passing through the die and displacing it. Apart from ensuring accurate centring of the die initially, it may be necessary to improve its fixing or to make the paste more plastic.

3.8 Characterisation of the Monolith

The prepared silicalite monoliths were characterised according to their adsorption breakthrough curves with propane, their crystal structure, pore size distribution and particle size. Commercial silicalite pellets were used for comparison.

3.8.1 Techniques of Characterisation

3.8.1.1 Adsorption Characterisation by the Breakthrough Curve Technique

The adsorption breakthrough curve experiment was performed on the silicalite monolith using the apparatus and procedure described in Chapter 2. Adsorption experiments were carried out to test the consistency of the formulation technique and the experimental repeatability. Two separate beds of square-channel monoliths which were prepared from different batches of paste, *viz.*, Batchs 1 and 2, consisting of similar silicalite:clay contents, i.e. 80:20 weight percent, were tested in the adsorption apparatus by determining the propane breakthrough curve. A comparative test was conducted using a packed-bed of the commercial beads of silicalite (1.0 x 1.18 mm mesh). The weights of the two beds were the same (i.e. 56.70 g) and 1000 ppm of propane in 500 cm^3/min of nitrogen was used as the feed.

3.8.1.2 Structural Characterisation by X-ray Diffraction Analysis

The aim of this study is to investigate the effect of high temperature treatment on the crystallinity of silicalite. The crystal structure of the silicalite monolith was analysed using the X-ray diffractometer, model Philips PW1710, with scan step size of 0.01 and scan angle of 5-60. The same technique was used on the commercial silicalite pellets and the silicalite powder. The effect of temperature on these materials was studied by heating them to various temperatures and carrying out further analyses. All adsorbent

materials were cleaned with distilled water and degassed in the oven overnight at 150°C. The materials were crushed in a pestle and mortar to obtain fine powders for the analysis.

3.8.1.3 Micropore Characterisation by Nitrogen Adsorption-Desorption

The objective of this analysis is to measure the microporosity and total pore volumes of the manufactured silicalite monoliths, commercial silicalite pellets, and silicalite powder. A Micromeritics surface area/pore volume analyser, model ASAP 2001 Micropore, was used to conduct the investigations. This technique measures the nitrogen adsorption isotherm at the temperature of liquid nitrogen. The instrument is supplied with software packages for computing the micropore data from the measured nitrogen isotherms using several models including BET and Langmuir, and the manufacturer default settings on the calculation parameters were used. Samples were thoroughly cleaned with distilled water and regenerated at 300°C overnight prior to analysis. Analysis was carried out on about 0.10 g of sample and the degassing procedure was performed at 300°C under vacuum followed by the nitrogen adsorption under increasing pressures.

3.8.1.4 Morphological Characterisation by Scanning Electron Microscopy

The Scanning electron microscopy (SEM) was employed for "rough" characterisation of the monoliths and pellets. The surface structure, particle size and distribution in the matrices were observed using the SEM T330 model. All samples were cleaned and dried at 120°C overnight before the test. The sample was frozen in liquid nitrogen for 20 seconds and then sectioned using a sharp blade. A small quantity of the adsorbent was mounted on a specimen stub with a carbon adhesive. It was then coated with a thin layer of gold under 3 mbarg pressure for 3-5 minutes in the Edwards

Sputter Coater (S150B). The SEM was operated in 15 kV and micrographs were taken of a number of areas on each sample using 60 seconds exposure time.

3.8.1.5 Cold-crushing Strength

The extruded silicalite monoliths were tested for cold-crushing strength using an Instron model 1122 compressive strength tester. A method similar to that described in the literature (DeLiso, 1991) was used to obtain an average value from 10 samples of each type of square-channel monolith. These samples had been used in the breakthrough experiments (to be described in Chapter 5) and were cut into lengths approximately equal to their diameter. They were washed thoroughly with distilled water and dried overnight at 250°C. The cold-crushing strength was measured by mounting each sample between two steel platens and applying an increasing mechanical load, using a crosshead speed of 1.0 mm/min, until the structure failed. The load at rupture was recorded.

3.8.2 Results of Characterisation

3.8.2.1 Repeatability of Results and Consistency in Monolith Formulation

Results in Figure 3.9 show good reproduction of experimental data for the two monoliths. Thus there is good consistency in paste formation and monolith fabrication. The equilibrium loading of propane on the monolith (which is represented by the area above the curve) is reasonably comparable with that on the pellets thereby confirming good paste formulation and suggesting that the monolith preparation has not significantly blocked the silicalite crystallites. The comparison also indicates that the commercially produced pellets probably contained 80 % silicalite and 20 % binder by weight although this information was not made available by the manufacturers. The shallower curves for the monolith show that the rate of propane mass transfer in the monolith is slower than that in the pellets. This is probably due to the different nature of the flow through the two quite different materials. The flow in the straight channel, which is usually laminar, gives rise to a very low pressure drop (Irandoust, 1988).

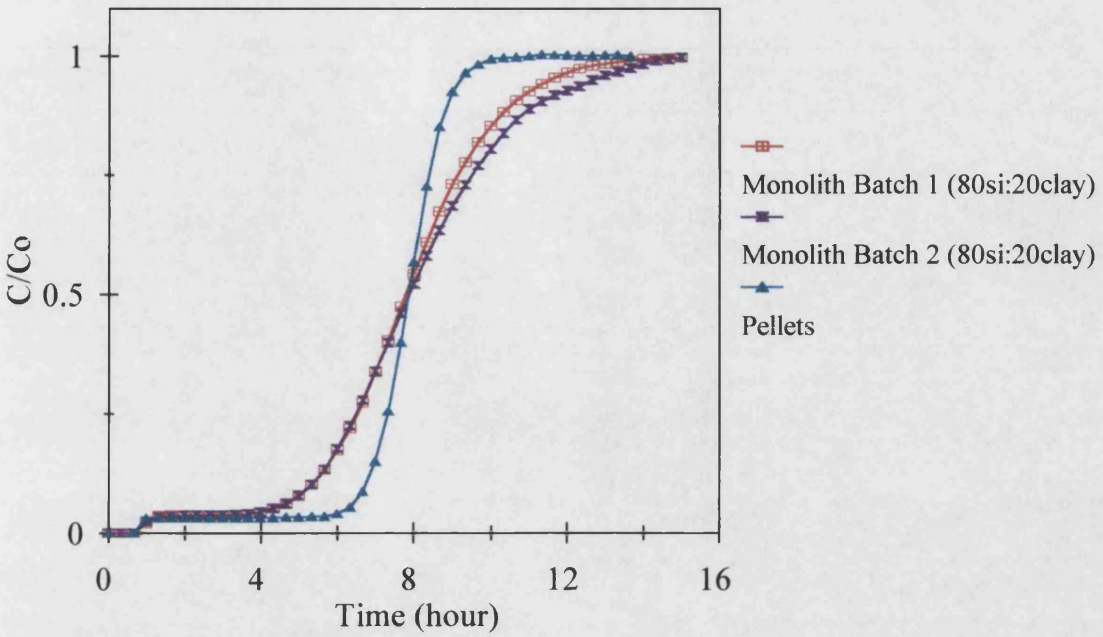

Figure 3.9 Adsorption of propane (1000 ppm) onto two identical square channel (1.25 mm square) silicalite monoliths prepared from two different batches and onto the commercial silicalite pellets (1.0 x 1.18 mm mesh)

3.8.2.2 Results of X-ray Diffraction Study

The diffraction results of the silicalite monolith (80 silicalite : 20 clay square channel type) and the powder are both in good comparison with data in the literature (Figure 3.10). The crystalline structure of silicalite did not change when it was heated to 700 and 800°C. X-ray patterns shown in Figure 3.11 indicate that the crystallinity of the silicalite monolith changed when heated to 900 and 1100°C. Hence, a firing temperature of 750°C, which has no effect on the zeolite, was selected during the formulation of silicalite monoliths.

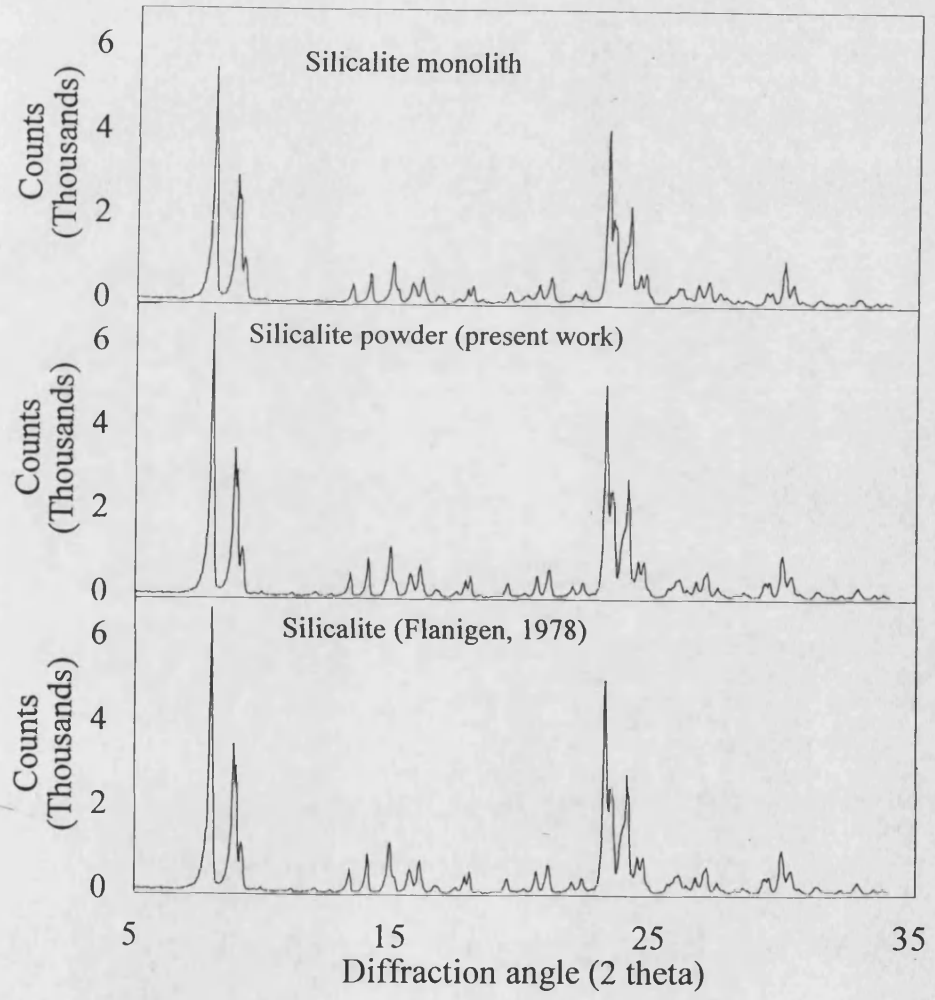

Figure 3.10 X-ray patterns for silicalite monolith, silicalite powder used in the study and that in the literature (Flanigen et. al., 1978)

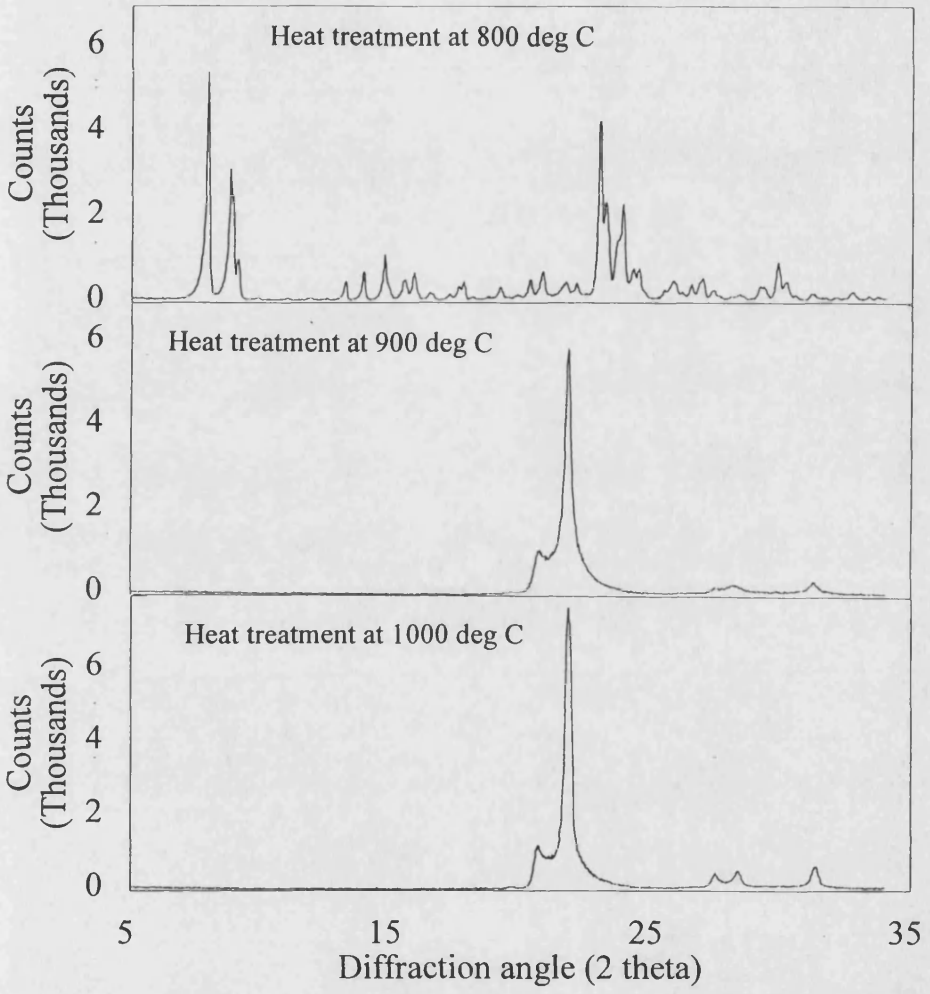

Figure 3.11 X-ray patterns for silicalite powder treated at different temperatures

3.8.2.3 Results of Micropore Measurements

The results from the micropore analysis are tabulated in Table 3.3. The average micropore diameter determined by the nitrogen adsorption at the cryogenic conditions for the silicalite monoliths is comparable with that of the powdered silicalite. This shows that the formulation technique has not affected the micropores of the silicalite significantly, e.g. by plugging the pores or disrupting the crystalline structure. The evaluation of the micropore surface area according to the BET method is reported as it is commonly used in industry for characterisation of the surface area. The results obtained from this method are lower than those based on the Langmuir model, under the same adsorption conditions. The discrepancy between the two values is due to different assumptions made in the two adsorption models. The BET isotherm (Brunauer et. al., 1938) based on physical adsorption assumes the formation of multiple adsorption layers while the Langmuir model is valid only for the formation of a single layer. The pore volumes calculated by the total pore model for the pellets are generally higher than for the monoliths. The micropore volume and diameter estimated by the Howarth-Kawazoe model are approximately the same for both the monoliths and pellets (Table 3.3).

Table 3.3 Results of micropore measurements of silicalite monoliths, powder and pellets

Adsorbent type	Methods of calculation				
	BET	Langmuir	Total Pore	Horvath-Kawazoe	
	Surface area (m^2/g)		volume (cm^3/g)	volume (cm^3/g)	diameter (nm)
Manufactured silicalite monoliths:					
Square channel thin wall 80si:20clay (wt) %	297	400	107	0.1400	0.560
Square channel thin wall 85si:15clay (wt) %	300	401	119	0.1449	0.560
Square channel thin wall 90si:10clay (wt) %	326	433	120	0.1559	0.560
Square channel thin wall 80si:20clay + 10 (wt) % pore agent	300	409	112	0.1531	0.550
Square channel thin wall 85i:15clay + 10 (wt) % pore agent	315	434	114	0.1573	0.550
Commercially available silicalite :					
Powder	342	451	130	0.1668	0.530
Pellets (1.10 x 1.18 mesh)	291	386	186	0.1407	0.510
Pellets (2.0 x 2.8 mesh)	299	396	192	0.1442	0.540

3.8.2.4 Results of Electron Microscopy Observation

Figures 3.12 and 3.13 show the particle distributions on the outer surface of the monolith and of the pellets, respectively. The monolith channel surfaces can be observed to consist of a layer of smooth crystallites with most of the cubic surfaces facing outwards (Figure 3.12). This is a characteristic of the extrusion process, where the particles tend to laminate and align themselves during pressure application. The surface of the pellets exhibits greater roughness with clusters of crystallites. The crystals on the monolith surface are relatively free from any impurities (Figure 3.12) when compared with the pellets which have amorphous particles distributed in the matrix (Figure 3.13). Figure 3.14 (at a lower magnification) shows the different particle arrangement on the external wall (lower section of the photograph) and internal wall (upper section of the photograph) of the square channel monolith. A closer packing can be seen at the outside compared to the inside. Figure 3.15 shows the more open structure which is obtained when 10 wt. % of a pore forming agent is incorporated into the monolith.

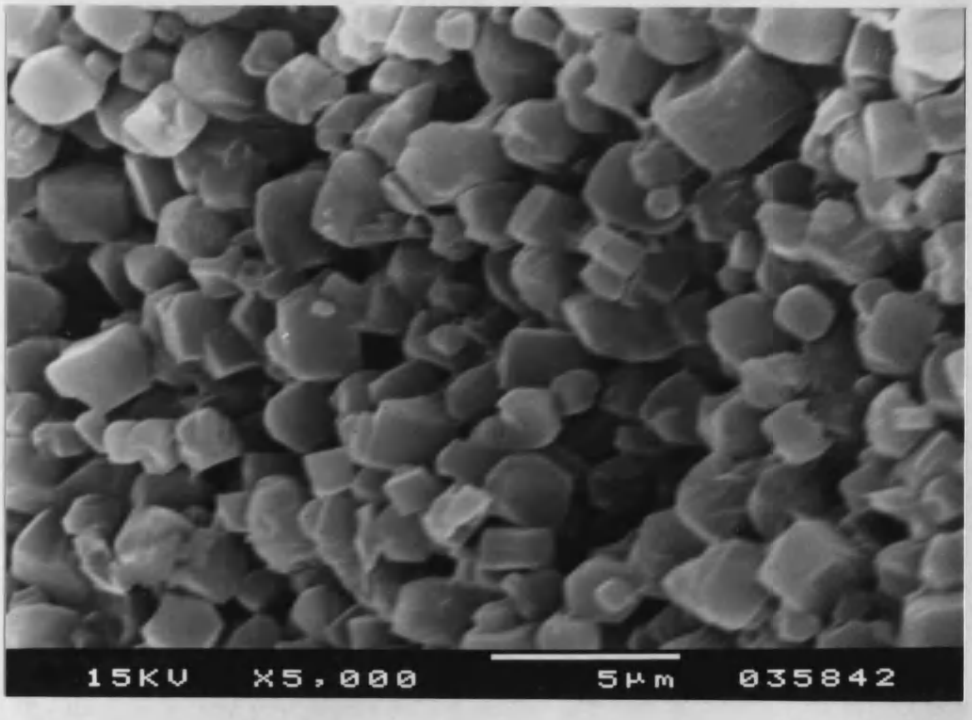

Figure 3.12 SEM photograph at square channel monolith wall (80si:20clay wt. %)

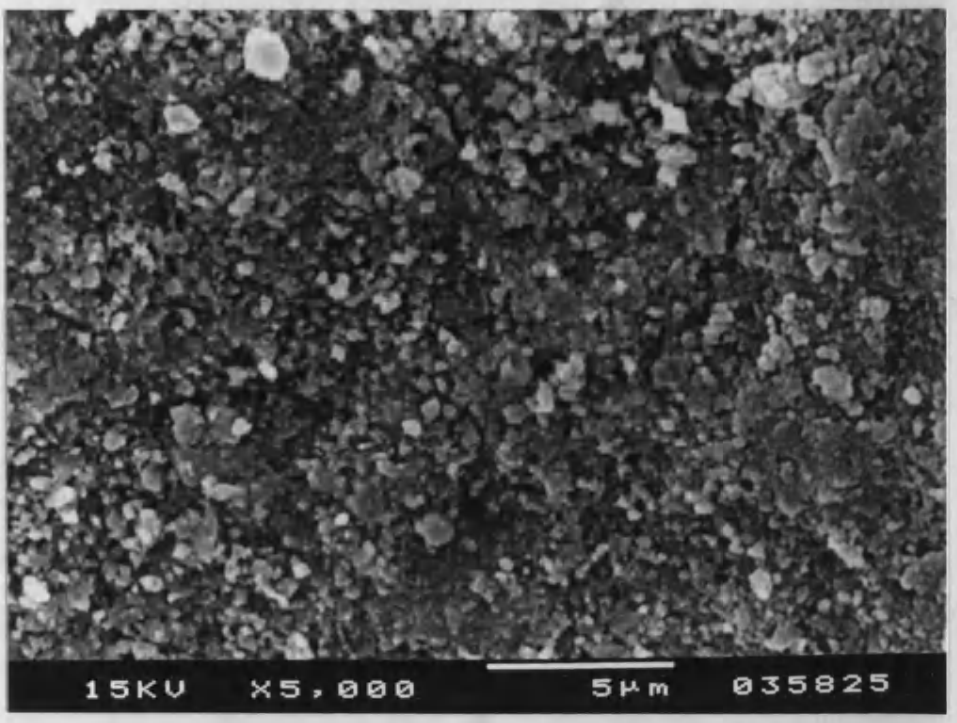

Figure 3.13 SEM photograph at pellets wall (1.0 x 1.18 mm)

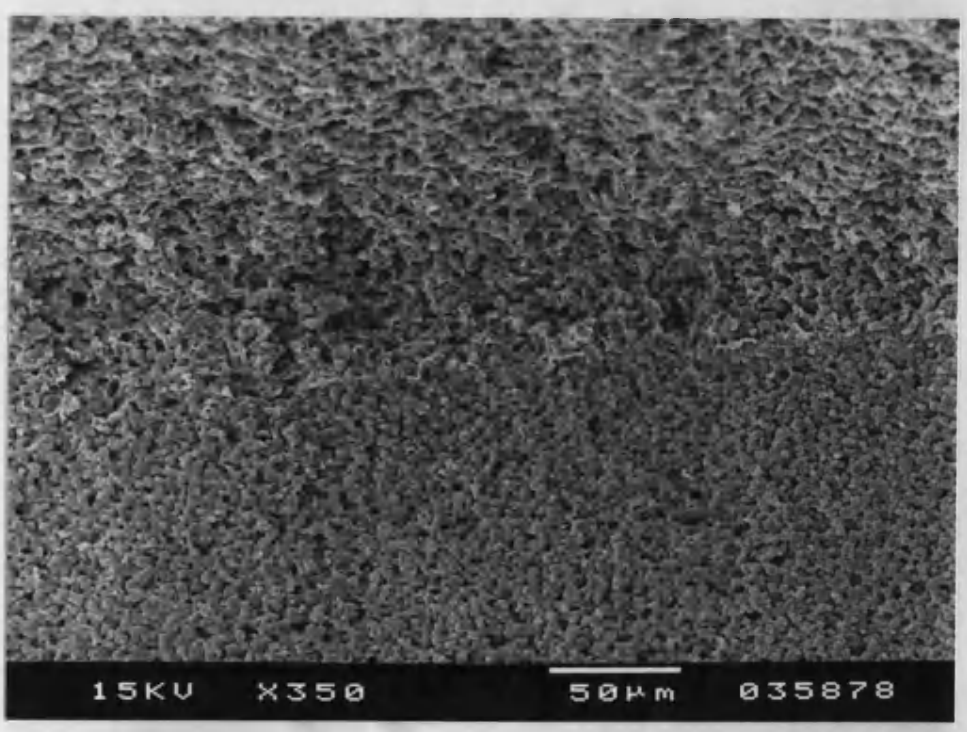

Figure 3.14 SEM photograph at square channel monolith wall (90si:10clay wt. %)

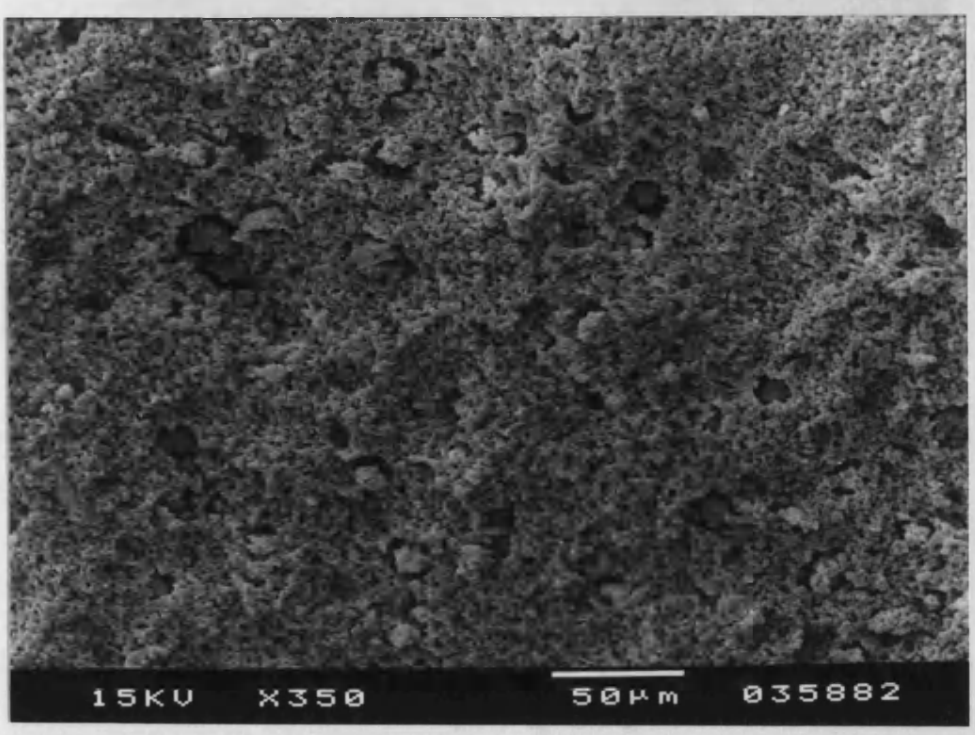

Figure 3.15 SEM photograph at square channel monolith wall (80si:20clay + 10 wt. % pore forming agent)

3.8.2.5 Results of Cold-crushing Strength

The cold-crushing strengths are shown in Table 3.4. Data obtained from literature (DeLiso, 1991) for activated carbon monolith samples made using various organic binders and monolith geometries are also listed for comparison. The results show that the monolith composed of 80:20 weight percent of silicalite to clay, and of the thick wall geometry has the highest resistance to stress. The weakest structure was the monolith of composition 90:10 weight percent of silicalite to clay. When comparing silicalite and activated carbon monoliths of similar structure, the silicalite monolith demonstrates values of crush strength which are in no case inferior to those of activated carbon and are in most cases distinctly superior.

Table 3.4 Results of crushing strength test on silicalite monoliths

Adsorbent type	Cell density (cells/cm^2)	Wall thickness (mm)	Cold-crushing strength (MPa)
Square channel monoliths :			
Thick wall 80si:20clay (wt) %	27	1.0	17.64
Thin wall 80si:20clay	28	0.59	9.98
Thin wall 80si:20clay (+ 10% pore forming agent)	30	0.58	6.62
Thin wall 85si:15clay	27	0.59	7.28
Thin wall 85si:15clay (+ 10 wt % pore forming agent)	28	0.55	6.45
Thick wall 90si:10clay	25	0.64	4.28
Activated carbon monoliths[3.1] :			
CI-170-1	62	0.15	4.37
CI-170-2	62	0.15	1.27
CR-170	31	0.38	1.13
CL-170	62	0.15	1.75
CM-170	62	0.15	1.27
CN-179	62	0.15	1.31
SAMPLE-4	31	0.38	6.88

[3.1] Data obtained from DeLiso (1991).

3.9 Optimisation of Monolith Design by Breakthrough Curve Analysis

This section is concerned with the optimisation of monolith designs based on the analyses of the propane adsorption breakthrough curves. The design considerations are the monolith physical structure (channel shape and wall thickness) and monolith compositions (silicalite:clay: pore forming agent).

The apparatus and experimental procedure described in Chapter 2 were employed for the investigation. A total gas flowrate of 500 cm^3/min was used and the weight of adsorbents was kept constant. Analysis of the breakthrough curves will be dealt with in more detail in Chapter 4, and so this section is concerned only with the breakthrough time and the sharpness of the curve. The geometric properties of monoliths and pellets are calculated using equations shown in Appendices VIII and IX, and a summary of the analyses is presented in Table 3.5. The monoliths prepared for the optimisation study are divided into the following catagories :

- different channel geometry, *viz.*, square and circular.

- different wall thickness for square channel geometry, *viz.*, thin- and thick wall.

- various silicalite contents in thin wall square channel, *viz.*, 80, 85 and 90 % by weight.

Comparison of the breakthrough behaviour in monoliths and packed beds was also carried out as follows :

- square channel monolith made of 80 wt. % silicalite versus packed-bed of pellets (mesh 1.18 x 1.0 mm).

- square channel monolith made of 90 wt. % silicalite versus packed-bed of pellets (mesh 2.0 x 1.70 mm).

The effect of incorporating a pore forming agent during the fabrication of the square channel monolith was studied. 10 % of starch was added to increase the porosity of the monolith. The following comparisons *vis a vis* breakthrough were made:

- square channel monolith made of 80 wt. % silicalite versus that made with 10 (total wt.) % of pore forming agent.

- square channel monolith made of 85 wt. % silicalite versus that made with 10 wt. % of pore forming agent.

Table 3.5 Physical properties of silicalite monoliths (The adsorbent weight is kept constant, i.e. 56.70 g)

	Monolith							Pellet (mm mesh)	
Property	Square channel		Circular channel	Square channel		Square with 10% pore-agent		1.0 x 1.18	1.70 x 2.0
	Thin wall	Thick wall	-	Thin wall	Thin wall	Thin wall	Thin wall	-	-
Si:clay wt. %	80:20	80:20	80:20	85:15	90:10	80:20	85:15	-	-
Bed length (cm)	29.30	21.80	21.10	29.10	29.0	33.5	31.0	18.50	19.50
Bed diameter (mm)	19.64	18.94	19.76	20.0	20.75	18.90	19.81	21.10	21.10
Wall thickness (mm)	0.59	1.00	-	0.59	0.64	0.58	0.55	-	-
Channel size (mm)	1.25	1.00	1.40	1.25	1.27	1.22	1.20	*Pellet size:* 1.09	1.85
Cell density ($cell/cm^2$)	28	27	11	27	25	30	28	*Pellet density:* 1.715	1.384
Specific surface area (m^2/m^3)	1476	828	473	1476	1393	1505	1568	2813	1949
Voidage	0.440	0.500	0.1656	0.440	0.442	0.460	0.470	0.4889	0.3992

3.10 Results of Optimisation by Breakthrough Curve Analysis

3.10.1 Adsorption onto Monoliths of Different Channel Shape

Monoliths of different channel geometry were prepared using the same silicalite:clay mix, i.e. 80:20 wt. % ratio. The length of the circular channel monolith was much shorter than that for the square channel bed for the same bed weight (see Table 3.5). A comparison of the breakthrough curves of the two monolith types is shown in Figure 3.16. The breakthrough performance of the square channel monolith is considerably better than the circular channel monolith, indicating the importance of its effective surface area in creating access to adsorption sites.

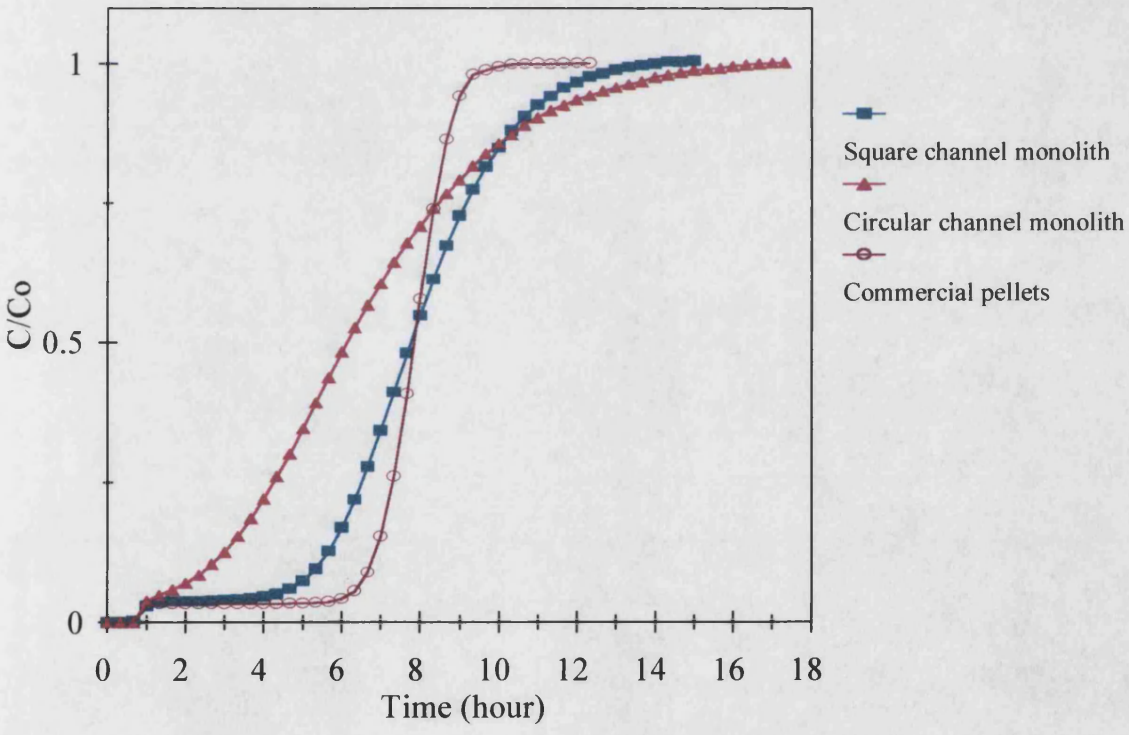

Figure 3.16 Adsorption of propane (1000 ppm) onto silicalite monoliths (80si:20clay wt. %) of various channel shapes (1.25 mm square and 1.40 mm circular channels) and onto commercial silicalite pellets (1.0 x 1.18 mm mesh)

3.10.2 Adsorption onto Square Channel Monoliths of Different Wall Thickness

From the above channel shape comparison, it is concluded that a square channel monolith shows a much better dynamic adsorption of propane due to its higher cell density and larger effective surface area. It would be desirable to produce a square channel monolith of higher cell density and much thinner wall. However this would require a very precise and fine die design. This work could not be carried out due to a lack of precision machinery for making the required die. Furthermore, a more powerful extruder would be required to create the much greater extrusion force necessary for the paste to flow through the finer orifices. Instead of producing a finer die design, a die for forming a thicker wall square channel monolith was made in order to test the effect of wall thickness (see Table 3.5).

Figures 3.17, 3.18 and 3.19 show the breakthrough curves of propane, at concentrations of 1000, 5000 and 10,000 ppm respectively, on square channel monoliths of two different wall thickness. The breakthrough curves are steeper for the thin wall monolith, this performance being consistent with the higher cell density. Also, thinner walls provide easier access to adsorption sites due to a lower pore diffusion resistance.

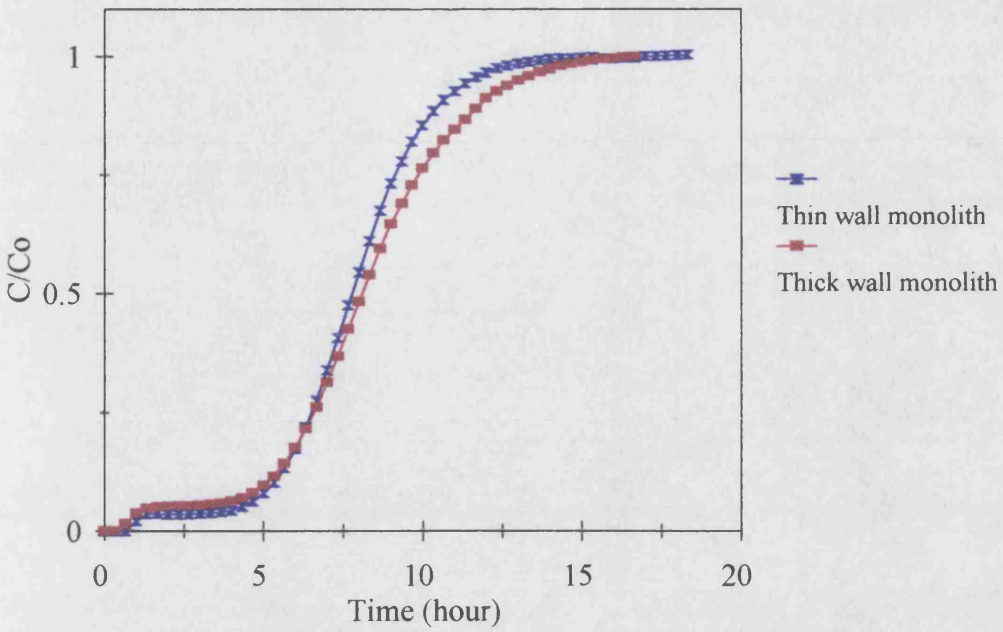

Figure 3.17 Adsorption of propane (1000 ppm) onto silicalite monoliths (80si:20clay wt %) of thin wall (0.6 mm) and thick wall (1 mm)

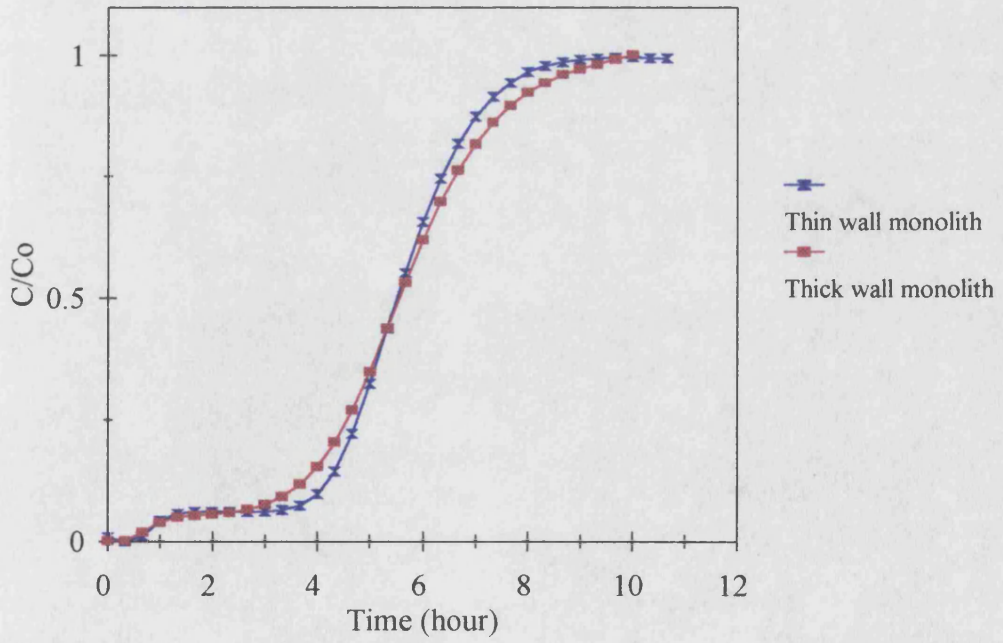

Figure 3.18 Adsorption of propane (5000 ppm) onto silicalite monoliths (80si:20clay wt %) of thin wall (0.6 mm) and thick wall (1 mm)

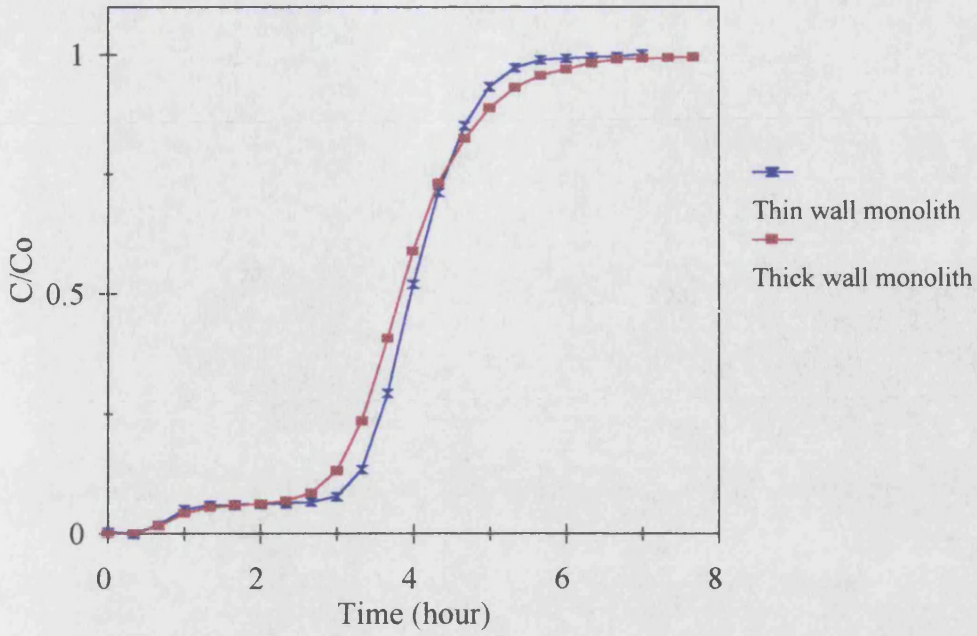

Figure 3.19 Adsorption of propane (10,000 ppm) onto silicalite monoliths (80si:20clay wt %) of thin wall (0.6 mm) and thick wall (1 mm)

3.10.3 Adsorption of Propane onto Square Channel Monoliths of Different Silicalite:Clay Ratio

Monoliths consisting of various silicalite:clay ratios were compared for their adsorption of propane. Breakthrough curves are shown in Figure 3.20. The breakthrough time and equilibrium loading, which is the area above the curve, increased with the percentage of silicalite in the monoliths (The weight of the monoliths is kept constant, i.e. 56.70 g). This clearly demonstrates the importance of the availability of adsorption sites as more silicalite crystals were present on the external surfaces of monolith. These results also show that the clay binder has not contributed to the adsorption of propane.

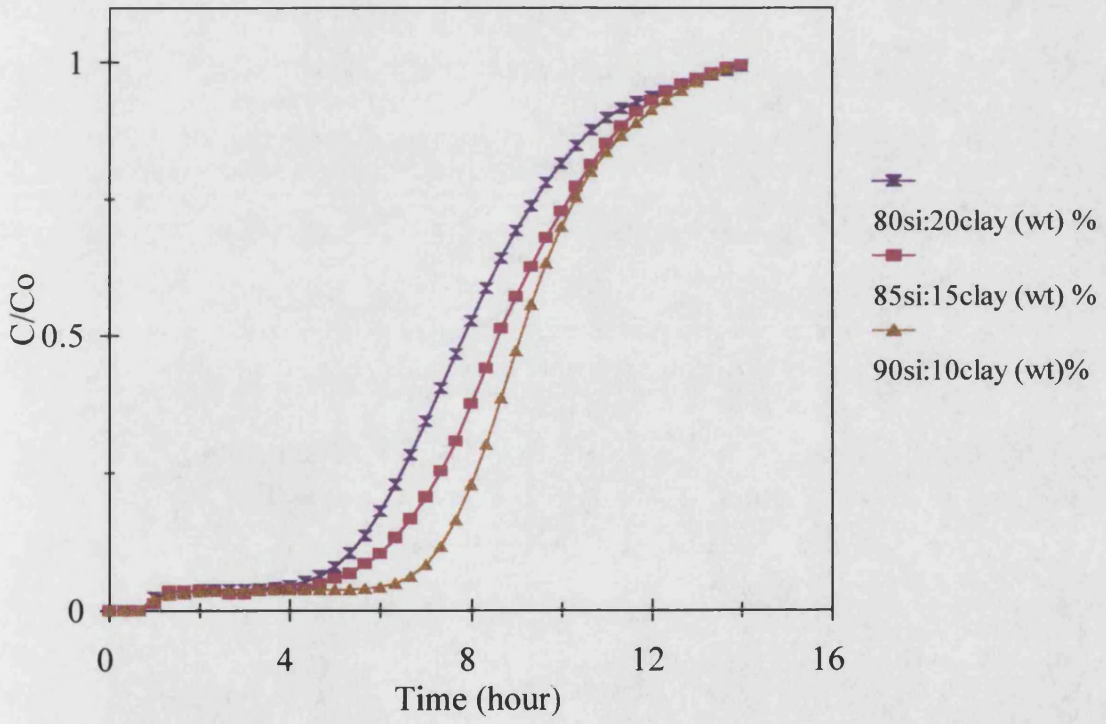

Figure 3.20 Adsorption of propane (1000 ppm) onto square channel monoliths of various silicalite:clay ratios

3.10.4 Breakthrough Comparison of Monoliths with Packed Beds

The monoliths used in this study were of the square channel thin wall type. The breakthrough curves in Figures 3.21 and 3.22 show that the packed-bed of 1.18 x 1.00 mm mesh pellets has a sharper curve than that of the 2.0 x 2.8 mm mesh as well as that of the monolith. The curve sharpness for the monolith comprising 90si:10clay is comparable with that of pellets of 2.0 x 2.8 mm mesh (Figure 3.22). This shows that there is a considerable resistance to mass transfer in the monolith comprising 80si:20clay, probably due to the consolidated packing of particles. As discussed previously, the flow in a monolith is normally laminar and hence the curve is broader than that of the pellets.

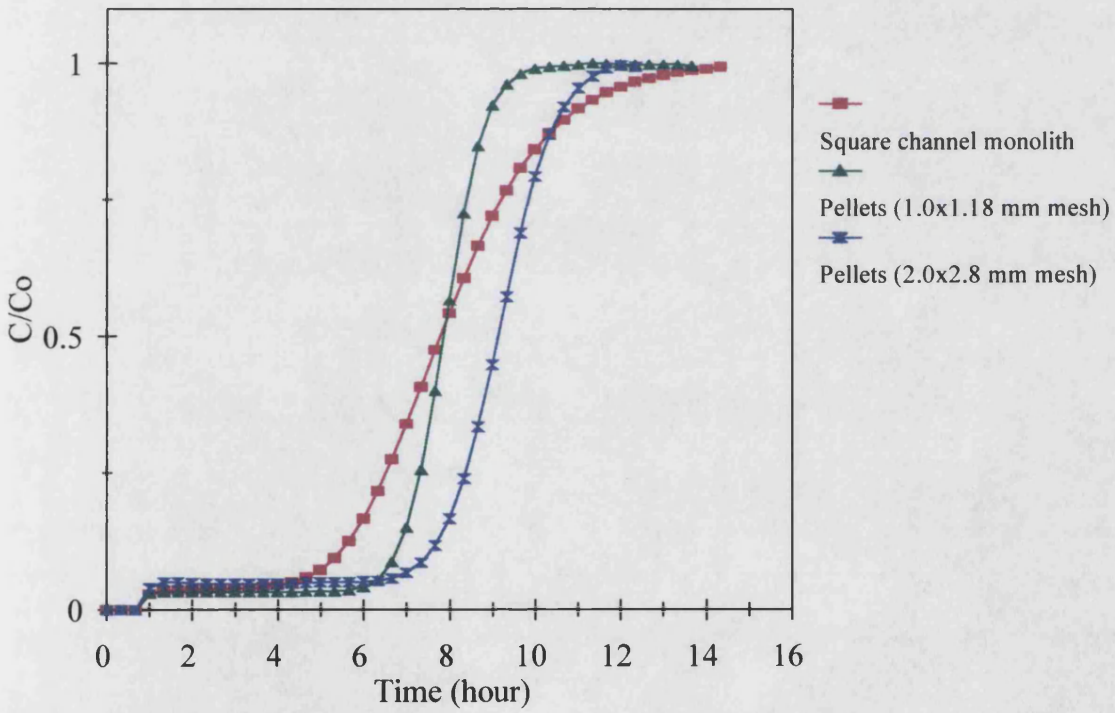

Figure 3.21 Adsorption of propane (1000 ppm) onto pellets of various sizes and thin wall square channel monolith of 80si:20clay wt. %

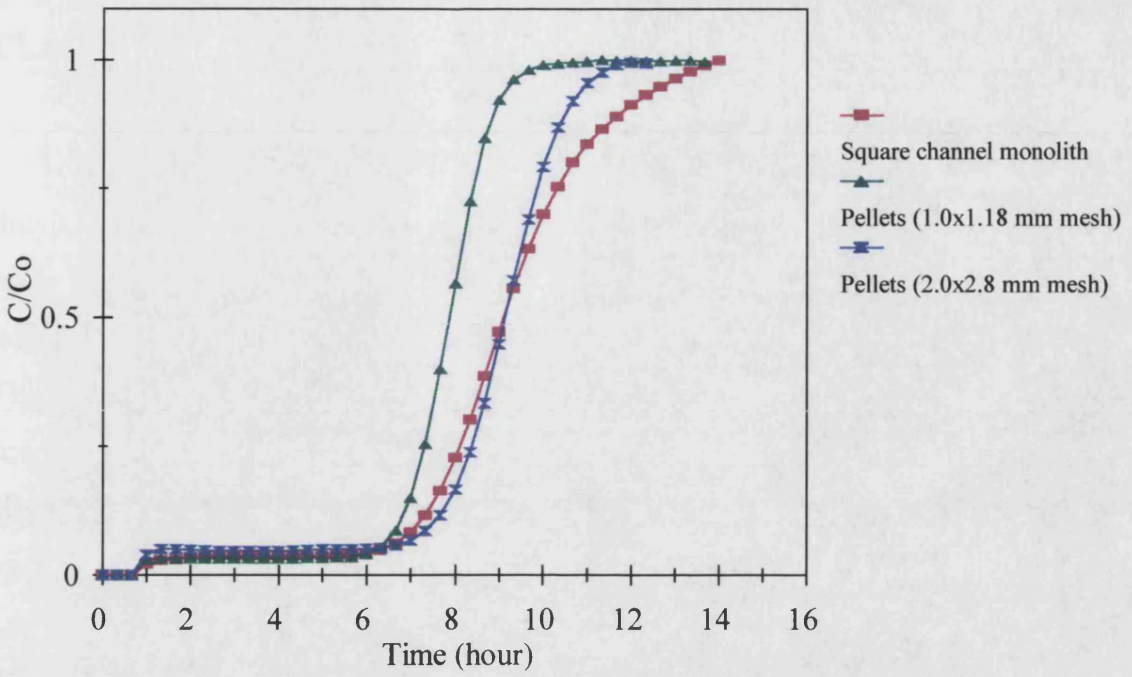

Figure 3.22 Adsorption of propane (1000 ppm) onto silicalite pellets and thin wall square channel monolith of 90si:10clay wt. %

3.10.5 Effect of 10 Weight % Pore Forming Agent in Square Channel Monoliths

From the above packed-bed to monolith breakthrough comparisons, it was decided to increase the porosity of the monolith by incorporating a pore-forming agent such as starch into the paste formulation. Only 10 wt. % of the pore-forming agent was added so as not to affect the structural strength. Breakthrough curves are shown in Figures 3.23 and 3.24 for various silicalite contents. They reveal that the pore agent has improved slightly the breakthrough time but not the sharpness of the breakthrough. The slight improvement in the breakthrough time may be due to the monoliths with pore agent being longer (Table 3.5) and/or silicalite crystals being more exposed to propane, i.e. the structures being more open. The breakthrough curve for the monolith of 85si:15clay is comparable with that of 90si:10clay, helping to justify the explanation. The attempt to increase the macroporosity was not quite successful and probably a much higher percentage of pore agent is required. However there is a consideration of loss of mechanical strength when more pore agent is used. The failure of using corn flour to increase macroporosity may be due to the fact that the organic compound was combusted at a temperature (~150°C) lower than the firing temperature of the green monolith (i.e. 650°C). The pores formed by the combustion of the pore agent at the lower temperature may be closed by the coalescence of fused clay particles during the calcination of the green monolith.

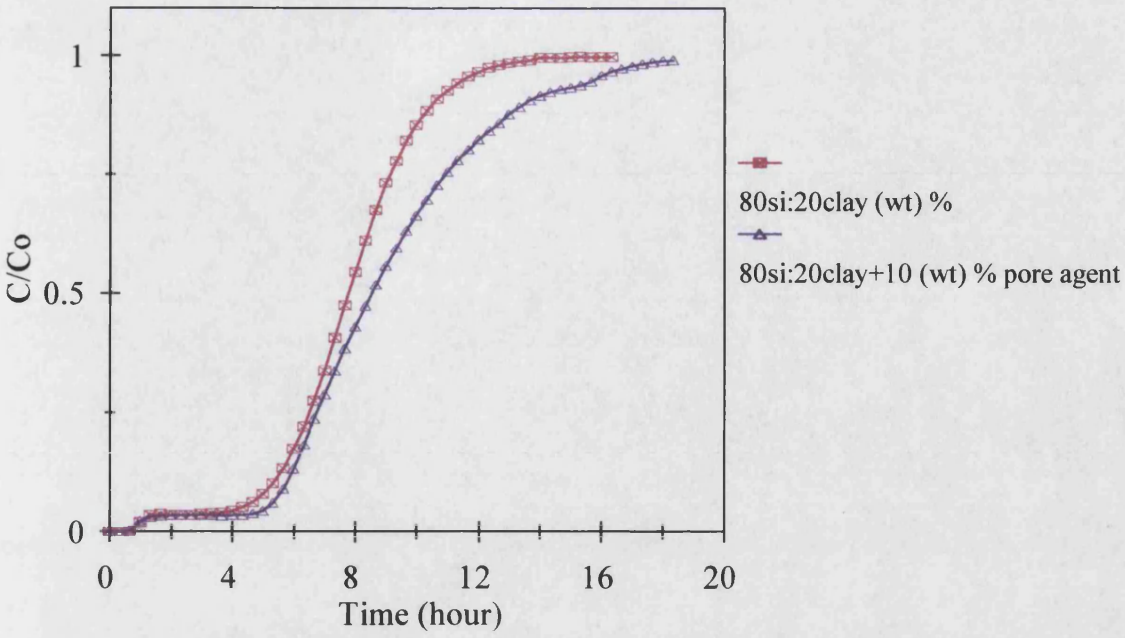

Figure 3.23 Effect of 10 wt. % of pore forming agent in a square channel monolith of 80si:20clay wt. % on propane (1000 ppm) adsorption

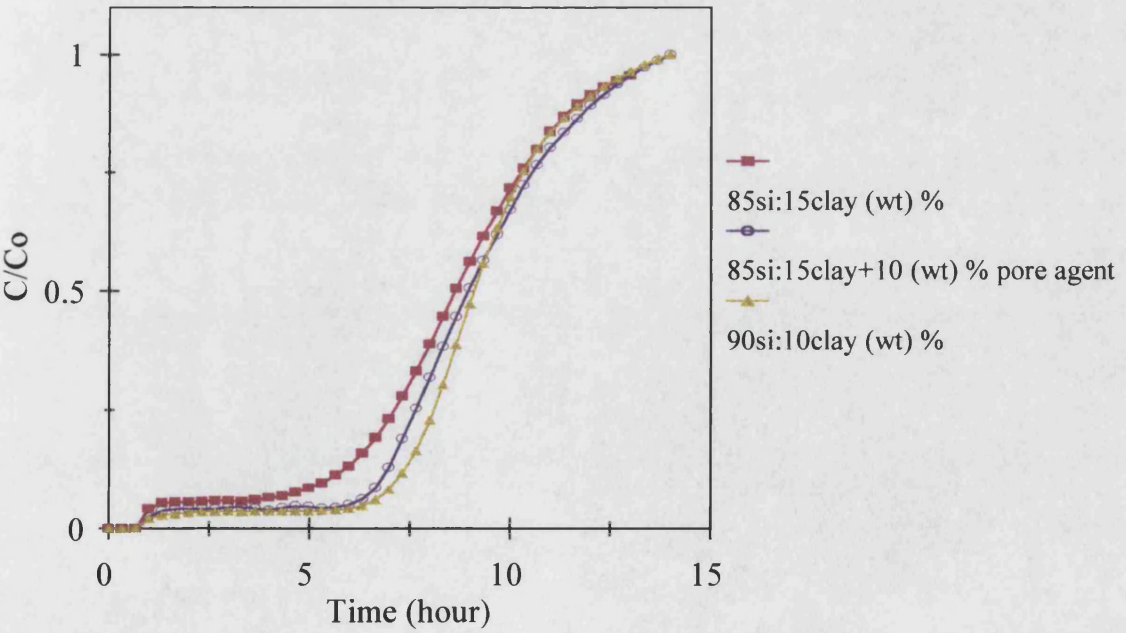

Figure 3.24 Effect of 10 wt. % of pore forming agent in a square channel monolith of 85si:15clay wt. % on propane (1000 ppm) adsorption

3.11 Conclusions

A chemical formulation and set of working procedures have been developed for the manufacture of a low pressure drop silicalite monolith suitable for the control of VOC emissions. Multichannel monoliths of various channel shapes (i.e. square and circular channels), diameters (i.e. 2.0 and 4.0 cm) and lengths up to 1.0 m were successfully manufactured. Monoliths containing up to 90 wt % silicalite and with cell densities up to 28 cells/cm^2 and adsorbent wall thicknesses down to 0.6 mm were produced. Although silicalite is generally more expensive than activated carbon, the use of bentonite as a dual-function binder and plasticiser adds little to the cost of raw materials. By contrast, the manufacture of activated carbon monoliths, which are unable to withstand the traditional firing or sintering steps, requires the use of comparatively expensive organic binders (e.g. acrylic resins, PVA, etc.) and plasticisers (e.g. cellulose ethers and derivatives) (DeLiso, 1991). These organic compounds might themselves become a source of pollution, especially if accidentally subjected to a temperature in excess of 300°C. Regeneration of carbon monoliths may therefore be possible only at relatively low temperatures, and may be incomplete. The novel silicalite monolith is free of organic material and can withstand temperatures of up to 750°C.

Silicalite monoliths exhibit lower thermal expansion than activated carbon monoliths, and may therefore be expected to have better mechanical resistance to thermal cycling, such as that encountered in vehicle exhausts. This could lead to a longer operating life.

Breakthrough studies have shown that a silicalite monolith with square channels performs better than a monolith with circular-channels. Thick wall square-passage monoliths are easier to fabricate than thin wall varieties and have higher mechanical strengths during the green state and after firing. Moreover, the length of a thick wall monolith is more comparable with that of a packed-bed containing the same weight of adsorbent. The thick wall monolith fulfils the criteria for manufacturing viability, bed length, robustness as well as adsorption kinetics. Despite these positive aspects, future work should be directed at making a monolith of much higher cell density and thinner

wall for a considerable improvement in adsorption performance, whilst maintaining the structural integrity of the monolith.

The optimal paste composition was found to be 85 % silicalite : 15 % clay with 10 % pore forming agent. This composition was found to be superior to 80 % silicalite : 20 % clay (with and without pore agent) and to behave comparably with a 90 % silicalite : 10 % clay monolith. Use of a pore forming agent necessitates a longer bed for the same weight of adsorbent. There is scope for further research into ways of increasing the intercrystalline porosity without compromising the mechanical strength. Techniques might include the use of different powder sizes and firing temperatures (Hamaguchi et. al., 1989).

Although a high silicalite content in the monolith is preferred, this has to be traded against mechanical strength and ease of manufacturing. The use of different clay binders, powder sizes and die geometries could be explored in future research.

Chapter 4

Results of Dynamic Adsorption of VOCs onto Packed Beds of High Silica Adsorbents

4.1 Introduction

This chapter describes the results of experimental investigations into the dynamic adsorption of VOCs onto packed beds of high-silica zeolites. The adsorption breakthrough curves are reported and discussed for single component adsorption. The effect of water vapour on the performance of the packed-bed is also described. From the breakthrough curves, the equilibrium loading of the bed, and the length and velocity of the mass transfer zone have been calculated. These results will be used as a basis for comparison with later work using the monolith adsorbent (to be described in Chapter 5).

4.2 Summary of Experiments

The experimental procedures described earlier in detail in Chapter 2 were used to investigate the breakthrough of VOCs in packed beds of high silica zeolite adsorbents. A series of tests was performed using either ZSM-5 or silicalite, under various conditions of VOC feed concentration and flowrate, and employing various bed lengths. A summary of the various experimental conditions is given in Tables 4.1-4.3 while the geometric characteristics of the packed beds are given in Table 4.4. Experiments with ZSM-5 pellets were carried out only with propane, whereas silicalite beads were used with propane, ethanol and methylene chloride. Further investigations were carried out to determine the effect on VOC adsorption of the presence of water, either preadsorbed onto the bed, or added as vapour into the feed stream. The desorption of propane from a packed bed of ZSM-5 was also investigated. The desorption experiments were carried out immediately following the adsorption experiments. All the experiments were performed at 25°C and atmospheric pressure. The abbreviation "$MeCl_2$" used in Tables 4.1 and 4.2, represents methylene chloride while the term

preconditioned (Table 4.2) refers to premoisturising of a bed with 70 % relative humidity (RH). The VOC concentration described in this Chapter is in ppm volume.

Table 4.1 A summary of the experimental conditions for single component adsorption study (at 25°C and atmospheric pressure)

Packed-bed number	Test run no.	Total flow (cm^3/min at STP)	Feed concentration (ppm)	
P104	1	470	Propane :	1000
(ZSM-5)	2	470		2500
	3	470		5000
	4	470		7500
	5	470		9900
P102	6	500	Propane :	1000
(Silicalite)	7	500		2500
	8	500		5000
	9	500		7500
	10	500		10,000
P101	11	500	Ethanol :	5300
(Silicalite)	12	500		18,500
	13	500		44,000
P101	14	500	$MeCl_2$:	9000
(Silicalite)	15	500		20,000
	16	500		44,000
P103	18	500	Propane :	1000
(Silicalite)	19	1500		1000
	20	3000		1000
P103	21	500	Propane :	5000
(Silicalite)	22	1500		5000
	23	3000		5000
P101	24	500	Propane :	1000
(Silicalite)	25	500		5000
	26	500		10,000

Table 4.2 A summary of the experimental conditions for binary component adsorption study (at 25°C and atmospheric pressure)

Packed-bed number	Test run no.	Total flow (cm^3/min)	Adsorbate (ppm)	Relative humidity (%)	Initial bed condition
P101			Propane :		
(Silicalite)	27	500	1000	55	Dry
	28	500	5000	55	Dry
	29	500	10,000	55	Dry
P101			Propane :		
(Silicalite)	30	500	1000	70	Dry
	31	500	5000	70	Dry
	32	500	10,000	70	Dry
P101			Propane :		
(Silicalite)	33	500	1000	70	Preconditioned
	34	500	5000	70	Preconditioned
	35	500	10,000	70	Preconditioned
P101			Ethanol :		
(Silicalite)	36	500	5300	70	Dry
	37	500	19,000	70	Dry
	38	500	44,000	70	Dry
P101			Ethanol :		
(Silicalite)	39	500	1000	70	Preconditioned
P101			$MeCl_2$:		
(Silicalite)	40	500	5300	70	Dry
	41	500	19,000	70	Dry
	42	500	44,000	70	Dry
P101			$MeCl_2$:		
(Silicalite)	43	500	1000	70	Preconditioned

Table 4.3 A summary of the experimental conditions for desorption study (at 25°C and atmospheric pressure)

Packed-bed number	Test run no.	Nitrogen purge (cm^3/min at STP)	Concentration on previous adsorption experiment (ppm)
P104			Propane :
(ZSM-5)	44	500	1000
	45	500	2500
	46	500	5000
	47	500	10,000

Table 4.4 Properties of the packed-beds of spherical zeolites[4.1]

Adsorbent type	Silicalite			ZSM-5
Packed-bed number	P101	P102	P103	P104
Particle diameter (mm)	1.09	1.09	1.85	2.40
Weight of bed (g)	56.70	91.70	89.20	55.11
Length of bed (cm)	18.50	30.50	30.50	21.60
Diameter of bed (cm)	2.11	2.11	2.11	2.11
Specific surface area of bed (m^2/m^3)	2813	2760	1959	1446
Voidage	0.4889	0.4986	0.3957	0.4214
Bulk density, (g/cm^3)	0.8765	0.8598	0.8364	0.7297
Specific surface area of pellets (m^2/m^3)	5504	5506	3243	2500
Particle density, (g/cm^3)	1.715	1.715	1.384	1.261

[4.1] The calculations of specific surface area, voidage, bulk and particle densities are presented in Appendix IX

4.3 Theory of Calculations

Important properties of the adsorption bed such as the equilibrium loading, the mass transfer zone (MTZ) length and velocity were evaluated directly from the breakthrough curves. The following sections describe the methods used to determine these parameters.

4.3.1 Equilibrium Loading

A typical breakthrough curve is represented by Figure 4.1 which shows the breakthrough time, t_b, and the equilibrium time, t_{eq}. The areas above the curve are denoted by A and B, and that below the curve by C. The equilibrium loading, q_{eq}, is defined to be the amount of the adsorbate on the adsorbent in equilibrium with the feed concentration. A material balance on the adsorbate up to the period of complete breakthrough leads to the following equation,

$$q_{eq} = \frac{F_{sorbate}}{W}(t_{eq} - \int_{t=0}^{t=t_{eq}} \frac{C}{C_o} dt) \qquad (4.1)$$

where $F_{sorbate}$ is the adsorbate feed flowrate, W is the adsorbent weight, C_o is the initial feed adsorbate concentration and C is the adsorbate concentration in the bed effluent at any general time t. The first term on the right hand side of the equation is equivalent to the sum of the areas A, B and C of Figure 4.1, while the second term on the right hand side represents the area C. A computer program, written in Fortran, was used to determine the area C using Simpson's rule (Appendix X). According to Equation 4.1, q_{eq} was thus calculated by subtracting the area C from the total amount of adsorbate fed into the bed up to the time t_{eq}.

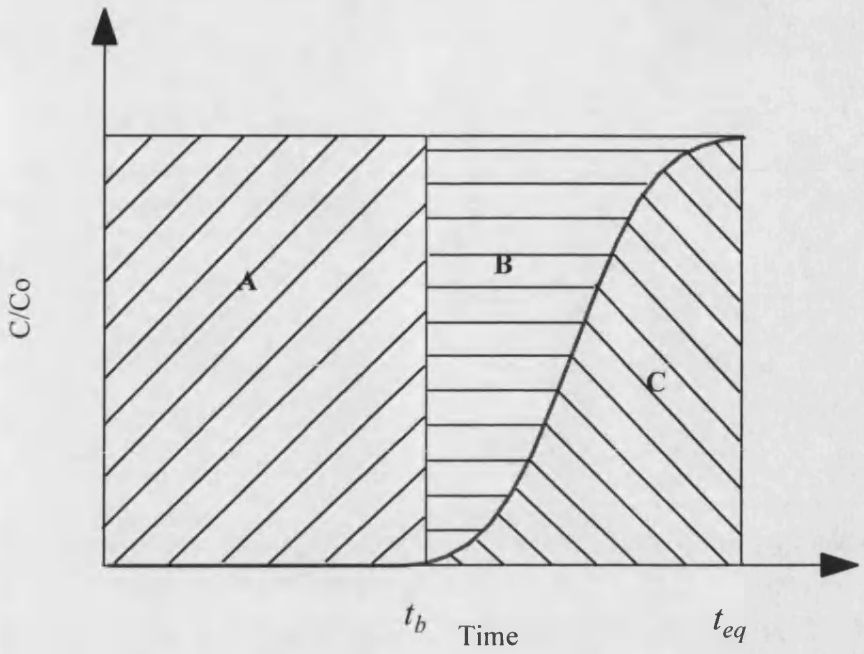

Figure 4.1 Breakthrough curve

4.3.2 Isotherm Prediction Using the Langmuir Model

Flanigen et. al. (1978) discussed the adsorption of n-hexane on silicalite and described the isotherm as being well represented by the Langmuir form. The assumptions of the Langmuir model are that:

- molecules are adsorbed at a fixed number of well-defined localised sites.
- each site can hold one adsorbate molecule.
- all sites are energetically equivalent.
- there is no interaction between molecules adsorbed on neighbouring sites.

The equilibrium data were fitted using the Langmuir equation which is of the form:

$$\frac{q}{q_{max}} = \frac{bp}{1+bp} \tag{4.2}$$

where q is the adsorbate concentration in the adsorbed phase, q_{max} is the concentration in the adsorbed phase when the monolayer is complete, p is the partial pressure of adsorbate in the fluid and b is the adsorption equilibrium constant. Linearisation of the Langmuir equation gives:

$$\frac{1}{q} = \frac{1}{(bq_{max})}\frac{1}{p} + \frac{1}{q_{max}} \tag{4.3}$$

The constants q_{max} and b were determined from the intercept and the slope of a plot of $1/q$ versus $1/p$, respectively.

Klein and Abraham (1983) have used the extended Langmuir equation to predict the adsorption of binary mixtures of ethanol and water vapours. Assuming the pore volume parameter is constant for each component, the model is given by

$$q_i = \frac{q_{max} b_i p_i}{1 + \sum_{j=1}^{N} b_j p_j} \tag{4.4}$$

where N is the total number of adsorbate species in the gas mixture. Thus, the equilibrium concentrations of the binary mixture adsorption were predicted by knowing the Langmuir constants q_{max}, b_i and b_j from the single component adsorption isotherms.

4.3.3 Mass Transfer Zone Length and Velocity

The mass transfer zone is that fraction of the bed which is partly loaded with adsorbate, in between the saturated adsorbent and the fresh adsorbent, as the adsorption front moves through the bed. Its length was calculated using the method given by Chi and Cummings (1978). For single component adsorption, the length of unused bed, LUB, and the MTZ length, MTZ_{length}, were given in terms of the areas shown in Figure 4.1 as follows:

$$LUB = L\left(\frac{B}{A+B}\right) \tag{4.5}$$

and

$$MTZ_{length} = \frac{LUB}{\xi} \tag{4.6}$$

where L is the overall bed length and ξ is the shape factor defined by $\left(\frac{B}{B+C}\right)$.

Thus,

$$MTZ_{length} = L\left(\frac{B}{A+B}\right)\left(\frac{B+C}{B}\right) = L\left(\frac{B+C}{A+B}\right) \tag{4.7}$$

The MTZ velocities were determined using the following definition for a non-symmetric breakthrough curve given by Schweitzer (1976),

$$MTZ_{velocity} = \frac{MTZ_{length}}{\Delta t_b} \tag{4.8}$$

where Δt_b was the time required for the MTZ to travel its own length, i.e. the duration of the breakthrough curve to increase from break-point to equilibrium concentration.

The type of flow in the packed bed may influence the MTZ properties. According to Coulson and Richardson (1991), the transition from laminar to turbulent flow in packed beds occurs at a modified Reynolds number of approximately 10. The modified Reynolds number for a packed bed of spheres is (Darby, 1996) :

$$Re_{PB} = \frac{2\rho d_p u_s}{3(1-\varepsilon)\mu} \tag{4.9}$$

in which ε is the bed voidage, u_s is the superficial velocity, d_p is the particle diameter, μ is the fluid viscosity and ρ is the fluid density. It was assumed that the flowrate remained constant and that the adsorption of VOC did not alter the fluid properties. Therefore, the properties of nitrogen at 25°C and atmospheric pressure were used in the determination of Re_{PB}.

4.4 Results and Discussions

4.4.1 Breakthrough Curves

Example breakthrough curves are shown in Figures 4.2-4.7. These figures show the effect of varying the adsorbate feed concentration, feed flowrate and bed length on the VOC breakthrough. For each curve, the effluent concentration gradually increases after the initial breakthrough until complete breakthrough of the adsorbate has occurred.

Most of the experiments involving propane were carried out using technical grade gas, on account of its lower cost. The curves obtained are characterised by a small early step increase in the effluent VOC concentration, which then remains constant until the main propane breakthrough. This is thought to be due to impurities in the gas (up to 5 %) which are mostly organic compounds of higher molecular weight (Table 4.5), and therefore only weakly adsorbed onto the bed. (The FID detection method used does not distinguish between different organic compounds). This explanation is supported by the absence of such step changes when using instrument grade propane (99.5 % pure), as shown in Figure 4.2, for concentrations of 1000, 5000 and 7500 ppm. The other reagents used (ethanol and methylene chloride) were also of high purity and do not exhibit this effect (Figures 4.4 and 4.5). Consequently, for technical grade propane, the initial breakthrough time, t_b, was defined as the time at which the effluent VOC concentration level reached 6 % of the feed concentration. For all other feedstocks, initial breakthrough was assumed to have occurred when the effluent concentration had attained 2 % of the feed concentration.

The equilibrium time, t_{eq}, was given the same definition for all the adsorbates tested, i.e. the time at which the effluent concentration reached 98 % of the feed concentration.

In Figures 4.2-4.7 it can be seen that increasing the feed concentration and the feed flowrate resulted in earlier breakthrough times. This was a direct consequence of the adsorbent being exposed to more adsorbate per unit time. As shown in Figure 4.8 the breakthrough time decreased with increasing feed flowrate. The effect on the propane

breakthrough curve of varying the bed length is shown in Figure 4.9. Changes in bed length do not appear to affect the shape of the breakthrough curve, thereby lending support to the presumption of a constant pattern waveform, but a shorter bed length results in a shorter breakthrough time. The breakthrough times were approximately in proportion to the amount of adsorbent in the bed, as illustrated in Figure 4.10.

Breakthrough curves from experimental runs where water vapour was introduced into the feed gas are given in Figures 4.12-4.14. For reference, the results shown in Figure 4.11 are from those experiments using a feed gas without water vapour. Comparing Figures 4.11 and 4.12, it can be seen that the presence of water vapour in the feed gives rise to a distinct change in the shape of the VOC breakthrough curves and to a shorter breakthrough time. The earlier breakthrough may be due to the competitive adsorption of water molecules. Effluent concentration peaks are observed in Figure 4.12, and the height of the peak is greater for a higher feed concentration. As shown in Figure 4.13, the effect is exacerbated if the water vapour level is increased to 70 % RH, and the effluent concentration peaks are larger. In contrast, a similar shape change is not observed in Figure 4.14, which shows the breakthrough of the same feedstocks from a pre-moisturised bed. However, the breakthrough times were reduced considerably when compared with the values for the dry bed (Figure 4.11). The shorter breakthrough time was probably due to the pre-occupation of part of the active sites of the adsorbent bed. Figure 4.15 shows that the 'peaks' on the propane breakthrough curves occur simultaneously with the breakthrough of water vapour, suggesting that the characteristic 'peak' may be due to the displacement of propane by the water front. Figure 4.16 shows that when a propane-water vapour mixture is applied to a preconditioned bed, water vapour breaks through immediately. This indicates that the bed was completely saturated with water vapour during the preconditioning, and consequently there would have been no further adsorption of water during the experiment. This may explain why 'peaks' are not observed in Figure 4.14.

Figure 4.17 shows that the presence of water vapour does not appreciably change the appearance of the ethanol breakthrough curves. This may be due to the total miscibility of ethanol with water, so that the ethanol solubilises into the condensed phase and then diffuses into the adsorption sites, displacing water from those sites.

The effect of water vapour on the uptake of methylene chloride is shown in Figure 4.18. Earlier breakthrough was observed when water vapour was present in the feedstock, but the shape of the curves was not affected. The moderate effect of water vapour on the adsorption of methylene chloride may be due to the limited miscibility of methylene chloride with water, which is higher than that of propane but lower than that of ethanol.

Table 4.5 Typical assay of impurities in technical grade propane

Component	Concentration[4.2] (ppm)	Molecular weight[4.3]
Ethane	100-300	30.07
Propylene	500	42.081
Isobutane	200-1500	58.124
N-Butane	550	58.124
Trans-2-Butene	200	56.108
Cis-2-Butene	100	56.108

[4.2] Information provided by BOC Ltd
[4.3] Data obtained from Reid and Sherwood (1958)

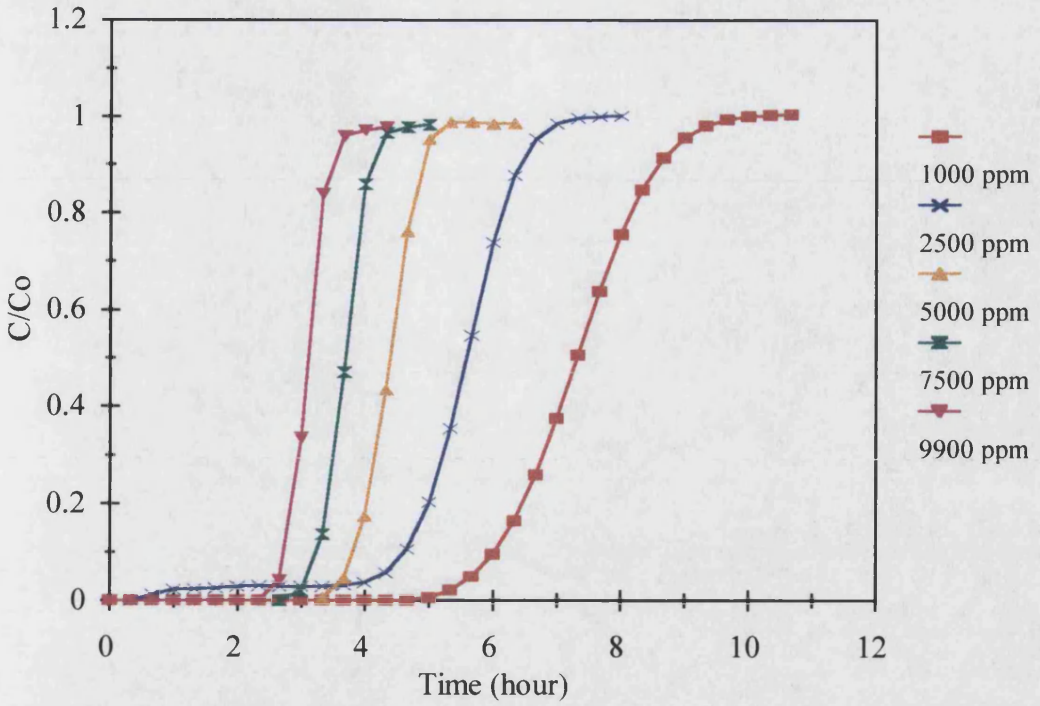

Figure 4.2 Dynamic adsorption of propane at different feedstock concentrations onto ZSM-5 packed bed

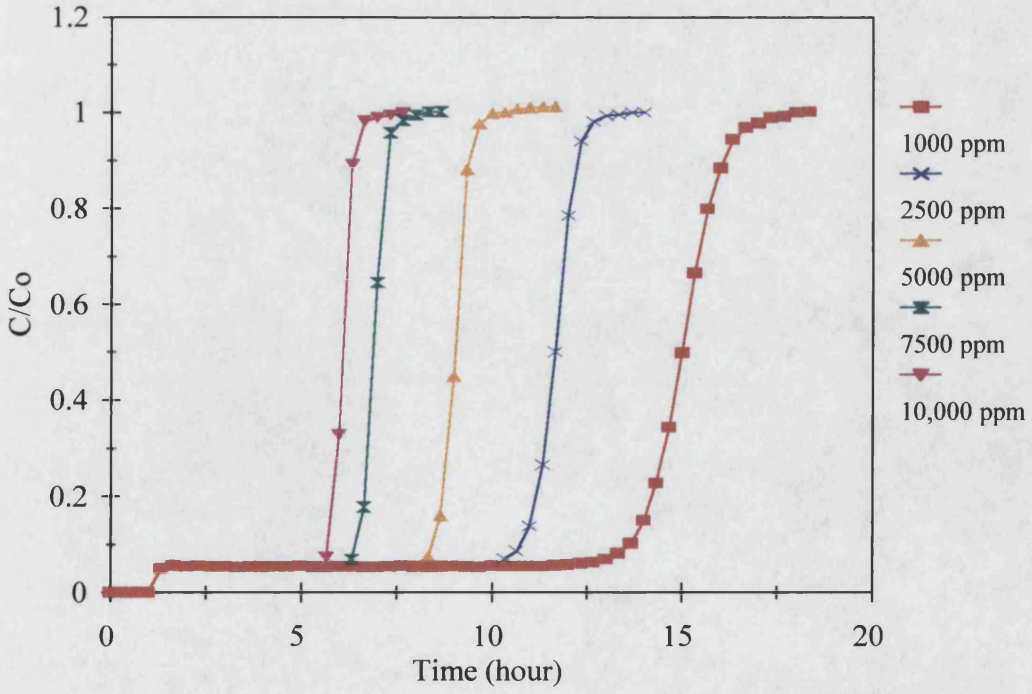

Figure 4.3 Dynamic adsorption of propane at different feedstock concentrations onto silicalite packed bed

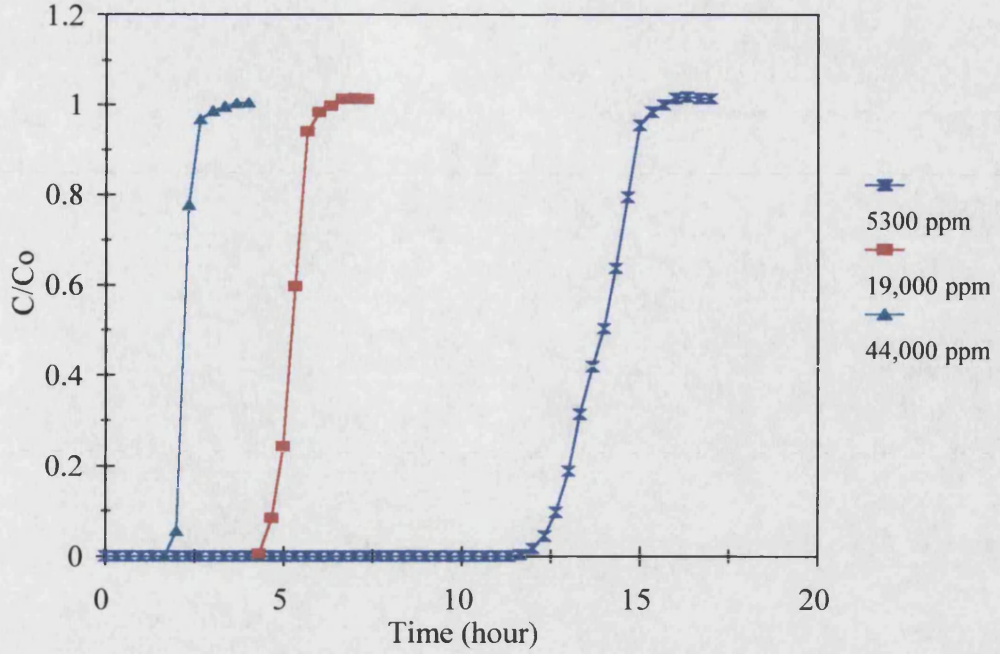

Figure 4.4 Dynamic adsorption of ethanol at different feedstock concentrations onto silicalite packed bed

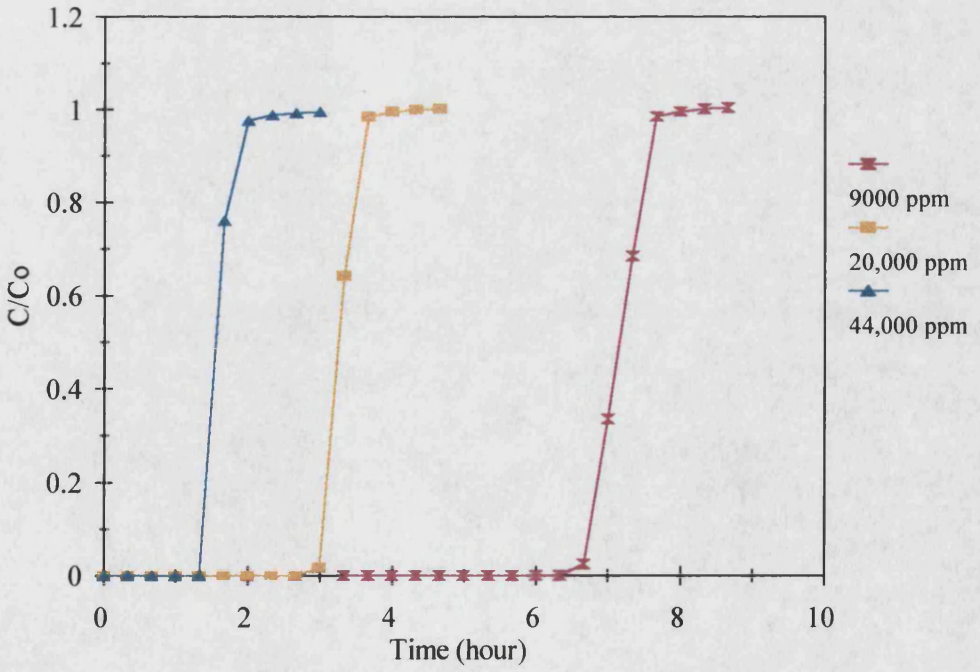

Figure 4.5 Dynamic adsorption of methylene chloride at different feedstock concentrations onto silicalite packed bed

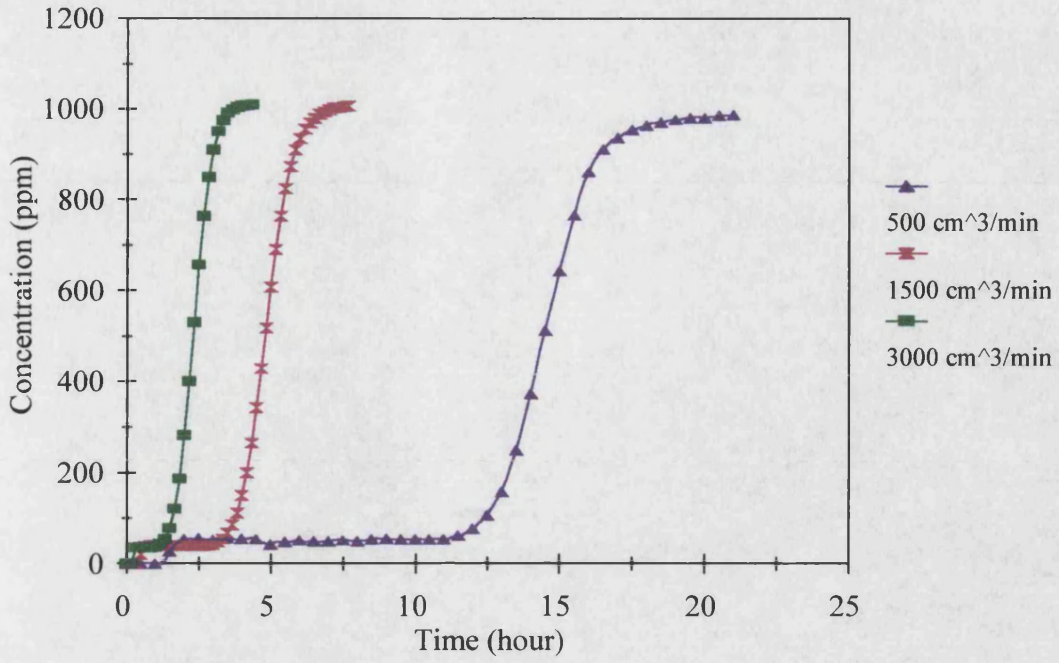

Figure 4.6 Effect of flowrate on the breakthrough curves of propane (1000 ppm) adsorption onto silicalite packed bed

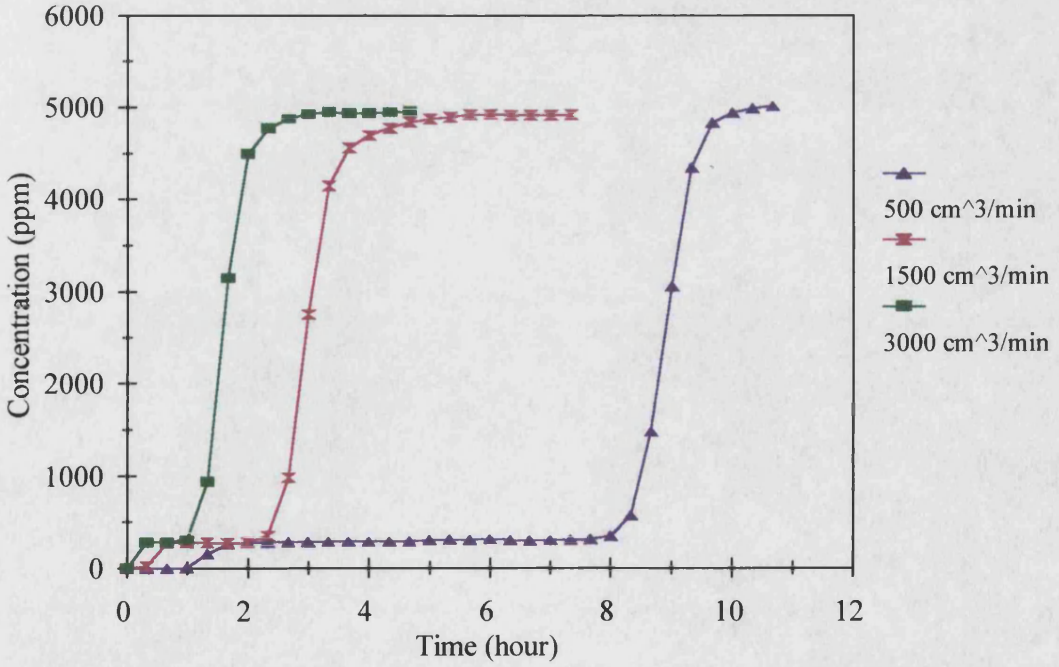

Figure 4.7 Effect of flowrate on the breakthrough curves of propane (5000 ppm) adsorption onto silicalite packed bed

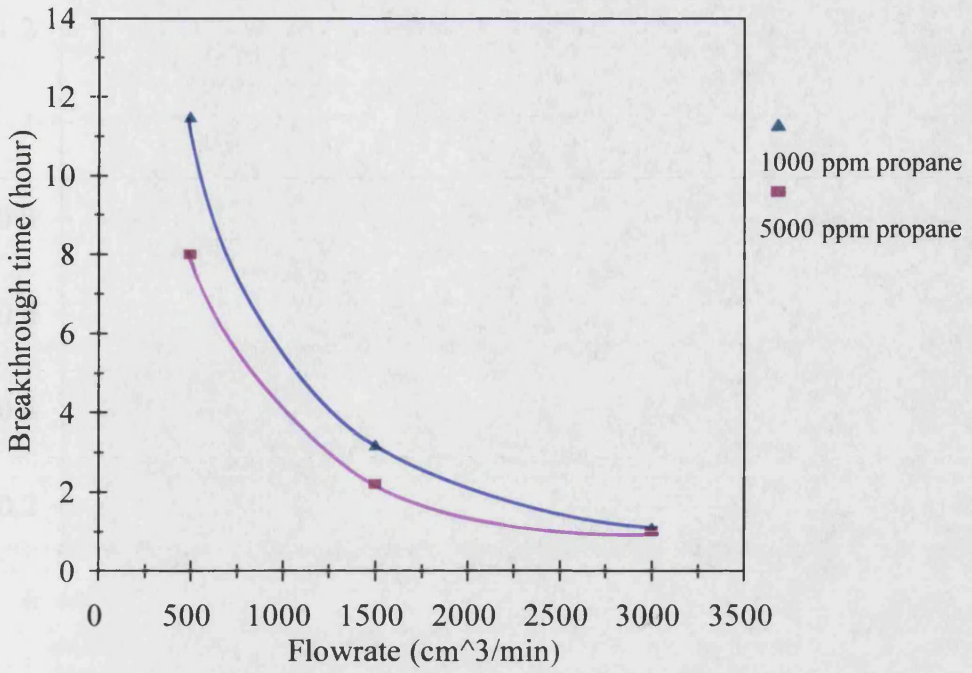

Figure 4.8 Variation of breakthrough times with flowrate through the silicalite packed bed

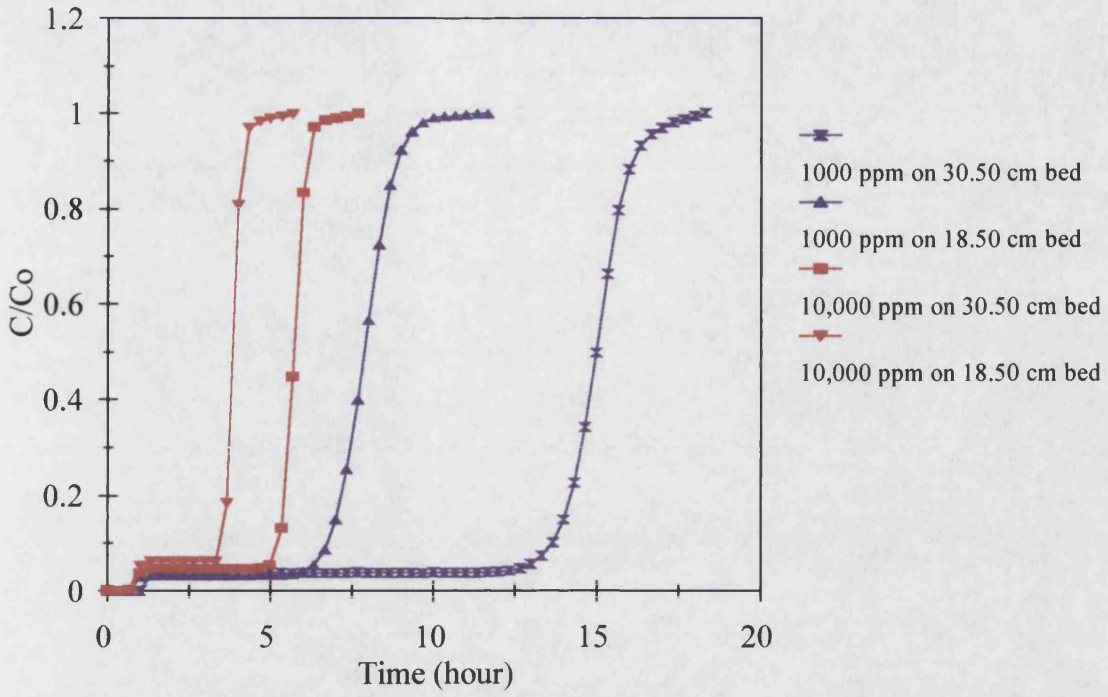

Figure 4.9 Propane adsorption onto silicalite packed beds of 18.50 cm and 30.50 cm length

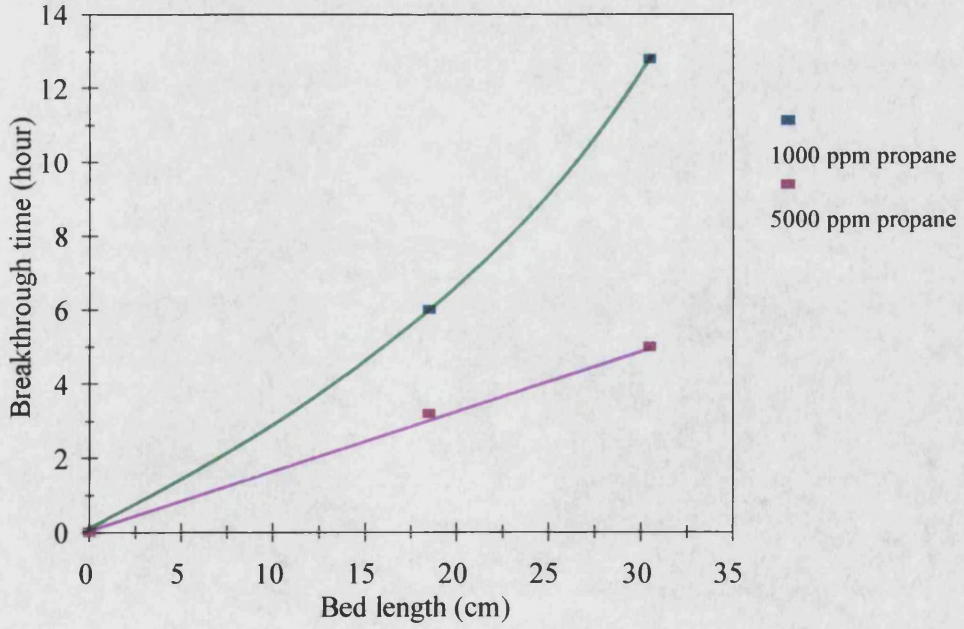

Figure 4.10 Variation of breakthrough time with bed length

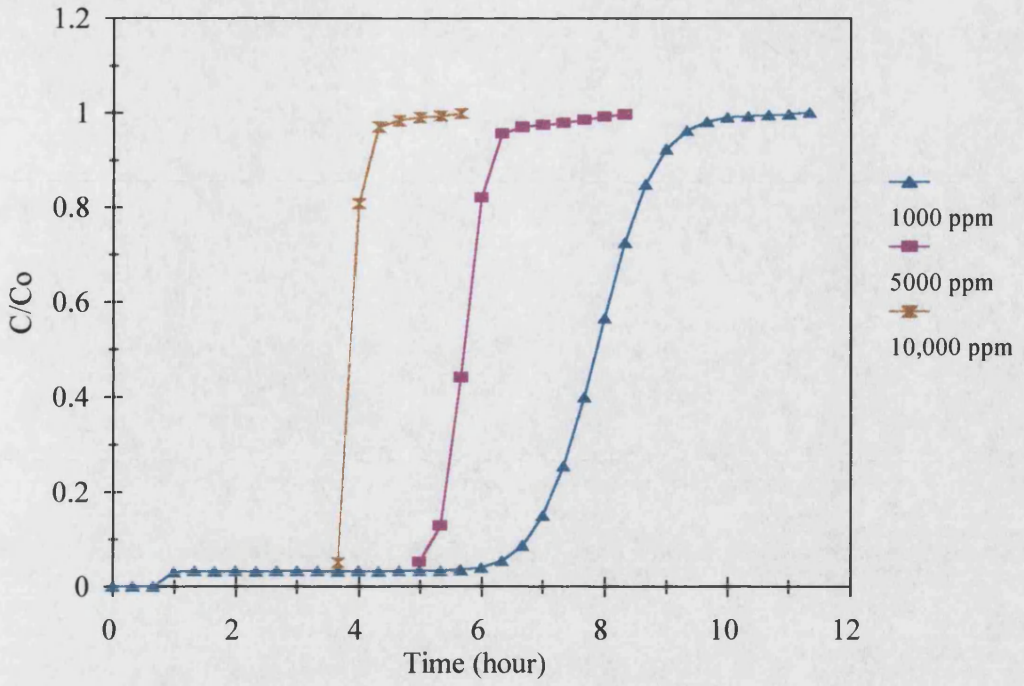

Figure 4.11 Adsorption of propane onto silicalite packed bed (no moisture present)

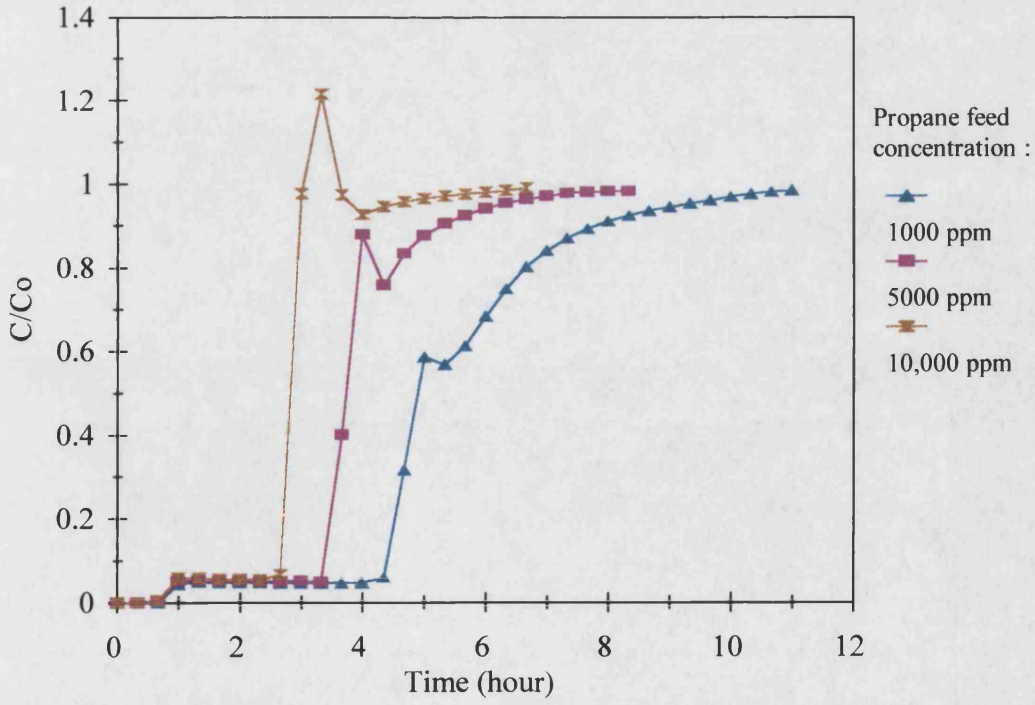

Figure 4.12 Adsorption of propane with 55 % RH water vapour onto silicalite packed bed

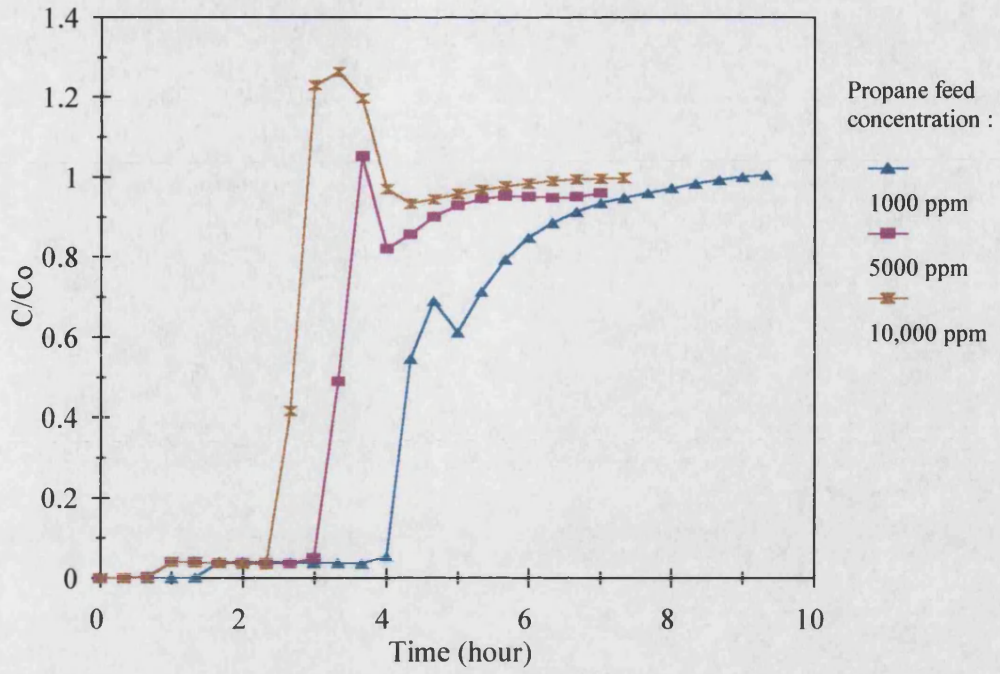

Figure 4.13 Adsorption of propane with 70 % RH water vapour onto silicalite packed bed

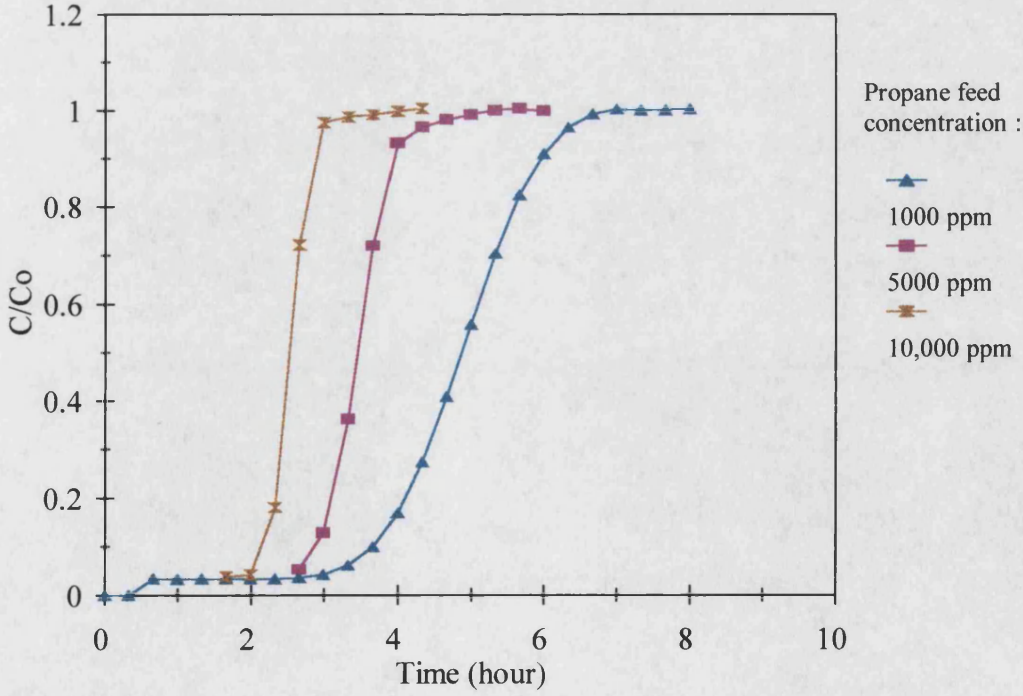

Figure 4.14 Adsorption of propane with 70 % RH water vapour onto preconditioned silicalite packed bed

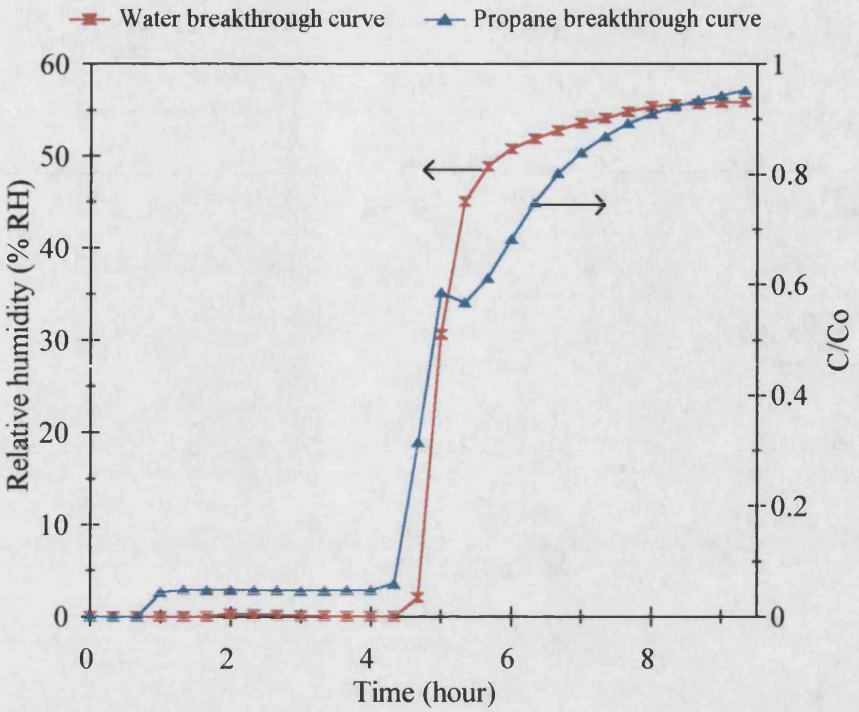

Figure 4.15 Effect of water vapour on the adsorption of propane (1000 ppm) onto dry silicalite packed bed

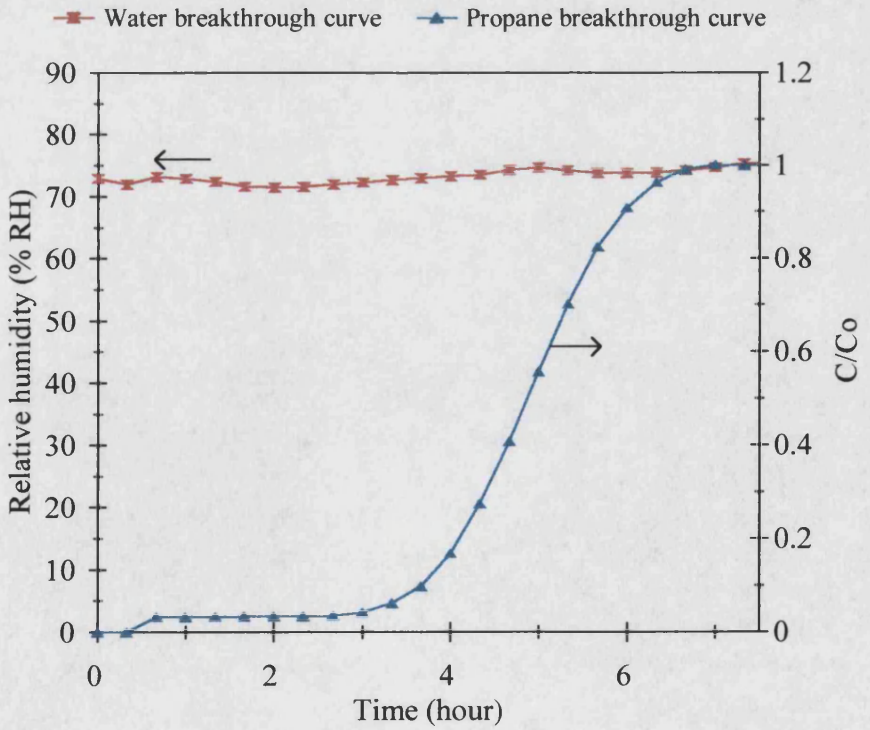

Figure 4.16 Effect of water vapour on the adsorption of propane (1000 ppm) onto preconditioned silicalite packed bed

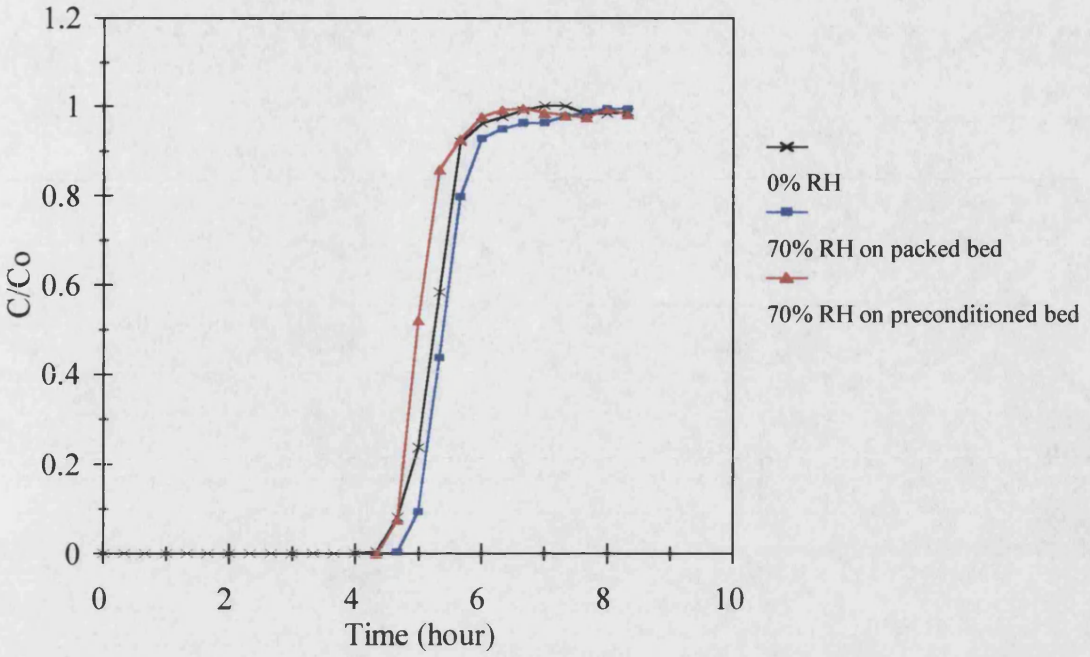

Figure 4.17 Effect of water vapour on the adsorption of ethanol (19,000 ppm) onto silicalite packed bed

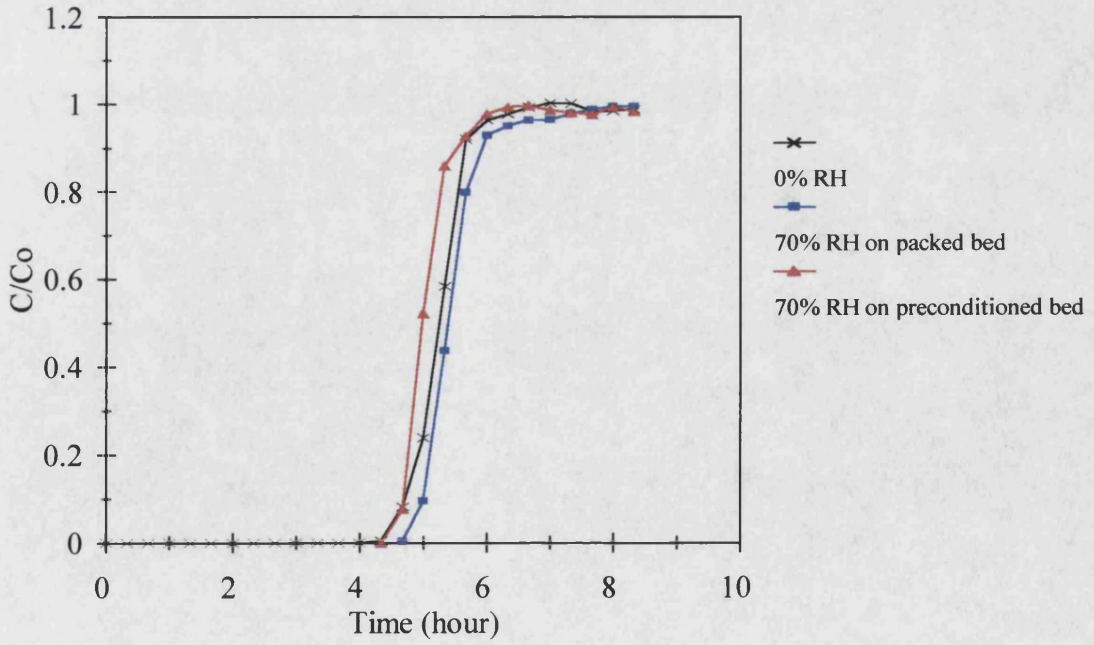

Figure 4.18 Effect of water vapour on the adsorption of methylene chloride (20,000 ppm) onto silicalite packed bed

4.4.2 Adsorption Isotherms

The adsorption isotherm for each organic vapour is shown in Figure 4.19. The adsorbability of the three VOCs onto silicalite is seen to decrease in the order of ethanol, methylene chloride and propane. This may be related to their kinetic diameters which increase in the same order. Since ethanol (kinetic diameter = 0.453 nm) is the smallest molecule amongst the three VOCs and much smaller than the average pore diameter of silicalite (0.60 nm), it is able to enter the pores most easily. Propane (0.512 nm) is the largest molecule under study and is adsorbed to the least extent. The isotherms for ethanol and methylene chloride are almost rectangular, i.e. the loadings are only weakly dependent on the gas phase concentration, indicating that the adsorbent is easily saturated with ethanol and methylene chloride. In contrast, the equilibrium adsorption of propane appears to be a much stronger function of the gas phase concentration. The amount of propane adsorbed is shown to increase with increasing gas phase concentration, without levelling off within the concentration range of 0 to 10,000 ppm.

Figure 4.19 also shows that silicalite has a higher equilibrium loading for propane than ZSM-5. However, the adsorption of propane on ZSM-5 exhibited the same basic characteristics as that on silicalite. This is expected since the crystal structure of these zeolites is the same. However, ZSM-5 contains a considerable amount of aluminium cations (while silicalite contains no aluminium) which may have contributed to the slightly lower capacity for propane (Flanigen et. al., 1978).

The effect of water vapour on the adsorption isotherms of the VOCs is shown in Figures 4.20-4.22. When water vapour was present in the feed:

- the equilibrium loading of propane was reduced, the severity of the reduction increasing with increased relative humidity.

- the isotherm of ethanol was not changed significantly.

- the loading of methylene chloride was slightly reduced but was not further affected when adsorption was performed onto a preconditioned bed.

These effects may be related to the miscibility of the respective VOC with water. As explained earlier (Section 4.4.1), ethanol and water are totally miscible. Therefore, ethanol solubilised into the water phase and adsorbed onto the pores. Propane is immiscible with water and thus it has to compete with water molecules for the adsorption sites. The miscibility of methylene chloride and water lies between that of propane and that of ethanol and therefore the effect is moderate.

The results of performing a linear regression on the isotherm data using the Langmuir model are presented in Table 4.6. According to the derivation of the Langmuir equation, the constant q_{max} is related to the number of adsorption sites per unit weight of adsorbent. Therefore, when the amount of organic adsorbed is expressed in terms of the volume per unit weight of adsorbent, the q_{max} values should be constant irrespective of adsorbate for adsorbates of similar molecular size. As shown in Table 4.6, this assumption is approximately valid for the systems studied. Figures 4.23-4.25 show that the experimental isotherms are well represented by the Langmuir model and indeed are favourable in shape.

A comparison of the experimental isotherms with those from the literature is made in Figures 4.24 and 4.25. The isotherm of ethanol agrees closely with that from the literature (Otto et. al., 1991), but that of methylene chloride deviates slightly from the literature (UOP, 1992). The literature data for methylene chloride was determined at a temperature of 22°C, while the author's own data were obtained at 25°C. An increase in temperature should lower the adsorbed phase concentration and thus this may account for the discrepancy between the two isotherms.

The adsorption isotherm of pure water vapour is shown in Figure 4.26. The experimental data agree reasonably well with those from the literature (Flanigen et. al., 1978). The water isotherm was also tested on the Langmuir model, but with a different numerical procedure. It is assumed that q_{max} for water, when expressed in volume units (cm^3/g), is equal to that for the organic vapour. The assumptions of the model used require that q_{max} be the same for all components. In addition, the water data are easily

fitted by a straight line through the origin, so these data do not allow reasonable prediction of two parameters. Thus the average value of q_{max}, i.e. 0.1358 cm^3/g, was used in the regression on the water data and resulted in a value of b of 0.0292 $mmHg^{-1}$.

The results of fitting the isotherms of two-component mixtures, i.e. VOC and water vapour, using the extended Langmuir expression are illustrated in Figures 4.27-4.29. The estimated isotherms do not agree well with the experimental data. Although the prediction does not fit the experimental data accurately, the shapes of the estimated curves do agree well with those obtained from experiment. The failure of the extended Langmuir model to fit the experimental data for binary mixture adsorption may be due to the adsorption mechanism of water which is expected to be predominantly of capillary condensation.

Table 4.6 Langmuir parameters for single component adsorption of VOCs onto packed bed

Adsorbate	Kinetic diameter[4.4] (nm)	Adsorbent type	q_{max} (mg/g)	q_{max} (cm^3/g)	b ($mmHg^{-1}$)
Propane	0.512	ZSM-5	50.24	0.1019	0.1830
Propane	0.512	Silicalite	70.33	0.1426	0.1450
Methylene chloride	0.489	Silicalite	142.84	0.1083	1.248
Ethanol	0.453	Silicalite	122.48	0.1564	0.4027

[4.4] Data obtained from Reid and Sherwood (1958)

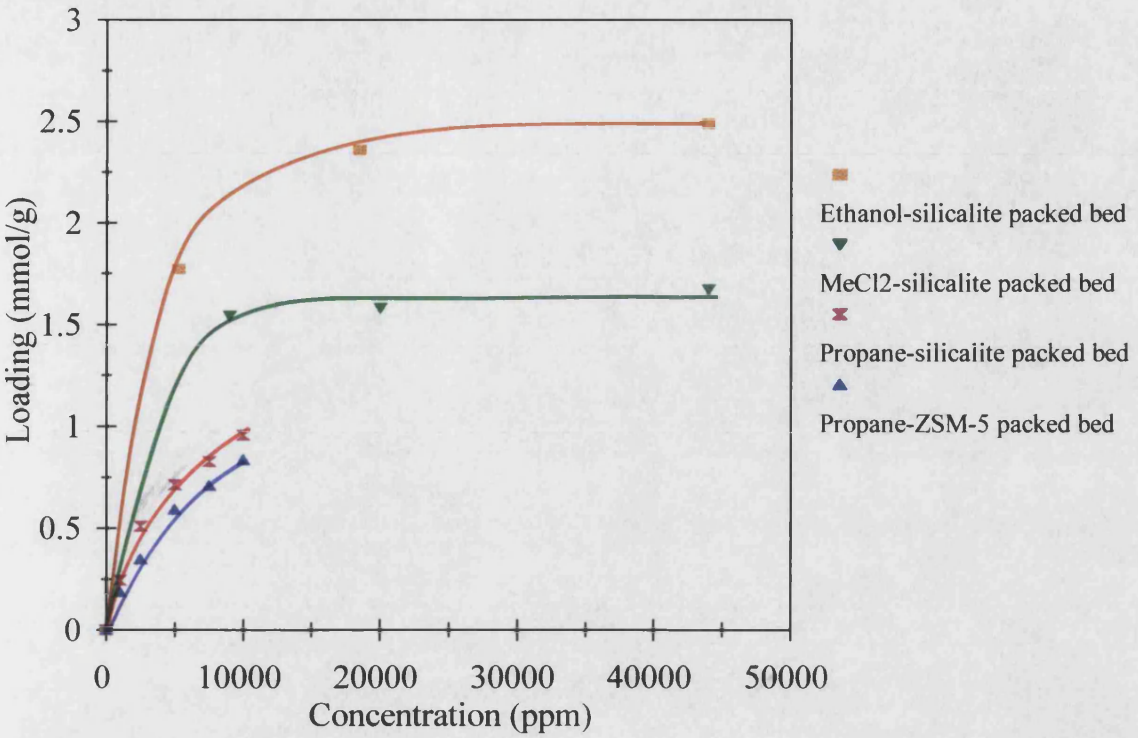

Figure 4.19 Adsorption isotherms of single-component VOCs onto silicalite and ZSM-5 packed beds (at 25°C)

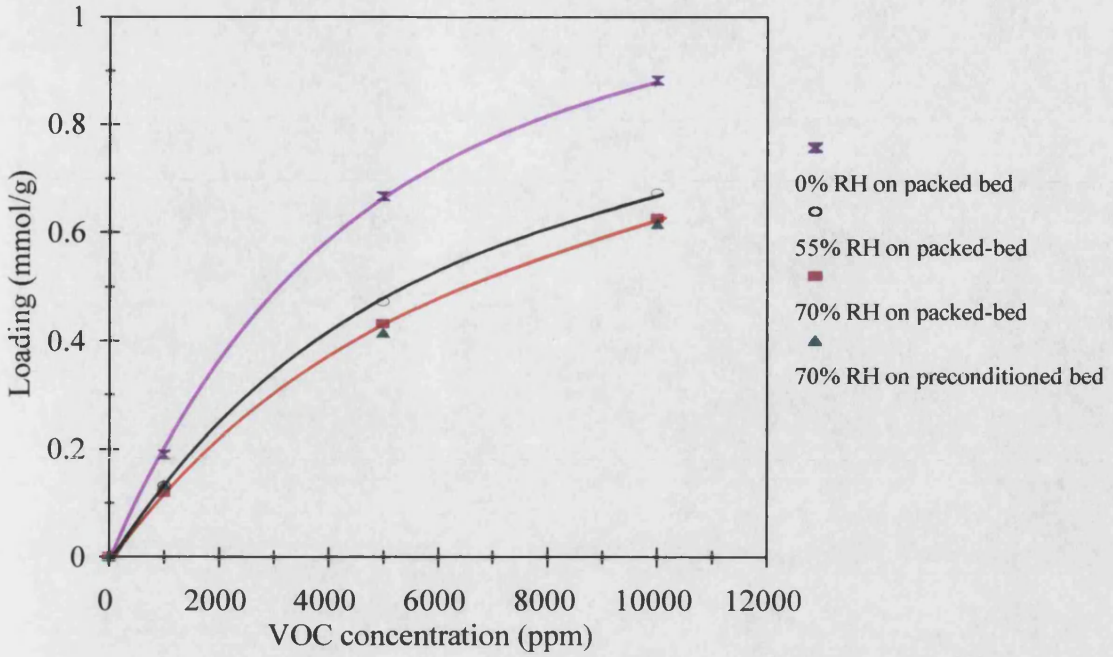

Figure 4.20 Effect of water vapour on the adsorption of propane onto silicalite packed-bed

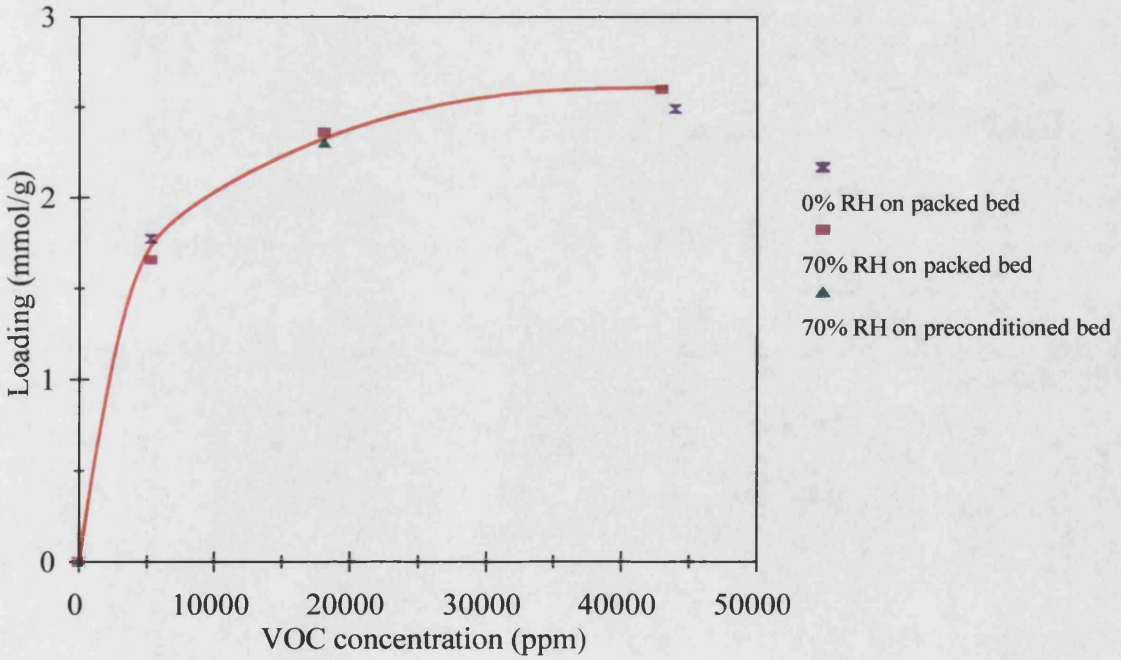

Figure 4.21 Effect of water vapour on the adsorption of ethanol onto silicalite packed-bed

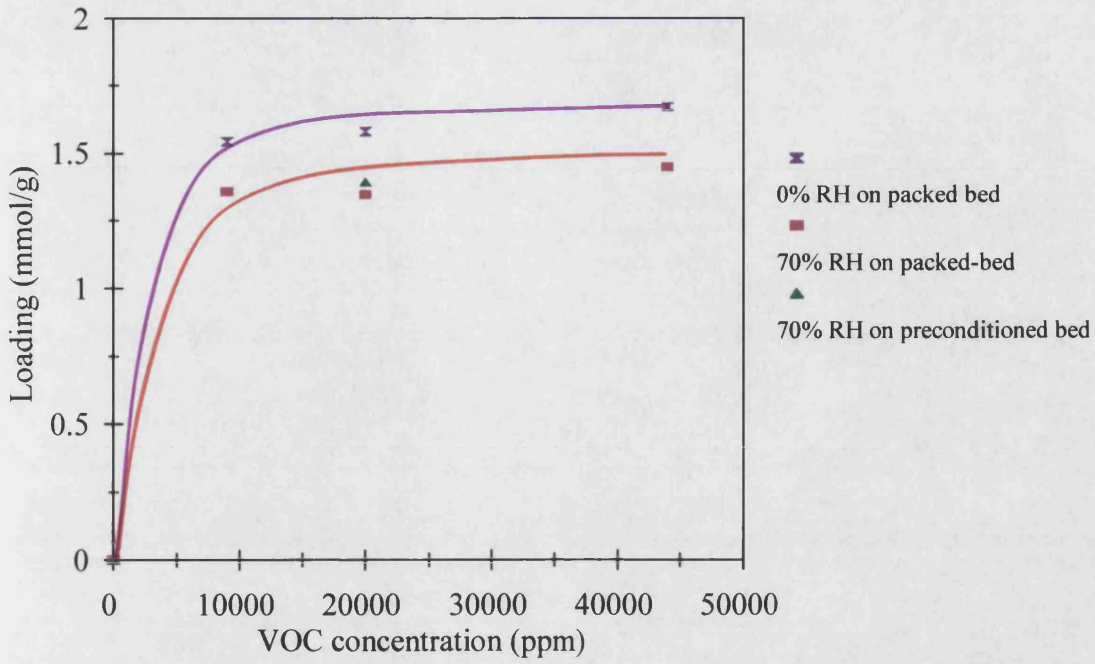

Figure 4.22 Effect of water vapour on the adsorption of methylene chloride onto silicalite packed-bed

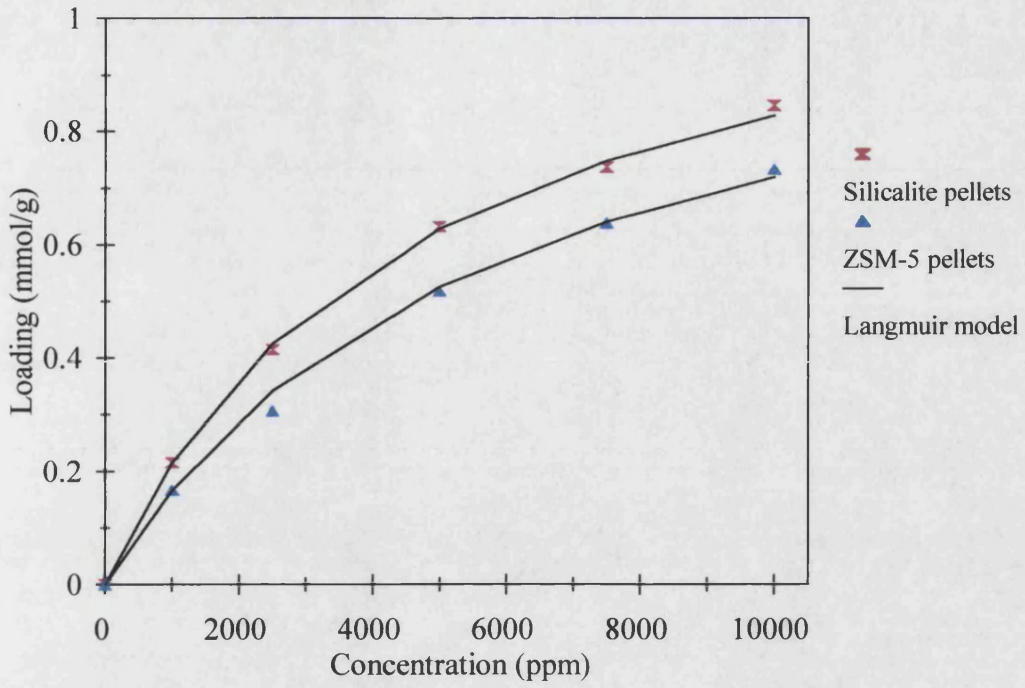

Figure 4.23 Comparison of the experimental isotherm of propane with the Langmuir model

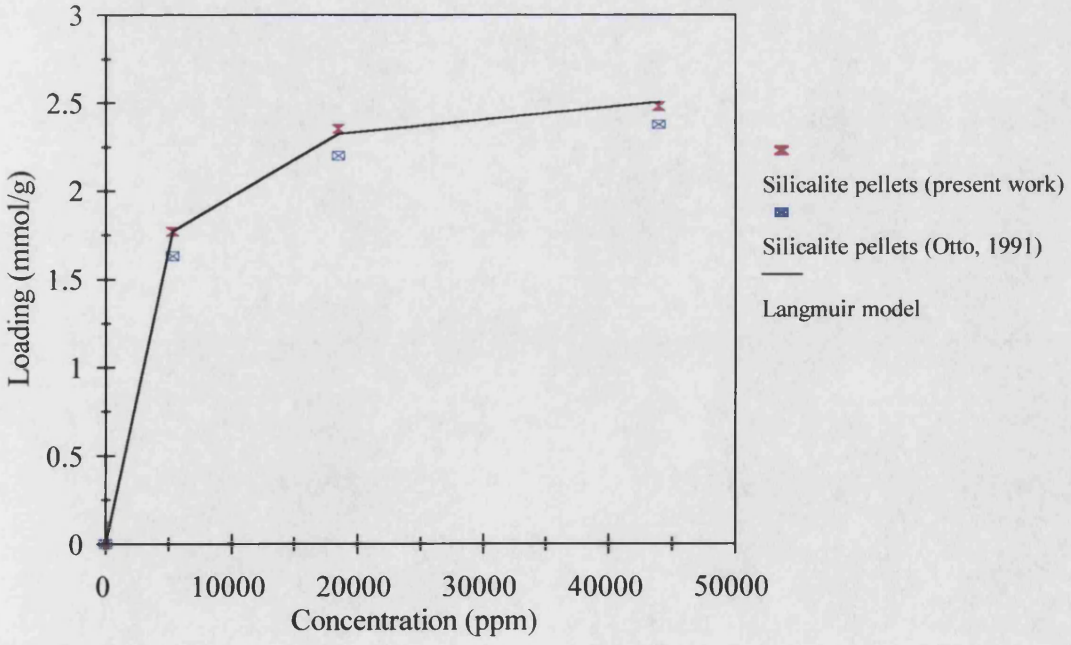

Figure 4.24 Comparison of the experimental isotherm of ethanol with the Langmuir model and literature data

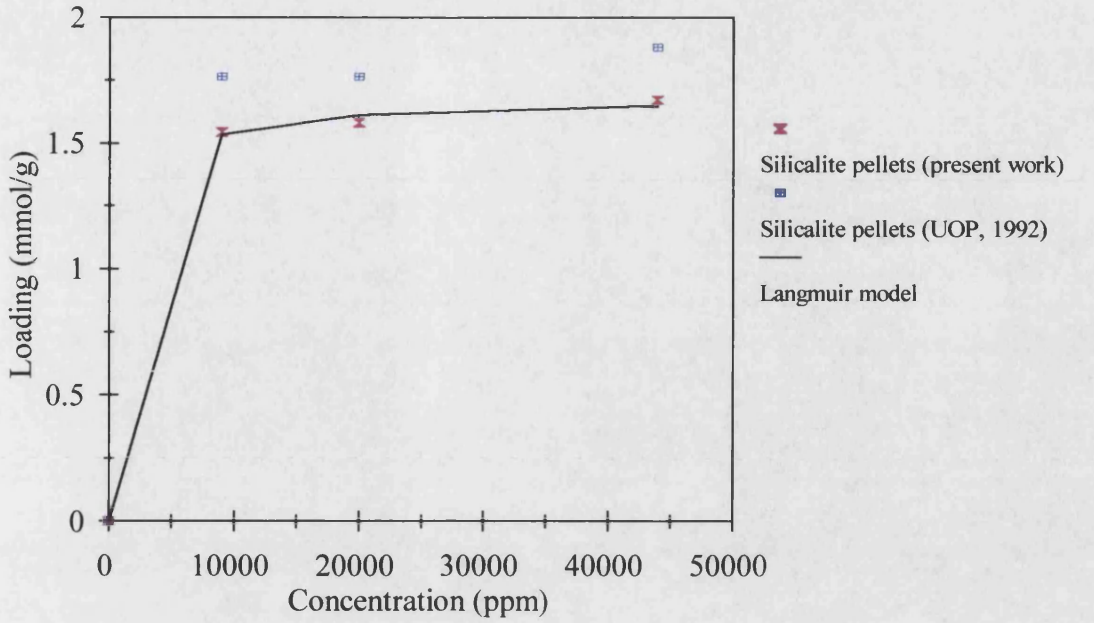

Figure 4.25 Comparison of the experimental isotherm of methylene chloride with the Langmuir model and literature data

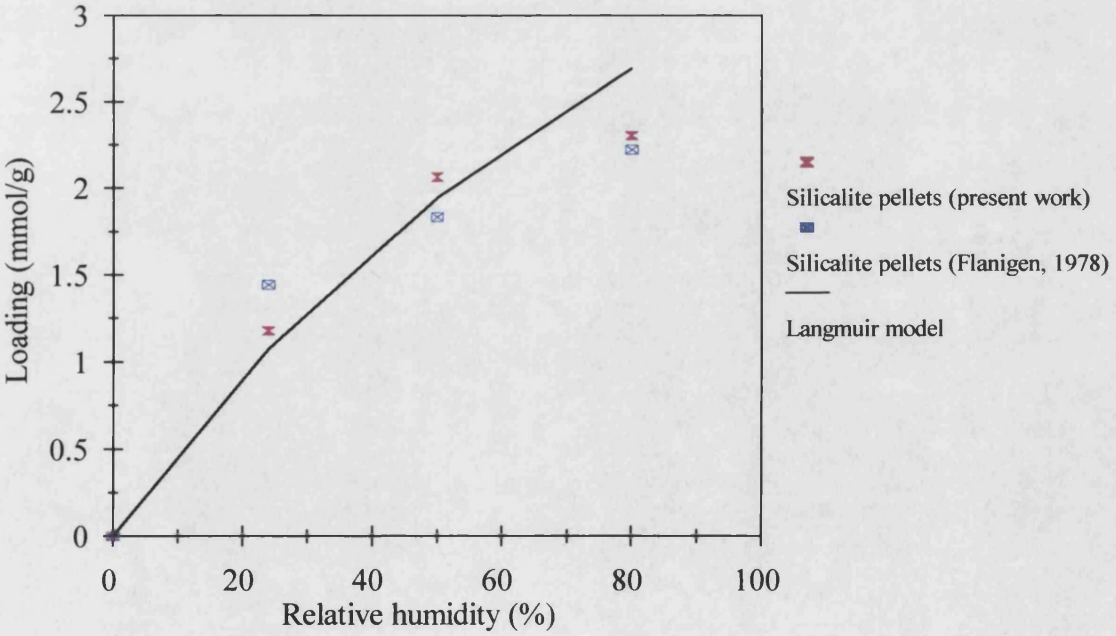

Figure 4.26 Comparison of experimental isotherm of water with the Langmuir model and literature data

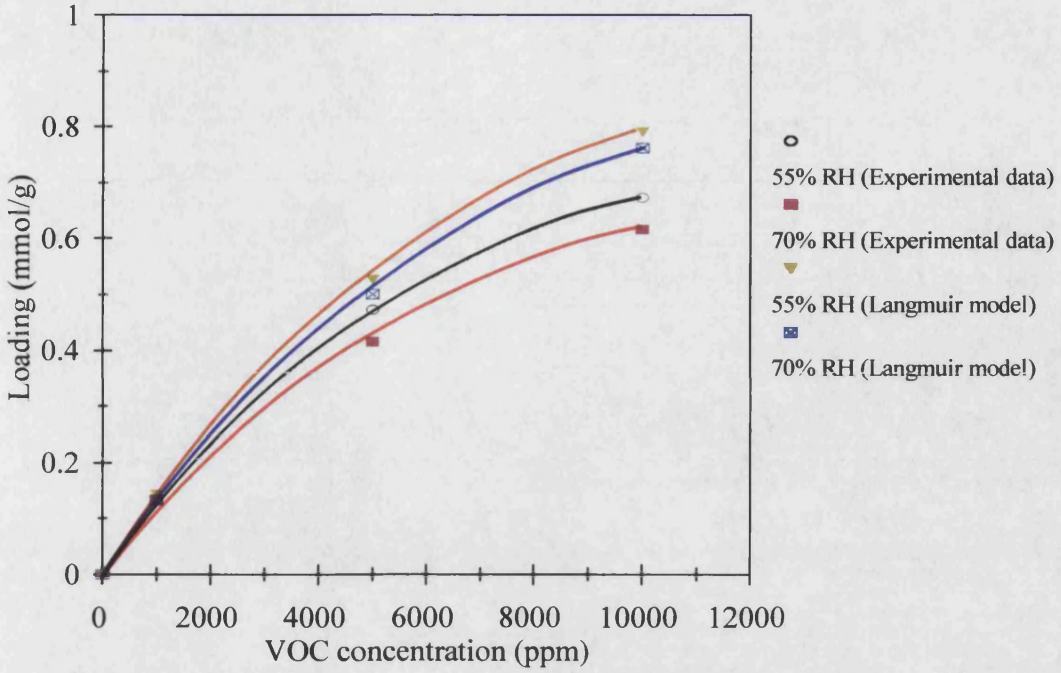

Figure 4.27 Comparison of the experimental isotherm of propane with the extended Langmuir model

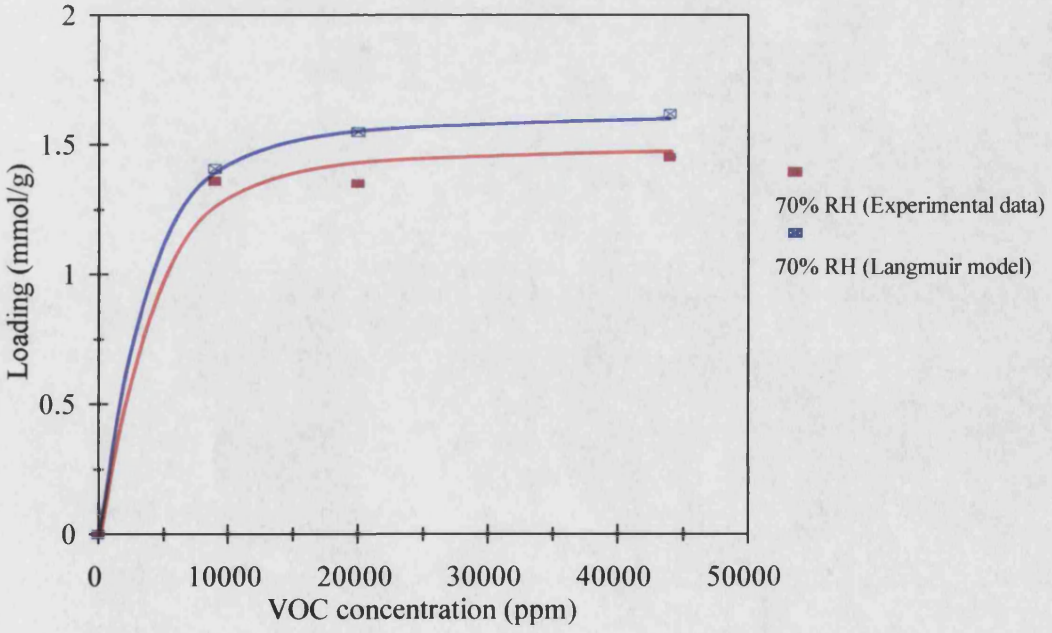

Figure 4.28 Comparison of the experimental isotherm of methylene chloride with the extended Langmuir model

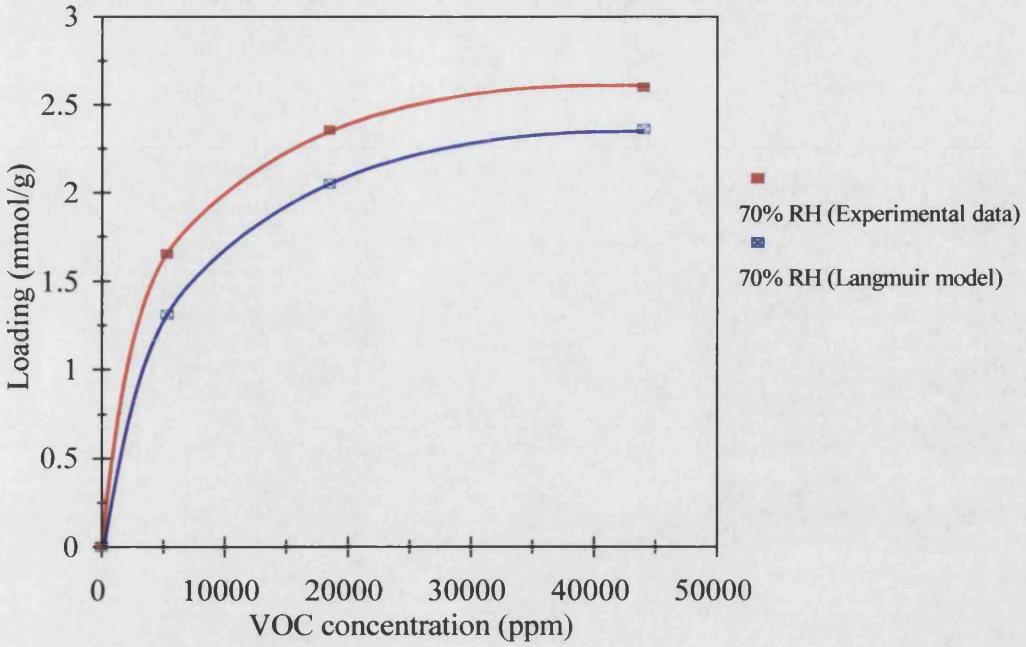

Figure 4.29 Comparison of the experimental isotherm of ethanol with the extended Langmuir model

4.4.3 The MTZ Length and Velocity

The MTZ lengths observed for single component VOC adsorption are shown in Figure 4.30. Increasing the propane concentration in the feed from 1000 to 10,000 ppm caused a reduction in the MTZ length. With ethanol and methylene chloride, the MTZ length was also reduced when the feed concentration was increased. However, a further increase in feed concentration from 20,000 to 44,000 ppm caused an increase in MTZ length. Examples of the calculated modified Reynolds number are listed in Table 4.7. The prevailing flow regime was laminar for all the experimental runs. The Reynolds number was affected most by the feed flowrates and the properties of the bed. In Table 4.7, P101, P102 and P103 were the different types of packed bed used in the respective experimental runs and their characteristics are summarised in Table 4.4. The effect of a lower feed concentration (1000-20,000 ppm) on the MTZ length may be due to a reduction of the fluid film mass transfer resistance in the laminar flow regime when the feed concentration is increased. More experimental data using various feed concentrations would be required to give a clearer picture of the behaviour in the range of 20,000-44,000 ppm.

The most noticeable effect of varying the feed concentration is the change in MTZ velocity. As shown in Figure 4.31, for all cases, the MTZ velocity is directly proportional to the feed concentration. There is an overall effect of faster forward movement of adsorbates in the axial direction as a result of shorter MTZ at increased feed concentrations. Thus, the steepness of the breakthrough curves rises as the feed concentration is increased.

The effect of changes in feed flowrate on the MTZ length and velocity are shown in Figures 4.32 and 4.33, respectively. Increasing the feed flowrate increases the MTZ length and velocity almost proportionally. Figures 4.34 and 4.35 show that the overall bed length has no significant effect on the properties of the MTZ.

Figures 4.36-4.38 show the effect of water vapour on the MTZ length. In the case of propane, the MTZ length is increased when water vapour is present in the feed, reducing the efficiency of the packed bed. This may be due to propane being immiscible

with water and resistance to propane adsorption into the pores was exhibited by the water molecules. In the case of ethanol, the length of the MTZ is not affected by the presence of water vapour. This is because ethanol, which is totally miscible with water, dissolves into the water phase and is adsorbed onto the pores. For methylene chloride the effect was only observed at certain feed concentrations, perhaps as a result of its moderate miscibility with water.

The effect of water vapour on the MTZ velocity is illustrated in Figures 4.39-4.41. For propane, the MTZ velocity was increased, and the effect was elevated when the level of water vapour was increased. In the case of ethanol, the MTZ velocity was not changed significantly, while that of methylene chloride was affected only at high feed concentrations.

Table 4.7 Results of the calculated modified Reynolds number

Packed-bed number	Total flow (cm^3/min at STP)	Feed concentration (ppm)		Modified Reynolds number, Re_{PB}
P102	500	Propane :	1000	2
(Silicalite)	500		5000	2
	500		10,000	2
P101	500	Ethanol :	5300	2
(Silicalite)	500		18,500	2
	500		44,000	2
P101	500	$MeCl_2$:	9000	2
(Silicalite)	500		20,000	2
	500		44,000	2

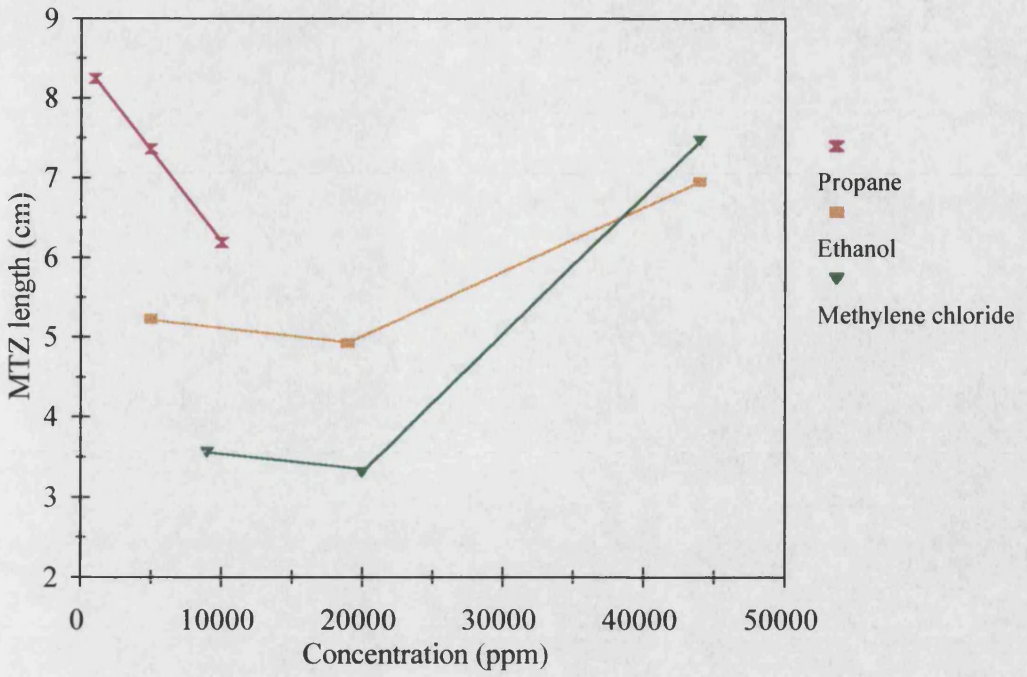

Figure 4.30 Variation of MTZ length with feed concentration for single component VOCs adsorption onto silicalite packed bed

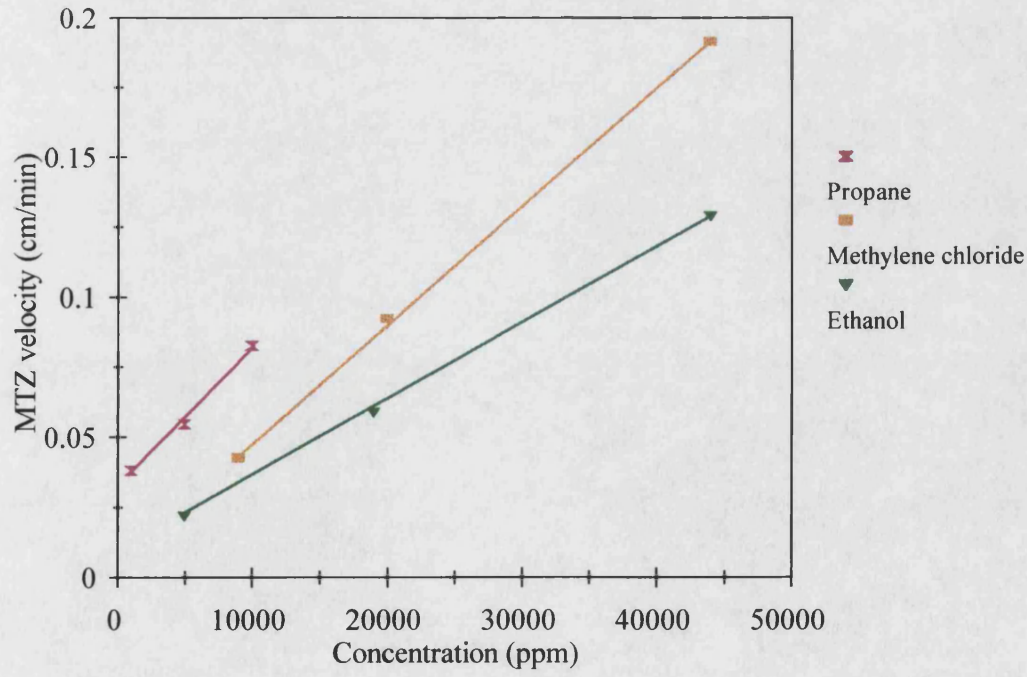

Figure 4.31 Variation of MTZ velocity with feed concentration for single component VOCs adsorption onto silicalite packed bed

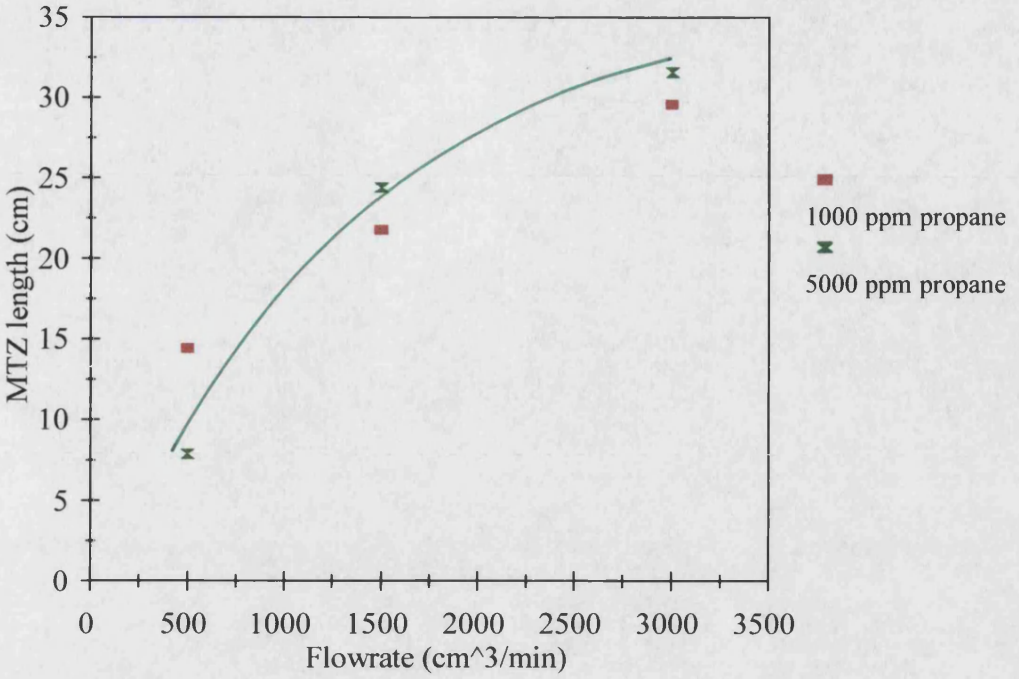

Figure 4.32 Variation of MTZ length with feed flowrates

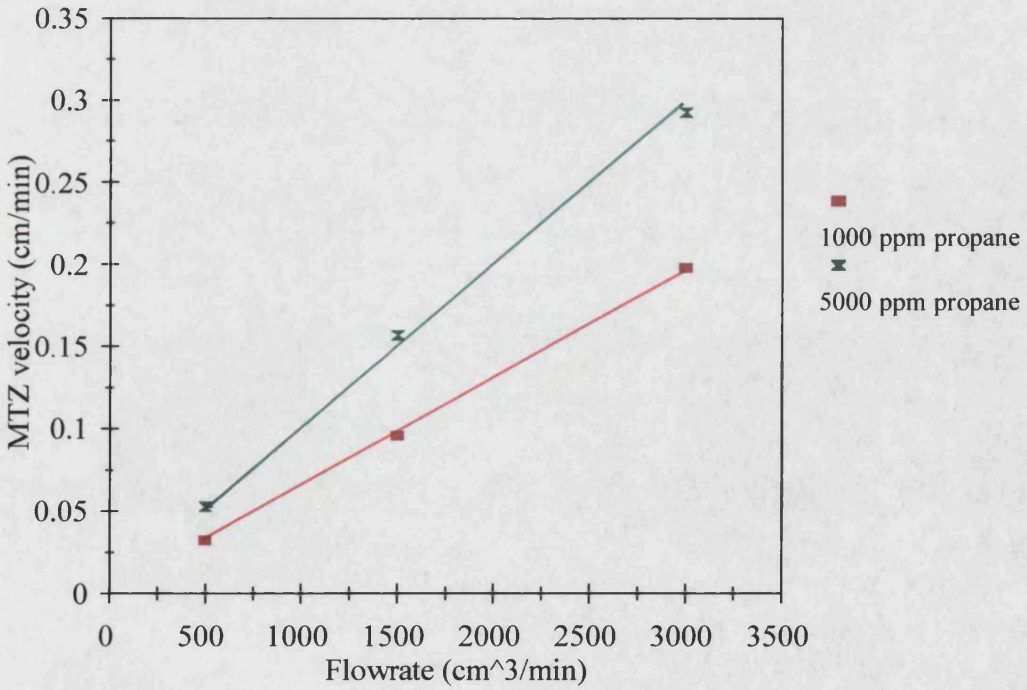

Figure 4.33 Variation of MTZ velocity with feed flowrates

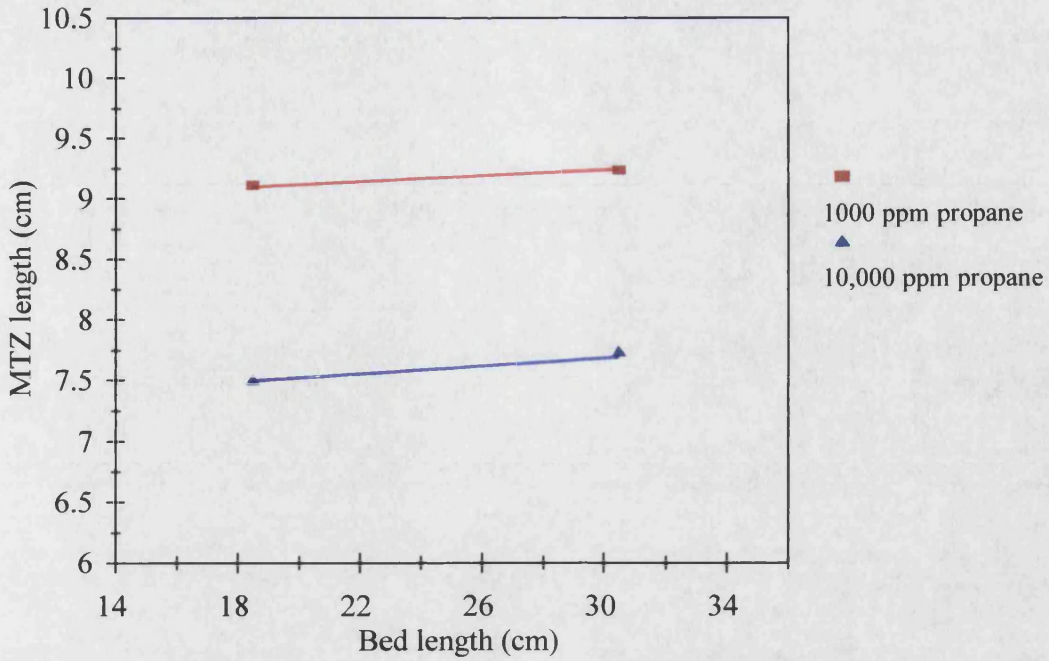

Figure 4.34 Variation of MTZ length with bed length

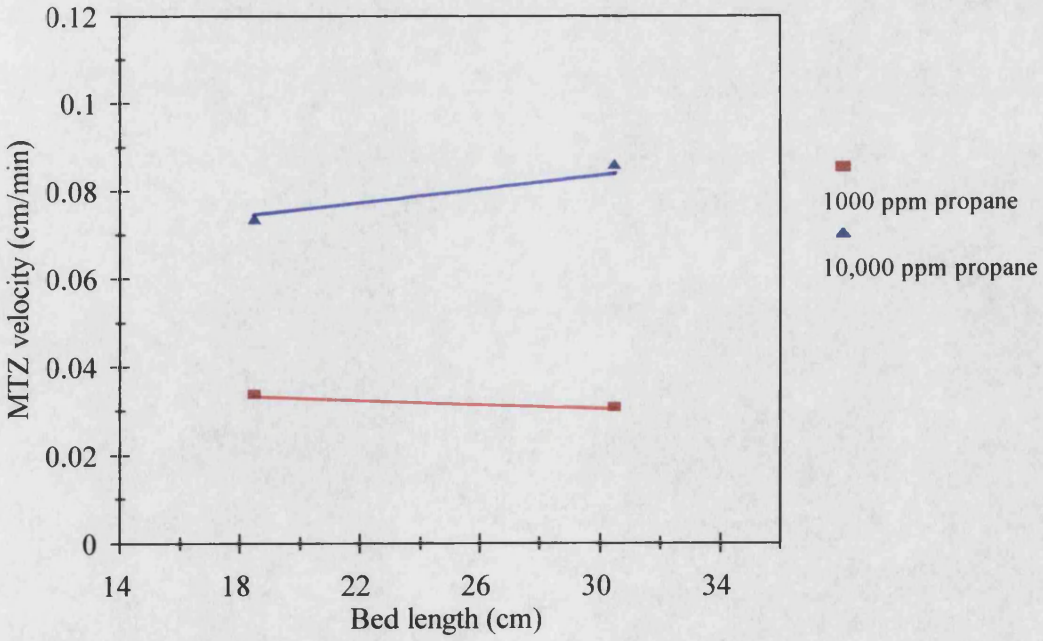

Figure 4.35 Variation of MTZ velocity with bed length

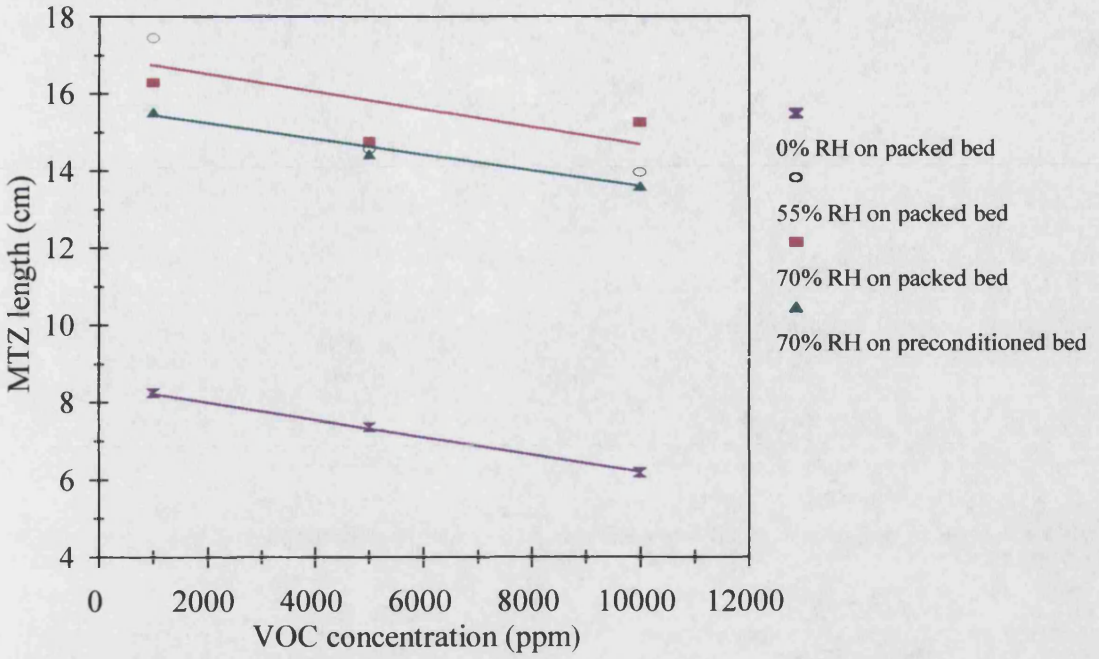

Figure 4.36 Effect of water vapour on the MTZ length of propane adsorption onto silicalite packed bed

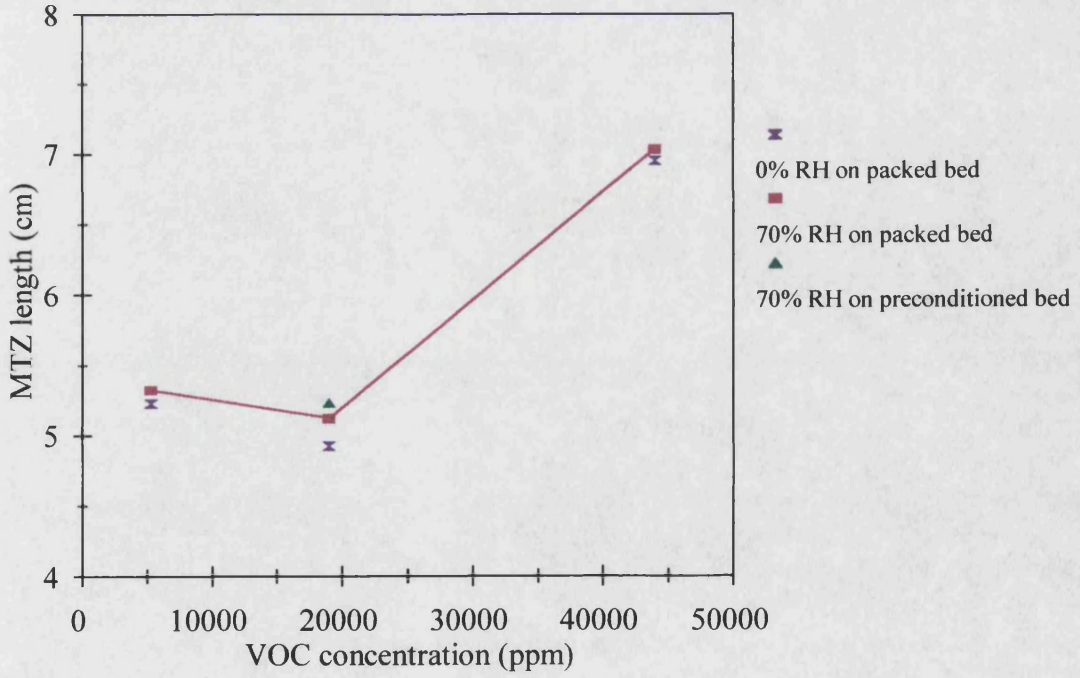

Figure 4.37 Effect of water vapour on the MTZ length of ethanol adsorption onto silicalite packed bed

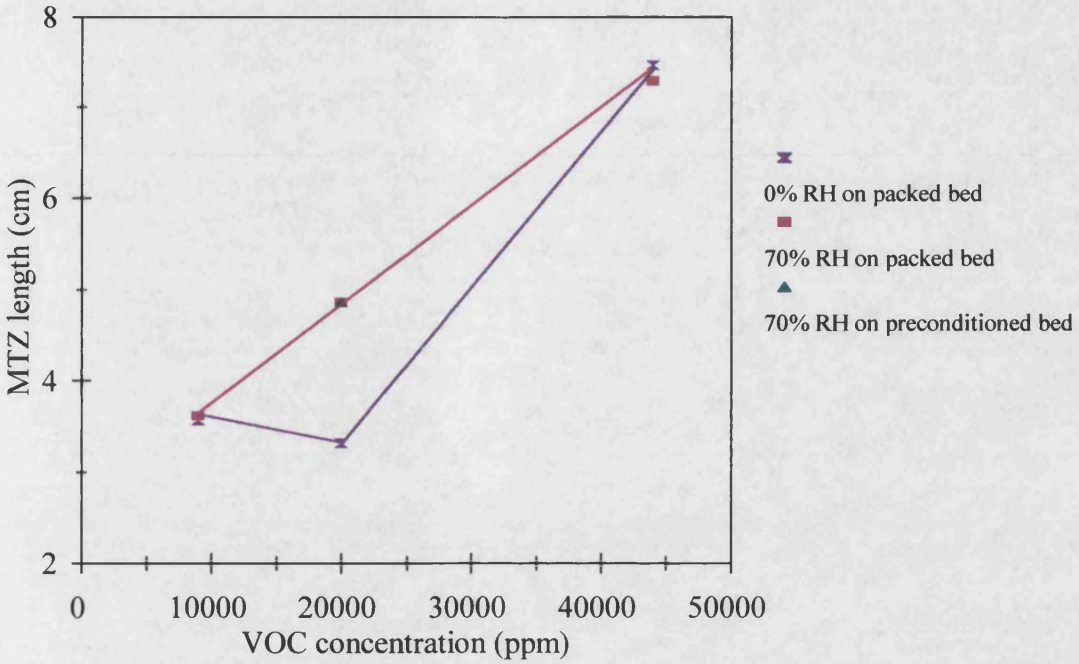

Figure 4.38 Effect of water vapour on the MTZ length of methylene chloride adsorption onto silicalite packed bed

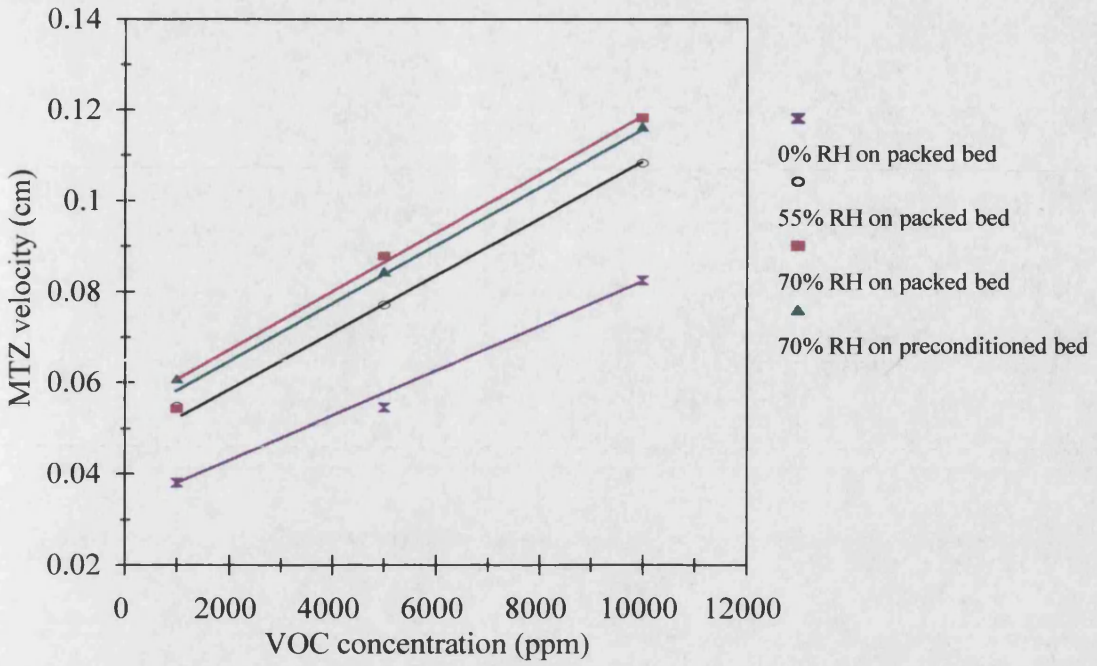

Figure 4.39 Effect of water vapour on the MTZ velocity for propane adsorption onto silicalite packed bed

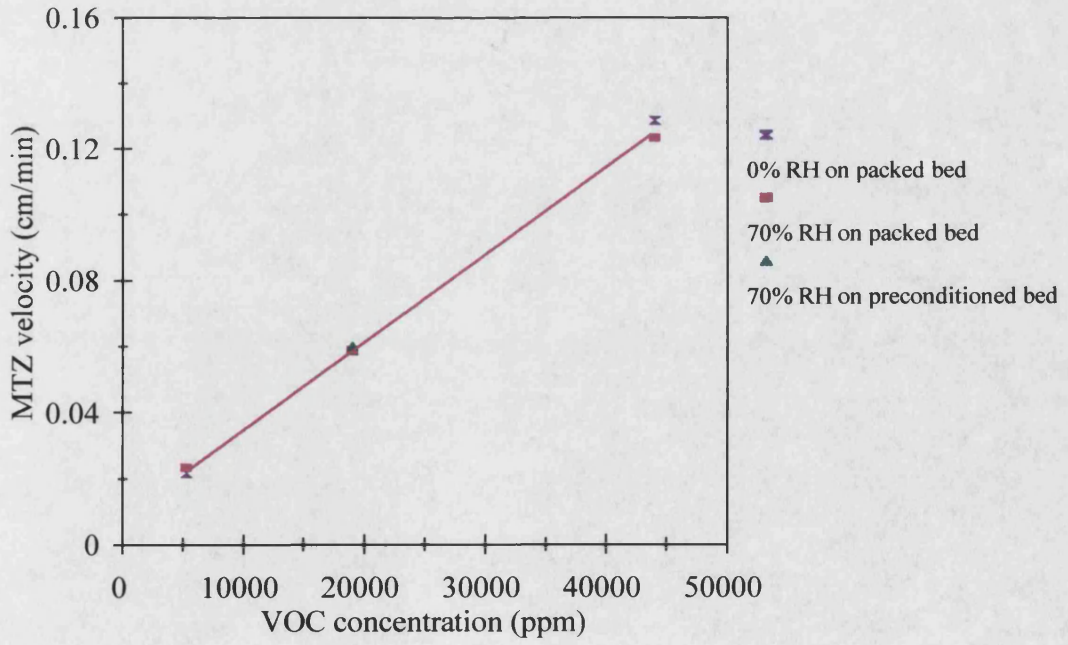

Figure 4.40 Effect of water vapour on the MTZ velocity for ethanol adsorption onto silicalite packed bed

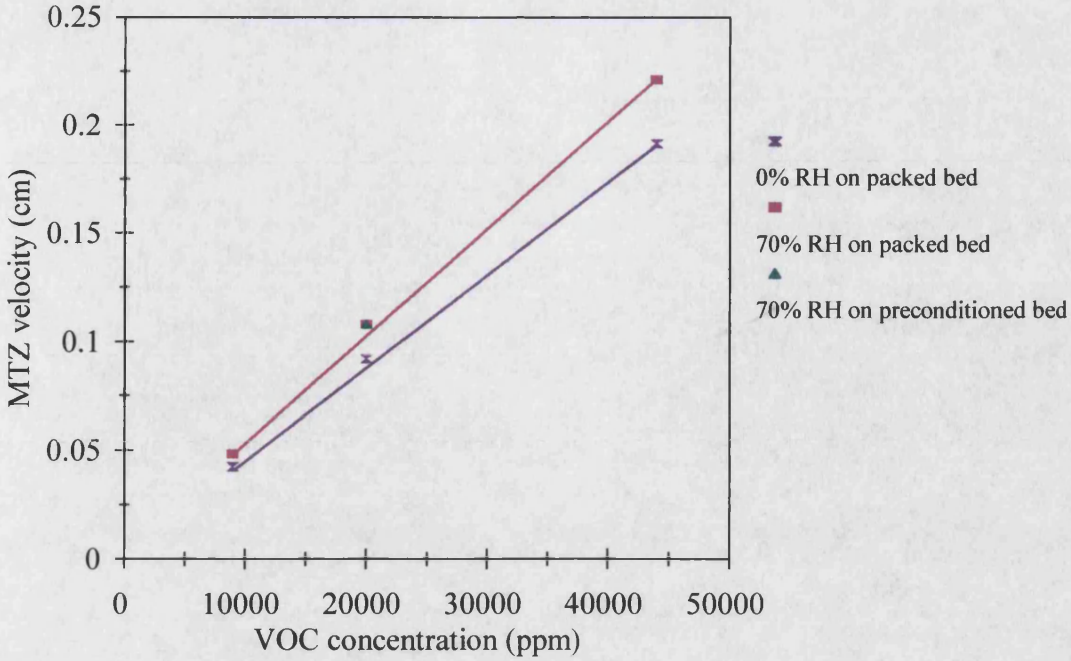

Figure 4.41 Effect of water vapour on the MTZ velocity for methylene chloride adsorption onto silicalite packed bed

4.4.4 Desorption Breakthrough Curves

Example desorption curves are shown in Figure 4.42. In Figure 4.43, it can be seen that the desorption curve is almost a mirror image of the adsorption curve for a low initial concentration of propane (i.e. 1000 ppm). For higher propane concentrations, the desorption curves are broader than the corresponding adsorption curves as shown in Figures 4.44-4.46. A longer time was required to regenerate the bed than was required for the previous adsorption step. The deviations from the mirror-image relationship between the adsorption and desorption profiles may be due to non-linearity in the adsorption isotherm.

A parameter is defined to identify the reversibility of the adsorption-desorption cycles as follows :

$$\Psi = \frac{q_{de}}{q_{eq}} \tag{4.10}$$

where Ψ is the reversibility factor, q_{de} is the amount of adsorbate being desorbed and q_{eq} is the amount adsorbed. The q_{de} and q_{eq} were calculated from the area below the desorption breakthrough curve and that above the adsorption breakthrough curve, respectively. The results shown in Table 4.8 indicate that the reversibility factor is greater than 98 % in most cases. This shows that propane desorption from the silica-rich zeolite is highly feasible at room temperature and atmospheric pressure. Regeneration at elevated temperature may not therefore be required.

Table 4.8 Results of the reversibility factor

Propane concentration (ppm)	Amount desorbed, q_{de} (mg/g)	Amount adsorbed, q_{eq} (mg/g)	Reversibility factor, Ψ (%)
1000	7.35	7.37	99.73
2500	13.47	13.53	99.55
5000	22.66	22.86	99.13
10,000	31.91	32.36	98.61

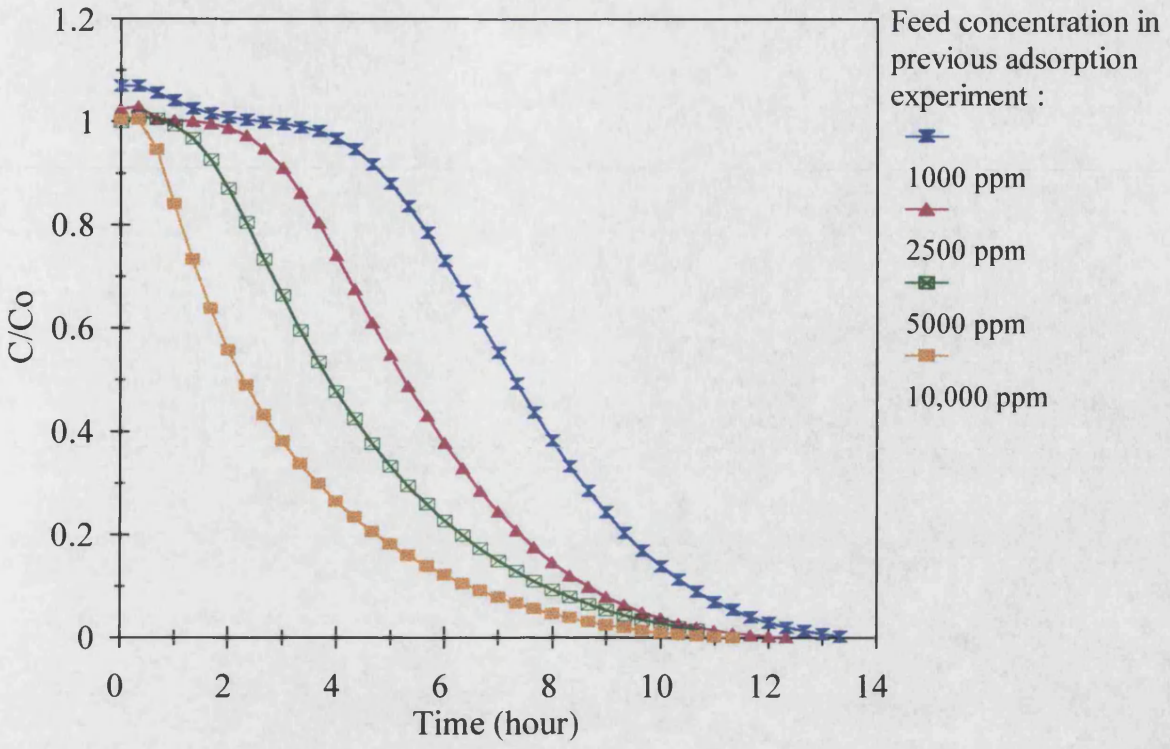

Figure 4.42 Desorption of propane from ZSM-5 packed bed under experimental conditions similar to those during adsorption (at 25°C)

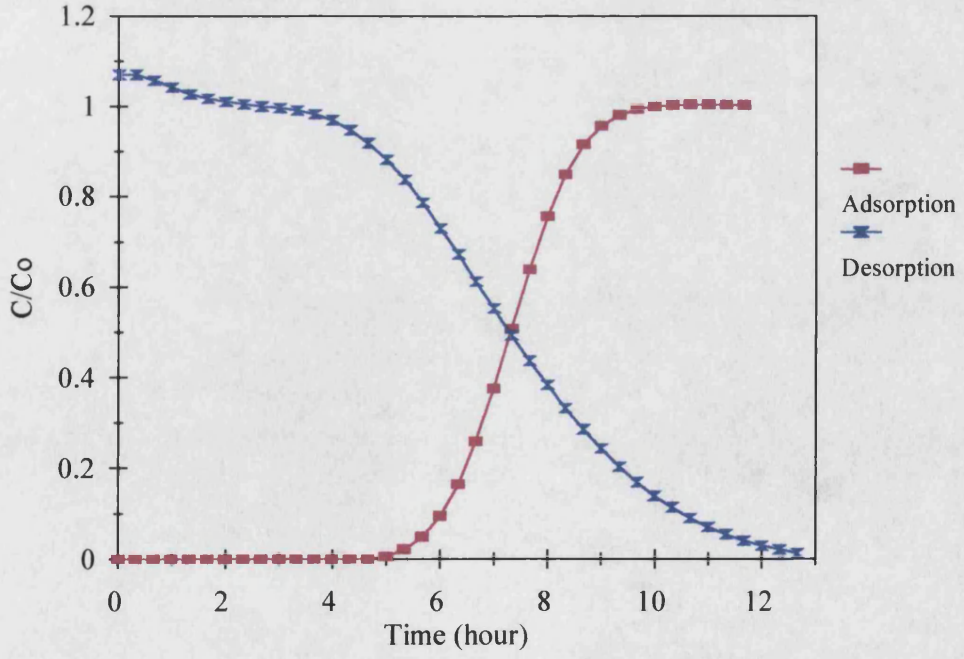

Figure 4.43 Adsorption and desorption curves of propane (1000 ppm) onto ZSM-5 packed bed

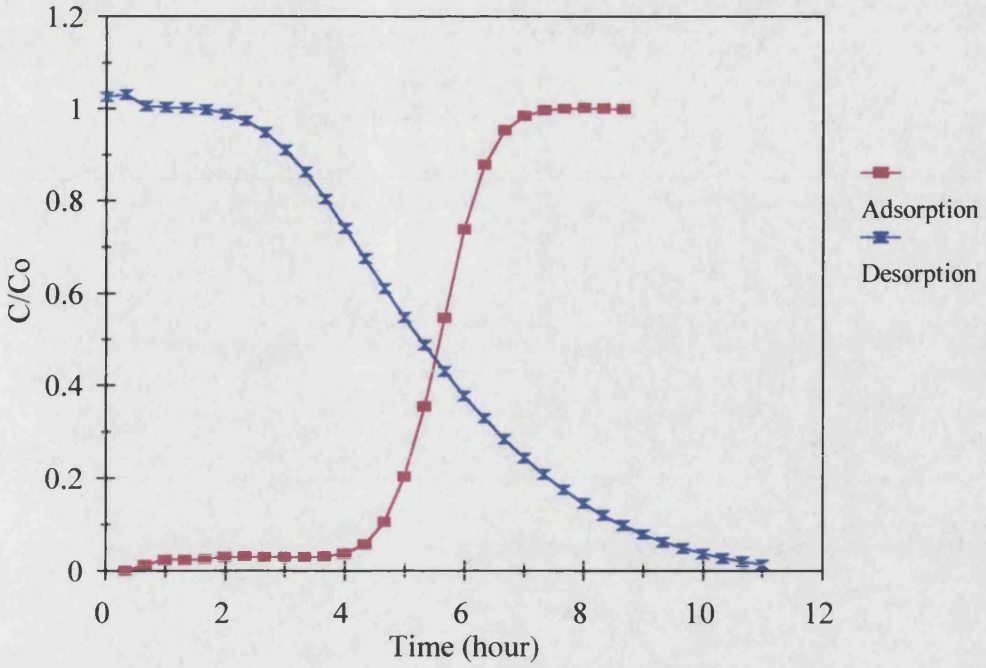

Figure 4.44 Adsorption and desorption curves of propane (2500 ppm) onto ZSM-5 packed bed

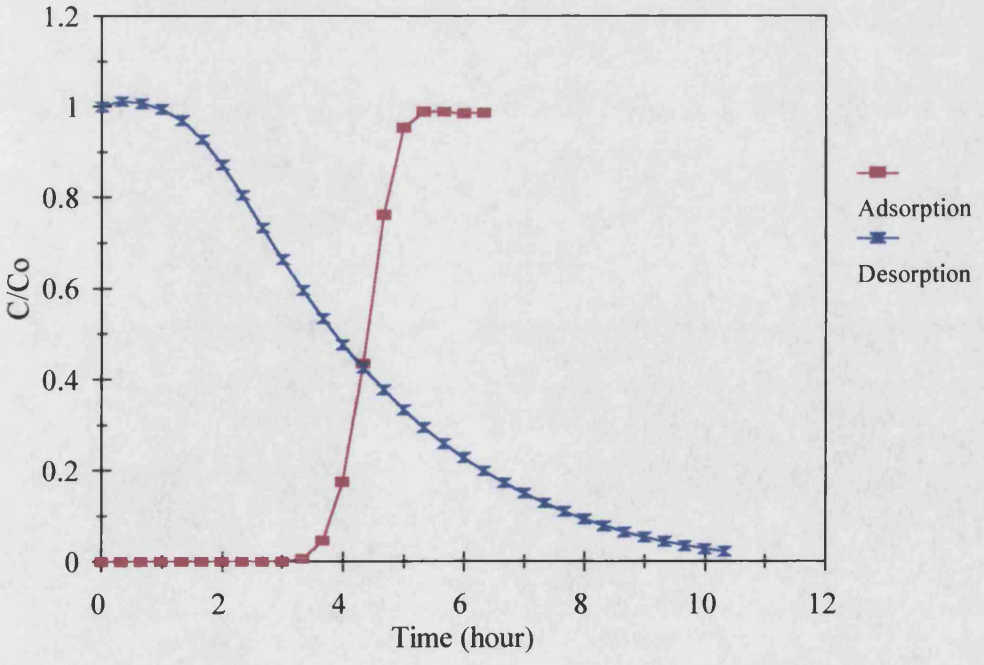

Figure 4.45 Adsorption and desorption curves of propane (5000 ppm) onto ZSM-5 packed bed

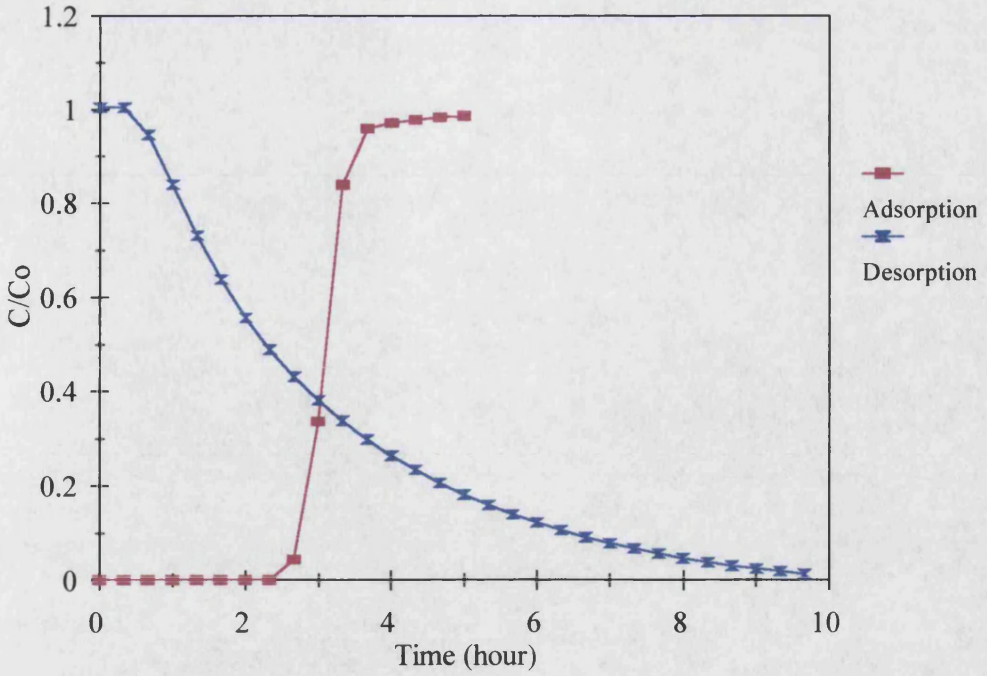

Figure 4.46 Adsorption and desorption curves of propane (10,000 ppm) onto ZSM-5 packed bed

4.5 Conclusions

The results described in this chapter of the thesis confirm that the adsorption of VOC onto a high silica zeolite packed bed is highly favourable.

The slope of the breakthrough curve increases with increasing feed concentration while the breakthrough time decreases. The increase in the slope of the curves was due to the shorter mass transfer zone (MTZ) at higher feed concentrations. For laminar flow through a packed bed, the limiting mass transfer may be dominated by bulk diffusion. As the feed concentration increases, the resistance to mass transfer in the fluid film is reduced and may result in a shorter MTZ. Earlier breakthrough was a direct consequence of a higher adsorbate input per unit time.

It was demonstrated that silicalite has a higher equilibrium loading for propane than ZSM-5 and thus is more effective in removing this VOC. This is probably due to the fact that silicalite does not contain any aluminium atoms in its crystalline structure. The adsorption of ethanol and methylene chloride onto silicalite pellets was found to be relatively independent of the VOC concentration in the range of 1000 to 40,000 ppm and highly favourable. Single component isotherms for these compounds are well represented by the Langmuir equation and agree reasonably well with the literature. Neither the flowrate nor the packed bed height has a significant effect on the equilibrium capacity. Study of the isotherms also reveals that silicalite pellets preferentially adsorbed VOCs in the order of ethanol, methylene chloride and propane. This may be due to the kinetic diameter of the ethanol being the smallest of the three VOCs.

Silicalite has successfully separated each VOC from a humidified stream. Methylene chloride showed little change in the shape of its breakthrough curve and a relatively small decrease in its adsorbability onto the adsorbent, up to about 70 % relative humidity (RH). On the other hand, propane adsorption was most affected by the presence of moisture, the loading reducing with increased water concentration at concentrations above 55 % RH. The reduction is greater when the adsorption bed is preconditioned with water vapour. The presence of moisture in the feed stream has

relatively little effect on the uptake of ethanol. Due to its high miscibility with water, ethanol diffuses into the water phase and is adsorbed onto the pores, displacing water molecules from these sites. An attempt was made to predict the isotherm of adsorption of a binary mixture of VOC and water using the extended Langmuir model. Predictions deviated from the experimental data and this may be due to water vapour adsorption being dominated by the capillary condensation mechanism.

The MTZ concept was employed to characterise the breakthrough curves. For single component uptake of VOC, there is a general increase in the MTZ velocity with feed concentration. In the case of propane, the MTZ length is reduced with increasing feed concentration. Thus higher bed efficiency is achieved when a higher propane feed concentration is used. For ethanol and methylene chloride, the MTZ length decreases to a point (from a feed concentration of 5000 ppm to 20,000 ppm) and then rises again with a further increase in feed concentration (from 20,000 to 44,000 ppm). Additional experimental data are required to give a clearer picture of this unexpected variation of MTZ length. The presence of water vapour does not change the properties of the MTZ of ethanol significantly, but for propane, the MTZ length is increased. In the case of methylene chloride, the effect is intermediate.

The desorption of propane from the silica-rich adsorbent is highly feasible under ambient conditions using a nitrogen purge. This is indicated by high values of the reversibility factor (greater than 98 % for all feed concentrations).

Chapter 5
Results of Dynamic Adsorption of VOCs onto Monoliths of Silicalite

5.1 Introduction

This chapter describes results obtained from experimental studies of kinetic and equilibrium adsorption of VOCs onto silicalite monoliths. The adsorption study was extended to include binary feed mixtures of VOC and water vapour, and adsorption onto premoisturised monolith. A comparison is made with the results obtained using a packed bed adsorber (Chapter 4) of similar adsorbent weight, under the same experimental conditions.

5.2 Summary of Experiments

Experiments were carried out using the equipment and experimental procedure described in Chapter 2. The monolithic adsorber was manufactured using a novel chemical formulation described in Chapter 3. The optimised monolith was composed of 80 wt. % silicalite and 20 wt. % of bentonite clay having channels of square cross section and a wall thickness of 1 mm. The structural properties of the monolith are summarised in Table 5.1. The monolith weight, which was similar to that of the comparative packed-bed, was 56.70 g. Adsorption experiments with the monolith were performed under conditions similar to those used with the packed bed (25 ^{o}C and atmospheric pressure). A summary of the experiments is given in Tables 5.2 and 5.3. The abbreviation "$MeCl_2$" in Tables 5.2 and 5.3 refers to methylene chloride. The VOC concentration is expressed in ppm volume. Experiments to determine the selectivity of the monolith for VOC over water vapour were conducted using both dry and preconditioned adsorbents. Preconditioning was performed by premoisturising the monolith using a humidified (70 % RH) nitrogen stream of 500 cm^3/min at room temperature for at least 12 hours. The breakthrough curves of both the organic and the

water vapour were monitored simultaneously from the break-point through to complete breakthrough. (The VOC breakthrough was detected by the FID and the water breakthrough was measured by the hygrometer). Desorption of VOCs from the monolith was carried out at low and elevated temperatures (Table 5.4) under a nitrogen purge. The effect, on propane desorption at low temperature, of varying the purge gas flowrate was also investigated.

Table 5.1 Properties of optimised square channel silicalite monolith

Monolith type	Thick wall square-channel
Silicalite:bentonite (wt. %)	80:20
Channel size (mm)	1.00
Wall thickness (mm)	1.00
Weight (g)	56.70
Length (cm)	21.80
Diameter (cm)	1.89
Cell density (cell number/cm^2)	25
Specific surface area (cm^2/cm^3)	10
Voidage	0.25

Table 5.2 A summary of the experimental conditions for single component breakthrough studies of silicalite monolith (at 25°C and atmospheric pressure)

Test number	Total flow (cm^3/min STP)	Adsorbate (ppm)
1	500	Propane : 1000
2	500	2500
3	500	5000
4	500	7500
5	500	10,000
6	500	Ethanol : 1000
7	500	3000
8	500	5300
9	500	9000
10	500	20,000
11	500	44,000
12	500	$MeCl_2$: 3000
13	500	19,000
14	500	44,000
15	500	Propane : 1000
16	1000	1000
17	1500	1000

Table 5.3 A summary of the experimental conditions for two-component breakthrough studies of silicalite monolith (at 25°C and atmospheric pressure)

Test no.	Total flow (cm^3/min STP)	Initial bed condition	Adsorbates (ppm)	(%)
18	500	dry	Propane : 1000	RH : 55
19	500	dry	5000	55
20	500	dry	10,000	55
21	500	dry	Propane : 1000	RH : 70
22	500	dry	5000	70
23	500	dry	10,000	70
24	500	Preconditioned	Propane : 1000	RH : 70
25	500	Preconditioned	5000	70
26	500	Preconditioned	10,000	70
27	500	dry	Ethanol : 5300	RH : 70
28	500	dry	19,000	70
29	500	dry	44,000	70
30	500	Preconditioned	Ethanol : 5300	RH : 70
31	500	Preconditioned	19,000	70
32	500	Preconditioned	44,000	70
33	500	dry	$MeCl_2$: 3500	RH : 70
34	500	dry	20,000	70
35	500	dry	44,000	70
36	500	Preconditioned	$MeCl_2$: 3500	RH : 70
37	500	Preconditioned	20,000	70
38	500	Preconditioned	44,000	70

Table 5.4 A summary of the desorption experiments

Test no.	Desorption temperature (°C)	Purge flowrate (cm^3/min STP)	Concentration on previous adsorption experiment (ppm)
39	25	500	Propane : 1000
40	25	1500	1000
41	25	3000	1000
42	180	500	1000
43	25	500	$MeCl_2$: 3500
44	25	500	20,000

5.3 Calculation Methods

The calculation methods described in Chapter 4 were used for the determination of equilibrium loading, and mass transfer zone (MTZ) length and velocity for VOC adsorption onto the monolith. The following section describes the experimentally obtained breakthrough curves, the results of calculations, and compares these with the results from the packed bed studies described in Chapter 4.

5.4 Results and Discussions

5.4.1 Breakthrough Curves

Breakthrough curves are shown in Figures 5.1-5.3. As the feed concentration was increased the breakthrough time was reduced for each single component. This is due to the increase in adsorbate feed input rate. The definitions of breakthrough and equilibrium times for monolith adsorption are the same as those used for the packed bed studies (Chapter 4). As with the packed bed, the premature concentration plateau prior to the main propane breakthrough is observed in the breakthrough curves for the monolith (Figure 5.1). As explained in Chapter 4, this effect has been attributed to the

impurities (5 %) present in the technical grade propane. The premature concentration plateau was not observed in the breakthrough curves for ethanol and methylene chloride (Figures 5.2 and 5.3)

Figure 5.4 shows the effect of feed flowrate on the breakthrough of propane. In general the shape of the curve does not alter but the breakthrough time is reduced as the flowrate is increased. This is a consequence of the higher adsorbate input per unit time. The relationship between the breakthrough time and the feed flowrate is illustrated in Figure 5.5.

Figures 5.7-5.9 show the effect of water vapour on the breakthrough curve of propane. For reference, Figure 5.6 shows the breakthrough of propane in the absence of water vapour. Comparing Figures 5.6 and 5.7, the propane breakthrough curves become broader and the breakthrough times are reduced considerably when moisture is present in the feed. The effect is more severe when the relative humidity is increased to 70 % RH (Figure 5.8) and when adsorption is carried out onto a preconditioned monolith (Figure 5.9). However, no concentration 'peak' is observed as in the case of packed bed (see Figures 4.12 and 4.13 in Chapter 4).

Figures 5.10 and 5.11 show the effluent concentrations of propane and water vapour versus time for a dry monolith and a preconditioned monolith, respectively. The breakthrough of water from the dry monolith occurs much earlier than that of propane. Where a preconditioned monolith was used, water vapour was detected in the effluent at the start of the experiment. This shows that the preconditioning step had fully saturated the monolith with water, so no further adsorption of water occurred during the adsorption experiment.

The effect of humidity on the adsorption of ethanol is shown in Figures 5.12-5.14. The breakthrough curves were not significantly affected by the presence of water vapour. This is probably due to the ethanol, being totally miscible with water, solubilising into the water phase and being adsorbed onto the sorption sites.

The influence of humidity on methylene chloride adsorption is shown in Figures 5.15-5.17. The effect is relatively small in comparison with that encountered for propane.

Figures 5.18-5.20 compare the breakthrough curves for the monolith with those for the packed bed. The breakthrough curves for the monolith are broader than those for the equivalent packed bed. Figures 5.21-23 compare the breakthrough times of monolith and packed bed. The breakthrough times for monolith adsorption are shorter than those for packed bed adsorption. The difference between the performance of the monolith and the packed bed is greatest for propane (Figure 5.21) and relatively small for ethanol (Figure 5.22) and methylene chloride (Figure 5.23). This may be due to the kinetic diameter of propane (0.512 nm) which is larger than that of ethanol (0.453 nm) and methylene chloride (0.489 nm), and thus it travels comparatively slower into the adsorption pore and is contained in lesser amount. On the other hand the ethanol molecule is the smallest and therefore can diffuse relatively faster into the pores and can be accommodated more. The shorter breakthrough time and the shallower breakthrough curve for the monolith are indicative of a greater resistance to adsorption in the monolith than in the packed bed. The portion of the breakthrough curves near the break-point for the monolith (Figures 5.18-5.20) is shallower than that for the packed bed. The reason for this discrepancy may be due to a greater external resistance in the monolith than in the packed bed. The external mass transfer resistance is expected to be higher in the monolith as manifested in its lower pressure drop. The external transfer properties will be calculated and explored further in Chapter 6.

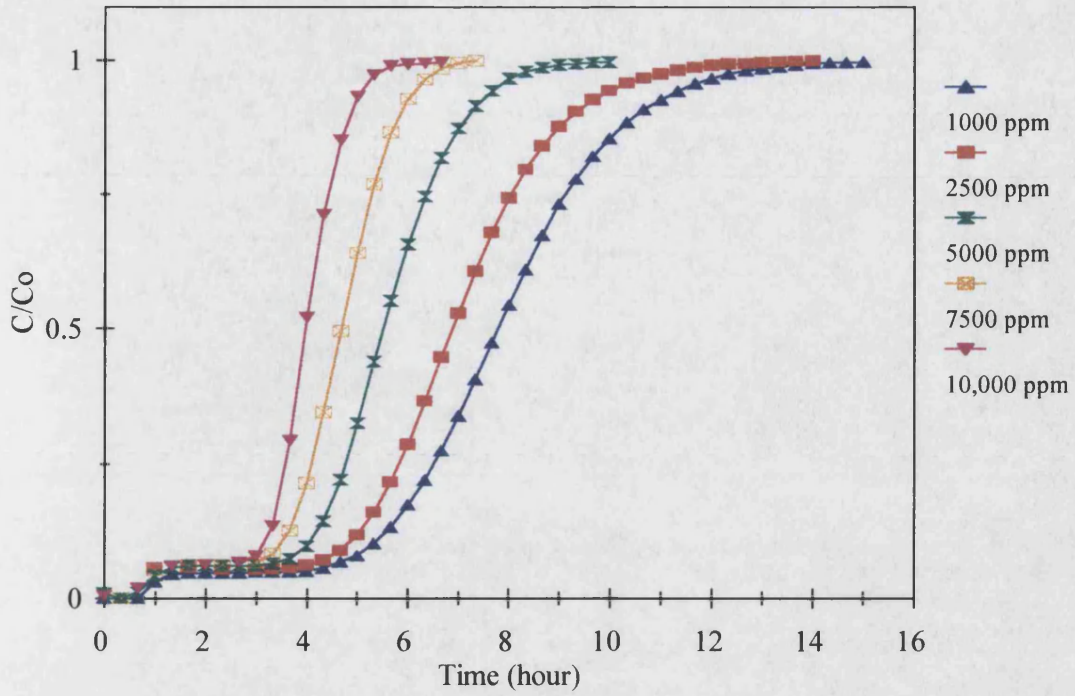

Figure 5.1 Dynamic adsorption of propane onto silicalite monolith at various feedstock concentrations

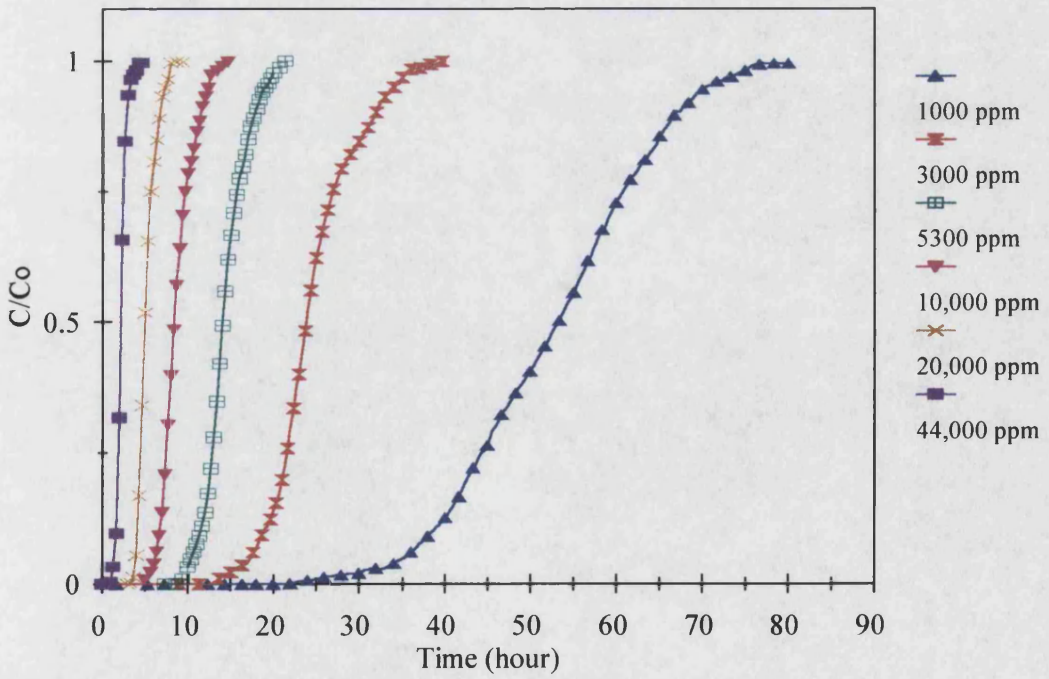

Figure 5.2 Dynamic adsorption of ethanol onto silicalite monolith at various feedstock concentrations

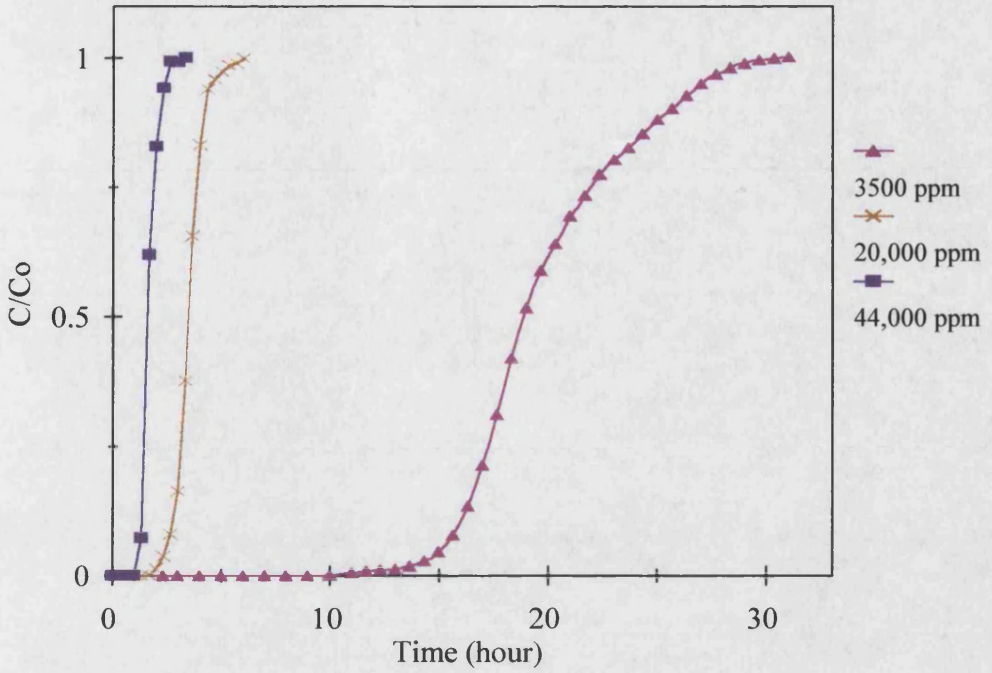

Figure 5.3 Dynamic adsorption of methylene chloride onto silicalite monolith at various feedstock concentrations

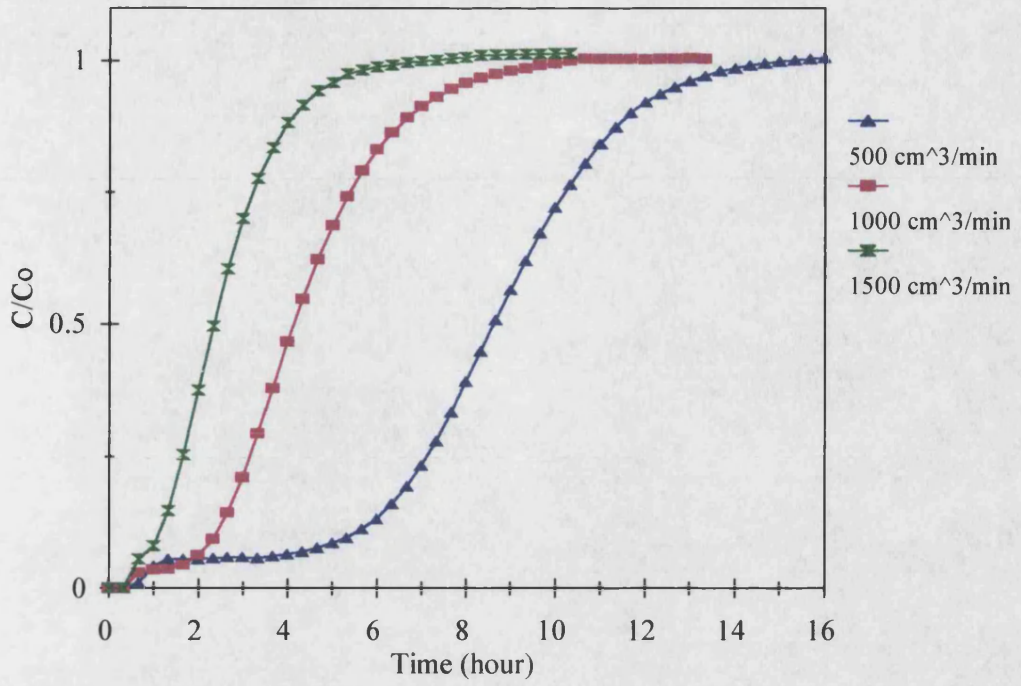

Figure 5.4 Effect of feed flowrate on the breakthrough of propane (1000 ppm) adsorption onto silicalite monolith

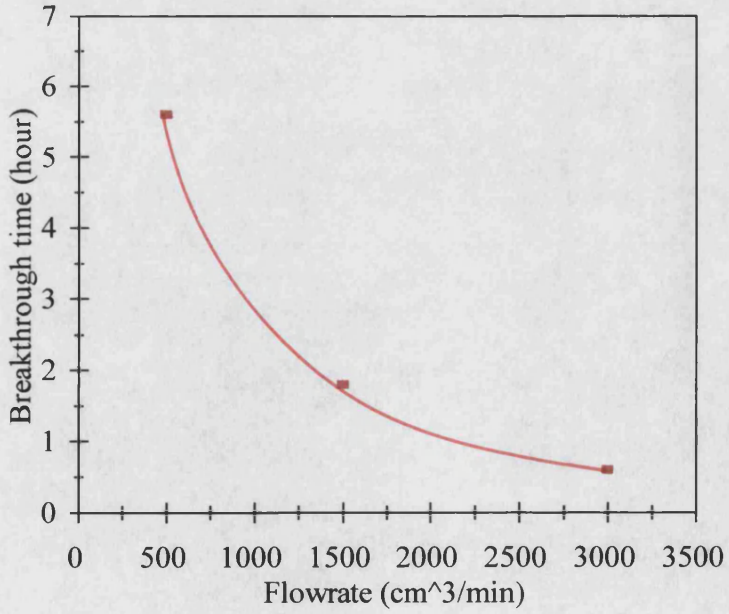

Figure 5.5 Variation of breakthrough time with feed flowrate

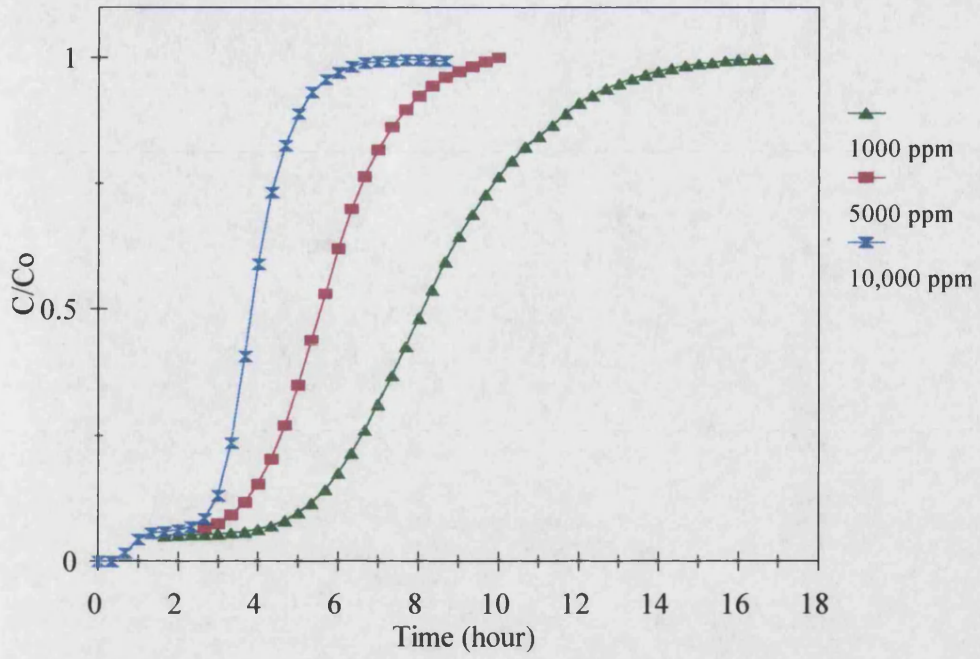

Figure 5.6 Adsorption of propane onto silicalite monolith (no moisture present)

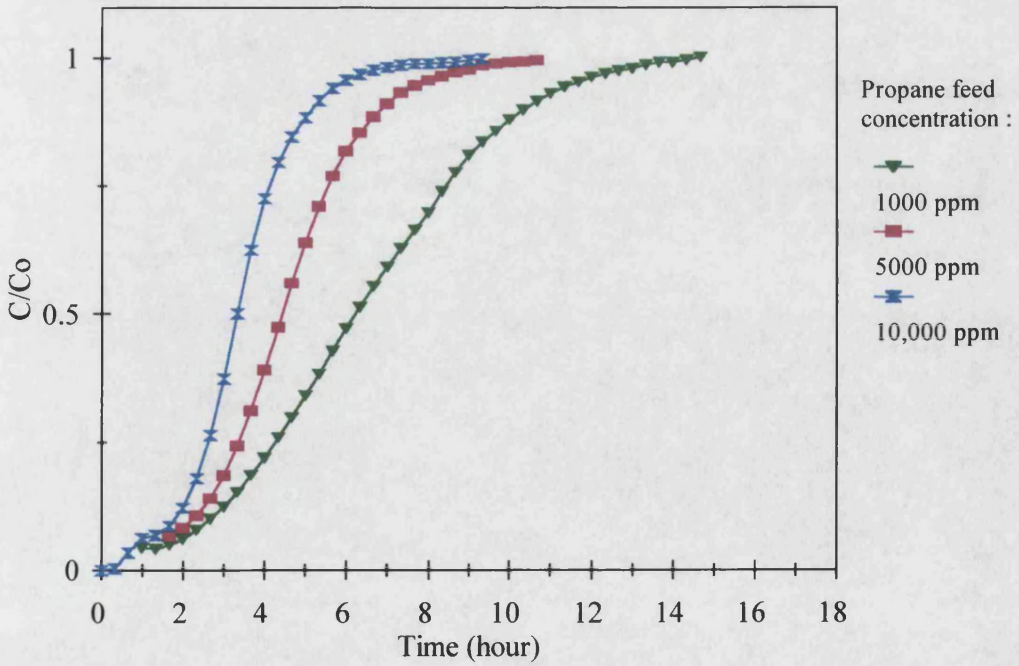

Figure 5.7 Adsorption of propane with 55 % RH water vapour onto silicalite monolith

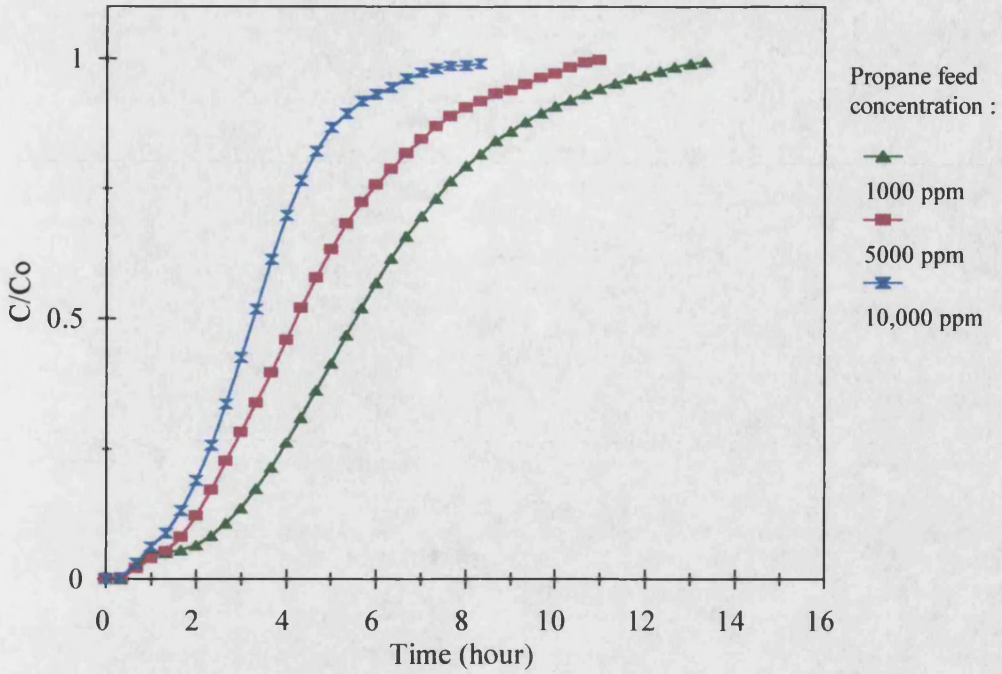

Figure 5.8 Adsorption of propane with 70 % RH water vapour onto silicalite monolith

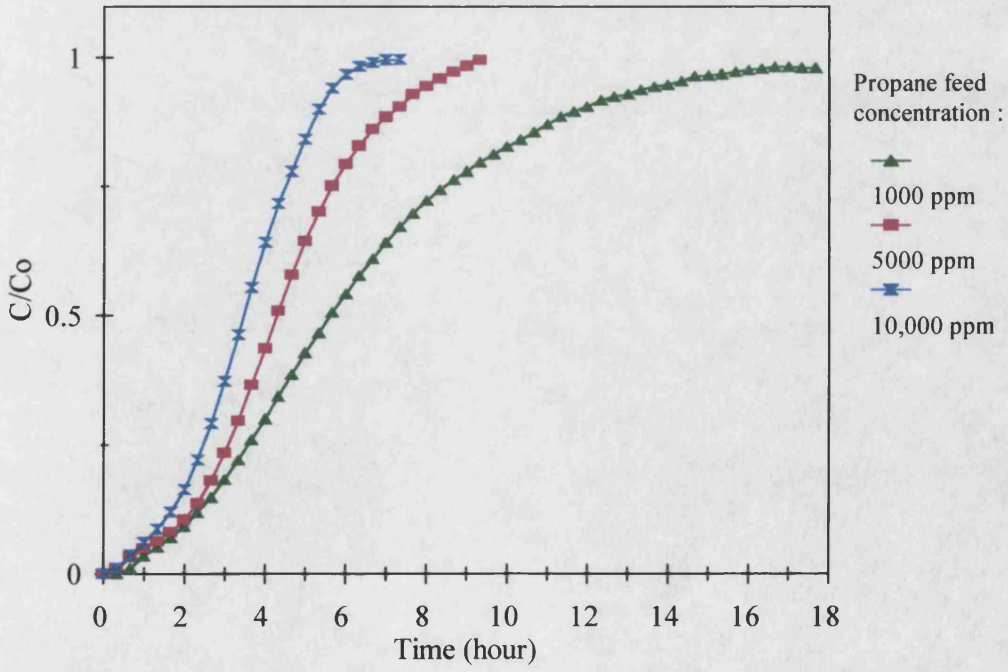

Figure 5.9 Adsorption of propane with 70 % RH water vapour onto preconditioned silicalite monolith

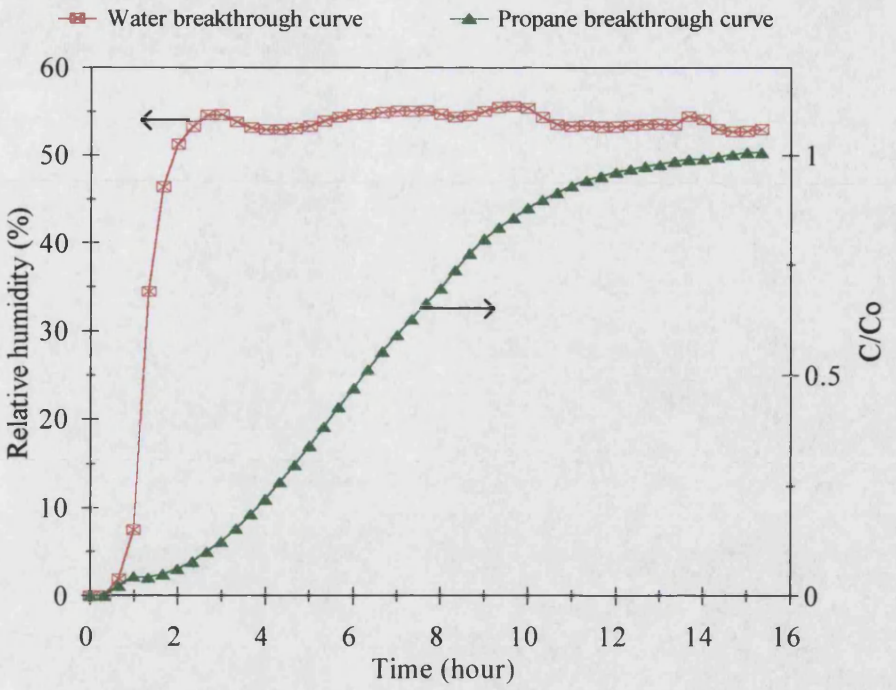

Figure 5.10 Effect of water vapour (55 % RH) on the adsorption of propane (1000 ppm) onto silicalite monolith

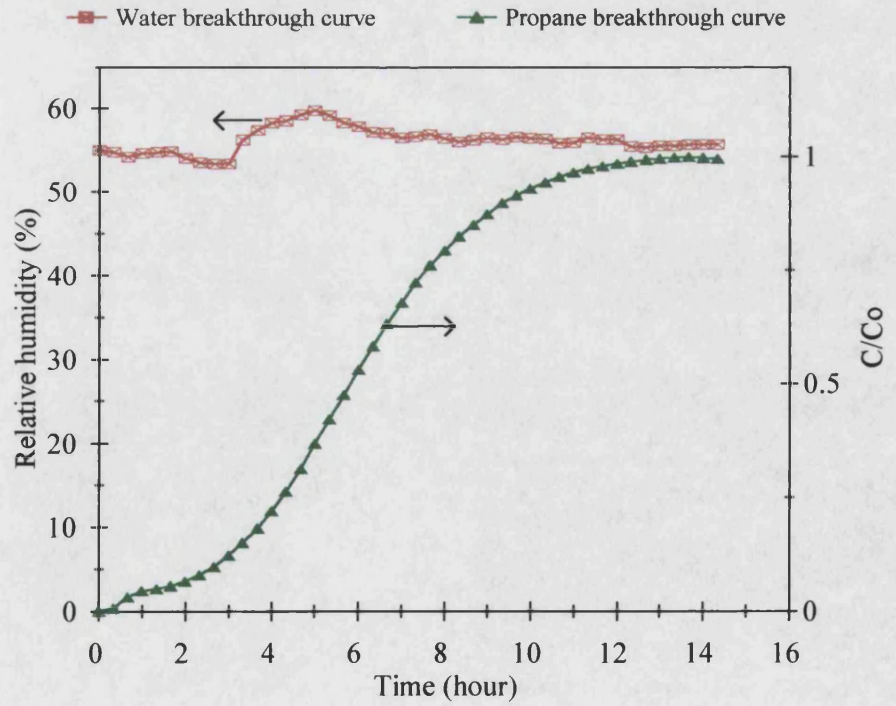

Figure 5.11 Effect of water vapour (55 % RH) on the adsorption of propane (1000 ppm) onto preconditioned silicalite monolith

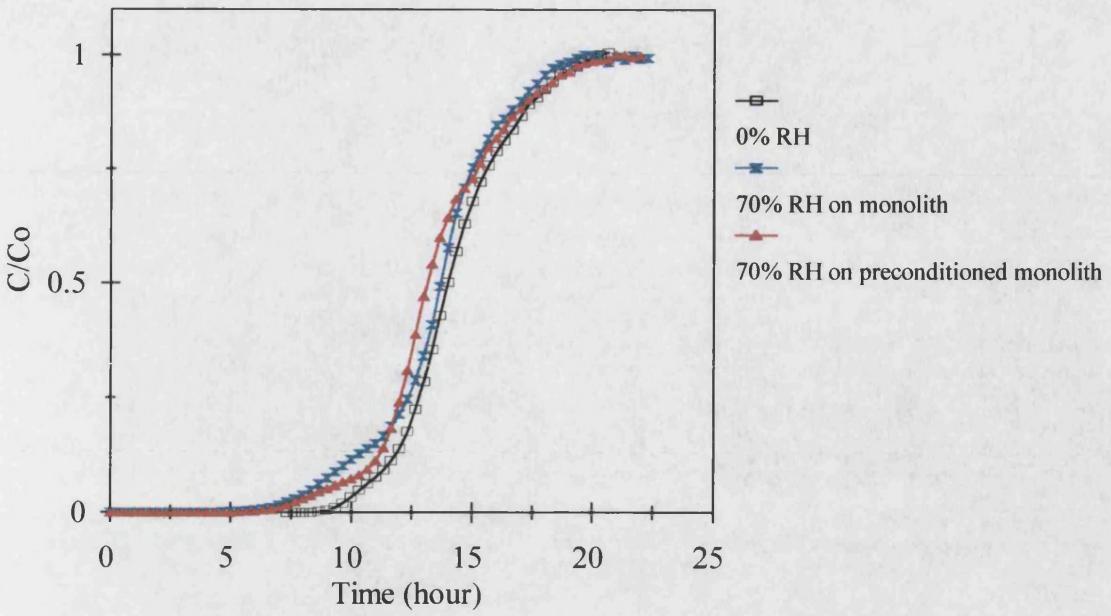

Figure 5.12 Effect of water vapour on the adsorption of ethanol (5000 ppm) onto dry and preconditioned silicalite monoliths

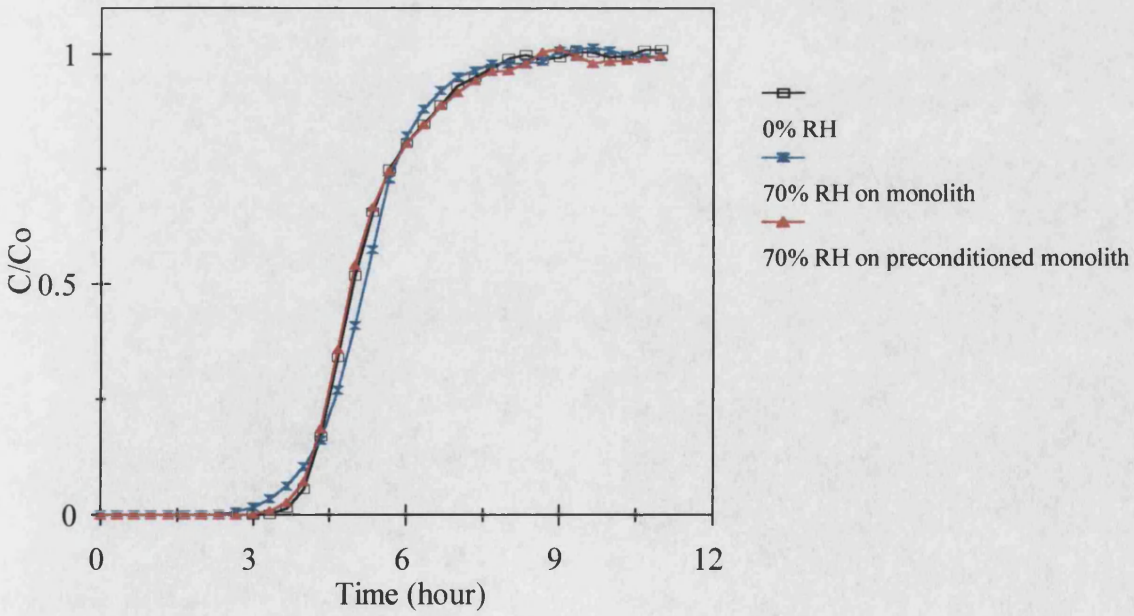

Figure 5.13 Effect of water vapour on the adsorption of ethanol (20,000 ppm) onto dry and preconditioned silicalite monoliths

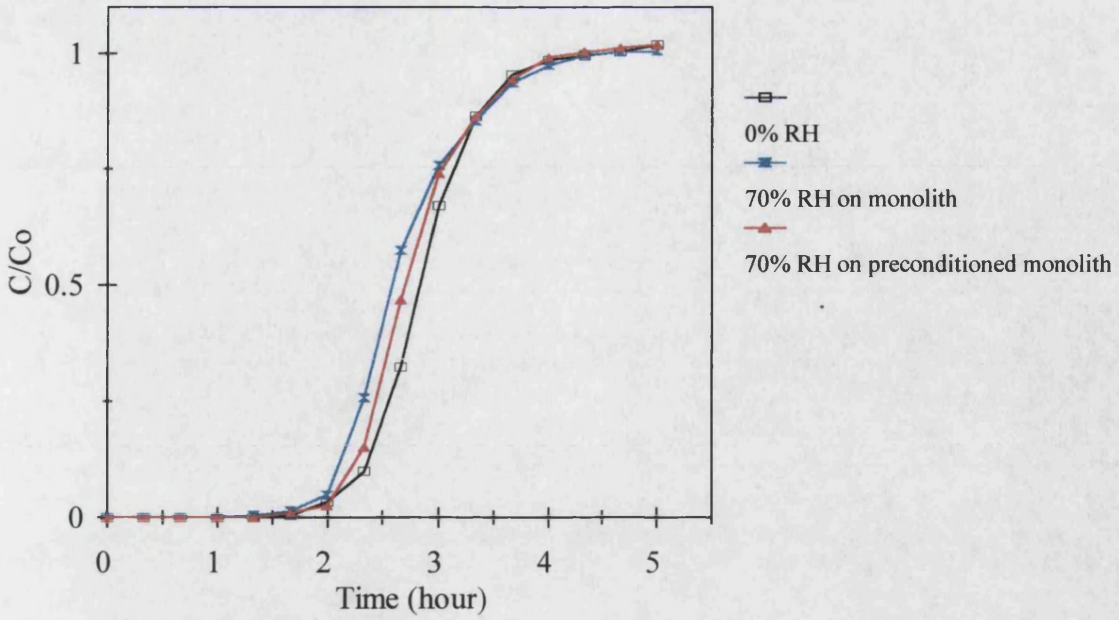

Figure 5.14 Effect of water vapour on the adsorption of ethanol (44,000 ppm) onto dry and preconditioned silicalite monoliths

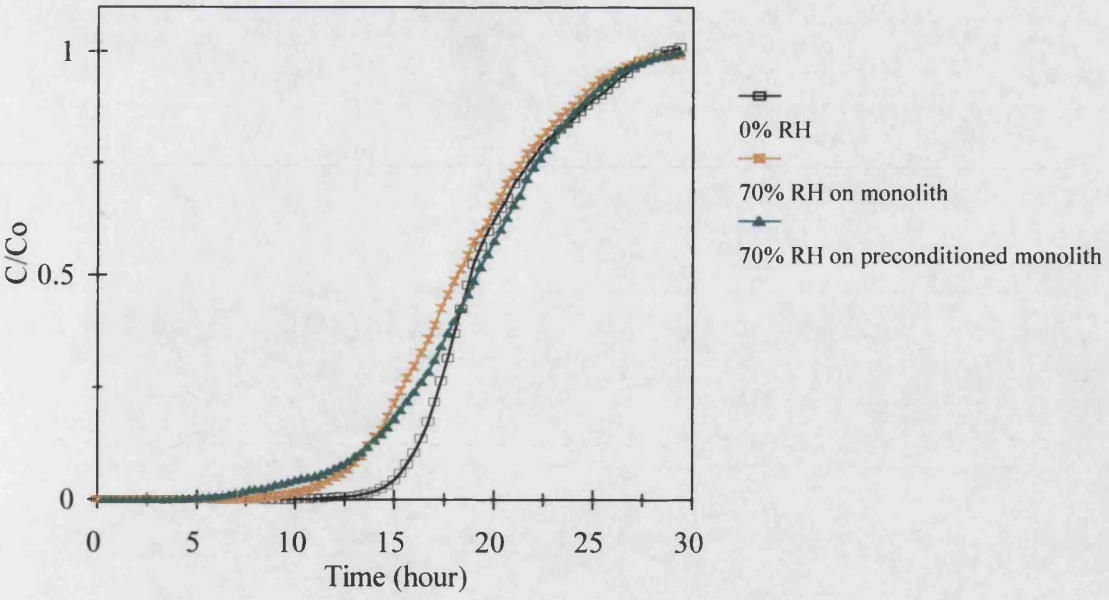

Figure 5.15 Effect of water vapour on the adsorption of methylene chloride (3300 ppm) onto dry and preconditioned silicalite monoliths

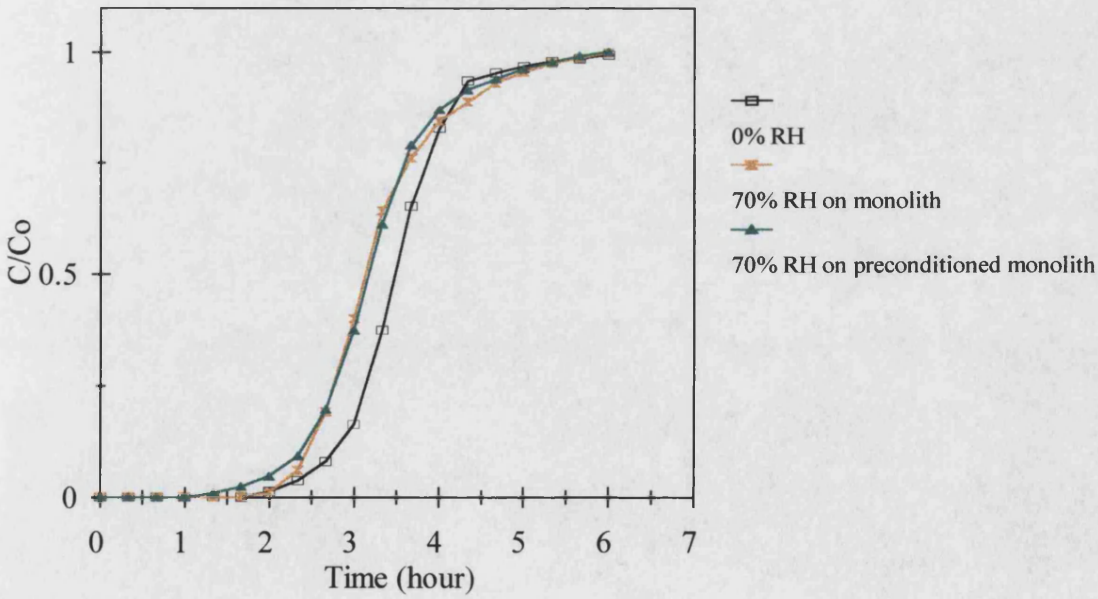

Figure 5.16 Effect of water vapour on the adsorption of methylene chloride (19,000 ppm) onto dry and preconditioned silicalite monoliths

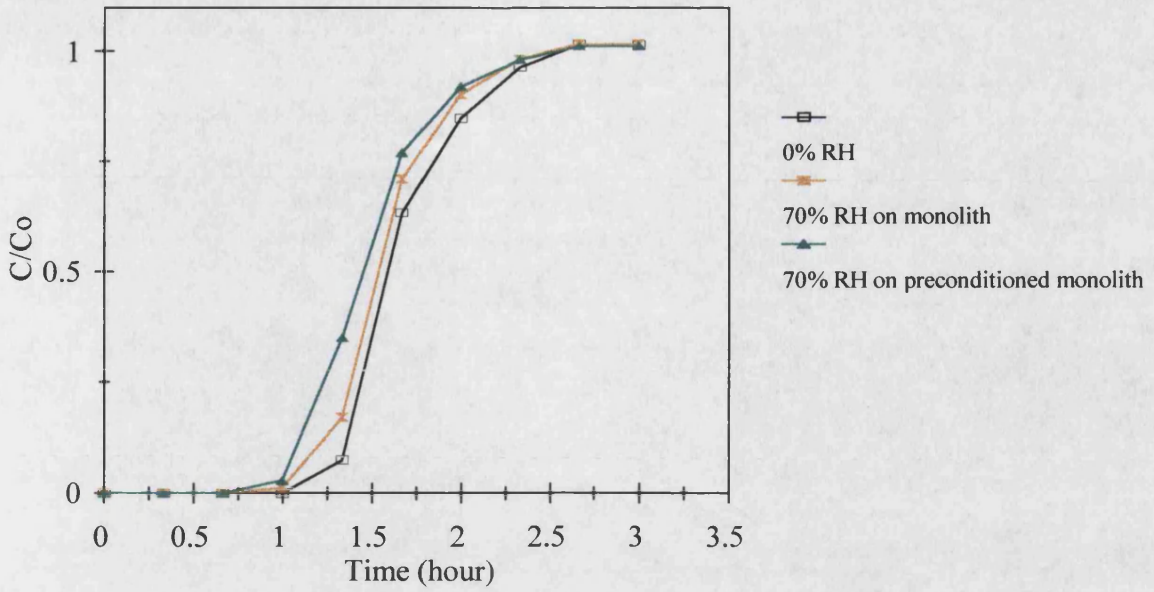

Figure 5.17 Effect of water vapour on the adsorption of methylene chloride (44,000 ppm) onto dry and preconditioned silicalite monoliths

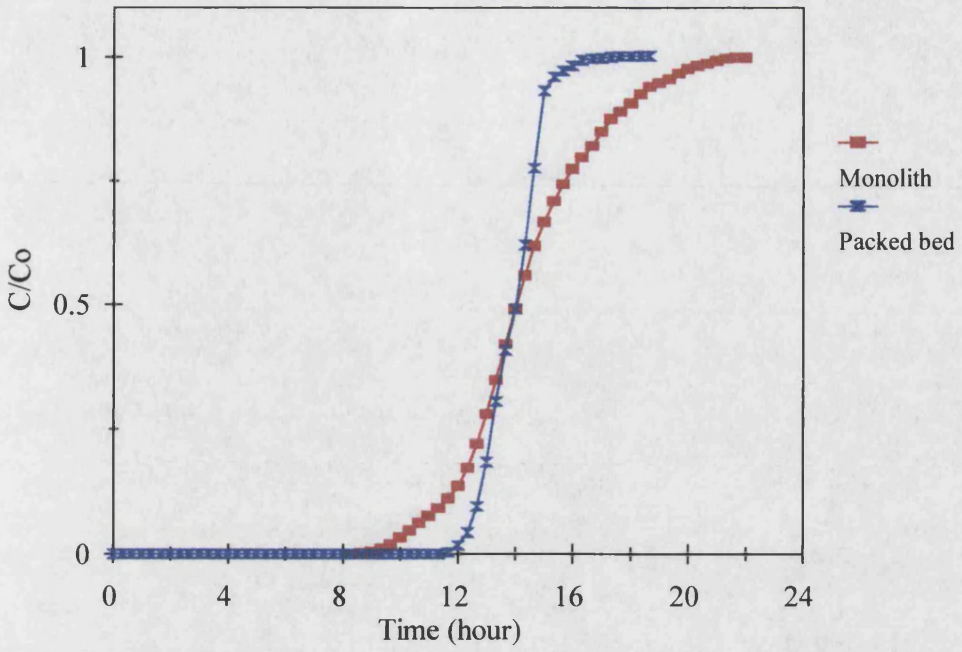

Figure 5.18 Comparison of ethanol (5000 ppm) adsorption onto silicalite monolith with adsorption onto silicalite packed bed

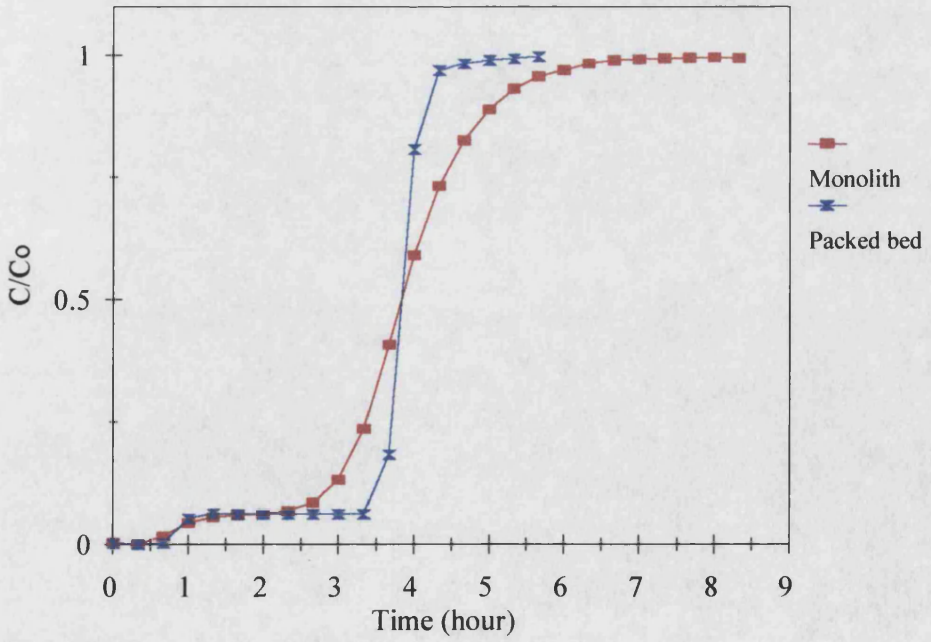

Figure 5.19 Comparison of propane (10,000 ppm) adsorption onto silicalite monolith with adsorption onto silicalite packed bed

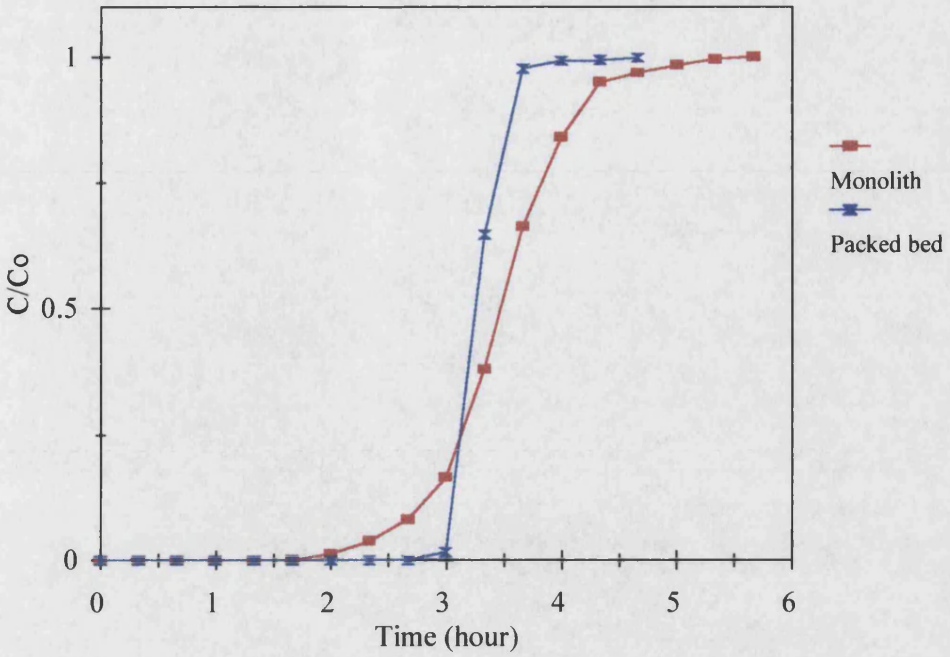

Figure 5.20 Comparison of methylene chloride (20,000 ppm) adsorption onto silicalite monolith with adsorption onto silicalite packed bed

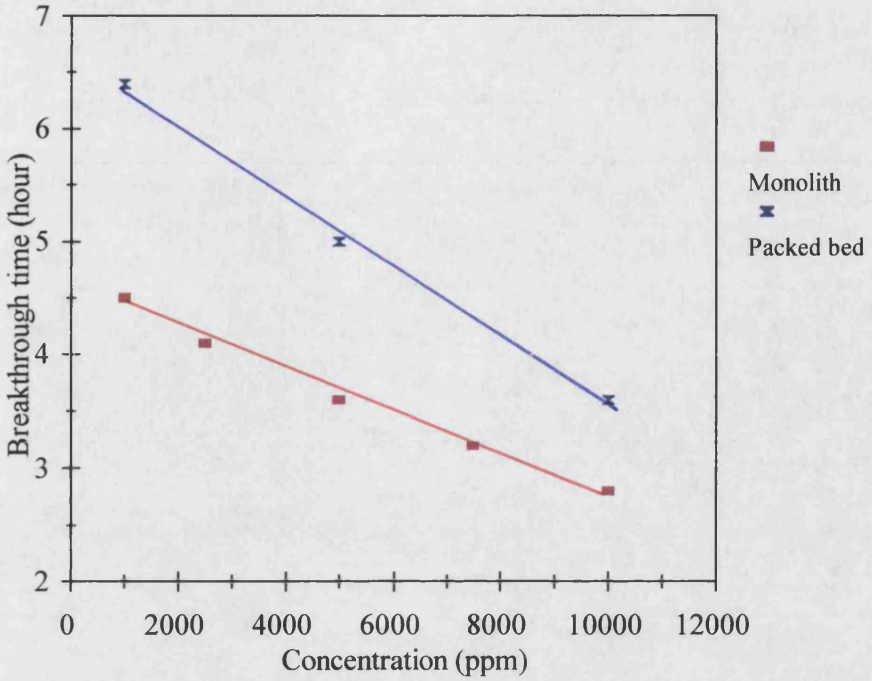

Figure 5.21 Comparison of breakthrough times of propane adsorption onto silicalite monolith with those of propane adsorption onto silicalite packed bed

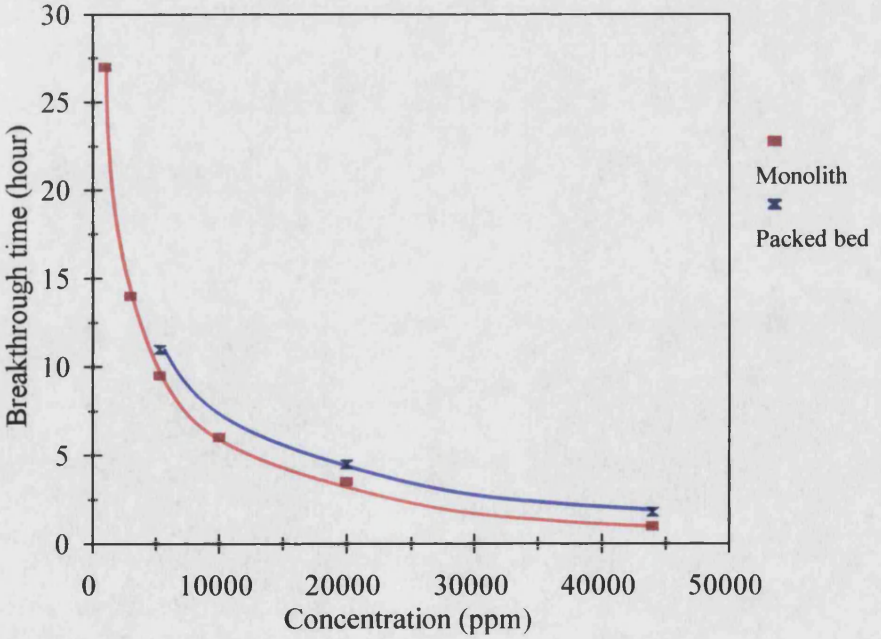

Figure 5.22 Comparison of the breakthrough times of ethanol adsorption ont silicalite monolith with those of ethanol adsorption onto silicalite packed bed

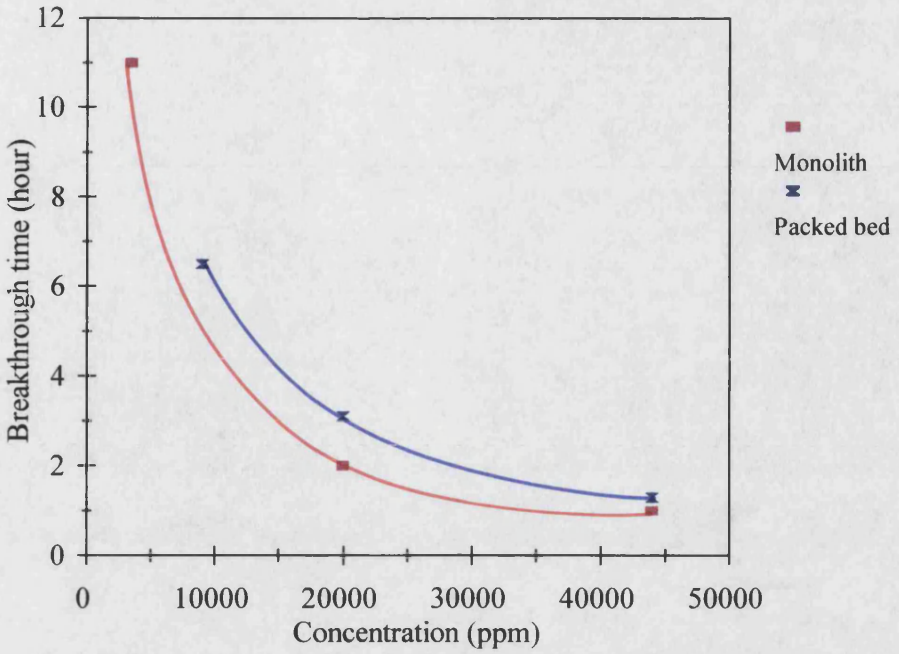

Figure 5.23 Comparison of breakthrough times of methylene chloride adsorption onto silicalite monolith with those of methylene chloride adsorption onto silicalite packed bed

5.4.2 Isotherms

Figure 5.24 shows the adsorption isotherms of VOCs onto silicalite monolith. The equilibrium loading for ethanol is greatest, followed by methylene chloride and then propane. This may be related to their kinetic diameters which increase in the order: ethanol, methylene chloride and propane. The equilibrium data are well represented by the Langmuir model. The parameters obtained from fitting the Langmuir equation to the experimental data are shown in Table 5.5. The values of q_{max} obtained for the monolith, when expressed in terms of volume per unit weight of adsorbent, are seen to be comparable with those obtained for the packed bed. This is to be expected since the maximum loading on the adsorbent should be independent of the geometric form of the material.

Table 5.5 Langmuir parameters for single component adsorption onto silicalite monolith

	Monolith				Packed bed
Adsorbate	Kinetic diameter (nm)	q_{max} (mg/g)	q_{max} (cm^3/g)	b ($mmHg^{-1}$)	q_{max} (cm^3/g)
Propane	0.512	69.76	0.1415	0.1510	0.1426
Ethanol	0.453	109.66	0.1400	1.1368	0.1564
Methylene chloride	0.489	150.76	0.1143	2.364	0.1083

The isotherm of pure water is shown in Figure 5.25, which compares the experimental results with those obtained using the packed bed (Chapter 4), and those from the literature (Flanigen et.al., 1978 and UOP, 1992). As can be seen in Figure 5.25, the equilibrium loading of water onto the monolith is the lowest, indicating that this material has a higher hydrophobicity. This may be due to the lower aluminium content of the monolith in comparison with that of the commercial pellets. The experimental isotherm for the monolith was fitted with the Langmuir equation using the numerical procedure described in Chapter 4, and the fit is also shown in Figure 5.25. The value of q_{max} is assumed to be constant and linear regression produces an adsorption equilibrium

constant of 0.0084 $mmHg^{-1}$, which is lower than that obtained for the packed bed (i.e. 0.0292 $mmHg^{-1}$).

The adsorption isotherms of VOCs in the presence of water vapour are shown in Figures 5.26-5.28 which include also the packed bed data described in Chapter 4. The equilibrium loading of propane on the monolith was found to be reduced in the presence of water vapour, the effect increasing with increasing water level (Figure 5.26). However, for a given relative humidity, the equilibrium loading of propane onto monolith was higher than that onto the packed bed. This may be due to the higher hydrophobicity of the monolith (Figure 5.25).

The isotherms of ethanol are not appreciably affected by the presence of water vapour (Figure 5.27). This may be related to the total miscibility of ethanol with water as explained in Chapter 4. The isotherms of methylene chloride adsorption onto the monolith are affected to a moderate degree (Figure 5.28). The miscibility of methylene chloride with water is higher than that for propane but lower than that for ethanol. However, for a given relative humidity, the monolith has a higher equilibrium capacity for methylene chloride than the packed bed.

The extended Langmuir expression for two-component adsorption, described in Chapter 4, was used to attempt to predict the isotherm of VOC adsorption with water vapour being present. The value of the maximum loading (i.e. q_{max} in Equation 4.4 described in Chapter 4) was assumed to be constant for the three organic compounds and it was taken as 0.1320 cm^3/g which was the average of the values shown in Table 5.5. The equilibrium adsorption constant of water on the monolith, equal to 0.0084 $mmHg^{-1}$, was determined by fitting the water isotherm (i.e. one of the b_j's of Equation 4.4 described in Chapter 4). The equilibrium adsorption constant of each of the VOCs (i.e. one of the b_j's of Equation 4.4 described in Chapter 4), as shown in Table 5.5, was determined by fitting the single component isotherm. The results in Figures 5.29-5.32 show good agreement between the experimental data and the prediction. As described in Chapter 4 the model is less successful, however, in predicting the isotherm data for the packed bed.

From the extended Langmuir model, it is possible to define a separation factor, α_{ij}, for the binary systems. This is the ratio of the adsorption equilibrium constants, b_i and b_j for the two components (i = VOC and j = water vapour) :

$$\alpha_{ij} = \frac{x_i / y_i}{x_j / y_j} = \frac{b_i}{b_j} \tag{5.1}$$

where x_i, x_j and y_i, y_j are the equilibrium mole fractions of components i and j in the adsorbed phase and the gas phase respectively. Table 5.6 shows that the separation factor for the monolith is higher than that for the packed bed for a given feedstock.

Table 5.6 Adsorption separation factors for binary mixtures based on the extended Langmuir model

	Silicalite Monolith			Silicalite Packed bed		
Binary mixture	b_i ($mmHg^{-1}$)	b_j ($mmHg^{-1}$)	α_{ij}	b_i ($mmHg^{-1}$)	b_j ($mmHg^{-1}$)	α_{ij}
Propane-water	0.1510	0.0084	17.98	0.1450	0.0292	4.97
Ethanol-water	1.137	0.0084	135.36	0.4027	0.0292	13.79
$MeCl_2$	2.364	0.0084	281.43	1.248	0.0292	42.74

In the case of the adsorption of ethanol without water vapour being present, the equilibrium loading onto the monolith and the packed bed are approximately the same. It might therefore be anticipated that the adsorption equilibrium constant, b, obtained by matching the experimental data to the linearised Langmuir equation, would be the same for both systems. However, as indicated in Table 5.6, this not the case. Figure 5.33 shows that the experiments on the packed bed have not covered the lower feed concentration range, thereby leading to a linearised Langmuir plot having a higher slope and lower intercept at the y-axis than expected (i.e. lower value of b). Clearly, there should be sufficient experimental data points to cover the entire concentration range

(from very low concentration to near saturation) in order to give accurate results. Despite this limitation, a comparison between the selectivity data of monolith and packed bed is still considered to be valid. This is because the value of the denominator in Equation 5.1 is different for the two adsorption systems (b_j = 0.0084 $mmHg^{-1}$ for monolith and b_j = 0.0292 $mmHg^{-1}$ for packed bed).

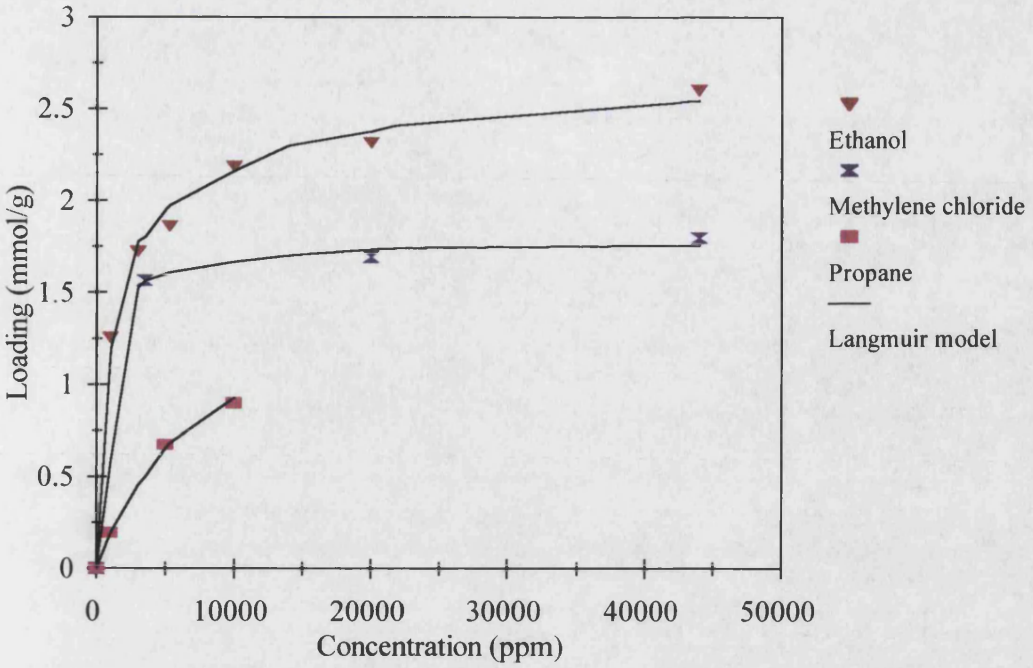

Figure 5.24 Adsorption isotherms of single component VOC onto silicalite monolith and the Langmuir model fit

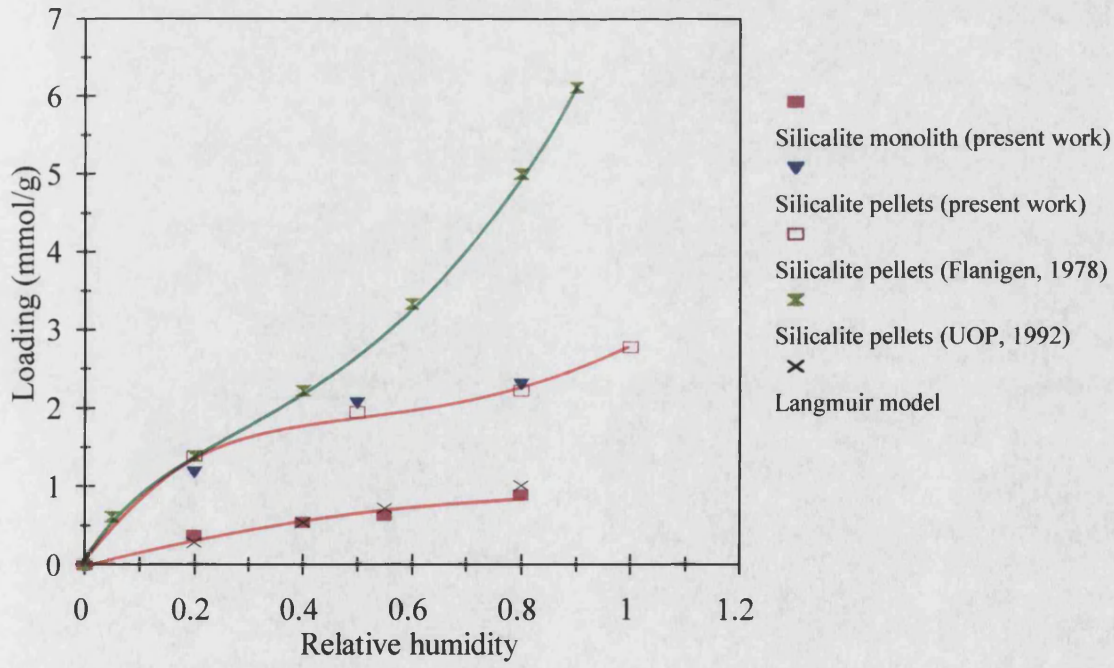

Figure 5.25 Comparison of the adsorption isotherms of water vapour onto silicalite monolith with those obtained using silicalite packed bed, values from the literature, and the Langmuir model fit

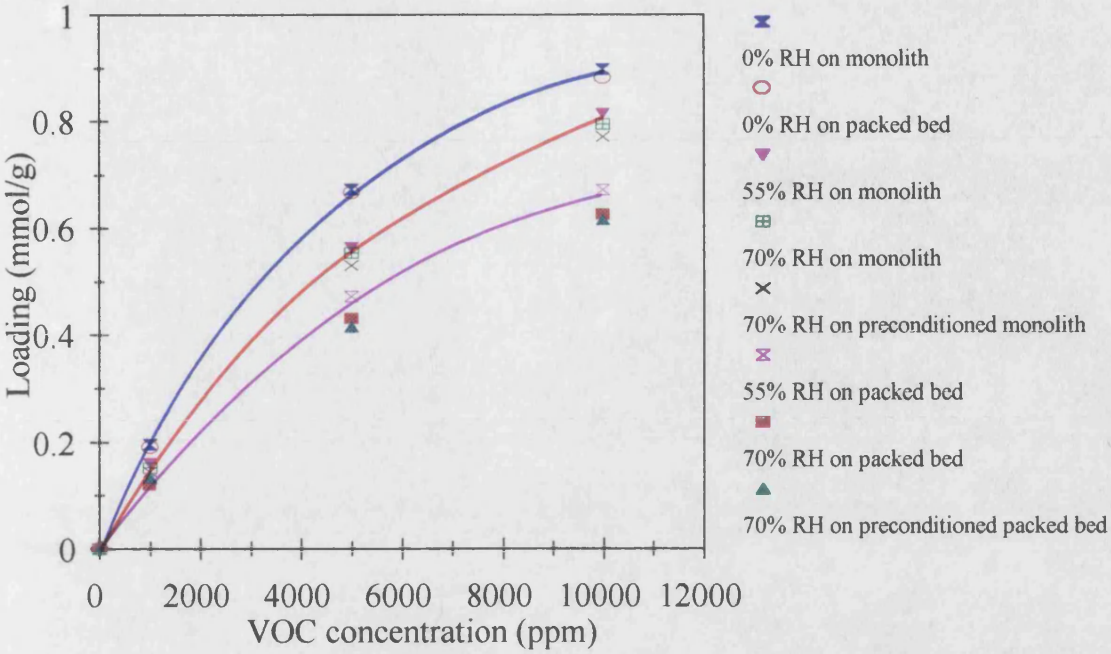

Figure 5.26 Effect of water vapour on the adsorption of propane onto silicalite monolith and comparison with the adsorption onto packed bed

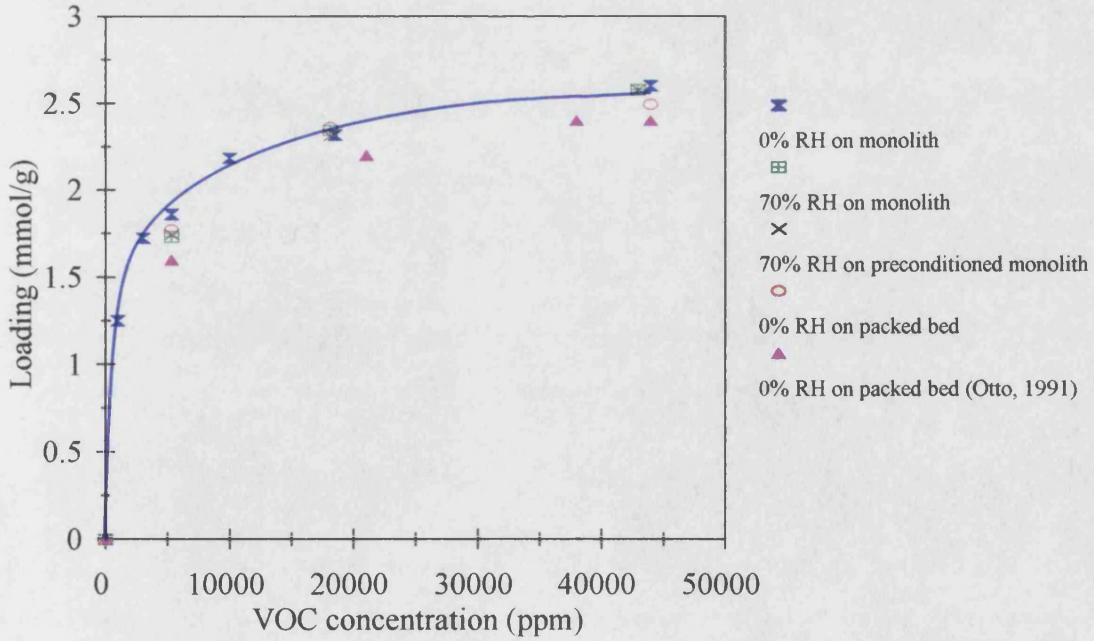

Figure 5.27 Effect of water vapour on the adsorption of ethanol onto silicalite monolith and comparison with the adsorption onto packed bed

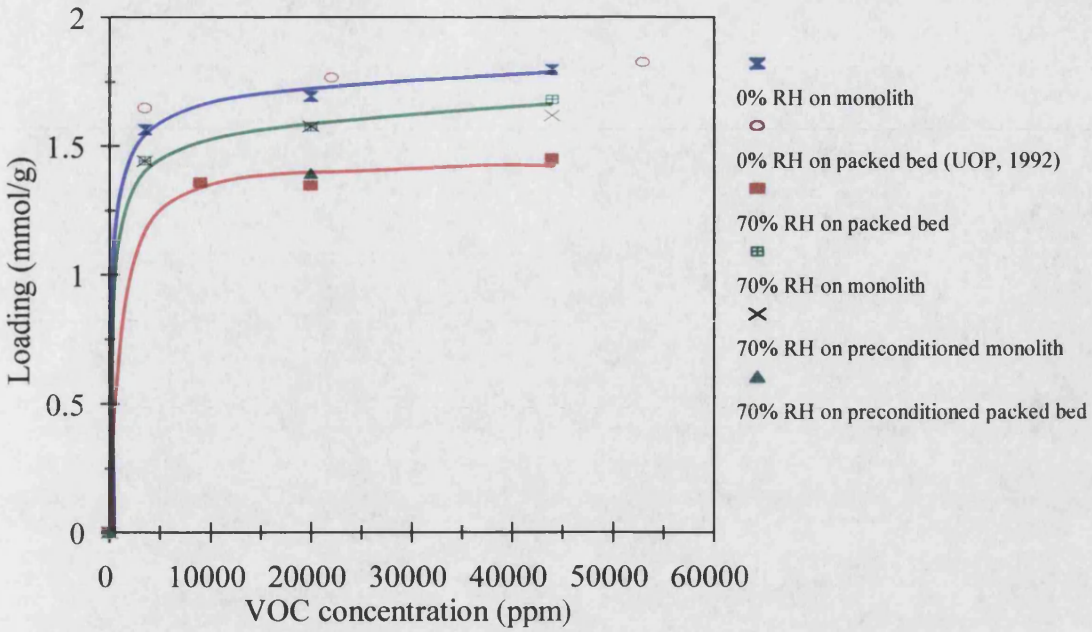

Figure 5.28 Effect of water vapour on the adsorption of methylene chloride onto silicalite monolith and comparison with the adsorption onto packed bed

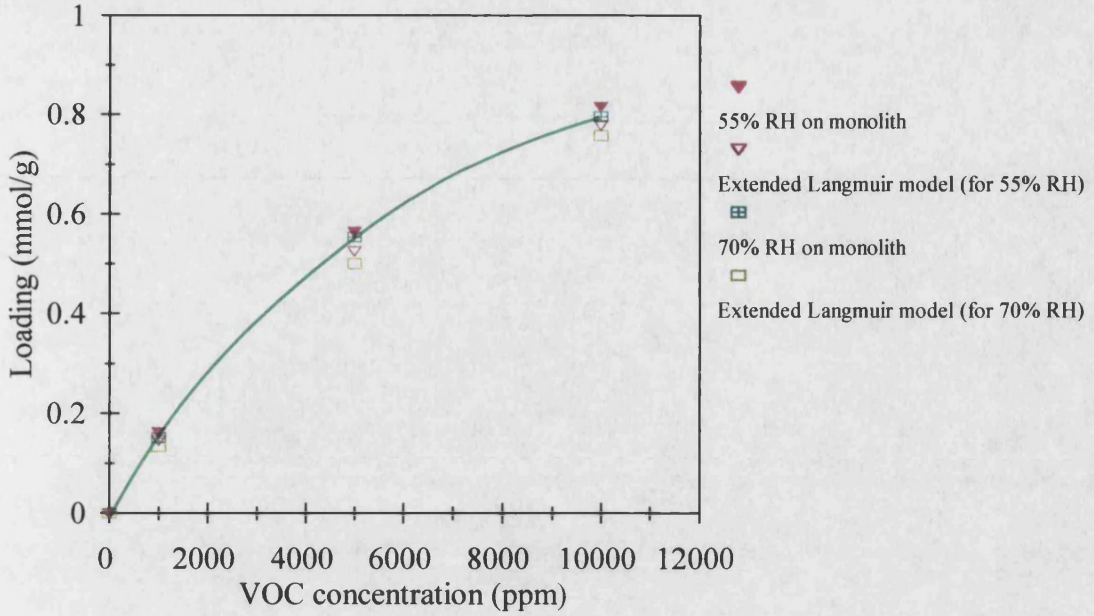

Figure 5.29 Comparison of the experimentally obtained propane isotherm with the extended Langmuir model

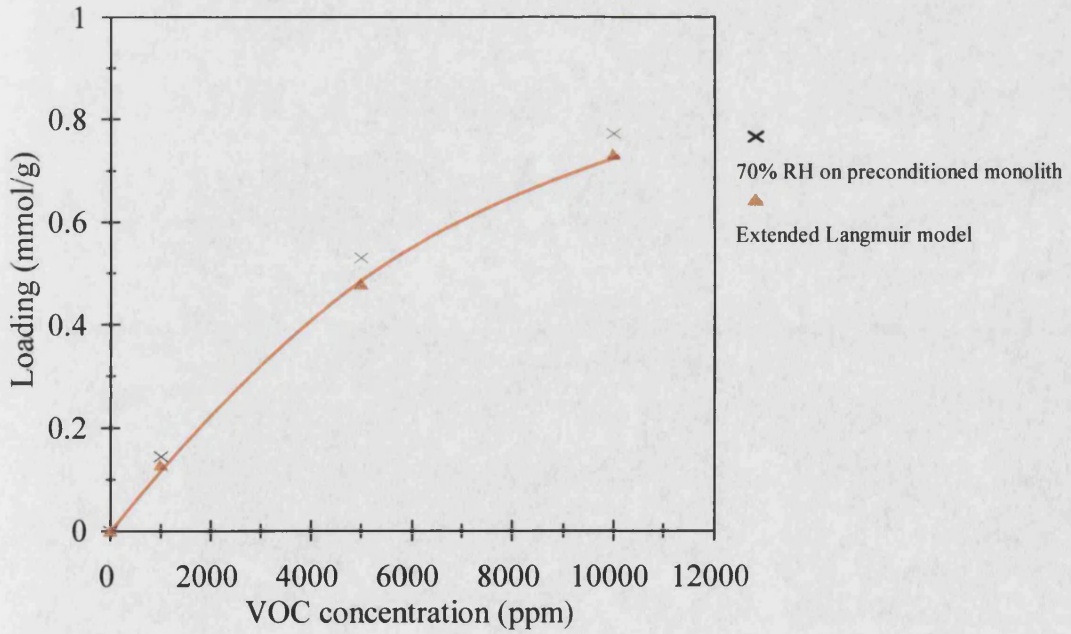

Figure 5.30 Comparison of the experimentally obtained propane isotherm with the extended Langmuir model

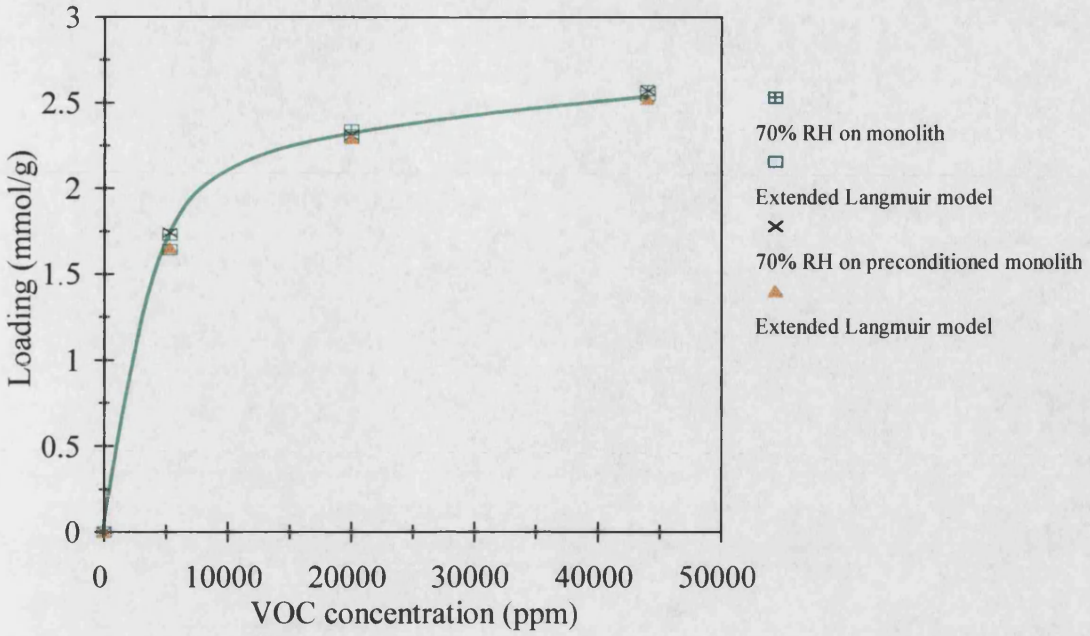

Figure 5.31 Comparison of the experimentally obtained ethanol isotherm with the extended Langmuir model

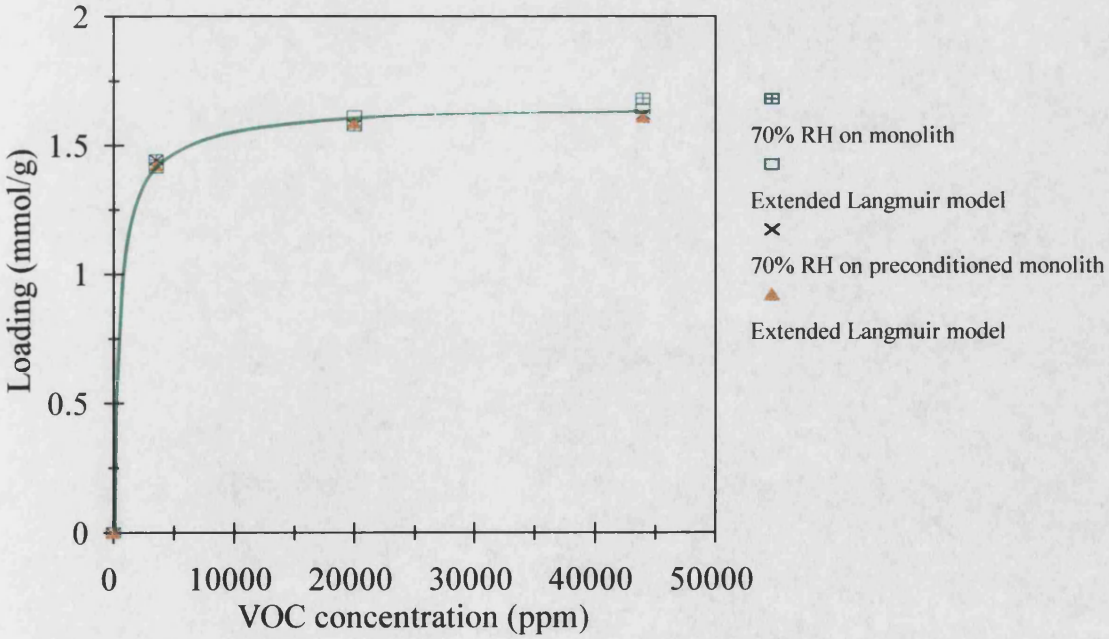

Figure 5.32 Comparison of the experimentally obtained methylene chloride isotherm with the extended Langmuir model

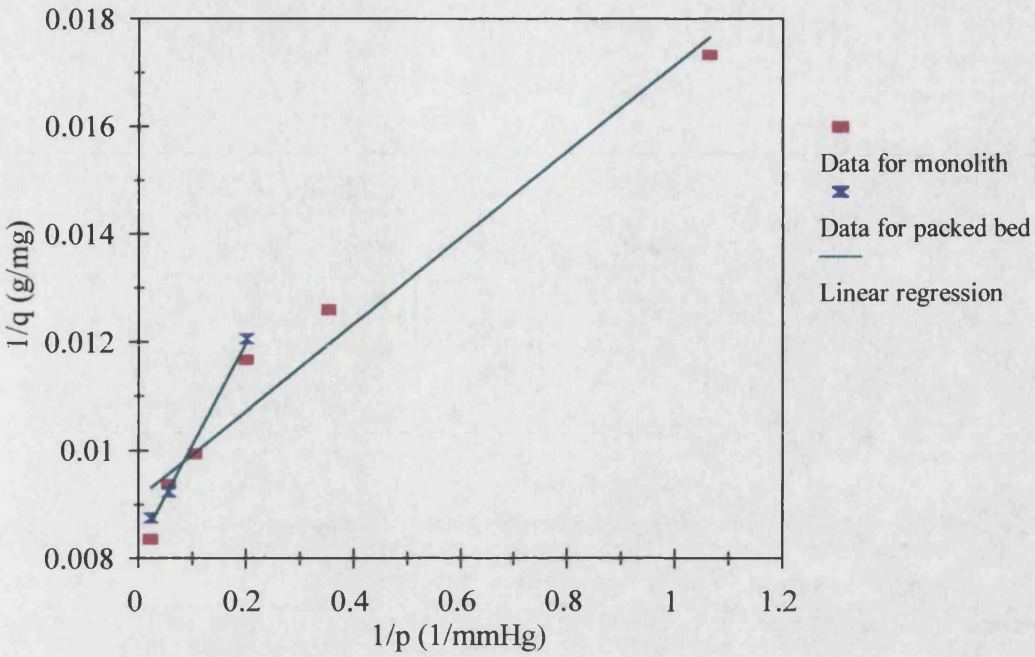

Figure 5.33 Langmuir plots showing conformity with the linearised Langmuir equation using equilibrium data for ethanol adsorption onto silicalite monolith and silicalite pellets

5.4.3 MTZ Length and Velocity

Figures 5.34-5.36 show the length of the MTZ as a function of the feed concentration. In the case of propane (Figure 5.34), the MTZ length decreases as the propane concentration is increased. For ethanol (Figure 5.35) and methylene chloride (Figure 5.36), the MTZ length initially decreases with increasing VOC concentration, but then rises again. The variation of MTZ length for the monolith follows a similar pattern as for packed bed (described in Chapter 4).

The Reynolds number for flow through a single monolith channel was calculated using the following equation (Votruba et. al., 1975) :

$$Re = \frac{\rho u_s d}{\varepsilon_m \mu} \tag{5.2}$$

where u_s is the superficial velocity, ε_m is the monolith voidage and d is the channel size. Example calculations are shown in Table 5.7, where the flow is laminar in all cases. In laminar flow the external mass transfer resistance may be significant in the monoliths. The reduction of MTZ length as the feed concentration is increased in the low Reynolds number region may be due to an increase in the fluid film mass transfer coefficient with feed concentration.

Table 5.7 Example of Reynolds number in the silicalite monolith

Test number	Total flow (cm^3/min STP)	Adsorbate (ppm)	Reynolds number
		Propane :	
1	500	1000	7
2	500	2500	7
3	500	5000	7
4	500	7500	7
5	500	10,000	7

Figure 5.34 also shows that, in the case of propane adsorption onto monolith, the presence of water vapour increases the length of the MTZ. The length of the MTZ is further increased with increasing water concentration. In the case of ethanol (Figure 5.35), the presence of moisture does not significantly affect the MTZ length, while for methylene chloride (Figure 5.36) there is a moderate increase. For all three VOCs, the MTZ length is greater in the monolith than in the packed bed, (given the same experimental conditions). This may be due to the higher overall mass transfer resistance in the monolith.

The rate of movement of the MTZ in the monolith as a function of feed concentration is shown in Figures 5.37-5.39. In all cases, the MTZ velocity increases with increasing feed concentration. For propane, the addition of water vapour of 55 % relative humidity causes the MTZ velocity to increase by approximately 20 %. However, there is no significant further increase when the level of humidity is raised to 70 % RH. In the case of ethanol and methylene chloride, the MTZ velocity is not significantly affected by the presence of water vapour. Figure 5.37 also includes, by way of comparison, results from the propane-packed bed adsorption studies. It shows that, in the absence of water vapour, the rate of movement of the MTZ is higher in the monolith than in the packed bed. However, when moisture of 55 % RH is introduced, the velocity in the packed bed rises by approximately 40 %, a significantly larger increase than that encountered in the monolith. When the humidity is increased to 70 % RH, the MTZ velocity again increases, the total increase now being approximately 55 %. For ethanol and methylene chloride, the MTZ velocity in the monolith is higher than that in the packed bed (Figures 5.38 and 5.39).

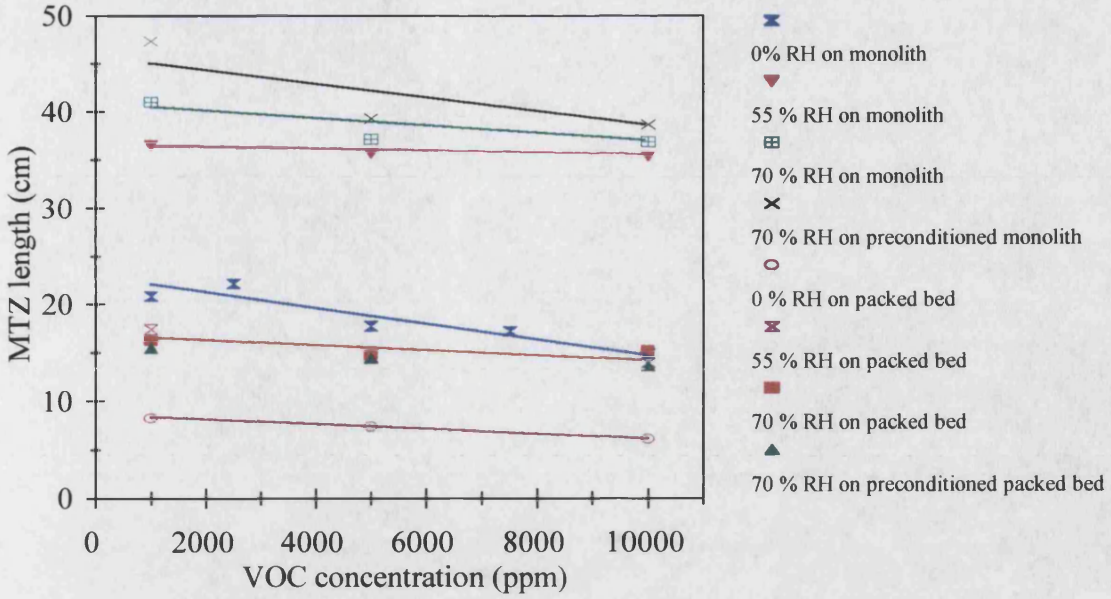

Figure 5.34 Effect of water vapour on the MTZ length of propane adsorption onto silicalite monolith, and comparison of the results with those of propane adsorption onto silicalite packed bed

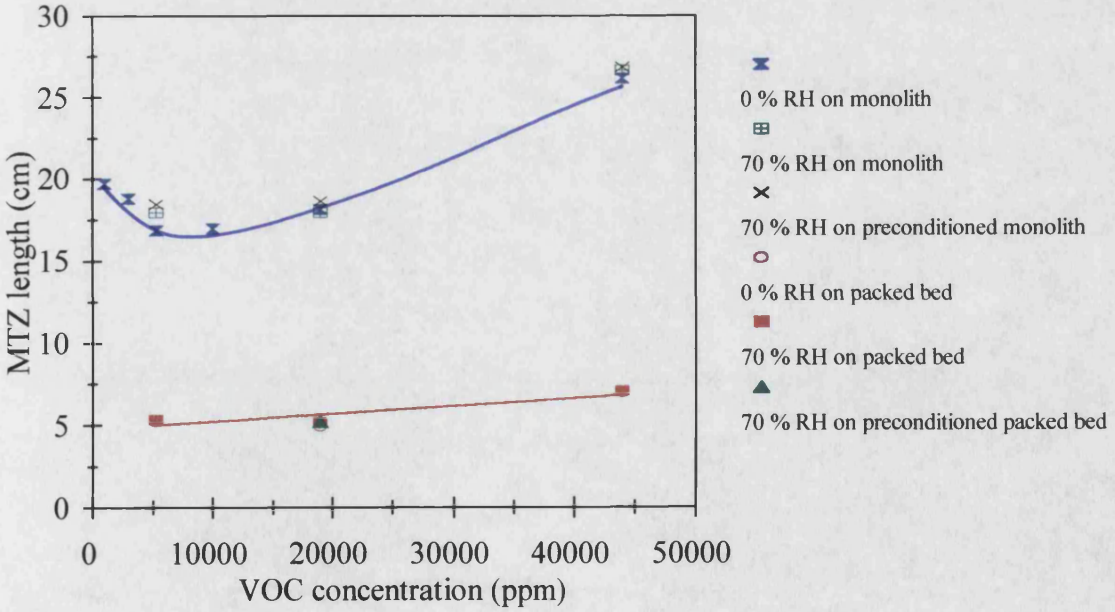

Figure 5.35 Effect of water vapour on the MTZ length of ethanol adsorption onto silicalite monolith, and comparison of the results with those of ethanol adsorption onto silicalite packed bed

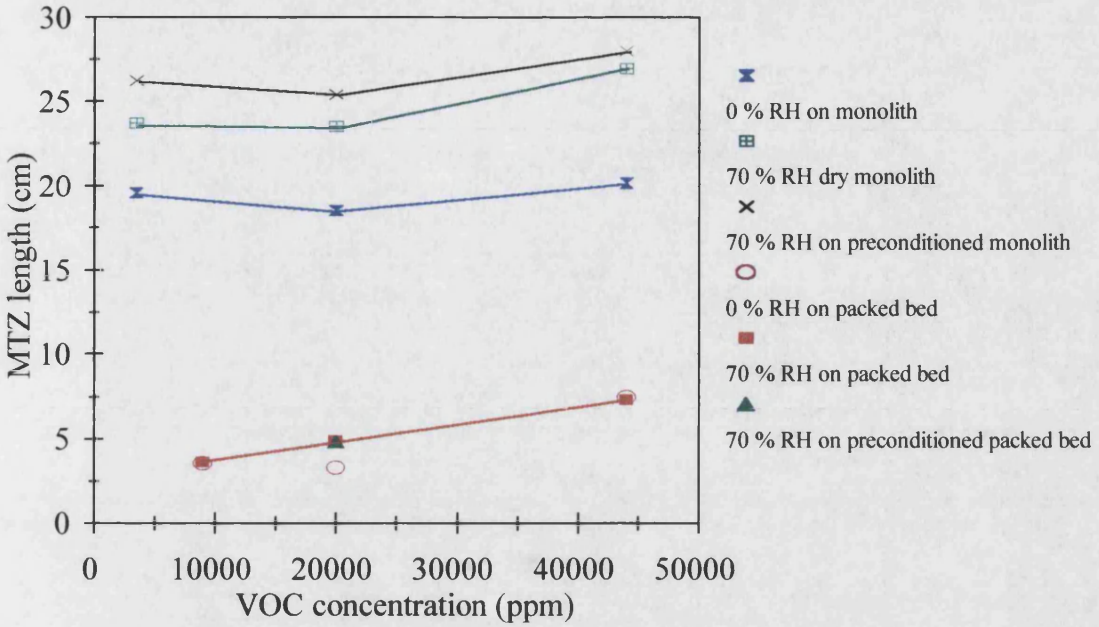

Figure 5.36 Effect of water vapour on the MTZ length of methylene chloride adsorption onto silicalite monolith, and comparison of the results with those of methylene chloride adsorption onto silicalite packed bed

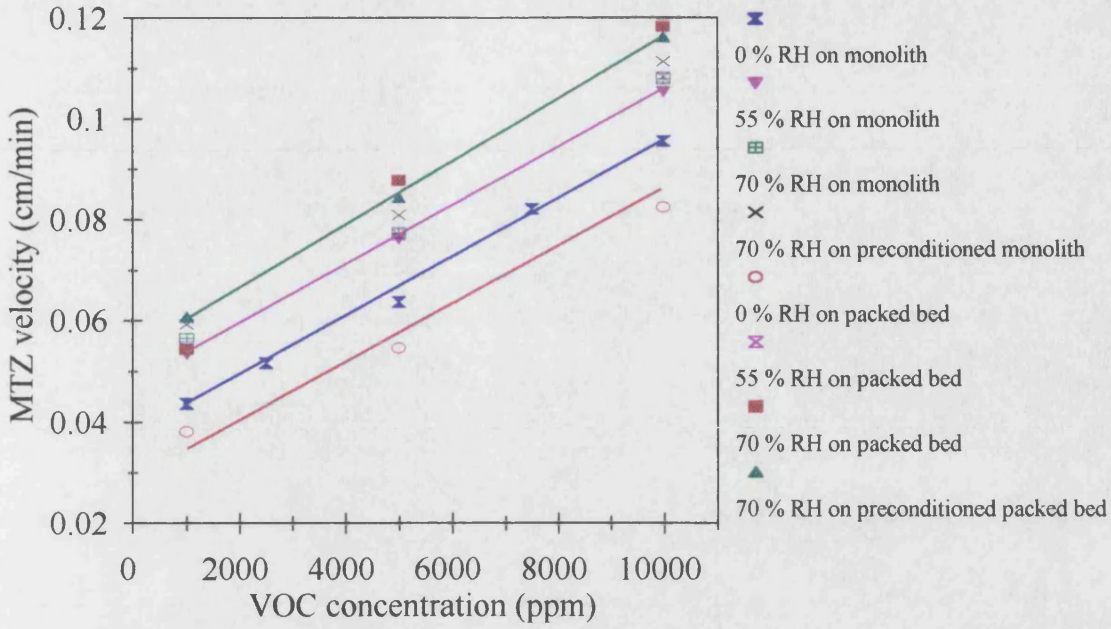

Figure 5.37 Effect of water vapour on the MTZ velocity of propane adsorption onto silicalite monolith, and comparison of the results with those of propane adsorption onto silicalite packed bed

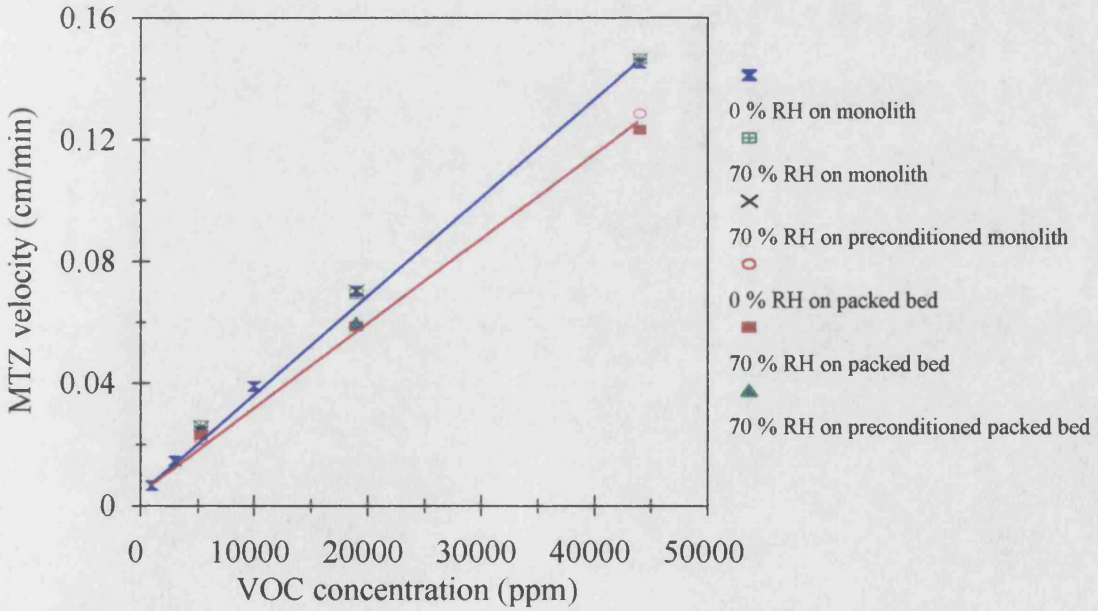

Figure 5.38 Effect of water vapour on the MTZ velocity of ethanol adsorption onto silicalite monolith, and comparison of the results with those of ethanol adsorption onto silicalite packed bed

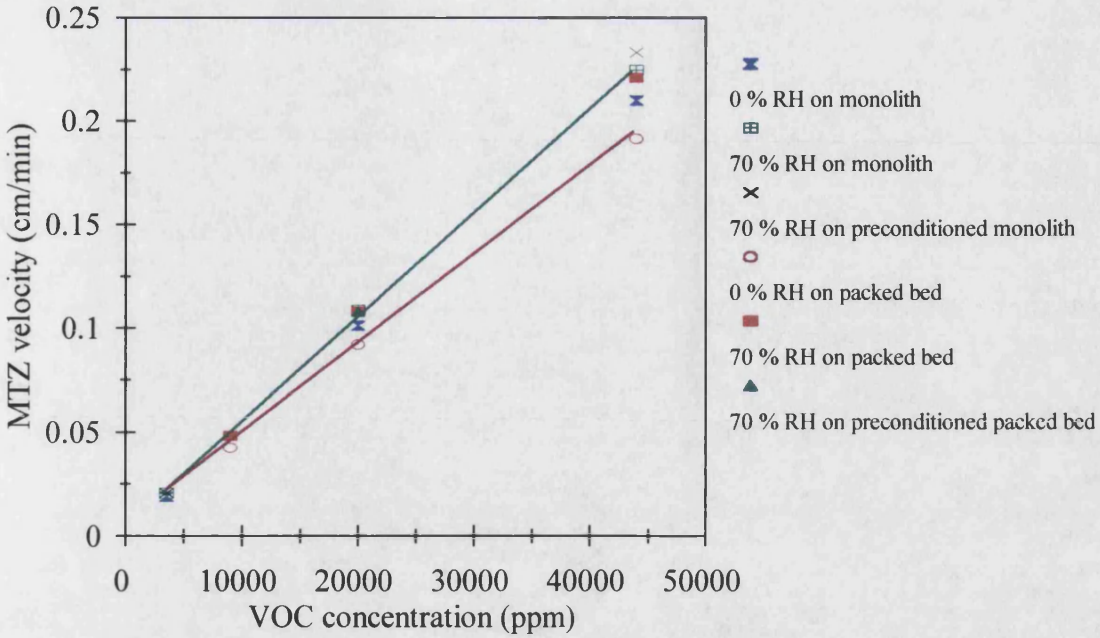

Figure 5.39 Effect of water vapour on the MTZ velocity of methylene chloride adsorption onto silicalite monolith, and comparison of the results with those of methylene chloride adsorption onto silcalite packed bed

5.4.4 Desorption Study

The effect on the desorption breakthrough curves of propane of varying the nitrogen purge flowrate is shown in Figure 5.40. Desorption was performed at atmospheric pressure and 25°C. The desorption time is reduced as the purge rate is increased. (The desorption cycle time is defined as the time at which the effluent concentration reached 2 % of the initial exit concentration). When a nitrogen flowrate of 500 cm^3/min is used for both adsorption and desorption, the desorption curve is almost a mirror image of the adsorption curve (Figure 5.40).

Results from a propane desorption study employing regeneration temperatures of 180°C (and under a nitrogen purge of 500 cm^3/min) are shown Figure 5.41, while the corresponding furnace and effluent stream temperature histories are shown in Figure 5.42. When using high temperature regeneration, the desorption time (i.e. 1.7 hours) is considerably reduced compared with low temperature regeneration (i.e. 13 hours).

Desorption curves for methylene chloride at 25°C are shown in Figures 5.43 and 5.44. These figures show that unlike with propane the monolith was not restored to its adsorbate-free state. Clearly a longer regeneration period may be required with this VOC.

The adsorption and desorption breakthrough curves for the monolith are compared with those of the equivalent packed bed in Figure 5.45. Both the adsorption and desorption curves of the monolith are broader than those of the packed bed, indicating that a higher overall mass transfer resistance exists in the silicalite monolith than in the packed bed (as mentioned earlier).

The reversibility factor, ψ, described in Chapter 4 was used to identify the effectiveness of regeneration under process conditions similar to those prevailing during adsorption. (It is assumed that the desorption of methylene chloride would have been complete had enough time been allowed. For the purpose of these calculations, therefore, the depletion curves were linearly extrapolated until they reached 2 % of the feed concentration). The results in Table 5.8 show that the reversibility factor is higher

than 95 % in all cases, indicating that regeneration under normal conditions is highly effective, and that high temperature regeneration may not be required. These results also show that the reversibility factor increases with increasing purge gas flowrate.

Table 5.8 Reversibility factors of the monolith

Adsorbate	Desorption flowrate (cm^3/min)	Desorption temperature (°C)	q_{de} (mg/g)	q_{eq} (mg/g)	ψ (%)
Propane of 1000 ppm	500	25	8.18	8.65	94.6
Propane of 1000 ppm	1500	25	8.44	8.65	97.6
Propane of 1000 ppm	3000	25	8.56	8.65	98.9
Propane of 1000 ppm	500	180	8.62	8.65	99.6
$MeCl_2$ of 3500 ppm	500	25	126.39	133.0	95.0
$MeCl_2$ of 20,000 ppm	500	25	140.43	152.71	97.6

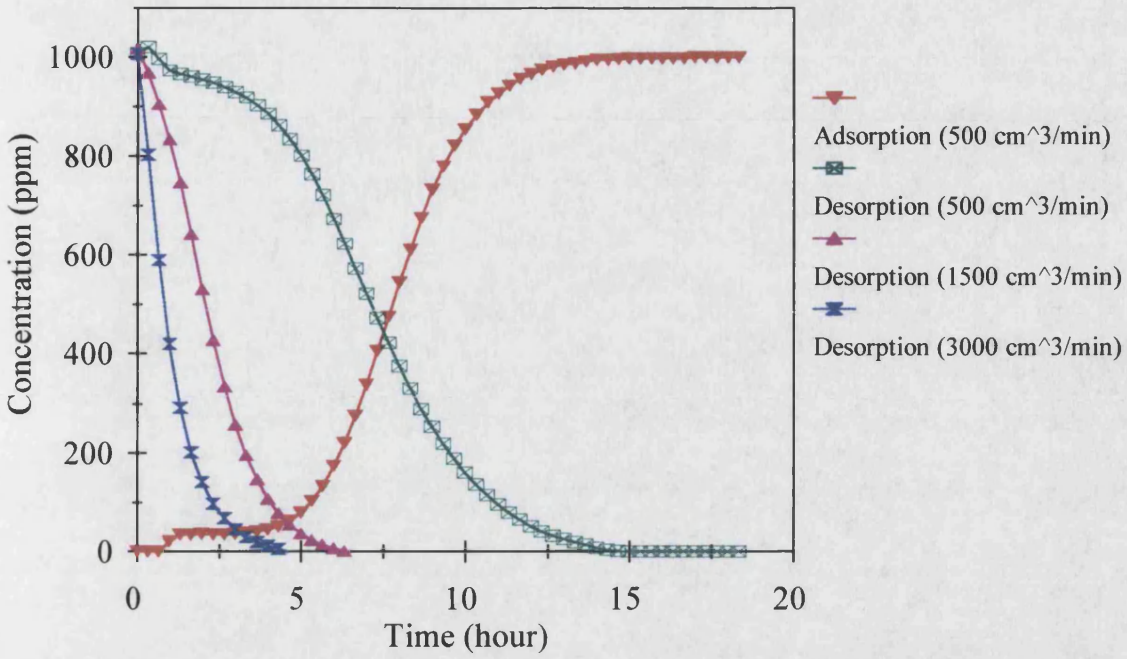

Figure 5.40 Effect of varying nitrogen purge rate on the desorption of propane (1000 ppm) from silicalite monolith at 25°C and atmospheric pressure, and comparison with propane (1000 ppm) adsorption breakthrough curve

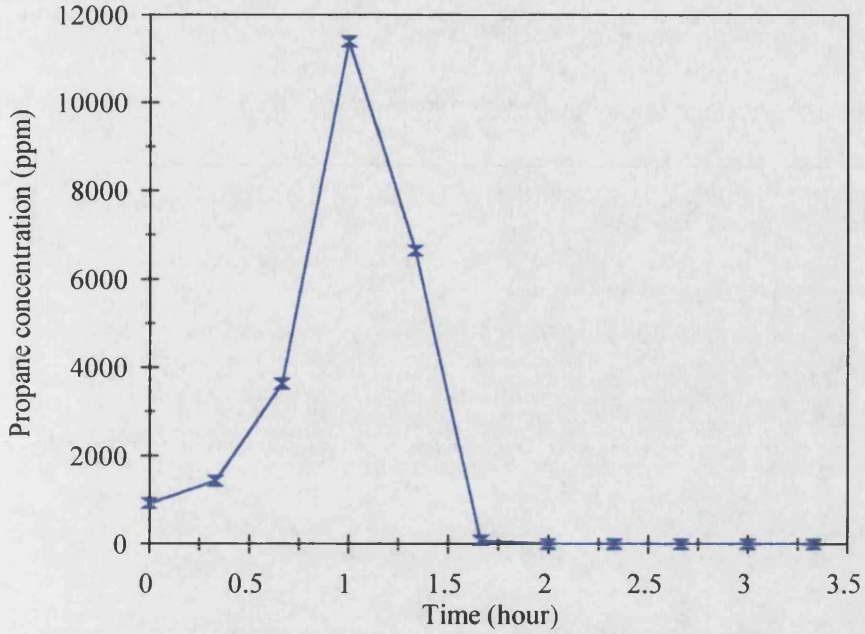

Figure 5.41 Desorption of propane (1000 ppm) from silicalite monolith at elevated temperature under a nitrogen purge of 500 cm^3/min

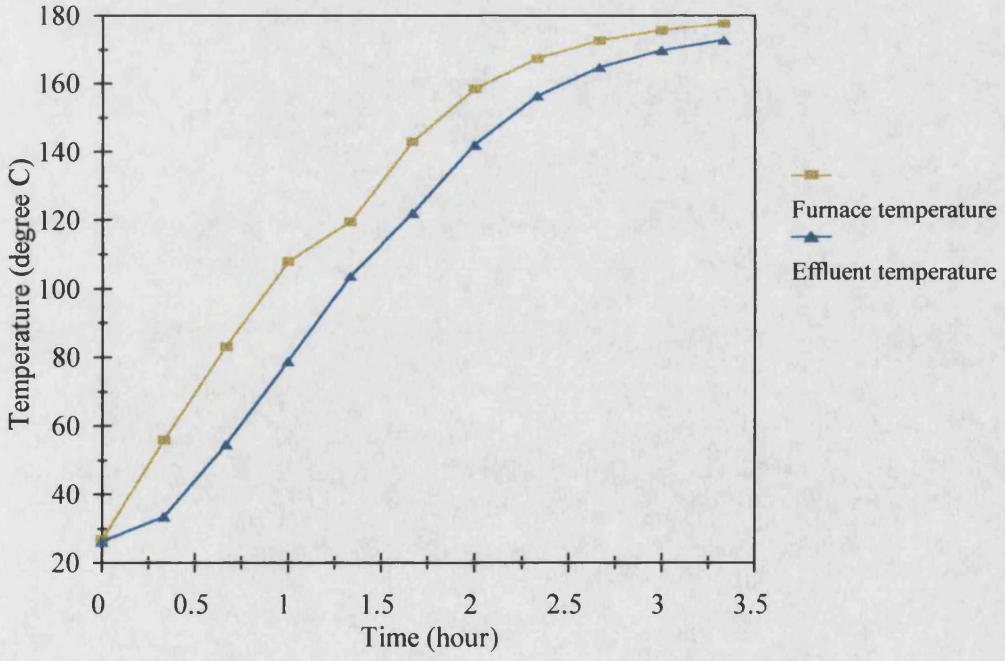

Figure 5.42 Temperature history of the furnace and effluent during the desorption of propane (1000 ppm) from silicalite monolith

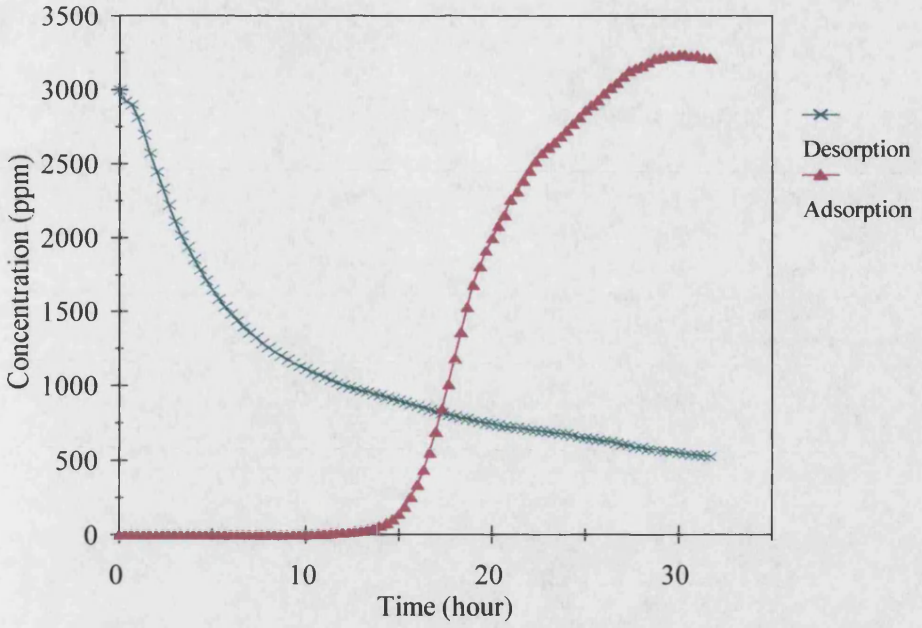

Figure 5.43 Adsorption and desorption curves of methylene chloride (3500 ppm)-monolith system at 25°C and atmospheric pressure

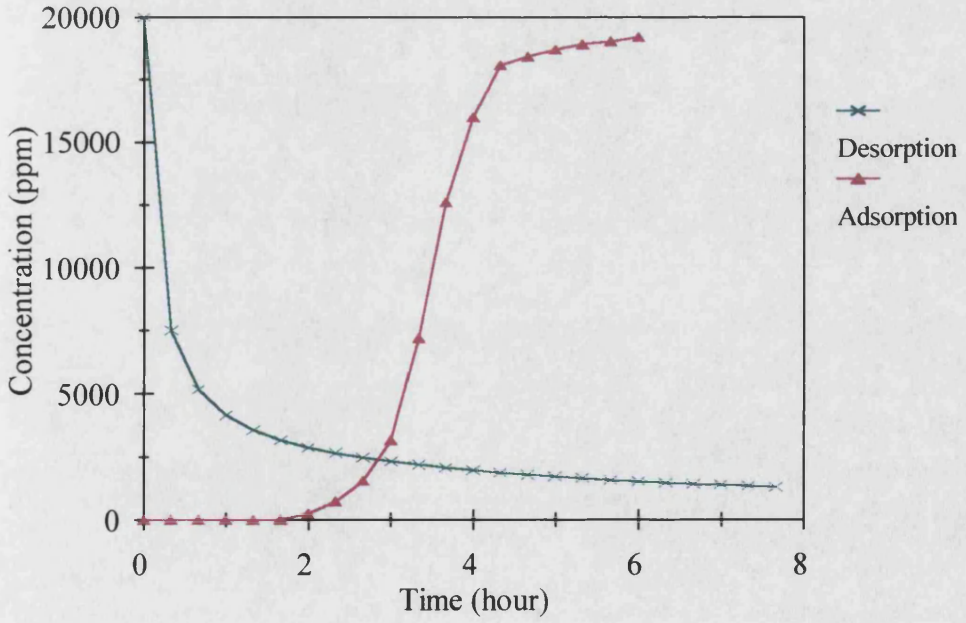

Figure 5.44 Adsorption and desorption curves of methylene chloride (20,000 ppm)-monolith system at 25°C and atmospheric pressure

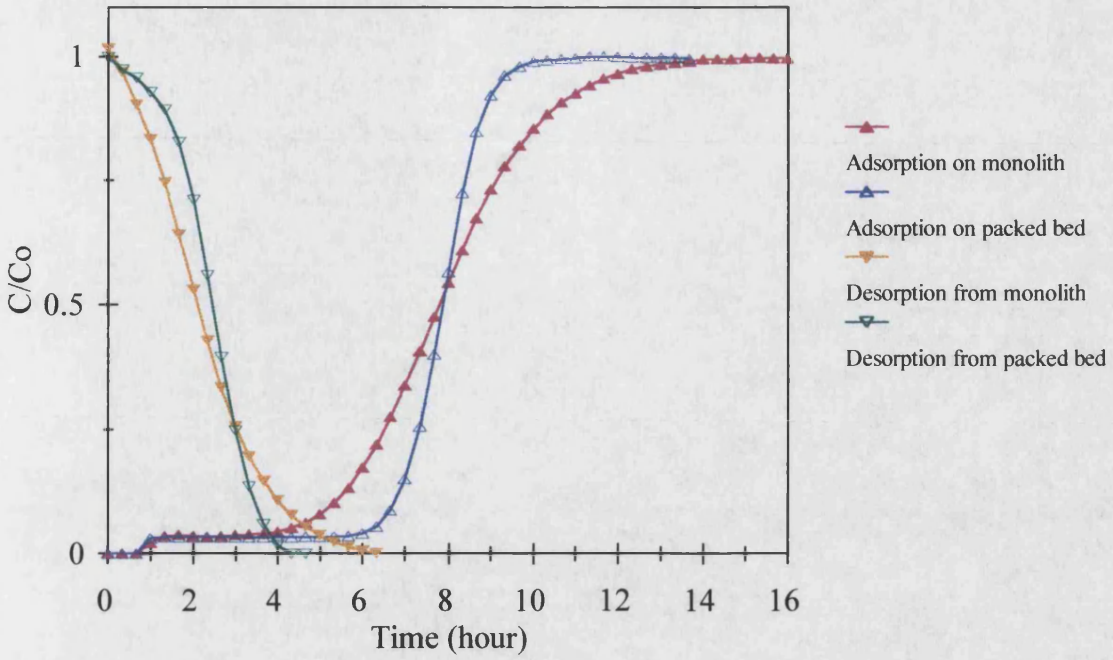

Figure 5.45 Adsorption and desorption curves of propane (1000 ppm) at 25°C and atmospheric pressure

5.5 Conclusions

The breakthrough curves for monoliths were found to be generally broader than those for packed beds. This may be due to a longer mass transfer zone, suggesting a higher overall resistance to mass transfer in the monolith when compared with the packed bed. The effective geometric surface area of the packed bed (2813 m^2/m^3) is considerably higher than that of the monolith (828 m^2/m^3). Under a laminar flow regime, the dominating mass transfer resistance is anticipated to be diffusion through the external film. Hence since the packed bed has a higher effective external surface area, the rate of mass transport into this type of bed is expected to be higher than into the monolith.

The equilibrium loadings of VOC onto a silicalite monolith are similar to those onto the equivalent packed bed. However, the loading of pure water onto the monolith is much lower than that onto the packed bed. This may be due to the lower aluminium content of the monolithic adsorber. The isotherms agree well with the literature and are well represented by the Langmuir equation.

Water vapour affects the adsorption of VOCs onto the silicalite monolith and packed bed in the following order of increasing severity : ethanol, methylene chloride, propane. Adsorption of ethanol onto silicalite, whether in monolith or packed bed form, is not significantly affected by the presence of water vapour. Ethanol is miscible with water and can therefore dissolve into the condensed phase and be separated by silicalite. This is demonstrated by the appearance of a separate breakthrough curve for the water vapour. Propane is immiscible with water in the liquid state and the loading of this compound is reduced when moisture is present in the feedstock, suggesting that water can compete with propane for adsorption sites on silicalite. The reduction in equilibrium loading when water is present is much greater for the packed bed than for the monolith, indicating a lower hydrophobicity for the latter. For methylene chloride, the reduction in loading is less than that for propane, possibly because the solubility of methylene chloride in water lies between that of propane and ethanol. The isotherms for binary adsorption onto the monoliths are well represented by the extended Langmuir model, though the model is unable to accurately predict the experimental data for the packed

bed system. This is probably due to water vapour having a milder influence on the monolith than on the packed bed. The calculated separation factor, based on the extended Langmuir model, is higher for the monolith than for the packed bed. This is a result of the higher hydrophobicity of the monolith.

The length of the mass transfer zone (MTZ) has been demonstrated to decrease with an increase in feed concentration for both the monolith and the packed bed. However, the MTZ length in the monolith is higher when compared with that in the packed bed. This may explain why the breakthrough curves with the monolith are broader than those with the packed bed. In the presence of water vapour, the MTZ length of propane in both the monolith and the packed bed increases, but the effect is greater in the packed bed than in the monolith. A further increase in the water level gives rise to a further increase in the MTZ length in the packed bed, but not in the monolith.

The rate of movement of MTZ increases with increasing concentration of VOC in the feed. For propane, the MTZ velocity in the monolith is higher than that in the packed bed as a consequence of a greater MTZ length in the former. When water vapour is added at 55 % RH, the MTZ velocity is increased to a larger degree in the packed bed than in the monolith. When the humidity is raised to 70 %, a further increase in MTZ velocity is observed in the packed bed, but not in the monolith. The studies revealed that the kinetic and equilibrium adsorption performance of the monolith are less affected by the presence of moisture than are those of the packed bed.

Desorption of propane from the silicalite monolith was found to be technically feasible under conditions identical to those prevailing during the adsorption process. The reversibility factor was found to be higher than 95 % in all cases. The rate of desorption has been shown to increase when the bed temperature or nitrogen purge flowrate is increased.

Chapter 6
Evaluation of Pressure Drop and External Mass Transfer Coefficients

6.1 Introduction

The pressure drop and external mass transfer properties of the monolith are compared with those of the packed bed for a range of operating conditions and geometric configurations.

It has been determined (Chapter 5) that, in general, the breakthrough curve exhibited by the monolith is broader than in the packed bed, and this may be due to a higher overall mass transfer resistance within the former. Since the flow in the monolith is laminar, the external mass transfer resistance may be contributing significantly to the overall mass transfer resistance, which also includes the macropore and micropore resistances. It is assumed that the external film coefficient of the monolith is lower than that of the packed bed and thus that portion of the monolith breakthrough curve near to the break point is more distended (Figure 6.1). As the concentration inside the solid increases the internal resistances may become limiting and this is reflected in the region of the breakthrough curve near to the saturation point (Figure 6.1). Thus, if the internal resistance is higher in the monolith than in the packed bed, this should manifest itself as a broadening of the monolith curve and hence a difference between the upper regions of the respective breakthrough curves.

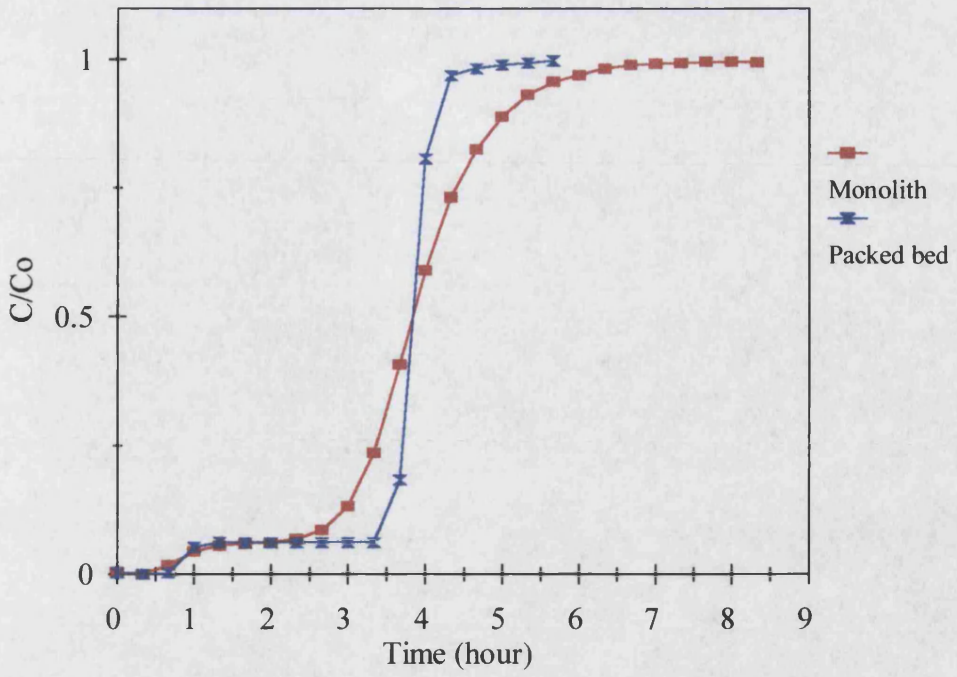

Figure 6.1 Comparison of propane (10,000 ppm) adsorption onto silicalite monolith with adsorption onto silicalite packed bed (same total flowrate, i.e. 500 cm^3/min)

6.2 Evaluation of Pressure Drop

The pressure drop was calculated for interstitial velocities up to the maximum allowable flow for the packed bed, i.e. before fluidisation occurs. According to Ruthven (1984) in order to prevent attrition from the movement of particles within the packed bed, the maximum interstitial velocity, u_{max}, in upwards flow should be less than about 80 % of the minimum fluidisation velocity, u_{mf}. The minimum fluidisation velocity is (Coulson and Richardson, 1991) :

$$u_{mf} = 0.0055 \frac{\varepsilon_{mf}^3}{(1-\varepsilon_{mf})} \frac{d_p^2(\rho_p - \rho)g}{\mu} \tag{6.1}$$

So, $$u_{max} = 0.8 u_{mf} \tag{6.2}$$

The voidage of the bed at the point when fluidisation is reached, ε_{mf}, will not be known accurately, so it is assumed to be the voidage of the fixed packed bed, ε.

The general equation for unit length pressure drop in a pipe of uniform cross section due to friction is :

$$\frac{\Delta P}{L} = 4f \frac{\rho u^2}{d} \tag{6.3}$$

where f is the friction factor, ρ is the fluid density, u is the average velocity in the pipe and d is the pipe diameter. Equation 6.3 is valid for both laminar and turbulent flows and the friction factor is half of the Fanning friction factor, i.e. $f = \frac{f_F}{2}$ (Darby, 1996).

For flow in a monolith of non-circular channels, d in Equation 6.3 is replaced by the hydraulic diameter, d_h. Since the hydraulic diameter approximation is not very accurate for laminar flow (Re < 2000) (Darby, 1996), the f in Equation 6.3 is replaced by the corrected friction factor for laminar flow through square ducts (Villermaux and Schweich, 1994 and Darby, 1996) :

$$f_F = \frac{14.2}{Re_{d_h}} \tag{6.4}$$

where $Re_{d_h} = \frac{\rho u d_h}{\mu}$ (6.5)

For monoliths having square channels of dimension d_c by d_c, the hydraulic diameter is equal to d_c. The u in Equations 6.3 and 6.5 is replaced by the interstitial velocity through the monolith channels :

$$u_i = \frac{u_s}{\varepsilon_m} \tag{6.6}$$

where u_s is the superficial velocity calculated over the whole cross section of the monolith, and ε_m is the voidage of the monolith. The final pressure drop equation for laminar flow through the square channel monolith is therefore:

$$\frac{\Delta P}{L} = 28.4 \frac{\mu u_s}{\varepsilon_m d_c^2} \tag{6.7}$$

For transition and turbulent flow in the monolith, the friction factor developed by Churchill, f_c, which is valid for both rough and smooth pipes is used (Darby, 1996). The hydraulic diameter of the monolith, d_h, replaces the pipe diameter in the equation. The surface roughness, φ, for the monolith is taken to be the same as that of a smooth concrete surface, i.e. 0.04 mm (Darby, 1996).

$$f_c = [(\frac{8}{Re_{d_h}})^{12} + \frac{1}{(A+B)^{3/2}}]^{1/12} \tag{6.8}$$

where $A = [2.457 ln \frac{1}{(\frac{7}{Re_{d_h}})^{0.9} + \frac{0.27\varphi}{d_h}}]^{16}$ (6.9)

$$B = [\frac{37530}{Re_{d_h}}]^{16} \tag{6.10}$$

For the packed bed, the friction factor given by Ergun (1952) is used :

$$f_{PB} = \frac{150}{Re_{PB}} + 1.75 \tag{6.11}$$

where Re_{PB} is the modified Reynolds number for the bed. The constants in the equation represent 640 experimental data involving various sized spheres, sand, pulverised coke and the following gases: carbon dioxide, nitrogen, methane and hydrogen (Ergun, 1952). The hydraulic diameter for a bed composed of uniform spherical particles can be written as

$$d_h = \frac{2d_p\varepsilon_p}{3(1-\varepsilon_p)} \tag{6.12}$$

where d_p is the particle diameter and ε_p is the bed voidage. The u in Equation 6.3 is substituted for the interstitial velocity, u_i, through the packed bed, which is related to the superficial velocity, u_s, as follows :

$$u_i = \frac{u_s}{\varepsilon_p} \tag{6.13}$$

The modified Reynolds number for the packed bed can thus be written by ignoring the numerical factor 2/3 as :

$$Re_{PB} = \frac{\rho u_s d_p}{(1-\varepsilon_p)\mu} \tag{6.14}$$

and Equation 6.3 is modified for the packed bed by neglecting the numerical factor 3 :

$$f_{PB} = \frac{\Delta P d_p \varepsilon_p^3}{L(1-\varepsilon_p)\rho u_s^2} \tag{6.15}$$

By inserting f_{PB} and Re_{PB} into Equation 6.11, the expression for pressure drop in the packed bed which is valid for all values of Reynolds number is therefore given by

$$\frac{\Delta P}{L} = \frac{(1-\varepsilon_p)}{\varepsilon_p^3}\left[\frac{150\mu u_s}{d_p^2}(1-\varepsilon_p) + \frac{1.75\rho u_s^2}{d_p}\right] \tag{6.16}$$

6.3 Evaluation of External Mass Transfer Coefficients

The dimensionless group characterising the external film mass transfer coefficient, k, is the Sherwood number, which is the analogue of the Nusselt number for heat transfer, defined as

$$Sh = \frac{kd}{D_v} \tag{6.17}$$

where d is either the particle diameter when the packed bed is considered, or the channel size of the monolith. The molecular diffusivity, D_v, for a binary gas mixture is evaluated from the Chapman-Enskog equation (Appendix XI).

The mass transfer in gas-solid packed bed systems has been well studied both theoretically and experimentally. Thus correlations for the mass transfer coefficient are well established. However, there appears to be no published data concerning mass transfer in silicalite monoliths. The closest approximation would be to adopt the correlations established for the performance of monolithic catalysts under non-reacting conditions, or to derive typical correlations from the analogy with heat transfer systems. Although monolithic catalysts are widely used as catalytic converters for the control of vehicle exhausts, there has been very little experimental study to validate the mass transfer correlations applied to such systems (Kolaczkowski et. al., 1996). The correlation for Sherwood number proposed by Hawthorn (1974) is based on the solutions compiled by Kays and London (1964) for heat transfer models. It is pertaining to laminar flow conditions in different matrix structures and of certain experimental data. The Hawthorn model is given as :

$$Sh = A(1 + 0.095\, Re\, Sc \frac{d_c}{L})^{0.45} \tag{6.18}$$

where A is 2.98 for square channels.

Votruba et. al. (1975) studied the vaporisation of water and some hydrocarbons from the surface of porous monolith structures. They showed that the Hawthorn model did not provide a good fit to their experimental data and developed the following empirical correlation :

$$Sh = 0.705(Re\frac{d_c}{L})^{0.43} Sc^{0.56} \tag{6.19}$$

for 3 < Re < 480, 0.57 < Sc < 3.3 and Pr=0.74. They concluded that, although the correlations could be used for the design of afterburner reactors, there was still a need for the acquisition of more experimental data. However, Heck et. al. (1976) and Boersma et. al. (1980) show that the Hawthorn model predicts their data more closely than the Votruba model (Irandoust and Andersson, 1988). No explanation was given for this discrepancy. On the other hand, Bennett et. al. (1991) and Ullah et. al. (1992) studied propane combustion and CO oxidation in catalytic monoliths, respectively, and determined Sherwood and Nusselt numbers which are closer to the results of Votruba et. al. (Kolaczkowski et. al., 1996).

Equation 6.18 may be compared with the developing flow of air in a square duct with constant wall temperature proposed by Hausen (Incropera and De Witt, 1990) :

$$Nu = 2.98 + \frac{0.0688Gz}{1 + 0.04Gz^{2/3}} \qquad \text{(for } Gz < 100\text{)} \tag{6.20}$$

where $Gz = \frac{d_c}{L} Re\, Sc$ (6.21)

Due to the uncertainty of the published mass transfer correlations, the Sherwood number derived from heat transfer analogies and Votruba model are used for laminar flow (Re < 2000) in the square channel monolith. For the transition region (2000 < Re < 10,000) the following equation is used (Perry and Chilton, 1973) :

$$Sh = 0.116(Re^{0.67} - 125)Sc^{0.33}(1 + (\frac{d_c}{L})^{0.67}) \tag{6.22}$$

For the packed bed, the mass transfer correlation which is valid for 3 < Re < 10,000 is given by Wakao and Funazkri (1978) :

$$Sh = 2.0 + 1.1Sc^{0.33}\ Re^{0.60} \tag{6.23}$$

This expression is applicable to highly favourable adsorption isotherms and the effect of axial dispersion has been taken into consideration. The corresponding axial dispersion coefficient, D_{ax}, expression is given by (Wakao and Funazkri, 1978) :

$$\frac{\varepsilon D_{ax}}{D_v} = 20.0 + 0.5Sc\ Re \tag{6.24}$$

The axial dispersion for laminar flow in monoliths, D_{axm}, was calculated from the following equation (Froment and Bischoff, 1990) :

$$D_{axm} = D_v + \frac{1}{192}\frac{u_i^2 d_c^2}{D_v} \tag{6.25}$$

The entrance effects on the velocity and concentration profiles in the monolith channels were also evaluated using the correlations for heat transfer. The criterion for the entrance length, l_v, in which the velocity profile becomes fully developed is given by (Incropera and De Witt, 1990) :

$$\frac{l_v}{d_c} = 0.05\,Re \tag{6.26}$$

The length required to obtain a fully developed concentration profile, l_c, can be estimated from (Incropera and De Witt, 1990) :

$$\frac{l_c}{d_c} = 0.05\,Re\,Sc \tag{6.27}$$

6.4 Calculation Parameters

The silicalite pellets described in Chapter 4 are of 1.09 mm diameter, while the silicalite monolith studied in Chapter 5 has both channel size and wall thickness of 1.0 mm. In order to study the effect of varying the channel size and wall thickness on the performance of monoliths, the geometric sizes of the monolith catalysts published by Howitt (1980) are used for illustrative purposes. It is assumed that the monolith weight and diameter are constant (i.e. 56.70 g and 18.94 mm). The structural properties of the monoliths and pellets are summarised in Tables 6.1 and 6.2 respectively.

The properties of nitrogen and propane at STP were used in the calculations of the pressure drop and mass transfer properties (Appendix XI). It is assumed that the concentration of VOC in the carrier gas is relatively small and that the adsorption process does not appreciably alter the fluid properties. The interstitial velocity used for the monolith (Chapter 5) is about 0.10 m/s while that used for the packed bed (Chapter 4) is 0.05 m/s.

Table 6.1 Structural properties of square channel monoliths

	Silicalite monolith described in Chapter 5	Catalyst monoliths from literature (Howitt, 1980)			
Cell density (cell/cm^2)	25	92	48	60	31
Wall thickness (mm)	1.0	0.15	0.30	0.15	0.30
Channel size (mm)	1.0	0.89	1.14	1.14	1.50
Specific surface area (m^2/m^3 bed)	1000	3280	2180	2725	1843
Porosity	0.25	0.73	0.62	0.78	0.69
Length (cm)	21.80	43.16	34.35	52.60	37.51
Density (g/cm^3 bed)	0.92	0.47	0.59	0.38	0.54

Table 6.2 Structural properties of packed beds

Spherical adsorbent type	Silicalite described in Chapter 4	Silicalite (UOP, 1992)	ZSM-5 (UOP, 1992)
Diameter (mm)	1.09	1.85	2.40
Bed length (cm)	18.50	19.50	21.60
Bed weight (g)	56.70	56.70	55.11
Bed diameter (cm)	2.11	2.11	2.11
Particle density (g/cm^3)	1.72	1.38	1.26
Bulk density	0.88	0.83	0.73
Specific surface area (m^2/m^3 bed)	2813	1948	1446
Voidage	0.49	0.40	0.42

6.5 Results and Discussions

The maximum allowable interstitial velocity for the pellets is shown in Table 6.3. It increases as the pellet size is increased.

Table 6.3 The maximum allowable interstitial velocity for the packed beds

Pellets diameter (mm)	Bed voidage	Particle density (kg/m^3)	Maximum interstitial velocity (m/s)	Reynolds number
1.09	0.490	1715	1.20	90
1.85	0.400	1384	1.30	90
2.40	0.420	1261	2.40	210

Figure 6.2 shows the pressure drop in the packed bed as functions of the interstitial velocity and the pellet size . It increases with increasing interstitial velocity and decreasing pellet size. The pressure drop in the monoliths, as shown in Figure 6.3, is proportional to the interstitial velocity and is increased as the channel size is reduced. It can be seen from Figures 6.2 and 6.3 that for a given interstitial velocity, the pressure drop is much lower in the monolith than in a packed bed of the same length. Figure 6.4 shows the pressure drop in the monolith calculated over a wider range of flow including laminar and transition. An advantage of monoliths is that they allow higher flowrates to be used without considerably increasing the pressure drop. The maximum pressure drop reached by the packed bed (1.09 mm pellets) is 6000 Pa/m corresponding to an interstitial velocity of 1.2 m/s (Figure 6.2). To achieve the same pressure drop in the monolith described in this thesis (25 cells/cm^2, 1.0 mm channel size and 1.0 mm wall), the interstitial velocity would be about 10 m/s. This indicates that monoliths can be used with much higher flowrates than packed beds.

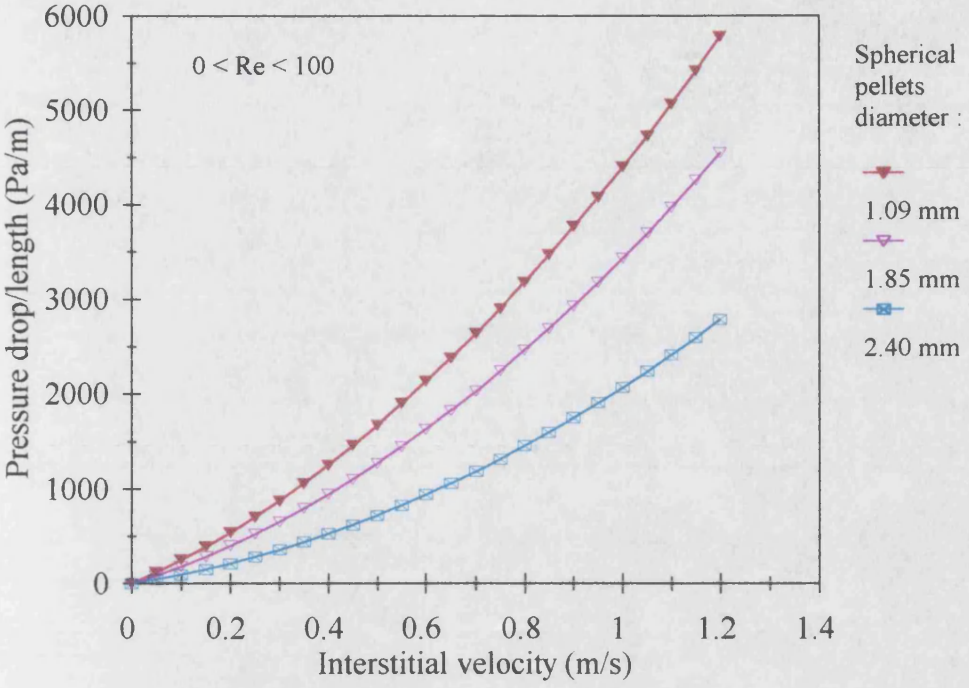

Figure 6.2 Variation of pressure drop with interstitial velocity for packed beds of various pellet sizes

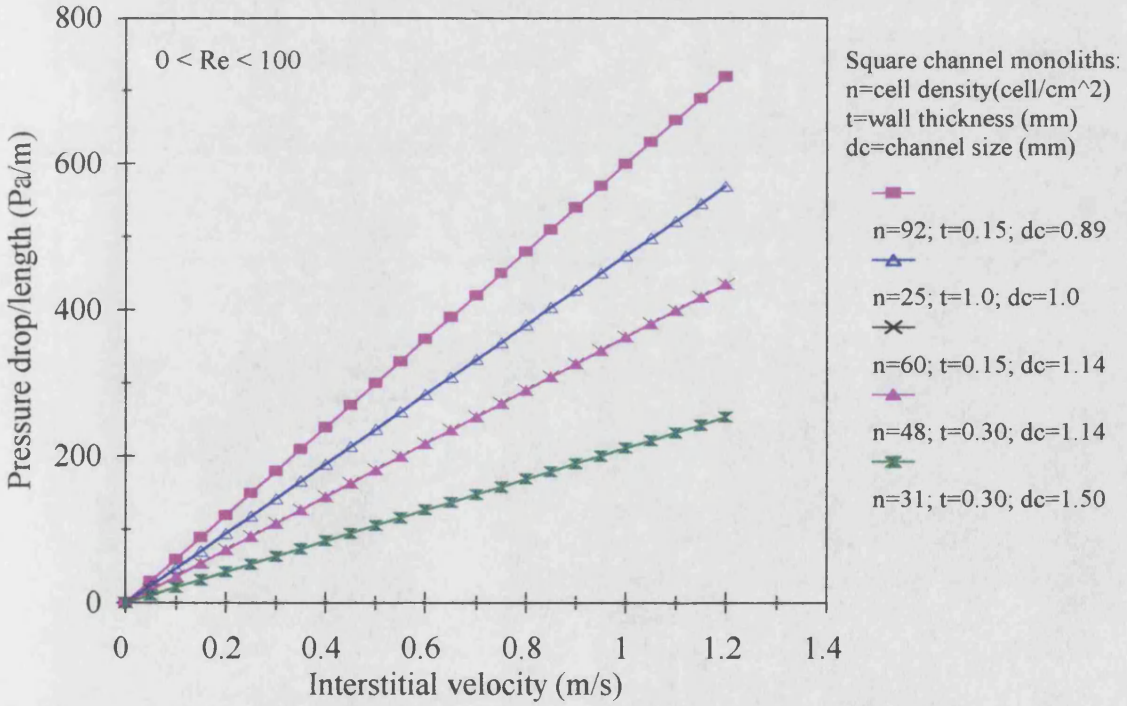

Figure 6.3 Variation of pressure drop with interstitial velocity for monoliths of various channel sizes and wall thicknesses

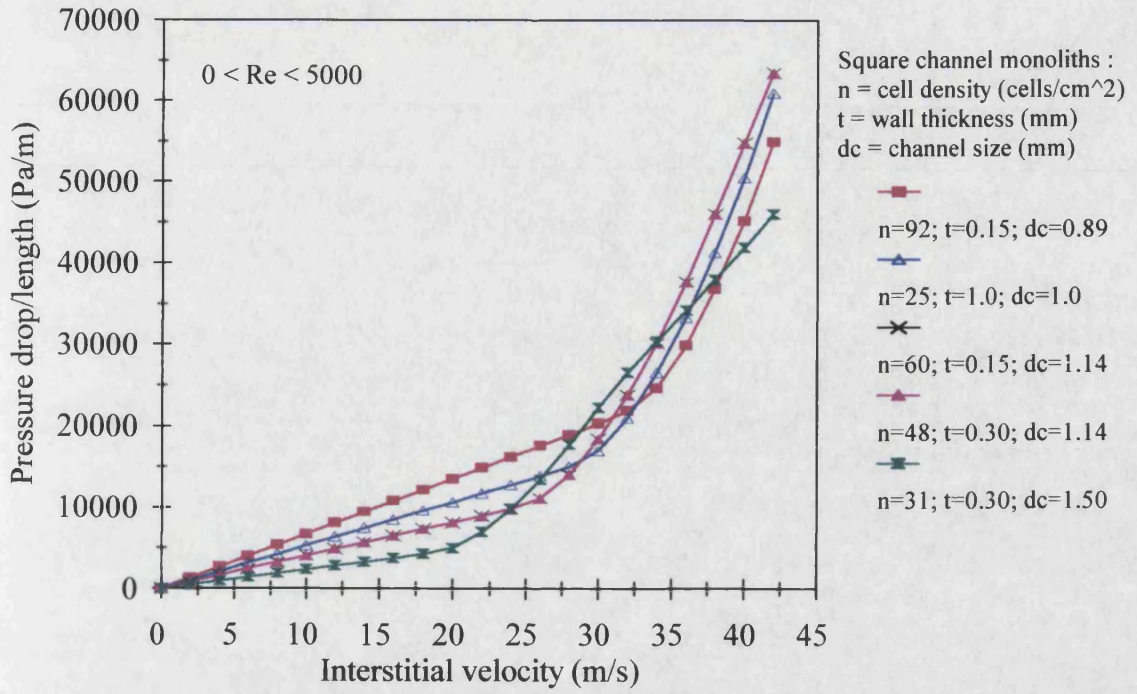

Figure 6.4 Pressure drop in monoliths of various geometric sizes

The fractional entrance lengths at which the velocity and concentration profiles are fully developed in the monolith are shown in Figure 6.5 as a function of interstitial velocity. The experiments described in this thesis were performed at an interstitial velocity of about 0.1 m/s. It can be seen that both velocity and concentration profiles are fully developed at a very small fraction of the total length, i.e. 0.25 %, of the monolith.

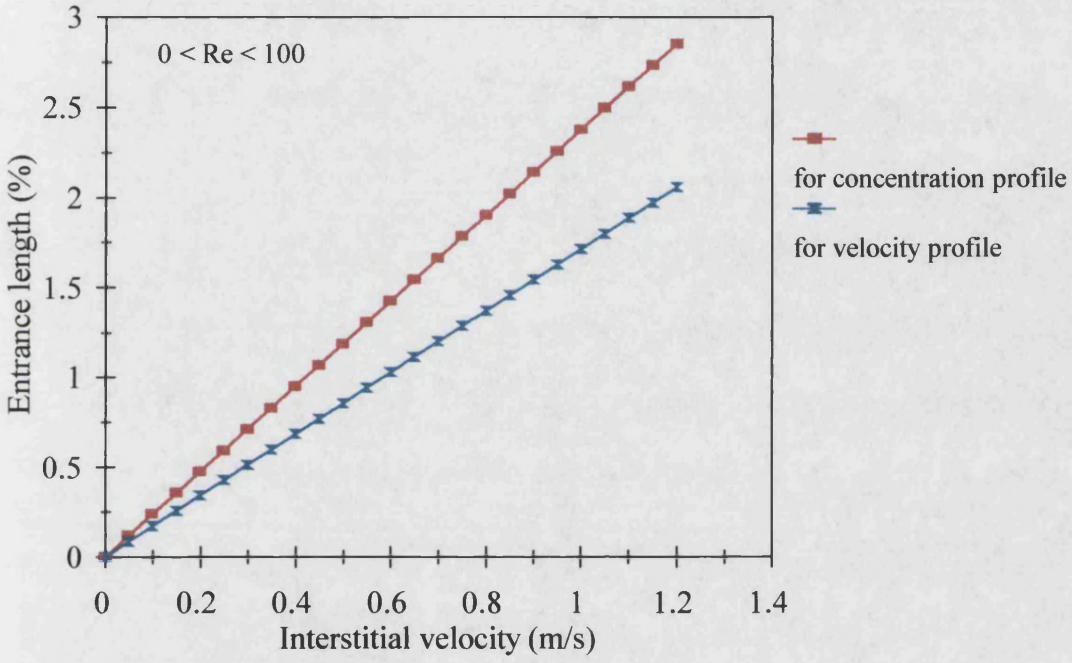

Figure 6.5 Effect of interstitial velocity on the entrance length of the monolith described in this thesis

Figure 6.6 shows the results of using different models to predict the Sherwood number for the square channel monolith used in the research described in this thesis (25 cell/cm^2, 1.0 mm channel size and 1.0 mm wall). The values calculated using the Hawthorn model agree well with those of the Hausen model. This is expected since the models were derived by analogy with heat transfer processes. On the other hand, the values calculated using the Votruba model are lower. As the interstitial velocity approaches zero, the models of Hawthorn and Hausen reach the asymptotic value (about 3.0), while the Votruba model tends to zero. The reason for this discrepancy is not

known, but may possibly be due to experimental errors, errors in calculation of the diffusivities and viscosities, or errors in the theoretical models.

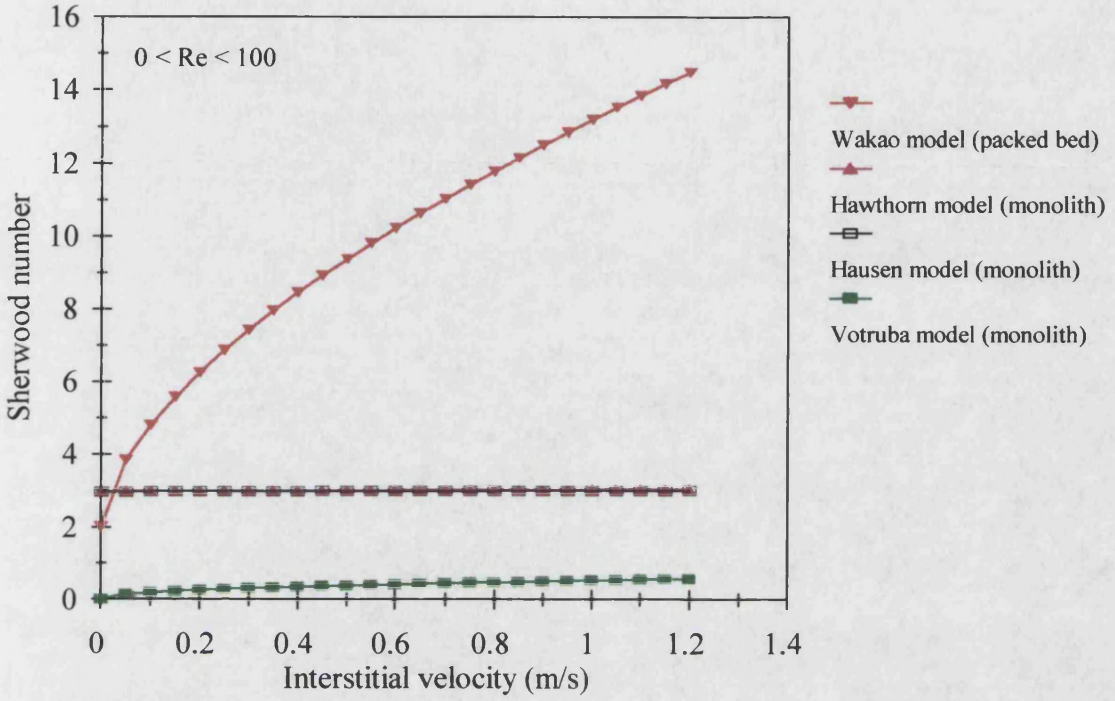

Figure 6.6 Sherwood number for the monolith (25 cells/cm^2, 1.0 mm wall and 1.0 mm square channels) and the packed bed (1.09 mm spheres) described in this thesis.

In Figure 6.6 the Sherwood number represented by the Wakao model is also plotted for the packed bed (1.09 mm spheres). At very low interstitial velocities, the Sherwood number for the monolith predicted using the heat transfer correlations is of the same order of magnitude as that of the packed bed, but at large velocities the Sherwood number for the packed bed is around an order of magnitude higher. When compared with the data predicted by the Votruba model, the differences in the Sherwood number are relatively high at all flowrates. The Sherwood number for the monolith calculated from the heat transfer correlations is about 3.0 as anticipated. Since the entrance effect is small in the case of the monoliths (Figure 6.5), i.e. the term d_c/L in Equations 6.18 and 6.20 is very small, the equations reduce to their asymptotes. The experiments in this research

were performed with an interstitial velocity of about 0.1 m/s and from Figure 6.6 it can be seen that the Sherwood number for the monolith is lower than that for the equivalent packed bed. Although the Sherwood number predicted for the monolith by the heat transfer models are of the same order of magnitude as that predicted for the packed bed using the Wakao model, the Sherwood number for the monolith predicted by the Votruba model is considerably lower.

The effect of geometry on the Sherwood number for packed beds and the monoliths is shown in Figure 6.7. The monoliths used for comparison include those described in the literature (Howitt, 1980) and in this thesis, while the pellets are commercially available materials (UOP, 1992). For packed beds, the Sherwood number increases as the interstitial velocity and pellet size are both increased. For monoliths, the Sherwood number estimated from the Hawthorn model remains relatively constant.

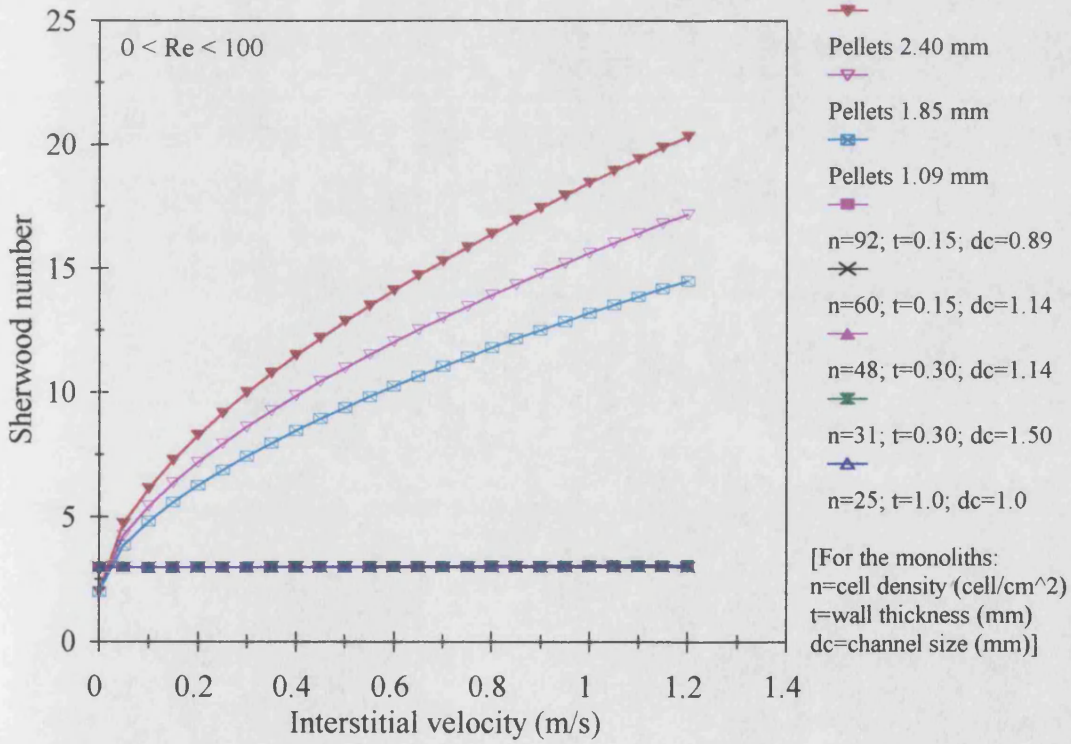

Figure 6.7 Sherwood number for the monoliths and packed beds of various geometric sizes.

The external film coefficient, k, for the various geometric sizes is shown in Figure 6.8. For packed beds, k increases when the interstitial velocity is increased and the pellet size is decreased. The external film coefficient for the monoliths determined from the Hawthorn model remains relatively unchanged with variation in interstitial velocity. However, it increases as the channel size is decreased. The k for the monolith (d_c=1.0 mm) described in this thesis at 0.1 m/s, (i.e. k_1=0.028 m/s) is slightly smaller than the k for the packed bed (pellet size=1.09 mm) described in this thesis at 0.05 m/s (i.e. k_2=0.035 m/s). However the k for the monolith predicted from the Votruba model are comparatively lower than for the packed bed (Figure 6.9).

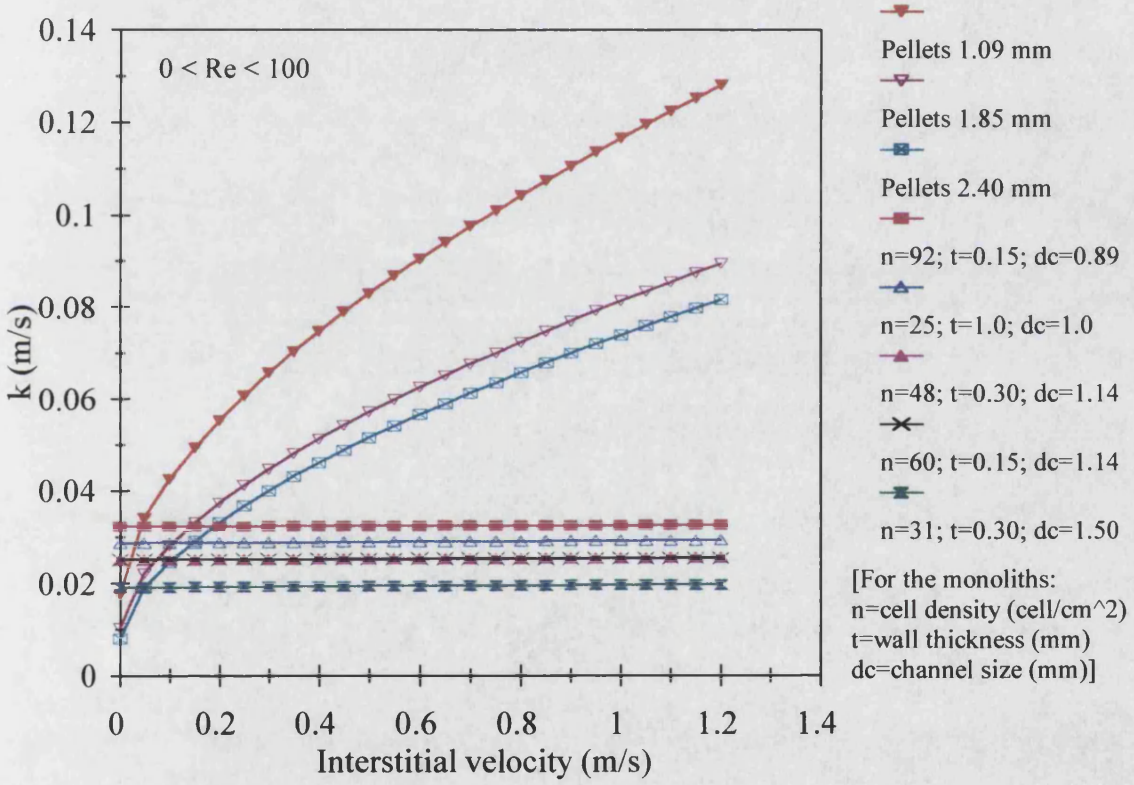

Figure 6.8 Variation of mass transfer coefficient, k, with interstitial velocity and geometry of the monoliths and the packed beds

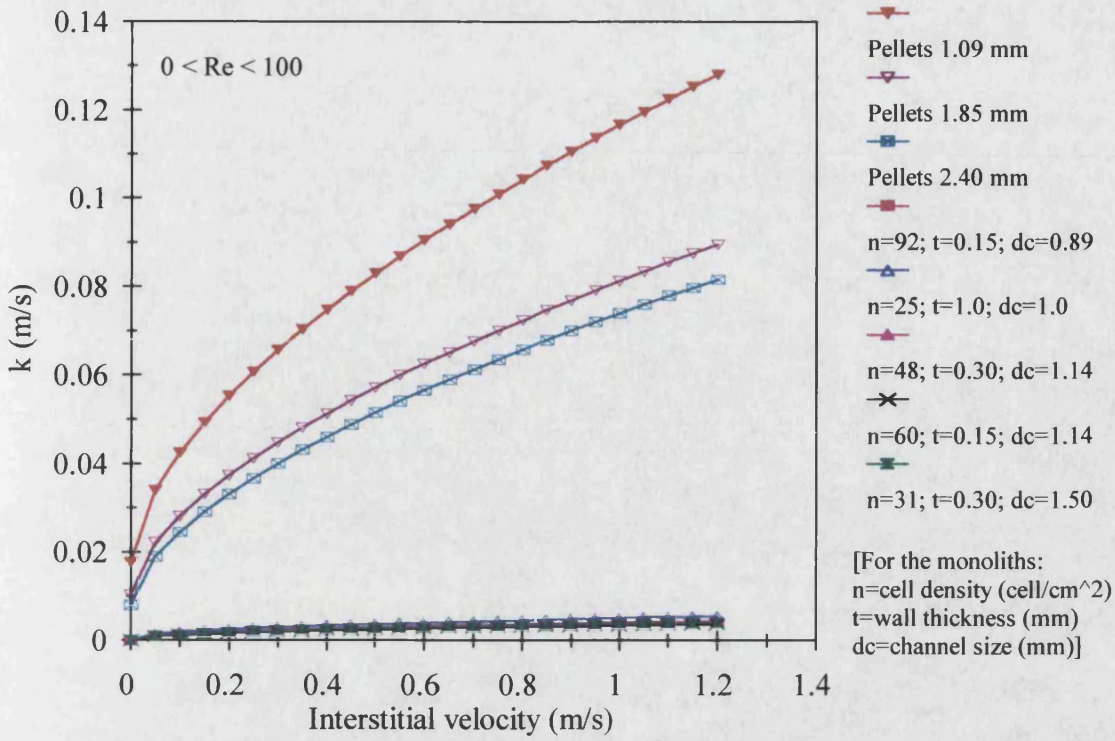

Figure 6.9 Variation of mass transfer coefficient, *k*, with interstitial velocity and geometry of the monoliths and the packed beds

The axial dispersion coefficient as a function of interstitial velocity and geometric size is shown in Figure 6.10. For the packed bed, the axial dispersion increases linearly with flowrate and pellet size. For the monolith, the axial dispersion coefficient does not vary linearly with the interstitial velocity but increases at a greater rate as the interstitial velocity is increased. At the interstitial velocity of 0.1 m/s, the axial dispersion coefficient in the monolith is very small when compared with the packed bed. As the velocity is increased, the axial dispersion coefficient in the monolith increases, and the increment is larger for monoliths having larger channel size. The axial dispersion coefficient for the monolith can be reduced by reducing the channel openings. However the higher pressure drop due to the reduction in channel size has to be considered.

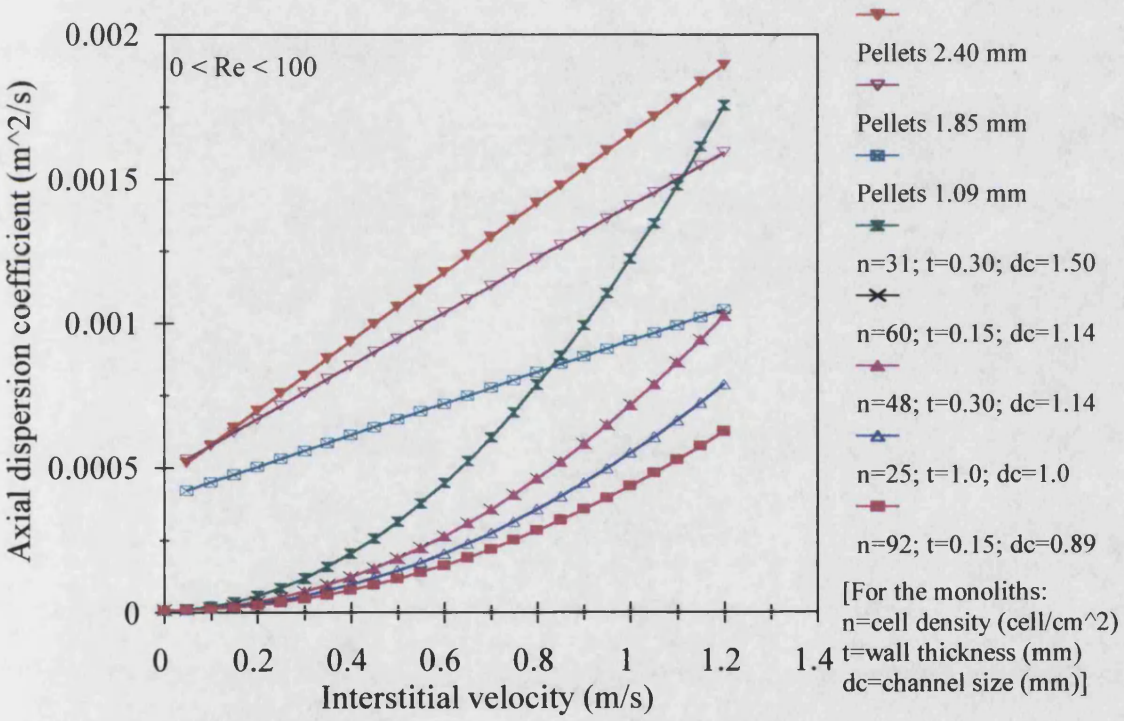

Figure 6.10 Variation of axial dispersion coefficient with interstitial velocity and geometry of the monoliths and the packed beds.

Figure 6.11 shows the Sherwood number for the monolith covering flow in the laminar and transition regions. The change from the laminar to transition flow is assumed to occur at a Reynolds number of about 2000. There is a sharp rise in the Sherwood number with increasing interstitial velocity beyond the transition point. Figure 6.12 shows the mass transfer coefficient, k, as a function of interstitial velocity including both laminar and transition flow. Again, the change from the laminar to the transition region is not smooth and there is a sudden rise in k at Reynolds numbers above 2000. For monoliths of larger channel size, the k in this region is larger than for monoliths with smaller channel size.

The k for the monolith and the packed bed described in this thesis are the same (i.e., k~0.035 m/s) at an interstitial velocity of about 10 m/s. The corresponding pressure drop in the monolith is about 500 Pa/m (Figure 6.4). Hence the desired value of k for the monolith can be achieved by increasing the interstitial velocity without the sacrifice of a high pressure drop. A higher value of k can also be achieved without having to increase the interstitial velocity considerably by using monoliths of higher cell density (i.e. 92 cell/cm^2, 0.89 channel size and 0.15 mm wall) (Figure 6.8).

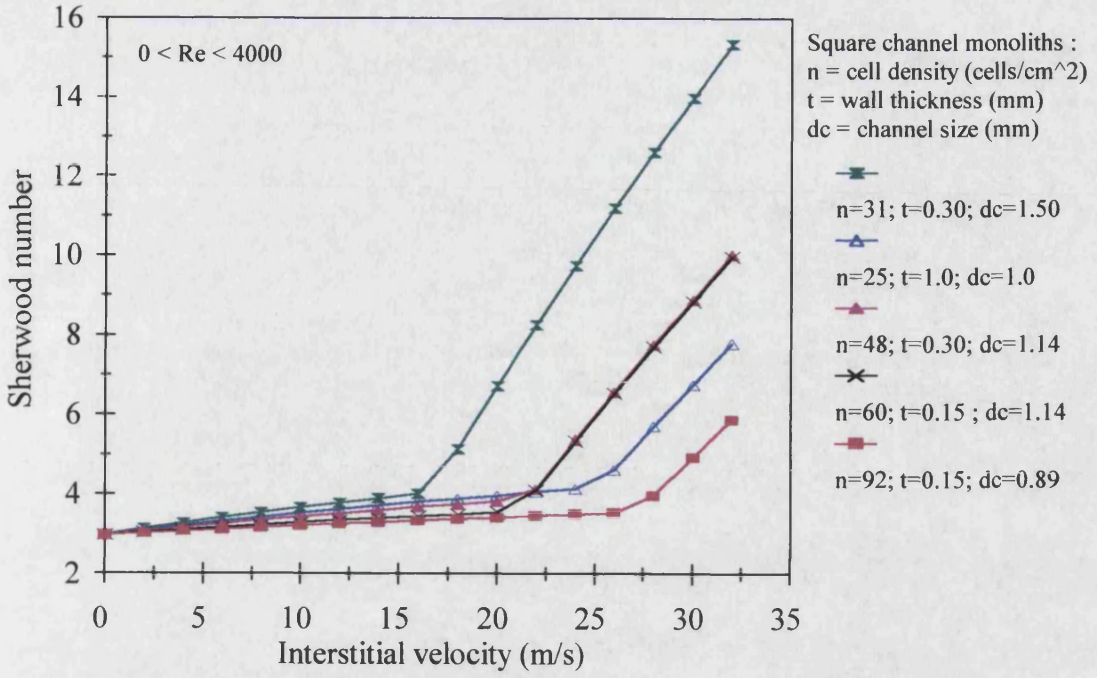

Figure 6.11 Variation of Sherwood number with interstitial velocity and geometry of the monoliths.

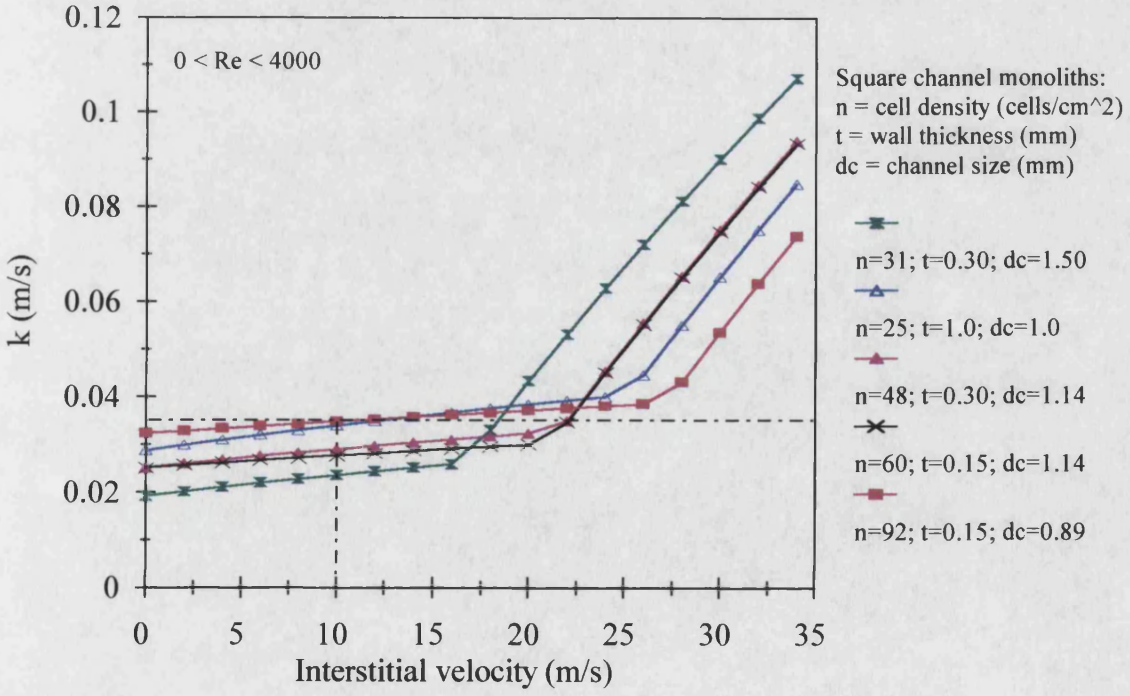

Figure 6.12 Variation of external mass transfer coefficient, *k*, with interstitial velocity and geometry of the monoliths

6.6 Conclusion

Compared with the packed bed, the pressure drop in the monolith is much lower. The monolith pressure drop increases with increasing interstitial velocity and reducing monolith channel and pellet diameters. For the monolith, the entrance effect is relatively small and axial dispersion is negligible under the experimental condition of interest.

The Sherwood number is generally higher for the packed bed than for the monolith. In the case of the packed bed, the Sherwood number can be increased by increasing the interstitial velocity and the pellet diameter. However, the Sherwood number for a monolith remains relatively unchanged in the laminar flow region with the flowrate and the geometric size ($Re < 2000$). A sudden rise in the Sherwood number is observed when the flowrate is increased beyond the transition region ($2000 < Re < 4000$). In the transition region, the Sherwood number for the monolith is seen to increase with the channel size.

The external mass transfer coefficient, k, for the packed bed is higher than for the monolith described in this thesis. In the laminar flow region, k for the packed bed is increased when the interstitial velocity is increased and the pellet size reduced. For the monolith the effect on k of the interstitial velocity is relatively small, but it increases as the channel size is reduced. However, in the transition flow regime, k for the monolith rises sharply with increasing interstitial velocity and increasing channel size. The k for the monolith described in this thesis can be made similar to that for the packed bed by increasing the experimental interstitial velocity of 0.1 m/s to 10 m/s. The resulting increase in the pressure drop is relatively small. Alternatively, a higher value of k can be obtained by increasing the cell density of the monolith. Catalyst monoliths with cell densities of 92 cells/cm^2 (0.89 mm channel size and 0.15 wall thickness) have been produced (Howitt, 1980). This monolith was demonstrated to have a value of k comparable to that of the packed bed of 1.09 mm pellets at the interstitial velocity of 0.1 m/s. The performance of the monolith can also be improved if a flowrate in the transition region ($2000 < Re < 6500$) is used. However this has to be traded against the resulting higher pressure drop and increased axial dispersion.

The validity of the Sherwood number correlations derived by analogy with heat transfer processes remains uncertain in the case of the monoliths. Future research work should be performed to measure the Sherwood number for the adsorption of VOCs onto the monoliths.

Chapter 7
Conclusions and
Recommendations for Future Work

7.1 Introduction

Because of the contribution made by VOCs to both primary and secondary pollution, regulatory pressure to control their emission into the atmosphere is increasing. VOCs may be toxic or mutagenic such as benzene and 1,3-butadiene which are carcinogens which can cause leukaemia. Some VOCs contribute to the formation of ozone in the troposphere (~0-14 km) and to destruction of ozone in the stratosphere (~12-40 km). Ozone concentrations at ground level can be raised to levels considered dangerous to human health, especially for those people with respiratory problems, and damaging to vegetation and building materials. The depletion of stratospheric ozone allows higher levels of harmful ultraviolet radiation to reach the earth's surface, worsening the ground level air quality. Some of the long-lived VOCs may absorb solar or terrestrial infrared radiation, thus contributing to global warming. It has been estimated that in the UK the emissions of VOCs (excluding methane) to the atmosphere in 1988 were around 3 million tonnes, the largest source being motor vehicles (972 kt/yr), followed by solvent usage (752 kt/yr) (DoE, 1993). In the UK, the legislative measures for the control of VOC emissions in the environment, for example the Environmental Protection Act 1990 (EPA 90), VOC protocol of the 1991 Long Range Transboundary Air Pollution (LRTAP) Convention, and EC Directives on petrol and petrol-vehicles, aim to achieve a reduction, by 1999, of 30 % of the total VOCs emitted in 1988.

The research described in this thesis is concerned with the control of VOC emissions by means of adsorption onto high silica zeolites. Adsorption is not only used to control the VOC emissions, but because it does not destroy the compounds it also enables their recovery for reuse. Furthermore, adsorption requires a lower energy consumption than distillation and thermal oxidation. High silica zeolites such as

silicalite and ZSM-5 are known to be hydrophobic and organophilic, and are considered for the recovery of VOCs in this research. There are problems associated with activated carbon as an alternative adsorbent because of the potential for bed fires, the restricted conditions under which it may be regenerated, its non-selectivity towards low molecular weight compounds, and its reduced adsorption capacity when humidity is present. The fact that silicalite is totally inorganic and thermally stable (it can withstand temperatures up to 1000°C) means that it would not suffer many of the drawbacks of activated carbon in VOC control applications.

VOC control with activated carbon has traditionally used this adsorbent in a packed bed of pellets. However, the pressure drop across the bed may be significant, and particle attrition can occur, especially when high flowrates are encountered. These problems will not arise if a monolith is used. Monoliths have a high surface area per unit volume and the low pressure drop associated with them could provide considerable savings in operational costs. Also, in contrast with the packed bed, the monolith structure would offer minimal resistance to the transport of particulates, should they be present in the gas phase.

In the first stage of the research described in this thesis, experiments were carried out using commercially available silicalite and ZSM-5 pellets to investigate the effectiveness of high silica zeolites in the recovery of VOCs. The flow-through adsorption column apparatus described in this thesis has enabled the equilibrium and kinetic performances of the pellets and monoliths to be determined. The effectiveness was represented quantitatively from the equilibrium loading and qualitatively from the shape of the isotherms. In parallel with this work, silicalite monoliths of novel composition were fabricated by extrusion and the monolith design was optimised using dynamic breakthrough experiments. Following the successful manufacture of suitable monoliths, experiments were performed to study the effectiveness of the monoliths in adsorbing selected VOCs, and the effect of humidity on their performance. The results were compared with those obtained using commercial silicalite pellets under similar operating conditions. Since the flow in a monolith is laminar, it is necessary to evaluate the external mass transfer coefficient and to compare it with that of the packed bed. The

pressure drops in the monolith and the packed bed were also compared. Conclusions about these results are provided under the following headings.

7.2 Monolith Manufacturing and Design Optimisation

Silicalite monoliths of novel chemical formulation were successfully manufactured using the extrusion technique. The extrusion paste was formulated using a very high ratio of silicalite to clay binder. The design of the monolith was optimised via the adsorption breakthrough experiments. The optimised monolith has square channels and a chemical composition of 80 wt. % of silicalite powder to 20 wt. % of clay binder. The thick wall square channel monolith has a wall thickness of 1.0 mm and a cell density of 25 cells/cm^2. The overall dimensions of the monolith test section were approximately 1.90 cm diameter and length about 21.80 cm. The monolith is easy to manufacture and has a greater crushing strength compared to the activated carbon monolith described in the literature (DeLiso, 1991). Although monoliths of 29 cells/cm^2 and lower wall thickness of 0.6 mm were produced, the thick wall design was chosen for study since its dimensions are comparable with those of a bed of similar weight but composed of 1.09 mm pellets. (The packed bed diameter is 2.11 cm and the length is 18.50 cm).

7.3 Kinetic Performances of Silicalite Monolith and Packed bed

The breakthrough curves using beds of pellets are generally sharper than those from the monolith. This is a result of the longer mass transfer zone in the monolith. A higher overall resistance to mass transfer in the monolith, when compared with the packed bed, may be due to conditions both external and internal to the adsorbent. In laminar flow, the diffusion through the external film may be a significant limiting factor. Since the flow in the monolith and the packed bed is laminar, it may be assumed that the external mass transfer coefficient is significant, and may be lower in the monolith. The packed bed has a higher total external surface area than the monolith and this may contribute to the lower overall mass transfer resistance in the former.

Micropore analysis revealed that both the monolith and the pellets have similar micropore volumes, but the total number of pores in the pellets is higher. It may be considered therefore that the pellets have greater macropore volume than the monoliths. This may provide easier access to internal adsorption sites. Modelling work performed by Shah et. al. (1995) showed that the performance of a monolith will be comparable with that of the equivalent packed bed only if the resistance to adsorption is controlled by micropore diffusion rather than macropore diffusion. Therefore it may be concluded that the macropore resistance may be higher in the monolith than in the packed bed.

The adsorption performance of a monolith may be improved by increasing the cell density and reducing the wall thickness. As shown in Figures 7.1-7.3, the steepness of the breakthrough curve improves when the cell density of the monolith is increased from 25 to 29 cells/ cm^2 and the wall thickness is reduced from 1.0 mm to 0.60 mm. A higher cell density provides a longer contact time and a thinner wall provides easier access to the active pores, thus reducing the influence of macropore resistance. In the manufacture of catalytic converters, cell densities in excess of 90 cells/cm^2 with a wall thickness as low as 0.10 mm have been achieved (Howitt, 1980). If these dimensions could be achieved in silicalite monoliths, then the adsorption performance might be expected to be comparable with that of the commercial pellets.

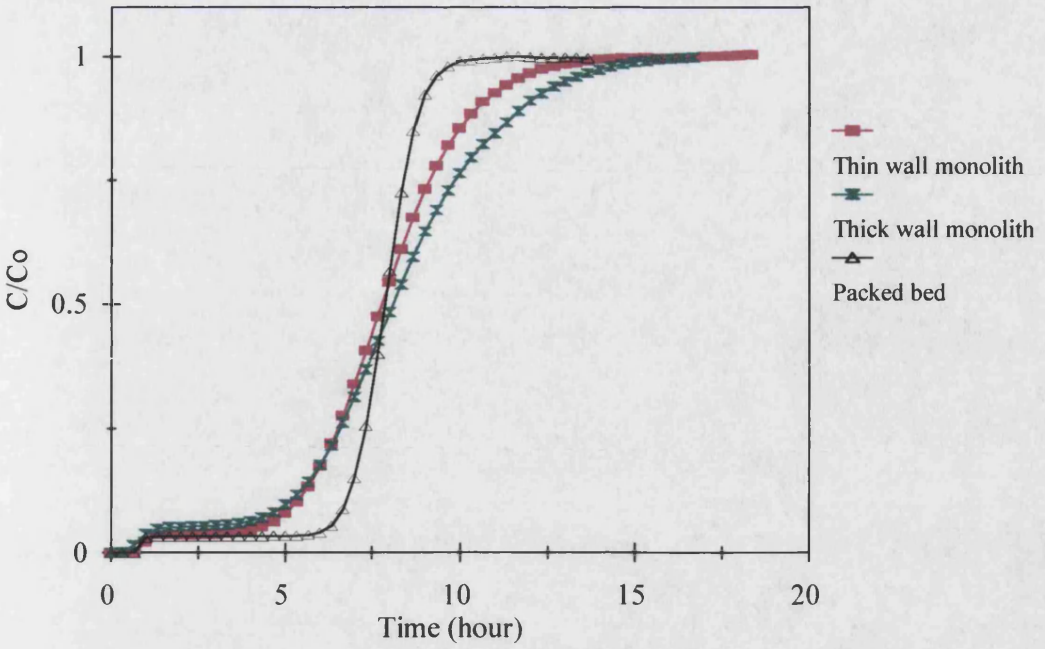

Figure 7.1 Adsorption of propane (1000 ppm) onto thick wall and thin wall monoliths (80si:20clay wt %) and packed bed (1.09 mm spheres) under same total flowrate of 500 cm^3/min

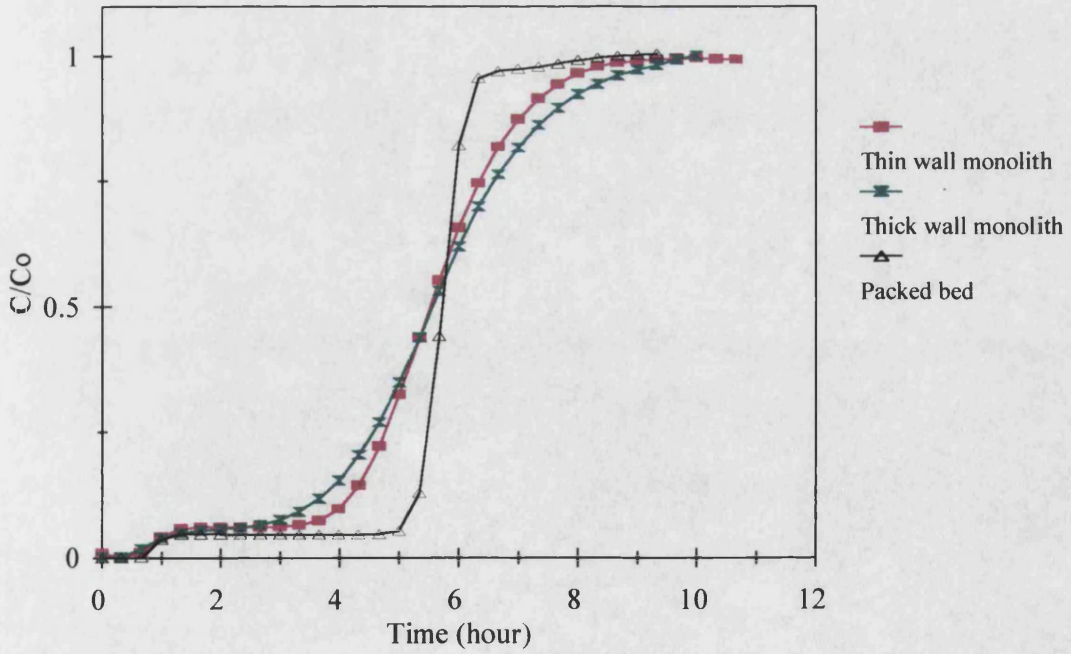

Figure 7.2 Adsorption of propane (5000 ppm) onto thick wall and thin wall monoliths (80si:20clay wt %) and packed bed (1.09 mm spheres) under same total flowrate of 500 cm^3/min

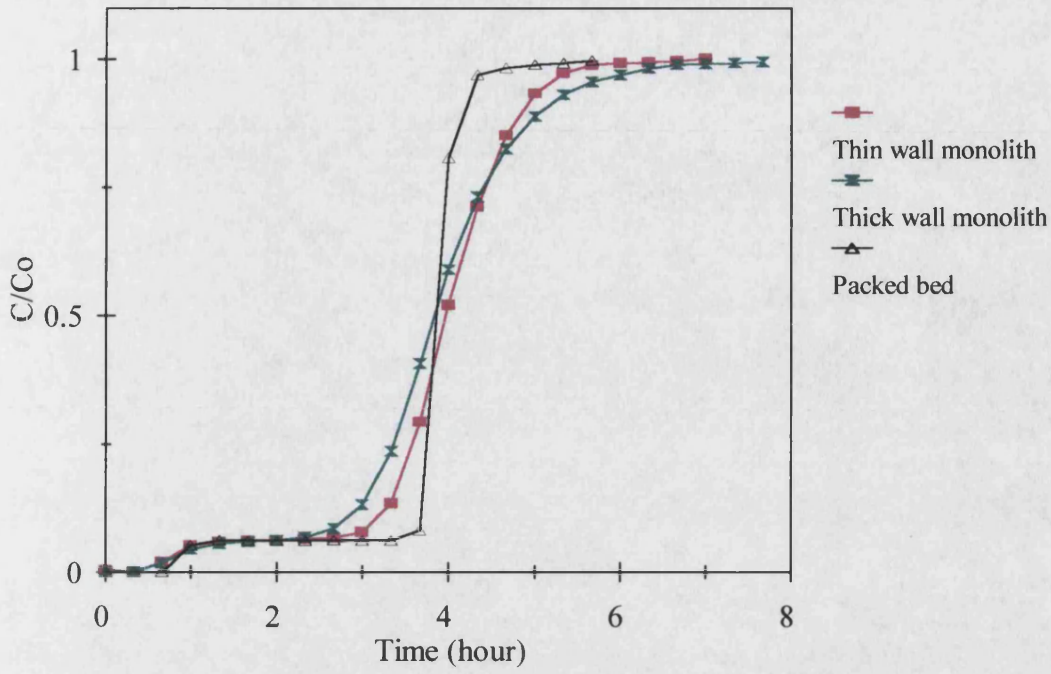

Figure 7.3 Adsorption of propane (10,000 ppm) onto thick wall and thin wall monoliths (80si:20clay wt %) and packed bed (1.09 mm spheres) under same total flowrate of 500 cm^3/min

7.4 Equilibrium Loading of Single Component VOCs

The isotherms determined for single component VOC adsorption onto the silicalite pellets (Figure 7.4) and monolith (Figure 7.5) are highly favourable. For example, the isotherms of ethanol and methylene chloride have a rectangular shape and the equilibrium loading is almost independent of the gas phase concentration. Silicalite is more effective than ZSM-5 for the recovery of VOCs as demonstrated by its higher equilibrium capacity for propane. This may be related to the fact the silicalite is totally free from aluminium, while ZSM-5 has a Si to Al ratio ranging from 20 to 8000 (Olson et. al., 1981). The equilibrium performance of the monolith is comparable with that of the pellets for single component VOC adsorption. The performance can be predicted well by means of the Langmuir model. The equilibrium loading is determined to be a function of the kinetic diameter of the VOC molecule. For example, the equilibrium loading of ethanol (kinetic diameter = 0.453 nm) is higher than the loading of methylene chloride (0.489 nm) which in turn is higher than that of propane (0.512 nm).

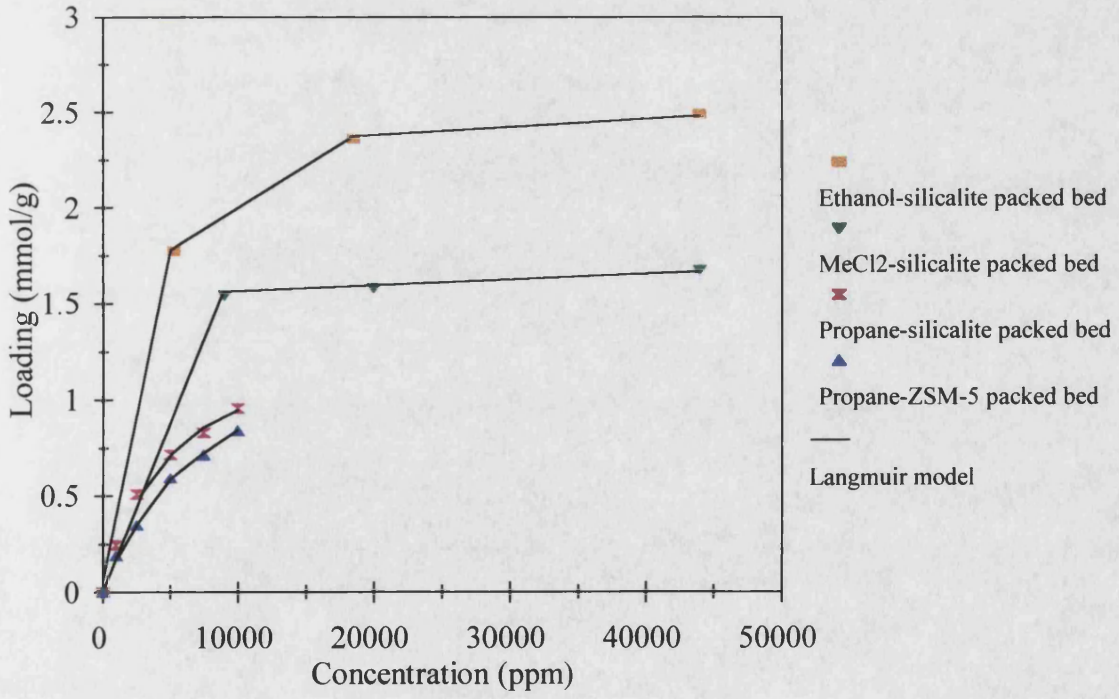

Figure 7.4 Adsorption isotherms of single component VOC onto silicalite and ZSM packed beds

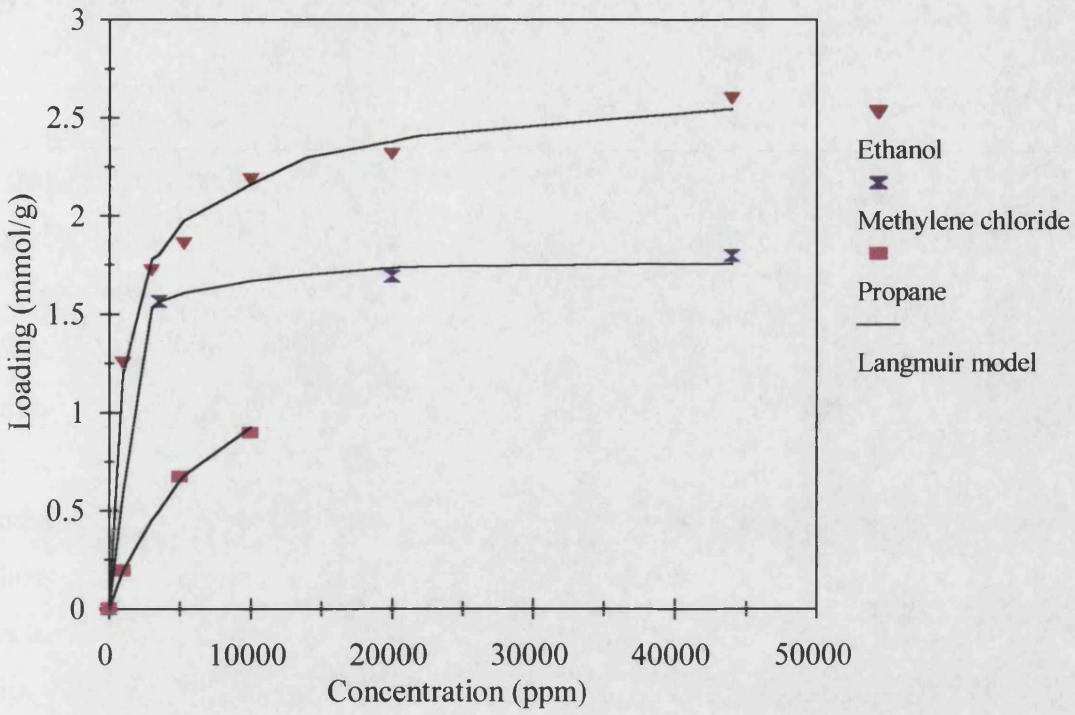

Figure 7.5 Adsorption isotherms of single component VOC onto silicalite monolith and the Langmuir model fit

7.5 Equilibrium Loading of Water Vapour

Silicalite pellets were demonstrated to have a capacity for water vapour similar to that described in the literature (Flanigen et. al., 1978). However the manufactured monolith was found to have a lower water equilibrium loading than the pellets as shown in Figure 7.6. This indicates that the novel chemical formulation has produced a monolith not only of low pressure drop but also of higher hydrophobicity than the commercial pellets. As explained by Flanigen et. al. (1978), silicalite is electrically neutral and there is therefore no strong interaction with water molecules. In the synthesis of silicalite, an organic template, hydroxyl ions and a silica source are used. When crystallisation is complete, the organic template is removed by chemical or thermal decomposition (usually in air at 500-600°C) to yield the micropores. As the silica framework is electrically neutral, the organic ion maintains its charge balance by interaction with the hydroxyl ion. Flanigen et. al. (1978) describe how any small amount of water adsorbed in silicalite may be associated with the residual impurities, such as hydroxyl groups, which persist in the silicalite precursor after thermal removal of the organic ion. Therefore, the higher degree of hydrophobicity of the manufactured monolith may be due to complete removal of any intracrystalline impurities during the firing of the green monolith (at 750°C) and/or a lower aluminium content of the clay binder used in the formulation of the monoliths compared with the binder used in the commercial pellets.

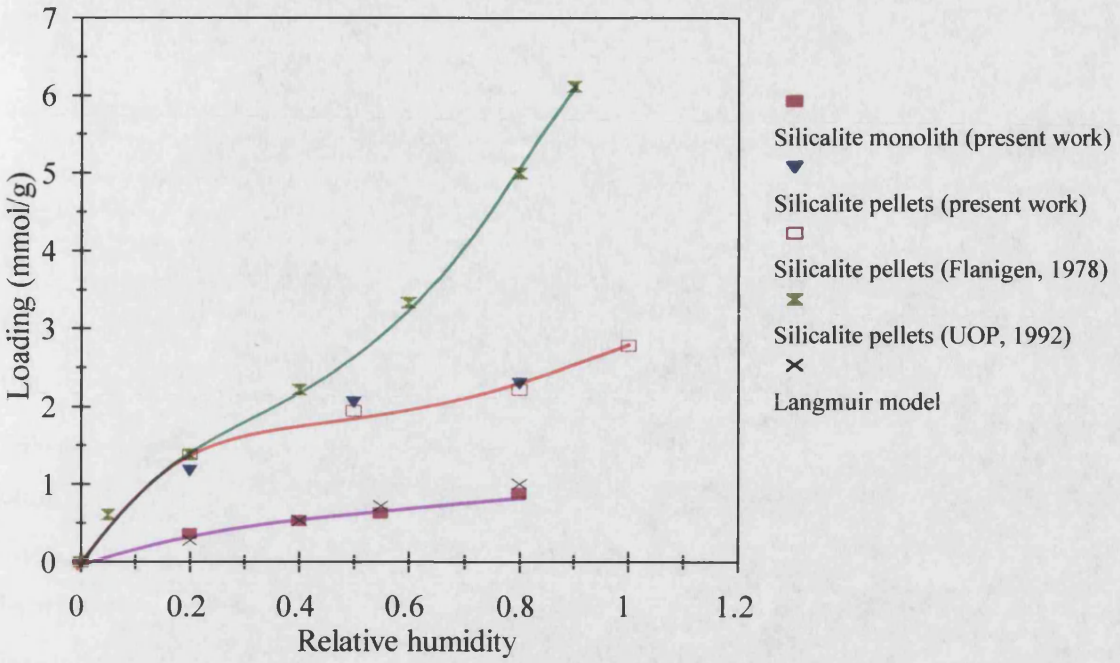

Figure 7.6 Comparison of the adsorption isotherms of water vapour onto silicalite monolith with those obtained using silicalite packed bed, values from the literature, and the Langmuir model fit

7.6 Equilibrium Loading of Binary Mixtures of VOC and Water Vapour

Silicalite monoliths and pellets successfully separated single VOCs from a humidified gas stream. The adsorption affinity may be related to the miscibility of the VOC in water. For example, the adsorption of ethanol is not appreciably affected by the humidity. As ethanol is totally soluble in water at any concentration, it is able to reach the adsorption sites without being impeded by any condensed phase. However, the equilibrium loading of propane, which is immiscible with water, is reduced under humid conditions. Propane molecules have to compete with water molecules for the active pore sites. The effect is worsened when the relative humidity is increased from 55 % to 70 %. In the case of methylene chloride the effect is moderate, since its solubility in water is intermediate between that of propane and ethanol. The trend of adsorption affinity is consistent for both the monoliths and the pellets. However, the performance of the monolith is better than that of the pellets with regard to the separation of a propane-water vapour mixture. As explained above, the monolith is more hydrophobic than the pellets. Therefore it is expected that the equilibrium loading of the low water solubility VOC species is higher in the monolith than in the pellets.

The simple extended Langmuir model for binary component mixtures is able to predict the performance of the monoliths better than that of the pellets. This is believed to be due to water vapour having a milder effect on the monolith.

7.7 Desorption

The desorption of propane from the silicalite adsorbents is technically feasible at room temperature by back-flushing with nitrogen. The rate of desorption is increased as the temperature in the bed and the flowrate of nitrogen is increased. The desorption curve for the pellets is sharper than for the monolith, which may be related to the longer mass transfer zone in the latter as explained above.

7.8 Pressure Drop and External Mass Transfer Properties

For the same length of bed, the pressure drop in the monolith (25 cells/cm^2) is predicted to be appreciably lower than in the packed bed (1.09 mm spheres). The pressure drop in the monolith and the packed bed increases with increasing interstitial velocity and decreasing channel size and pellet size (Figure 7.7). The external mass transfer coefficient evaluated for the monolith is lower than for the packed bed (at the interstitial velocity of 0.1 m/s) as shown in Figure 7.8. Figure 7.9 shows that the external film coefficient for the monolith can be improved by increasing the cell density and reducing the wall thickness. The performance of the monolith can also be improved by using a higher flowrate, however this has to be traded against a higher pressure drop and possibly greater axial dispersion. The results shown in Figures 7.8 and 7.9 for the monoliths are subject to the accuracy of the theoretical mass transfer models (described in Chapter 6) which were derived by analogy with heat transfer.

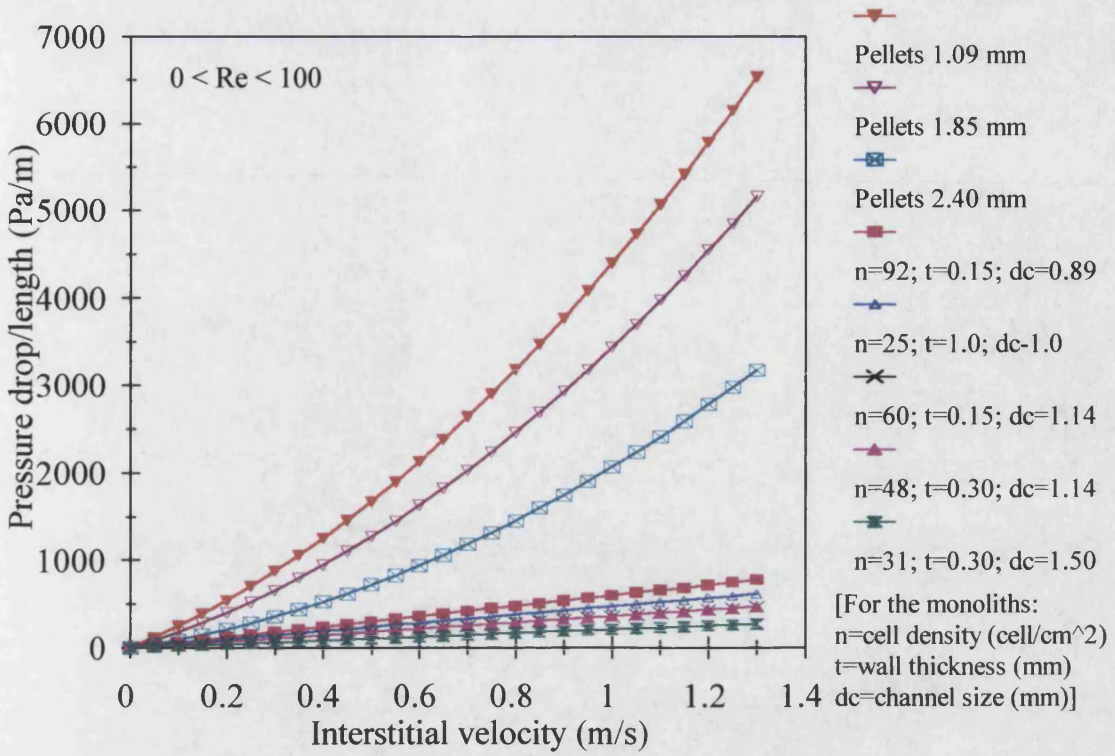

Figure 7.7 Comparison of pressure drop in monoliths with that in packed beds

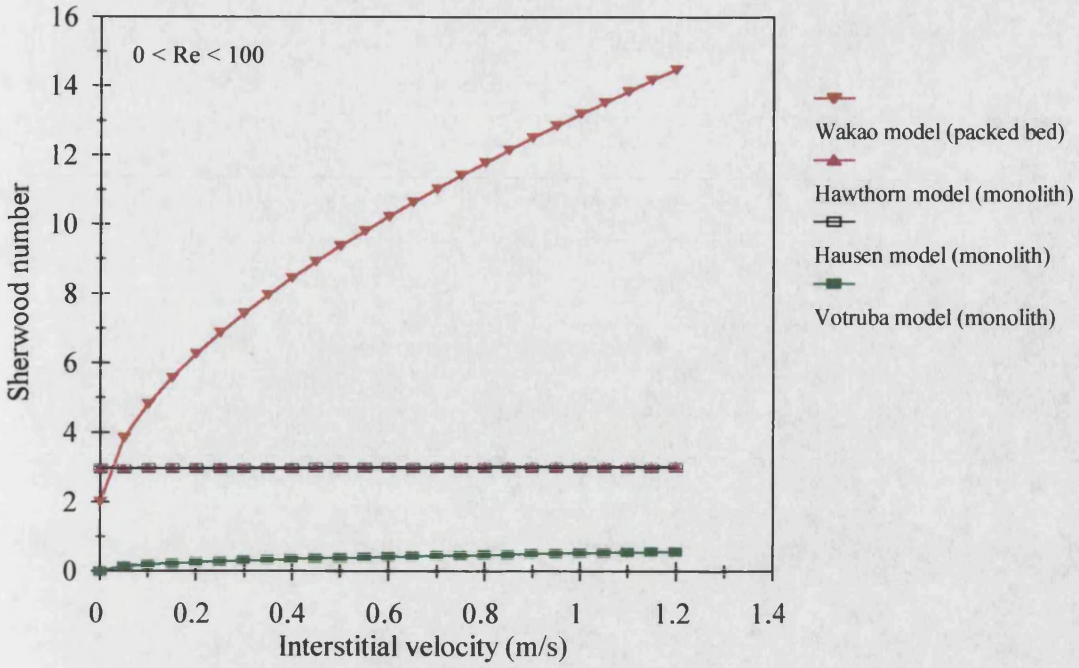

Figure 7.8 Sherwood number for the monolith (25 cells/cm^2, 1.0 mm wall and 1.0 mm square channels) and packed bed (1.09 mm spheres) described in this thesis.

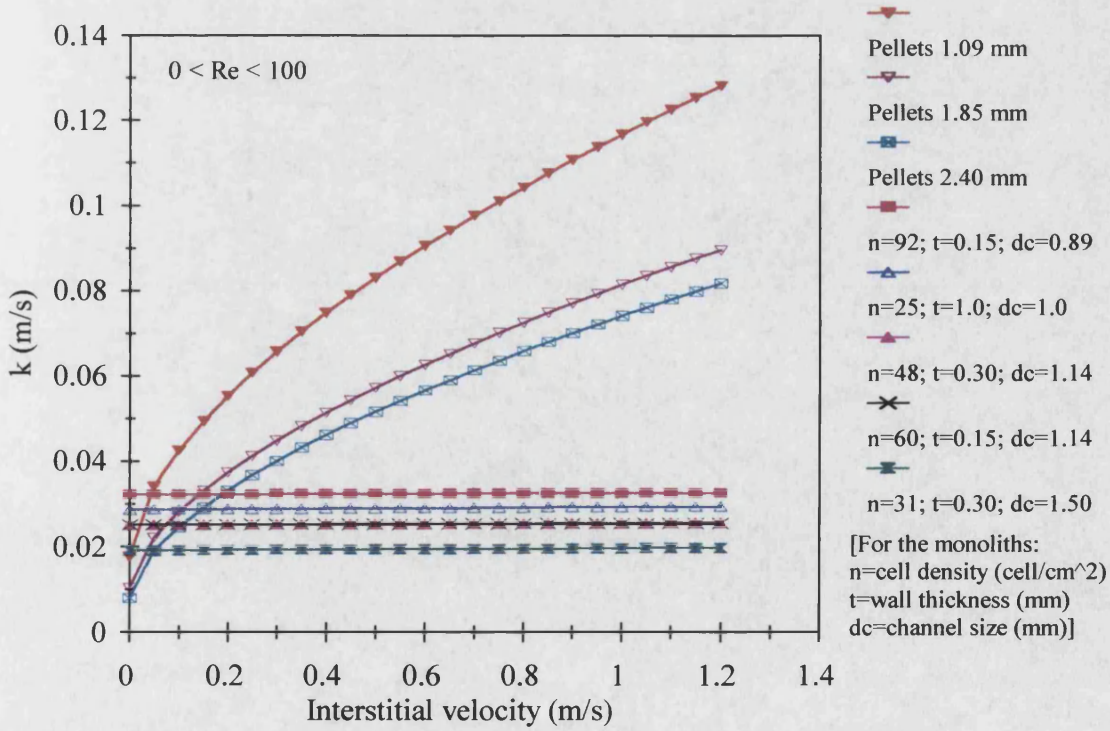

Figure 7.9 Variation of mass transfer coefficient, *k*, with interstitial velocity and geometry of the monoliths and the packed beds

Although the adsorption kinetics of the monolith are generally worse than that of the equivalent packed bed, the performance can be improved by increasing the cell density and reducing the wall thickness. It was shown that with silicalite in a monolith configuration, a low pressure drop advantage can be gained with a bed size approximately equivalent to the packed bed. It was also determined that:

- the monolith has a higher adsorption equilibrium loading for propane and methylene chloride when moisture is present.

- the adsorption isotherms of binary VOC-water vapour for the monolith can be represented by a simple model, *viz.* the extended Langmuir model.

7.9 Future Work

7.9.1 To Manufacture Monoliths of Higher Cell Density and Thinner Wall

It was demonstrated that the kinetic performance of the monolith can be improved by increasing the cell density and reducing the wall thickness. For a fixed diameter, the cell density may be increased by reducing the wall thickness and/or reducing the channel size. The kinetic performance of the monolith may also be improved by increasing the macropore volume and increasing the silicalite content in the structure. However, as described in Chapter 3, the attempt to increase the macroporosity using corn starch failed. This may have been due to the starch being combusted at a temperature (~150°C) below that at which the clay binder was calcined (~650°C). After the macropores were formed by the removal of the starch, a further increase in the firing temperature may have caused the macropores to close via coalescence of fused clay particles. In any case, an increase in macropore volume or silicalite content could lead to an undesirable reduction in mechanical strength.

7.9.2 To Study the Adsorption of Multi-component VOC Mixtures

The emissions of VOC from processes such as paint spraying, print-work, oil refinery and sealant applications usually consist of complex mixtures of volatile materials. For example, the toxic air emissions from the aerospace industry consist of VOC mixtures as shown in Table 7.1 (Kenson, 1994). Aerospace manufacturing and maintenance involve operations such as cleaning of aircraft parts using solvent, maskant application to protect aircraft parts during machining/forming steps, adhesive bonding which requires the spraying of an adhesive coating onto the aerospace parts to allow good bonding to other parts, composite lay-up which requires the cleaning and bonding of multiple material layers, paint stripping and painting of aerospace parts. Further experiments should therefore be performed to study the adsorption of the complex VOC mixtures onto the silicalite monolith and the silicalite packed bed.

Table 7.1 VOC emissions from aerospace processes

Process operations	VOC emission
Cleaning	Chlorinated hydrocarbons (HCs), ketones, aromatics, paraffins
Maskant application	Aromatics, chlorinated HCs
Adhesive bonding	Ketones, aromatics, alcohols, chlorinated HCs
Composite lay-up	Styrene, ketones, aromatics, chlorinated HCs
Paint stripping	Chlorinated HCs, ketones
Painting	Ketones, aromatics, alcohols, glycol ethers, acetates

7.9.3 To Carry Out Experiments to Measure the External Mass Transfer Coefficient

It was determined by calculation that the external mass transfer coefficient for the monolith is lower than that of the packed bed. However, the theoretical models used to predict the Sherwood number have not been tested on the silicalite monolith. Therefore it is suggested that experiments be performed to measure experimentally the external mass transfer coefficient in the monoliths.

7.9.4 To Model the Experimental Data in Order to Assess the Contribution of Intraparticle Resistances

The internal resistances within a monolith have been investigated theoretically in a numerical model by Shah et. al. (1995). The model has not been validated with any experimental data, and should therefore be tested, making use of the experimental data on the performance of the monoliths described in this thesis.

References

AEA Technology (1993). *Draft report of the abatement of volatile organic compounds from stationary Sources*, Air Pollution Abatement Review Group (AEA), Oxford.

Akubuiro, E.C. and Wagner, N.J. (1992). Assessment of activated carbon stability toward adsorbed organics. *Ind. Eng. Chem. Res.*, **31**, 1, pp339-349.

Antia, J.E. and Govind, R. (1995). Conversion of methanol to gasoline-range hydrocarbons in a ZSM-5 coated monolithic reactor. *Ind. Eng. Chem. Res.*, **34**, pp140-147.

Bagley, R.D. (1973). Corning Glass. *Extrusion die*. U.S. Pat. 3,837,783.

Baker, R.W., Kaschemekat, J., Wijmans, J.G. and Simmons, V.L. (1992). *Membrane vapour separation systems for recovery of VOCs*. Presented at the 85th annual meeting of the Air and Waste Management Association, Kansas City, Missouri.

Benbow, J.J., Oxley, E.W. and Bridgwater, J. (1987). The extrusion mechanics of pastes-the influence of paste formulation on extrusion parameters. *Chem. Eng. Sc.*, **42**, 9, pp2152-2162.

Benbow, J.J., Jazayeri, S.H. and Bridgwater, J. (1991). The flow of pastes through dies of complicated geometry. *Powder Tech.*, **65**, pp393-401.

Bennett, C.J., Kolaczkowski, S.T. and Thomas, W.J. (1991). Determination of heterogeneous reaction kinetics and reaction rates under mass transfer controlled conditions for a monolith reactor. *Trans. I. Chem. E.*, **69**, Part B, pp209-220.

Blocki, S.W. (1991). New solvent control strategies: the systems house approach, hydrophobic zeolite adsorbent. *Soc. Manuc. Eng.*, FC91-385.

Boersma, M.A.M., Spierts, J.A.M., Van Lith, W.J.G. and Van Der Baan, H.S. (1980). The oxidation of ethene in an empty and packed tubular wall reactor operating in the reaction- and diffusion-controlled regimes. *Chem. Eng. J.*, **20**, pp177-183.

Brown, S.M. and Woltermann, G.M. (1979). Engelhard Minerals and Chemicals Co. *Zeolitised honeycomb structure*. U.K. Pat. 2,017,520.

Brunauer, S., Emmett, P.H. and Teller, E. (1938). Adsorption of gases in multimolecular layers. *J. Am. Chem. Soc.*, **60**, pp309-319.

Bulow, M., Schlodder, H., Rees, L.V.C. and Richards, R.E. (1986a). Molecular mobility of hydrocarbons in ZSM-5/silicalite systems studied by sorption uptake and frequency response methods. **In:** *New developements in zeolite science and technology, Proc. 7th Int. Conf. Zeolites, Tokyo*, pp579-586. Amsterdam: Elsevier.

Bulow, M., Schlodder, H. and Struve, P. (1986b). Sorption uptake of the molecular mobility of n-paraffins in ZSM-5 type zeolite. *Ads. Sci. Tech.*, **3**, p229.

Caro, J., Bulow, M., Schirmer, W., Karger, J., Heink, W., Pfeifer, H. and Zdanov, S.P. (1985). Microdynamics of methane, ethane and propane in ZSM-5 type zeolites. *J. Chem. Soc. Farad. Trans. I*, **81**, pp2541-2550.

Chi, C.W. and Cummings, W.P. (1978). *Kirk-Othmer's Encyclopedia of Chemical Technology,* pp559-561, vol 1. New York: McGraw Hill.

Chiang, A.S., Dixon, A.G. and Ma, Y.H. (1984a). The determination of zeolite crystal diffusivity by gas chromatography: I. Theoretical. *Chem. Eng. Sci.*, **39**, pp1451-1459.

Chiang, A.S., Dixon, A.G. and Ma, Y.H. (1984b). The determination of zeolite crystal diffusivity by gas chromatography: II. Experimental. *Chem. Eng. Sci.*, **39**, pp1461-1468.

Chorley, S.R., Crittenden, B.D. and Kolaczkowski, S.T. (1991). Adsorption of trihalomethanes onto zeolites. **In:** *Thomas, G. and King, R. ed. Advances in water treatment and environmental management*, pp181-190. London: Elsevier Applied Science.

Coulson, J.M. and Richardson, J.F. (1991). *Chemical engineering volume 2, particle technology and separation processes*, 4th ed. UK: Pergamon Press.

Crittenden, B.D. (1994). Environmental control with pentasil zeolites: limitations and opportunities. **In:** *International conference in catalysis and adsorption in environmental protection*, Oct 13-15, Szklarska Poreba, Poland, pp113-118.

Crompton, D. and Gupta, A. (1993). Removal of air toxics: a comparison of the adsorption characteristics of activated carbon and zeolites. *Air & Waste. Manage. Asso.*, 93-TP-31B.06.

Darby, R. (1996). *Chemical engineering fluid mechanics*, pp183-189, pp139-152. New York: Marcel Dekker Inc.

DeLiso, E.M. (1991). Corning. *Activated carbon structures.* E. Pat. 0,492,081A1.

DeLuca, J.P. and Campbell, L.L. (1977). Monolithic catalyst supports. In: *Advanced materials in catalysis,* Chapter 10. London: Academic Press.

De Never, N. (1995). *Air pollution control engineering*, pp275-327. USA: McGraw-Hill Inc.

Department of Environment, DoE. (1993). *Reducing emissions of volatile organic compounds (VOCs) and levels of ground level ozone: A UK strategy.* GPC/03784. UK: Crown.

Dowd, E.J., Sheffer, W.M. and Addison, G.E. (1992). *A historical perspective on the future of catalytic oxidation of VOCs*. Presented at the 85th annual meeting of the Air and Waste Management Association, Kansas City, Missouri.

Eic, M. and Ruthven, D.M. (1989). Intracrystalline diffusion of linear paraffins and benzene in silicalite studied by the ZLC method. *Zeolites: facts, figures, future*, pp897-905. Amsterdam: Elsevier.

Eichhorn, R. and Sauber, M. (1969). *A Carrier for Catalyst*. U.K. Pat. 1,142,800.

Elsom, D. (1996). *Smog alert; managing urban air quality*, pp57-59. London: Earthscan Publications Ltd.

ENDS Report (May 1996). *Government takes softly, softly approach to indoor air pollution*, Mayer, M. ed., **259**, pp16-20. London: Environmental Data Service Ltd.

ENDS Report (January 1997). *Local Authority Air Pollution Control (LAAPC) guides for petrol processes*, Mayer, M. ed., **264**, p36. London: Environmental Data Service Ltd.

ENDS Report (March 1997). *Oil industry looses out over petrol refuelling controls*, Mayer, M. ed., **259**, pp16-20. London: Environmental Data Service Ltd.

Environmental Management. (1995). *Government response to VOC air pollution report*, p3. UK: Croner.

Environmental Protection Act 1990 (1994). Technical Guidance Note (Abatement) A2, *Pollution abatement technology for the reduction of solvent vapour emissions*, HMIP.

Ergun, S. (1952). Fluid flow through packed columns. *Chem. Eng. Prog.*, **48**, 2, pp89-94.

Flanigen, E.M., Bennett, J.M., Grose, R.W., Cohen, J.P., Patton, R.L. and Kirchner, R.M. (1978). Silicalite a new hydrophobic crystalline silicalite molecular sieve. *Nature*, **271**, pp512-516.

Froment, G.F. and Bischoff, K.B. (1990). *Chemical reactor analysis and design*, pp531-532, 2nd ed. New York: John Wiley & Sons.

Griffith, R.M. (1966). The extrusion of silica and alumina powders. *Can. J. Chem. Eng.*, **44,** Part I, pp108-110.

Hairston, D.W. (1996). Zealous Zeolites. *Chem Eng*, July, pp57 - 60.

Hamaguchi, K., Harada, T., and Hamanaka, T. (1989). NGK Insulator ltd. *Porous ceramic honeycomb filter and method of producing the same*. E. Pat. 0,354,721A3:

Hampson, A and Rees, L.V.C. (1992). Sorption of ethene and propane and their binary mixtures in zeolite. **In:** *Suzuki, M. ed. Fundamentals of adsorption, proc. IVth Int. Conf. on fundamentals of adsorption, Kyoto, May 17-22,* pp259-266. Copublished by Kodansha Ltd., Tokyo and Elsevier Science Publisher B.V., Amsterdam.

Harrison, R.M. (1996). *Pollution: causes, effects and control*, 3rd ed, pp162-164. Cambridge: Royal Society of Chemistry.

Hawthorn, R.D. (1974). Afterburner catalysts-effects of heat and mass transfer between gas and catalyst surface. *AIChE Sym. Ser.*, **70**, 137, pp428-438.

Hayhurst, D.T. and Paravar, A. (1988). Diffusion of C_1 to C_5 normal paraffins in silicalite. *Zeolites*, **8**, pp27-29.

Hayman, G.C. and Jenkin, M.E. (1991). Atmospheric chemistry of VOCs. *Environ. Protect. Bull.*, **010**, pp6-16.

Heck, R.H., Wei, J. and Katzer, J.R. (1976). Mathematical modeling of monolithic catalysts. *AIChE J.*, **22**, pp477-484.

Howitt, J.S. (1980). Thin wall ceramics as monolithic catalyst supports. *SAE Tech. Paper,* 800082.

Hufton, J.R. and Danner, R. P. (1991). Gas-solid diffusion and equilibrium parameters by tracer pulse chromatography. *Chem. Eng. Sci.*, **46**, pp2079-2091.

Hufton, J.R. and Danner, R. P. (June 1993). Chromatographic study of alkanes in silicalite: Transport properties. *AIChE*, **39**, 6, pp962-974.

Incropera, F.P. and De Witt, D.P. (1990). Fundamental of heat and mass transfer, 3rd ed, pp494-495. New York: John Wiley & Sons.

Irandoust, S. and Andersson, B. (1988). Monolithic catalysts for nonautomobile applications. *Catal. Rev. Sci. Eng.*, **30**, pp341-392.

Isenhour, C.T. (1979). Influence of die design on the quality of extrudate. *Am. Ceram. Soc. Bull.*, **58**, p766.

Jenson, B.I. and Jeffreys, G.V. (1963). *Mathematical methods in chemical engineering*, pp356-360. London: Academic Press.

Jobic, H., Bee, M. and Kearley, G.J. (1989). Translational and rotational dynamics of methane in ZSM-5 zeolite: a quasi-elastic neutron scattering study. *Zeolites*, **9**, p312.

Jobic, H., Bee, M. and Caro, J. (1992a). Translational mobility of n-butane and n-hexane in ZSM-5 zeolite measured by quasi-elastic neutron scattering. *Int. Zeolite Conf., Montreal, July 5-10.*

Jobic, H., Bee, M. and Kearley, G.J. (1992b). Dynamics of ethane and propane in ZSM-5 zeolite studied by quasi-elastic neutron scattering study. *Zeolites*, **12**, p146.

Karger, J. and Ruthven, D.G. (1992). *Diffusion in zeolites and other microporous solids*, pp467-512. Canada: John Wiley & Sons, Inc.

Kays, W.M. and London, A.L. (1964). *Compact heat exchanger*, 2nd ed. New York: McGraw-Hill.

Kenson, R.E. (Nov. 1985). Catalytic incineration in cogeneration systems. *Chem. Eng. Prog.*, pp57-62.

Kenson, R.E. (1994). Applications of air toxic/VOC emission control systems in the aerospace industry. *Air & Waste. Manage. Asso.*, 94-MP8.07.

Kiely, G. (1997). *Environmental engineering*, pp348-349. UK: McGraw-Hill

Klein, S.M. and Abraham, W.H. (1983). Adsorption of ethanol and water vapours by silicalite. *AIChe Sym. Ser.*, **230**, 1, pp53-59.

Kolaczkowski, S.T., Thomas, W.J., Titiloye, J. and Worth, D.J. (1996). Catalytic combustion of methane in a monolith reactor: heat and mass transfer under laminar flow and pseudo-steady-state reaction conditions. *Combust. Sci. and Tech.*, **118**, pp79-100.

Kodama, A., Goto, M. and Hirose, T. (1993). Experimental study of optimal operation for a honeycomb adsorber operated with thermal swing. *J. Chem. Eng. Japan*, **26**, 5, pp530-535.

Kuma, T. (1995). Thermally activated honeycomb dehumidifier for adsorption cooling system. *Solar Eng.*, **2**, pp1267-1275.

Lachman, I.M. and Patil, M.D. (1989).Corning Glass Works. *Method of crystallising a zeolite on the surface of a monolithic ceramic substrate*. U.S. Pat. 4,800,187.

Liepa, A.L. (1977). Procter & Gamble Co. *Beverage carbonation device*. U.S. Pat. 4,007,134.

Marlowe, I.T. ed. (1992). *Emission of volatile organic compounds in the United Kingdom: A review of emission factors by species and process*, pp257-259. DoE reference: PECD 7/12/03. UK: Warren Spring Laboratory.

Mitchell, W.J., Moore, W.F. and Tonawanda, N.Y. (1961). Union Carbide. *Bonded molecular sieves*. U.S. Pat. 2,973,327.

Mizuno, J., Fukami, A. and Okamoto, K. (1983). Nippon Soken Inc. *Apparatus for adsorbing fuel vapor*. U.S. Pat. 4,386,947.

Mukhopadhyay, N. and Moretti, E.C. (1993). VOC control: current practices and future trends. *Chem. Eng. Prog.*, pp20-25.

Ogawa, Y. and Asami, S. (1981). Nippon Gaishi Kabushiki. *Ceramic honeycomb body*. U.K. Pat. 2,071,640A.

Olson, D.H., Kokotailo, G.T., Lawton, S.L., and Meier, W.M. (1981). Crystal structure and structure-related properties of ZSM-5. *J. Phys. Chem.*, **85**, pp2238-2243.

Otto, K., Montrueil, C.N., Todor, O., McCabe, R.B. and Gandhi, H.S. (1991). Adsorption of hydrocarbons and other exhaust components on silicalite. *Ind. Eng. Chem. Res.*, **30**, pp2333-2340.

Parks, J.R. and Hill, M.J. (1959). Design of extrusion augers and the characteristic equation of ceramic extrusion machines. *J. Am. Ceram. Soc.*, **42**, 1, pp1-6.

Paravar, A. and Hayhurst, D.T. (1983). Direct measurement of diffusivity for butane across a single large silicalite crystal. **In:** *New developments in zeolite science and technology, Proc. 6th Int. Conf. Zeolites, Reno, Nevada*, pp217-224. UK: Butterworths.

Patil, M.D. and Lachman, I.M. (1988). Methanol conversion on ceramic honeycombs coated with silicalite; In: *ACS Sym. Ser. 368: Perspective in molecular science*, pp492-499. Washington: ACS.

Perry, R.H. and Chilton, C.H. (1973). *Chemical engineers handbook*, 5th ed. New York: McGraw-Hill.

Prakash, D.S., Athota, K.V. and Greene, H.L. (1995). Sorption and catalytic destruction of chlorinated VOCs using fresh and dealuminated Y and ZSM-5 zeolite. *AIChE Sym. Ser.*, Novel adsorbents and their environmental applications, **91**, 309, pp1-17.

Price, D.B. and Reed, J.S. (1983). Boundary conditions in electrical porcelain extrusion. *Am. Ceram. Soc. Bull.*, **62**, pp1348-1350.

Raupp, G.B., Junio, C.T., Mallele, R.H. and Phillips, L.A. (1992). *Destruction of organics in gaseous streams over UV excited alumina.* Presented at the 85th annual meeting of the Air and Waste Management association, Kansas City, Missouri.

Refractory Co. (1977). *Extrusion die.* U.K. Pat. 1,471,217.

Reid, R.C. and Sherwood, T.K. (1958). *The properties of gases and liquids*, 2nd ed. New York: McGraw-Hill.

Ruddy, E.N. and Carroll, L.A. (1993). Select the best VOC control strategy. *Chem. Eng. Prog.*, July, pp28-35.

Ruthven, D.M. (1984). *Principles of Adsorption and Adsorption Processes*, pp4-26, pp48-55, pp208-218. New York: Wiley and Sons Inc.

Ryan, W. (1978). *Properties of ceramic raw materials*, 2nd ed. London: Pergamon Press.

Schweitzer, P.A. (1976). *Handbook of separation techniques for chemical engineers*, pp3.24-3.38. London: McGraw-Hill.

Seidel, R. and Staudte, B. (1993). The influence of clay binder material on the physical properties of the CaNaA molecular sieve used in a hydrocarbon separation process. *Zeolites*, **13,** pp92-96.

Shah, D.B., Perera, S.P. and Crittenden, B.D. (1995). Adsorption dynamics in a monolithic adsorber. *Proc. 5th Int. Conf. on fundamentals of adsorption, Pacific Grove, California*, in press.

Shen, D., Rees, J.V.C., Caro, J. Bulow, M., Zibrowius, B. and Jobic, H. (1990). Diffusion of C_4 hydrocarbons in silicalite-1. *J. Chem. Soc. Farad. Trans.*, **86**, pp3943-3948.

Sing, K. S., Everett, D.H., Haul, R.A., Moscou, L., Pierotti, R.A., Rouquerol, J. and Siemieniewska, T. (1985). Reporting physisorption data for gas/solid system with special reference to the determination of surface area and porosity. *Pure & Appl. Chem.*, **57**, 4, pp603-619.

Spencer, R.J. (1992). *Cryogenic condensation and recovery of VOCs*. Presented at the 85th annual meeting of the Air and Waste Management Association, Kansas City, Missouri.

Sterling, D.A. (1985). Volatile organic compounds in indoor: An overview of sources, concentrations, and health effects. **In:** Gammage, R.B. and Kaye, S.V., ed. *Indoor air and human health*, pp387-402. USA: Lewis Publishers

Tien, C. (1994). *Adsorption Calculations and Modelling*, pp15-69. USA: Butterworth-Heinemann.

Ullah, U. Waldram, S.P. Bennett, C.J. and Truex, T. (1992). Monolithic reactors: mass transfer measurements under reacting conditions. *Chem. Eng. Sci.*, **47**, pp2413-2418.

UOP (1992). Molecular sieves for emissions control. Prepared by Yon, C.M. and Gautam, R. for *AIChE 1992 Annual Meeting*, Miami Beach, November 1-6.

Utiger, L., Cresswell, D.L. and Kershenbaum, L.S. (1991). *Chlorocarbon removal from process effluents.* The 1991 IChemE Research Event, The Institution of Chemical Engineers, Rugby, pp17-19.

van den Begin, N.G. and Rees, L.V.C. (1989). Diffusion of hydrocarbons in silicalite using a frequency-response method. *Zeolites: facts, figures, future*, pp915-924. Amsterdam: Elsevier.

van den Begin, N.G., Rees, L.V.C., Caro, J. and Bulow, M. (1989). Fast adsorption-desorption kinetics of hydrocarbons in silicalite-1 by the single-step frequency response method. *Zeolites*, **9**, p287.

Villermaux, J. and Schweich, D. (1994). Is the catalytic monolith reactor well suited to environmentally benign processing? *Ind. Eng. Chem. Res.*, **33**, pp3025-3030.

Visscher, K. and Brinkman, J. (1989). Biological degradation of xenobiotics in waste management. *Haz. Waste Haz. Mat.*, **6**, 2, pp201-212.

Votruba, J., Mikus, O., Nguen, K., Hlavacek, V. and Skrivanek, J. (1975). Heat and mass transfer in honeycomb catalysts. *Chem. Eng. Sc.*, **30**, pp201-206.

Wakao, N. and Funazkri, T. (1978). Effect of fluid dispersion coefficients on particle-to-fluid mass transfer coefficients in packed bed. *Chem. Eng. Sci.*, **33**, pp1375-1384.

Yamamoto, S., Suzuki, Z., Asano, M. and Ito, T. (1982). Nippon Soken Inc. *Extrusion die for extruding honeycomb structures having a peripheral wall.* U.K. Pat. 2,095,158A

Yang, R.T. (1987). *Separation by Adsorption Processes*. USA: Butterworth.

Appendix I Examples of Photochemical Ozone Creation Potential (POCP) Values

VOC type		POCP
Alkanes	ethane	8.2
	propane	42.1
	n-butane	41.4
	i-butane	31.5
	n-pentane	40.8
	i-pentane	29.6
	n-hexane	42.1
	2-methylpentane	52.4
	3- methylpentane	43.1
	2,2-dimethylbutane	42.1
	2,3-dimethylbutane	38.4
	n-heptane	52.9
	2-methylhexane	49.2
	3-methylhexane	49.2
	n-octane	49.3
	methylheptanes	46.9
	n-nonane	46.9
	methyloctanes	50.5
	n-decanes	46.4
	methylnonanes	44.8
	n-undecane	43.6
	n-duodecane	41.2

(continued next page)

(cont. Appendix I)

VOC type		POCP
Alkenes	ethylene	100
	propylene	103
	1-butene	95.9
	2-butene	99.2
	1-pentene	93
	2-pentene	105.9
	2-methyl-1-butene	77.7
	3-methyl-1-butene	89.5
	2-methyl-2-butene	77.9
	butylene	64.3
	acetylene	16.8
Aromatic	benzene	18.9
	toluene	56.3
	o-xylene	66.6
	m-xylene	99.3
	p-xylene	88.8
	ethylbenzene	59.3
	n-propylbenzene	49.2
	i-propylbenzene	56.5
	1,2,3-trimethylbenzene	117
	1,2,4-trimethylbenzene	120.3
	1,3,5-trimethylbenzene	114.5
	o-ethyltoluene	66.8
	m-ethyltoluene	79.4
	p-ethyltoluene	72.5

(continued next page)

VOC type		POCP
Aldehydes	methanal	42.1
	ethanal	52.7
	propanal	60.3
	butanal	56.8
	iso-butanal	63.1
	pentanal	68.6
	benzaldehyde	-33.4
Ketones	acetone	17.8
	methyl ethyl ketone	42.3
	methyl isobutyl ketone	63.3
Alcohols	methanol	12.3
	ethanol	26.8
Esters	methyl acetate	2.5
	ethyl acetate	21.8
	i-propyl acetate	21.5
	n-butyl acetate	32.3
	s-butyl acetate	33.2
Chlorinated HC	dichloromethane	0.9
	1,1,1-trichloroethane	0.1
	tetrachloroethene	0.5
	trichloroehtene	6.6

Appendix II PG 6 Process Guidance Notes

PG 6/(no.)	Title	Year	ISBN
1	Animal by-product rendering	1991	0117524611
2	Manufacture of timber and wood-based products	1991	0117524034
3	Chemical treatment of timber and wood-based products	1991	0117524026
4	Processes for the manufacture of particleboard and fibreboard	1991	0117523879
5	Maggot breeding processes	1991	0117523968
6	Fur breeding processes	1991	0117523917
7	Printing and coating of metal packaging	1991	011752462x
8	Textile and fabric coating and finishing processes	1991	0117524662
9	Manufacture of coating powder	1991	0117524719
10	Coating manufacturing	1992	0117525952
11	Manufacture of printing ink	1992	0117525960
12	Production of natural sausage casing, tripe, chitterlings and other boiled green offal products	1991	0117524654
13	Coil coating processes	1991	0117524727
14	Film coating processes	1991	0117524778
15	Coating in drum manufacturing and reconditioning processes	1991	0117524751
16	Printworks	1992	0117525979
17	Printing and flexible packing	1992	0117525987
18	Paper coating	1992	0117525995
19	Fish meal and fish oil	1992	0117526002
20	Paint application in vehicle manufacturing	1992	0117526010
21	Hide and skin processes	1992	0117526029
22	Leather finishing	1992	0117526037
23	Coating of metal and plastic	1992	0117526045
24	Pet food manufacturing	1992	0117526053
25	Vegetable oil extraction and fat and oil refining	1992	0117526061
26	Animal feed compounding	1992	011752607x
27	Vegetable matter drying	1992	0117526088
28	Rubber processes	1992	0117526096
29	Di-isocyanate processes	1992	011752610x
30	Production of compost for mushrooms	1992	0117526118
31	Powder coating	1992	0117526126
32	Adhesive coating	1992	0117526134
33	Wood coating	1992	0117526142
34	Respraying of road vehicles	1992	0117526150
35	Metal and other thermal spraying processes	1992	0117526169
36	Tobacco processing	1992	0117526177
37	Knackers yards	1992	0117526185
38	Blood processing	1992	0117526193
39	Animal by-product dealers	1992	0117526207

Appendix III Summary of C_1-C_4 Alkane Diffusion Data On Silicalite/ZSM-5 (Hufton and Danner, 1993)

T (K)	D (cm^2/s)	Experiment
	Methane	
297	$1.3x10^{-10}$	CPC[2]
343	$4.6x10^{-10}$	CPC[2]
400	$1.3x10^{-9}$	CPC[2]
304	$1.1x10^{-4}$	PFG-NMR[3]
293	$9.2x10^{-5}$	PFG-NMR[3]
281	$8.5x10^{-5}$	PFG-NMR[3]
268	$9.2x10^{-5}$	PFG-NMR[3]
266	$7.2x10^{-5}$	PFG-NMR[3]
256	$7.6x10^{-5}$	PFG-NMR[3]
241	$6.8x10^{-5}$	PFG-NMR[3]
233	$6.2x10^{-5}$	PFG-NMR[3]
334	$1.1x10^{-6}$	MBR[5]
197	$7.0x10^{-6}$	FR[8]
200	$2.8x10^{-5}$	QENS[9]
250	$5.0x10^{-5}$	QENS[9]
	Ethane	
299	$5.0x10^{-5}$	PFG-NMR[3]
282	$5.7x10^{-5}$	PFG-NMR[3]
282	$4.5x10^{-5}$	PFG-NMR[3]
266	$5.0x10^{-5}$	PFG-NMR[3]
267	$3.7x10^{-5}$	PFG-NMR[3]
298	$6.5x10^{-8}$	FR[4]
318	$1.2x10^{-7}$	FR[4]
338	$1.8x10^{-7}$	FR[4]
334	$2.2x10^{-7}$	MBR[5]
323	$3.0x10^{-5}$	FR[7]
298	$1.3x10^{-5}$	FR[8]
273	$1.0x10^{-5}$	FR[8]
252	$6.0x10^{-6}$	FR[8]
298	$3.1x10^{-8}$	TPC[11]
300	$2.0x10^{-5}$	QENS[13]
	Isobutane	
297	$1.9x10^{-8}$	MBR[1]
334	$5.5x10^{-8}$	MBR[1]
433	$2.3x0^{-11}$	CPC[2]
473	$6.5x0^{-11}$	CPC[2]
493	$9.1x0^{-11}$	CPC[2]

T (K)	D (cm^2/s)	Experiment
	Propane	
403	$2.9x10^{-11}$	CPC[2]
423	$5.6x10^{-11}$	CPC[2]
446	$1.1x10^{-10}$	CPC[2]
308	$3.9x10^{-5}$	PFG-NMR[3]
296	$4.0x10^{-5}$	PFG-NMR[3]
286	$3.2x10^{-5}$	PFG-NMR[3]
277	$4.0x10^{-5}$	PFG-NMR[3]
298	$3.5x10^{-8}$	FR[4]
318	$6.3x10^{-8}$	FR[4]
338	$9.3x10^{-8}$	FR[4]
313	$1.0x10^{-5}$	SU[4]
298	$2.0x10^{-7}$	SU[4]
253	$3.0x10^{-8}$	SU[4]
223	$4.0x10^{-9}$	SU[4]
188	$4.0x10^{-10}$	SU[4]
334	$7.3x10^{-8}$	SU[4]
303	$7.4x10^{-8}$	MBR[5]
303	$8.2x10^{-8}$	ZLC[6]
323	$1.2x10^{-7}$	ZLC[6]
348	$1.6x10^{-7}$	ZLC[6]
279	$1.7x10^{-7}$	ZLC[6]
323	$6.0x10^{-6}$	ZLC[6]
351	$1.0x10^{-5}$	FR[8]
333	$5.0x10^{-6}$	FR[8]
238	$3.0x10^{-6}$	FR[8]
300	$1.2x10^{-5}$	QENS[13]
373	$1.8x10^{-5}$	QENS[13]
453	$2.4x10^{-5}$	QENS[13]
	n-Butane	
297	$5.7x10^{-8}$	MBR[1]
334	$1.1x10^{-7}$	MBR[1]
393	$4.1x10^{-12}$	CPC[2]
423	$1.3x10^{-11}$	CPC[2]
453	$3.8x10^{-11}$	CPC[2]
334	$3.7x10^{-8}$	MBR[5]
323	$5.4x10^{-7}$	FR[7]
348	$9.6x10^{-7}$	FR[7]
323	$1.5x10^{-6}$	FR[10]
300	$1.0x10^{-5}$	QENS[12]

(continued next page)

Key to Sources of Diffusion Data for C_1-C_4 Alkane /Silicalite Systems

Symbol	Reference (see Hufton and Danner, 1993)
MBR[1] (Membrane technique)	Paravar and Hayhurst, 1983
CPC[2] (Concentration pulse chromatography method)	Chiang et. al., 1984
PFG-NMR[3] (Pulsed field gradient nuclear magnetic resonance)	Caro et. al., 1985
FR[4] (Frequency resonance method)	Bulow et. al., 1986
SU[4] (Sorption uptake)	
MBR[5]	Hayhurst and Paravar, 1988
ZLC[6] (Zero-length chromatography)	Eic and Ruthven, 1989
FR[7]	van den Begin and Rees, 1989
FR[8]	van den Begin et. al., 1989
QENS[9] (Quasi-elastic neutron scattering)	Jobic et. al., 1989
FR[10]	Shen et. al., 1990
TPC[11] (Tracer pulse chromatography)	Hufton and Danner, 1991
QENS[12]	Jobic et. al., 1992a
QENS[13]	Jobic et. al., 1992b

Appendix IV Computer Program for Data Acquisition

(written by Mr. John Bishop of Bath University)

This is the include file required by the main program.

```
'                    P C Super Interface Procedures
'                   ================================
'                     for Borland Turbo Basic
'
'                   Program Name :- PCSUPER.INC
'                   Program No :- 61G
'                   Issue No :- 2
'                   Date :- 16/3/90
'
'=================================================================
'
'           Procedure to return PC Super Card Status.
'         ============================================
'==========
 sub Status (Ad%,St%)
'==========
        St% = inp(Ad%+2)
end sub

'           Procedure to wait for Comms Busy Flag False.
'           ============================================
'========
 sub Busy (Ad%)
'========
        delay (0.001)                   'Wait 1mS
        while inp(ad%+2) >= 128                 'Wait for Busy False
                print "";               'Enable Keyboard Break
        wend
end sub

'           Procedure to Check if A-D is finished.
'           ======================================
'===========
 sub Finished (Ad%)
'===========
        delay (0.001)                   'Wait 1mS
        while (inp(Ad%+2) and 176) <> 0          'Bits 128 + 32 + 16 False
                print "";          'Enable Keyboard Break
        wend
end sub

'           Procedure to Output Data to Card.
```

```
'                ===================================
'============
 sub DataOut (Ad%,Cmd$,St%)
'============
        local I%,C%
        C$ = Cmd$ + chr$(13)                    'Add Carriage Return
        for I% = 1 to len(C$)                   'One Character at a time
                call Busy (Ad%)                 'Check Card Comms free
                out (Ad%), asc(mid$(C$,I%,1))   'Output the Character
        next I%
        St% = inp(Ad%+2)                        'Check Status when finished
end sub

'               Procedure to Input Data from Card.
'               ===================================
'===========
 sub DataIn (Ad%,D%(1),NoOfReadings%,St%)
'===========
        local I%,HiByte,LoByte,D
        for I% = 1 to NoOfReadings%             'One Reading at a time
                call Finished(Ad%)              'Check not converting
                HiByte = inp(Ad%+1)             'Input HiByte
                call Busy(Ad%)
                LoByte = inp(Ad%+1)             'Input LoByte
                D = ((HiByte * 256) + LoByte) - 32768
                D%(I%) = int(D)                 'DataArray (NoOfReadings)
        next I%
end sub

'=================================================================
```

Appendix V Experimental Data Error Analysis

The error analysis given in this appendix has been conducted by the method outlined by Jenson and Jeffreys, 1963.

V.1 Temperature

Error in reading analogue temperature indicator = ±1 °C

Therefore, accuracy of temperature measurement = ±1.0°C over the range 0-350 °C

V.2 Pressure

Error in reading digital pressure indicator = ±0.01 barg over the range 0-2 barg

V.3 Composition Analysis

V.3.1 Flame Ionisation Detector (FID)

For sample compositions in the range of 1000-10,000 ppmv, the maximum deviation found between 5 consecutive analyses was generally ±2 (v)%. For those in the range 20,000-44,000 ppmv, the maximum deviation compositions determined was ±5 (v)%.

V.3.2 Relative Humidity Measurement

The maximum deviation for 3 consecutive experiments was found to be ±1 % relative humidity (RH) for 55-70 % RH water samples.

V.4 Adsorption/Desorption Feed Flowrate

For flowrate of 500 cm^3/min,

the error in reading the mass flow controller $= \pm 0.25\ cm^3/min$

Therefore, the percentage error $= (\frac{\pm 0.25}{500})100$

$= \pm 0.05\ \%$

For flowrate of 1500 cm^3/min,

the error in reading the mass flow controller $= \pm 0.75\ cm^3/min$

Therefore, the percentage error $= \pm 0.05\ \%$

Appendix VI Dimensions of Extrusion Dies

The dimensions of the dies for extruding the thin-wall and thick-wall square channel monoliths are presented in Table VI.1, and illustrated in Figure VI.1.

Table VI.1 The dimensions of the dies for extruding square channel monoliths

	Thin wall	Thick wall
a (mm)	20.55	20.60
b (mm)	5.61	5.50
c (mm)	0.50	1.00
d (mm)	15.00	15.40
e (mm)	12.00	12.00
f (mm)	1.50	1.00
g (mm)	0.50	1.00
h (mm)	26.10	26.10

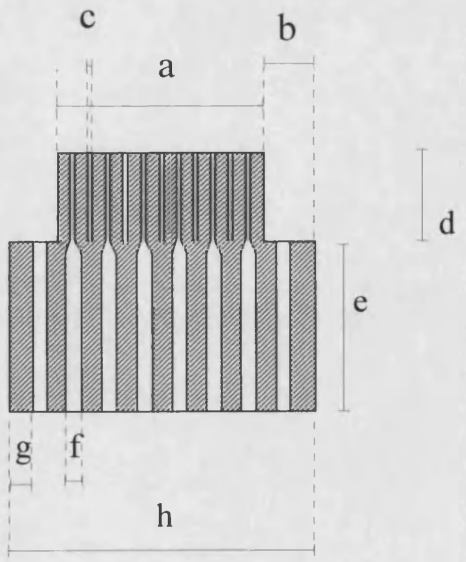

Figure VI.1 The dimensions of the die for extruding square channel monoliths

Appendix VII Properties of Bentonite, CCB and Hyplas 71

These data sheets were supplied by Cookson Ceramics and Minerals, ltd., 1994.

Table VII.1 Typical characteristics of bentonite

Major mineral constituent	Montmorillonite, $Al_2O_3.5SiO_2.7H_2O$
Appearance	Fine light grey powder
Chemical analysis :	wt %
SiO_2	54.63
Al_2O_3	6.71
Fe_2O_3	3.59
Cao	1.36
MgO	2.13
Na_2O	2.03
K_2O	0.53
Moisture content (100 °C)	12.49
Loss on ignition (105-1000 °C)	5.15
Bulk density	900 kg/m^3

Table VII.2 Typical characteristics of CCB

Chemical analysis :	Weight %
SiO_2	66.0
Al_2O_3	22.0
Fe_2O_3	1.0
Cao	1.0
MgO	1.0
Na_2O	3.0
K_2O	3.0
Loss on ignition (105-1000 °C)	7.0
Appearance	Fine dark grey powder

Table VII.3 Typical characteristics of Hyplas 71

Typical constituents :	Weight %
Kaolinite	40
Micaceous material	22
Quartz	37
Carbonaceous material	<1.0
Appearance	Fine light grey powder
Chemical analysis :	wt %
SiO_2	70
Al_2O_3	19
Fe_2O_3	0.8
Cao	0.2
MgO	0.4
Na_2O	0.5
TiO_2	1.6
K_2O	2.0
L.O.I	5.4
C	0.1

Appendix VIII Calculation of Geometric Properties of Monoliths

VIII.1 Calculation of Voidage and Specific Surface Area for Square Channel Monoliths

The voidage of a square channel monolith, ε_m , was calculated from an equation given by DeLuca and Campbell, 1977:

$$\varepsilon_m = \frac{D^2}{(D+t)^2} \qquad \text{(VIII.1)}$$

where D is the size of the channel and t is the thickness of the wall. The Equation VIII.1 was derived based the "void volume/total bed volume" for constant diameter and channel size. (Results are shown in Table 3.4)

The specific surface area, S_c, was determined from the following expression (DeLuca and Campbell, 1977) :

$$S_c = \frac{4(\sqrt{\varepsilon} - \varepsilon)}{t} \qquad \text{(VIII.2)}$$

VIII.2 Calculation of Voidage and Specific Surface Area for Circular channel Monoliths

The geometric properties of a circular channel monolith were calculated using empirical values. The voidage was determined as the following :

$$\varepsilon_m = \frac{Vol_{Single} \times Channel_{Total}}{Vol_{Total}} \qquad \text{(VIII.3)}$$

where Vol_{Single} is the volume of a channel, $Channel_{Total}$ is the total number of circular channels and Vol_{Total} is the total volume of the monolith.

The specific surface area, S_c, of the circular channel monolith is the total surface area of all passages per unit volume of bed. Thus,

$$S_c = \frac{Area_{Single} \times Channel_{Total}}{Vol_{Total}} \qquad \text{(VIII.4)}$$

where $Area_{Single}$ is the surface area of a single passage.

Appendix IX Calculation of Geometric Properties of Pellets

The weight of a spherical adsorbent was determined by weighing 100 randomly selected pellets which were sieved through a British Standard Sieve (see Table 3.4). Its density, ρ_p, was calculated from the ratio of weight to volume,

$$\text{Volume of pellet} = \pi(\frac{d_p^3}{6}) \qquad \text{(IX.1)}$$

$$\rho_p = \frac{6(weight)}{\pi d_p^3} \qquad \text{(IX.2)}$$

where d_p is the diameter of the pellet.

The bulk density, ρ_b, of the packed-bed was based on the total weight of pellets to the total volume of the bed:

$$\rho_b = \frac{Weight_{Bed}}{\pi r^2 L} \qquad \text{(IX.3)}$$

where r is the radius of the bed and L is the length of the bed.

Therefore, the bed voidage can be evaluated using Equations IX.2 and IX.3:

$$\varepsilon = 1 - \frac{\rho_b}{\rho_p} \qquad \text{(IX.4)}$$

The specific surface area, S_B, of the packed-bed was calculate using the following expression (Coulson and Richardson, 1991) :

$$S_B = \frac{6(1-\varepsilon)}{d_p} \qquad \text{(IX.5)}$$

Appendix X A Computer Fortran Program for the Evaluation of the Area Above the Breakthrough Curve

==========

```
C     This Fortran program is to read the experimental data from the data acquisition
C     card and then to calculate the area under the breakthrough curve using Simpson's
C     Rule The following is to declare the data types.

      Dimension Tme(8000),Concv(8000),Concp(8000),T1(8000),
     *  T2(8000),T3(8000),T4(8000),T5(8000),T6(8000)
      Character Fint*20, Fout*20
      Integer k, Ext, Ndat, Sort, i, ppm
      Real Aund, Atop, Step, F, W, Co, Void, Vtot, Vo, x, y, z, q, g
      k=1000000000


C     The following is to remind user to sort-out the 'raw' experimental data.

      Print *,'Have you sort-out expt. data ?'
      Print *,'Type 0 for NO and 1 for YES '
      Read (5,*) Sort
      If(Sort.EQ.0) Then
            Print *,'Open expt data file :'
            Print *,'(i) make sure first data is the time'
            Print *,'(ii) input 9 large negative values
     *      (ie. -1,000,000) at end of file'
            Stop
      Endif


C     The following is to read data from experimental data file.

      Print *,'Input filename :'
      Read (5,*) Fint
      Open (1,FILE=Fint)
      Do 11 i=1,k
      Read (1,*) Concv(i), Concp(i), Tme(i), T1(i), T2(i),
     * T3(i), T4(i), T5(i), T6(i)
      If(Concv(i).LE.-1000000) Go To 21
      If(Concp(i).LE.-1000000) Go To 21
      If(Tme(i).LE.-1000000) Go To 21
      If(T1(i).LE.-1000000) Go To 21
      If(T2(i).LE.-1000000) Go TO 21
      If(T3(i).LE.-1000000) Go To 21
      If(T4(i).LE.-1000000) Go To 21
      If(T5(i).LE.-1000000) Go To 21
      If(T6(i).LE.-1000000) Go To 21
11    Continue
```

```
21    Close (1)

        Ndat=i-1
        Print *,'Ndat :',Ndat
        Print *,'Data extraction step :'
        Read (5,*) Ext
        Print *,'Output filename :'
        Read (5,*) Fout
        Open (2,FILE=Fout)
        Write (2,100) 'FID Read(v)','Conc(ppm)','Tme(s)','T1(degC)'
     * ,'T2(degC)','T3(degC)','T4(degC)','T5(degC)','T6(degC)'

        Write (2,110) (Concv(i), Concp(i),(Tme(i)-Tme(1)), T1(i),T2(i),
     * T3(i),T4(i),T5(i),T6(i), i=1,Ndat,Ext)

        Write (6,110) (Concv(i), Concp(i),(Tme(i)-Tme(1)),T1(i),T2(i),
     * T3(i),T4(i),T5(i),T6(i), i=1,Ndat,Ext)
        Close (2)
100    Format (a11,1x,a9,2x,6a,1x,8a,8a,8a,8a,8a,8a)
110    Format (f6.0,1x,f7.2,1x,f8.2,1x,f7.4,1x,f7.4,1x,f7.4,1x,f7.4,1x,
     * f7.4,1x,f7.4)


C      This section is to calculate the area under the breakthrough curve by Simpson's
C      Rule, where
C      Aund denotes area under breakthrough curve
C      Atop denotes area above curve

        Step = Tme(2) - Tme(1)
        If (MOD(Ndat,2).EQ.0) Ndat=Ndat-1
        Call Simp(Ndat, Step, Aund, Concp)
        Atop = ((Concp(Ndat)*(Tme(Ndat)-Tme(1)))
     * - Aund)*0.41903236/10**6
        Aund=Aund*0.41903236/10**6
        Write (6,120) 'Atop (mmol)','Aund (mmol)','Concp (ppm)','Time
     * (s)'
        Write (6,130) Atop, Aund, Concp(Ndat), Tme(Ndat)-Tme(1)
120    Format (5x, a12, 3x, 5x, a12, 3x, 5x, a11, 4x, 5x, a8, 7x)
130    Format (4(5x, f15.6))


C      Defining:
C      Co  mole sorbate (mmol/m3)
C      W   wt adsorbent (gram)
C      Void  fractional voidage
C      Vtot  volume of column (m3)
C      F   total flowrate (mmol/s)

        W  = 55.11
        Void = 0.4
```

```
      Vtot = 0.000062831
      F = 0.41903236
      Print *,'Input initial fractional concentration (ppm) :'
      Read (5,*) ppm
      Co = ppm * 0.0502838


C     This section is the subroutine for Simpson's Rule,where:
C     N is total number of expt data (ODD no.)
C     H is interval between two data
C     F is experimental data

      Subroutine Simp(N, H, Rintg, F)
      Real F
      Dimension F(5000)
      Integer N
      Real H, Rintg

C     Initial value

      Sum1=0
      Sum2=0
      Sum3=0

      Do 10 i=1,N
      If (i.EQ.1) Sum1 = Sum1 + F(i)
      If (i.EQ.N) Sum1 = Sum1 + F(N)

10    Continue

      Do 20 i=2, N-3, 2
      Sum2 = Sum2 + F(i)
      Sum3 = Sum3 + F(i+1)

20    Continue
      Sum2 = Sum2 + F(N-1)
      Rintg = (H/3)*(Sum1 + 4*Sum2 +2*Sum3)
      End
```

Appendix XI Calculation of Molecular Diffusivity

At STP (0°C and 101325 N/m^2) the density of nitrogen is 1.25 x 10^{-3} g/cm^3 and its viscosity is 1.67 x 10^{-5} Ns/m^2 (Perry and Chilton, 1973).

The diffusion coefficient for a binary mixture of gases A and B is estimated from the Chapman-Enskog equation (Reid and Sherwood, 1958) :

$$D_v = \frac{0.0018583T^{1.5}\left(\frac{M_A + M_B}{M_A M_B}\right)^{0.5}}{P\sigma_{AB}^2 \Omega_D} \qquad \text{(XI.1)}$$

where D_v is the molecular diffusivity (cm^2/s), T is the absolute temperature (K), M_A, M_B are the molecular weights of the two species, P is the total pressure (atm), Ω_D is the collision integral, which is a function of kT/ε_{AB} where $\varepsilon_{AB} = \sqrt{\varepsilon_A \varepsilon_B}$, $\sigma_{AB} = \frac{1}{2}(\sigma_A + \sigma_B)$, ε, σ are the Lennard-Jones force constant and k is the Boltzmann constant. Tabulations of the force constants are given by Reid and Sherwood (1958). The data used for nitrogen-propane mixtures are as follows :

$$\sigma_{AB} = \frac{1}{2}(0.3798 + 0.5118) = 0.4458nm \qquad \text{(XI.2)}$$

$$\frac{kT}{\varepsilon_{AB}} = \frac{kT}{\sqrt{\varepsilon_A \varepsilon_B}} = \frac{k \times 273}{\sqrt{71.4k \times 237.1k}} = 2.0982 \qquad \text{(XI.3)}$$

From Reid and Sherwood (1958) at $\frac{kT}{\varepsilon_{AB}} = 2.0982$,

$$\Rightarrow \Omega_D = 1.057$$

Therefore, $D_v = \frac{0.001858 \times 273^{1.5}\left(\frac{28+44}{28 \times 44}\right)^{0.5}}{1 \times 4.458^2 \times 1.057} = 0.09645\,\text{cm}^2/\text{s}$ (XI.4)

Appendix XII Calculations of Pressure Drop and External Mass Transfer Coefficients

The experimental total flowrate was 500 cm^3/min. At 0°C and 101325 N/m^2, the density of nitrogen was 1.25 x 10^{-3} g/cm^3 and its viscosity was 1.67 x 10^{-5} Ns/m^2 (Perry and Chilton, 1973).

The pressure drop in the monolith was calculated using the following equation (described in Chapter 6) :

$$\frac{\Delta P}{L} = 28.4 \frac{\mu u_s}{\varepsilon_m d_c^2} \qquad \text{(XII.1)}$$

Thus, $$\frac{\Delta P}{L} = \frac{28.4 \times 1.67 \times 10^{-5} \times 0.03}{0.25 \times 0.001^2} = 56.91 Pa/m$$

The pressure drop in the packed bed was determined from the Ergun equation (Ergun, 1952) :

$$\frac{\Delta P}{L} = \frac{(1-\varepsilon_p)}{\varepsilon_p^3}\left[\frac{150\mu u_s}{d_p^2}(1-\varepsilon_p) + \frac{1.75\rho u_s^2}{d_p}\right] \qquad \text{(XII.2)}$$

$$\frac{\Delta P}{L} = \frac{(1-0.49)}{0.49^3}\left[\frac{150 \times 1.67 \times 10^{-5} \times 0.024}{0.00109^2}(1-0.49) + \frac{1.75 \times 1.25 \times 0.024^2}{0.00109}\right]$$

Thus, $$\frac{\Delta P}{L} = 116.88 Pa/m$$

The external mass transfer coefficient in the monolith was determined using the Hawthorn model (Hawthorn, 1974) :

$$Sh = 2.98(1 + 0.095\, Re\, Sc \frac{d_c}{L})^{0.45} \qquad \text{(XII.3)}$$

where $Sh = \frac{kd}{D_v}$

Thus, $k = \frac{9.64 \times 10^{-6} \times 2.98}{0.001}[1 + (0.095 \times 8.98 \times 1.38 \times \frac{0.001}{0.218})]^{0.45} = 0.0287 m/s$

The equation for the external mass transfer coefficient in the packed bed was given by Wakao and Funazkri (1978) :

$$Sh = 2.0 + 1.1 Sc^{0.33}\, Re^{0.60} \qquad \text{(XII.4)}$$

Thus, $k = \frac{9.64 \times 10^{-6}}{0.00109}[2.0 + 1.1(1.38^{0.33} \times 1.95^{0.60})] = 0.034 m/s$